The influence of spreading particles on the stability of thin liquid films

Promotor: Dr. A. Prins
Hoogleraar in de fysica en de fysische chemie van levensmiddelen met bijzondere aandacht voor de zuivel

Co-promotor: Dr. Ir. H.J. Bos
Universitair docent in de theoretische aerodynamica

Stellingen

1. Het aanwezig zijn van oppervlaktestructuren is zeer bepalend voor het gedrag van een schuim of een emulsie. Het onderkennen van deze structuren wordt vaak nagelaten, omdat hun bestaan moeilijk te bewijzen is.

2. Voordat een belangrijke wetenschappelijke ontdekking in de publiciteit wordt gebracht zou haar wetenschappelijk en maatschappelijk draagvlak op een voldoende rationele en relativerende wijze moeten worden getoetst om een mogelijke publieke onrust te vermijden.

3. "De bulkfase werd door God geschapen, maar het oppervlak door de duivel" (citaat Prof. W. Pauli (1900-1958)). Volgens dit citaat zou men oppervlaktereologie dus ergens tussen hemel en hel moeten plaatsen, omdat men bij deze leer de bulkfase en het oppervlak niet los van elkaar kan zien.

4. De uitspraak: "Wat met kracht niet lukt, zal met meer kracht wel lukken" is onjuist. Men zou de toegediende effectieve energie als graadmeter moeten gebruiken.

5. Voor de bij de Europese eenwording voorgestelde noodzakelijke integratie-snelheid van de verschillende culturen in de verschillende landen zouden de beleidsmakers bijzonder gebaat zijn bij een goede kennis der historie, die geleid heeft tot deze cultuurverschillen en in het bijzonder de rol die de tijdsfactor hierin heeft gespeeld.

6. De tegenstanders van het "alternatieve pedagogische geleuter" in het huidige onderwijs (1997), waarbij de alternatieve en losbandige opvoeding hoogtij zou vieren, zouden hun doelstellingen voor meer ouderwets onderwijs eerder bereiken door het ondersteunen van nog meer vrije denkbeelden in dit onderwijs: "er wordt nergens sneller orde geschapen dan bij complete chaos".

7. Om een taak goed te kunnen uitvoeren moet men openstaan voor kritiek en deze kritiek gebruiken om in de toekomst beter voorbereid te zijn.

8. Veel belangrijke beslissingen worden in een ongedwongen sfeer genomen.

9. Een vergadering kan als geslaagd worden gezien als aan het eind ervan beslissingen worden genomen. Heeft men veel geslaagde vergaderingen, dan is er nauwelijks tijd over om deze beslissingen uit te voeren.

10. "Scherven brengen geluk" luidt het spreekwoord. Dit zou betekenen dat, wanneer alles al gebroken is, men het geluk op een andere manier moet zoeken.

11. De benaming "scharrelvlees" betekent niet dat de dieren, waarvan het vlees afkomstig is, volkomen vrij waren in hun doen en laten. Indien men dit als voorwaarde zou stellen, zou men uitsluitend wild moeten eten.

12. Het nadeel van zogenaamde "upgrades" van computerprogramma's is, dat je oudere versies van het programma moet bewaren.

13. Als je in het buitenland een woordenboek Engels-Nederlands of Nederlands-Engels op je bureau hebt liggen, loop je de kans om voor Marxist te worden aangezien.

14. Roken is verslavend. Op het moment dat men er mee wil stoppen is men echter opgezadeld met een tweede verslaving om van de eerstgenoemde af te komen.

Stellingen behorende bij het proefschrift "The influence of spreading particles on the stability of thin liquid films" door C.G.J. Bisperink. Wageningen, 27 mei 1997.

The influence of spreading particles on the stability of thin liquid films

Christiaan G.J. Bisperink

Proefschrift
ter verkrijging van de graad van doctor
op gezag van de rector magnificus
van de Landbouwuniversiteit Wageningen,
dr. C.M. Karssen,
in het openbaar te verdedigen
op dinsdag 27 mei 1997
des namiddags te één uur dertig in de Aula

Omslagontwerp: Thomas Wansing

Druk: Grafisch Service Centrum, Van Gils B.V.

ISBN 90-5485-717-X

Voor mijn ouders

ABSTRACT

Bisperink, Chr.G.J. The influence of spreading particles on the stability of thin liquid films. Ph.D. thesis, Wageningen Agricultural University (210 pp., English summary)

Keywords: Foam, films, coalescence, coarsening, spreading particles, lipids, surface rheology

The influence of spreading particles on the stability of thin liquid films was investigated. Due to the spreading of a particle, i.e. an oil droplet, over a surface of a thin liquid film the latter becomes thinner and may rupture. The following steps in the whole process were distinguished: 1) transport of the particle to the film surface, 2) dewetting of the particle ensuring physical contact between the particle surface and the film surface, 3) spreading of the particle over the film surface and 4) movement of the film bulk liquid induced by the surface movement due to spreading material.

An attempt was made to develop a theory that describes the spreading process quantitatively. It describes the film thinning process as a result of the liquid drag due to the surface motion initiated by the spreading material by using the parameters film thickness, droplet radius, liquid bulk viscosity, liquid bulk density and the surface rheological properties of the oil droplet and the film liquid.

Model systems of foaming liquid and lipid material were used to study this spreading process. The latter was done on a relative macroscopic scale over bulk surfaces which is different compared to the dimensions and conditions which are valid for spreading particles on a foam film. It was assumed that the developed theory could be applied to both dimensions. The experimental results pointed in this direction. This was verified by the experimental results of introducing small spreading emulsion droplets on thin liquid films. A clear correlation between the above mentioned parameters and film rupture initiated by the spreading droplets was found.

VOORWOORD

"Het boekje" zoals dit proefschrift in mijn familiekring wordt genoemd. Nu U dit leest is het dus daadwerkelijk afgerond. Alleen mijn naam staat op de voorkant en dat is naar mijn mening ten onrechte. Het nadeel van een voorwoord waarin namen worden genoemd is dat je er uiteraard ook enkele zult vergeten. Daarom wil ik de mensen die ik hieronder niet bij naam noem, maar die toch op enigerlei wijze hebben bijgedragen aan het totstandkomen van dit proefschrift, bedanken.

Ruim vijf jaar heb ik op de toenmalige sectie Zuivel en Levensmiddelennatuurkunde doorgebracht, waarvan de laatste anderhalf jaar aan dit onderzoek zijn besteed. Gedurende deze tijd zijn voornamelijk de daadwerkelijke experimenten uigevoerd. Er werd gestoeid met Langmuir troggen, ringtroggen, vallende films, overlopende cylinders, overlopende goten en theoriën. Tijdens deze hectische periode was er altijd de persoon die openstond voor ideën, kritisch was, meedacht, hulp bood, discussieerde, rust bracht en aanspoorde. Ik heb het over mijn promotor Albert Prins. Albert, het is voor mij een eer geweest om met jou te mogen werken. Van jou heb ik geleerd de natuur te vragen "hoe ben jij?". Mijn huidige baas zegt altijd: "Freedom promotes creativity". De vrijheid heb ik tijdens het werken onder jouw leiding steeds ervaren en kreativiteit kon daardoor volledig gestalte krijgen. Albert ik bedank je hiervoor. Mijn co-promotor Hans Bos bedank ik voor de hulp, de vruchtbare discussies en z'n kritische kijk op de theorie. Hans, zonder jou inbreng had ik een groot deel van dit proefschrift niet kunnen schrijven. Ik heb veel van je geleerd.

De drie leden van de "knokploeg", zoals ik ze thuis altijd noemde, wil ik bedanken. Hierin was de grootste "vechtersbaas" wel Aliza de Groot. Met een engelengeduld hielp ze me steeds weer met het opbouwen van apparatuur, het maken van oplossingen en het doen van metingen. Aliza, bedankt voor alles en ik ben jaloers op de mensen die nu met je mogen werken. Gerard de Jong was de man die de vallende film wist te bedwingen. Gerard, de manier waarop jij de experimentele problemen wist op te lossen bewonder ik zeer. De resultaten van jouw experimenten zijn in dit onderzoek van groot belang geweest. Bedankt voor je inzet. Johan Hayer

VOORWOORD

wil ik bedanken voor z'n ontelbare pogingen om de spreidsnelheid van een vetdruppel te kunnen meten. Johan, je gelooft het misschien niet maar jouw werk heeft veel bijgedragen om het spreidende deeltjes mechanisme te leren begrijpen.

Mijn sponsor wil ik bedanken voor de mogelijkheid die mij geboden is om dit promotie-onderzoek te kunnen doen. Verder wil ik Nestlé bedanken voor de tijd die mij gegeven is om dit proefschrift te kunnen afronden.

Ik wil in het bijzonder alle, vaak vergeten, medewerkers van de technische diensten bedanken. Door jullie hulp en inzet zou menig onderzoek, inclusief het mijne, niet mogelijk zijn geweest. Jullie verdienen een pluim en ik bedank jullie allemaal.

Alle medewerkers van de sectie bedank ik voor de prettige samenwerking, hun interesse, discussies, hulp en collegialiteit gedurende de tijd die ik bij de sectie heb doorgebracht.

Aart de Groot bedank ik dat hij mijn paranymf wil zijn en voor alle hulp die hij geboden heeft om mijn promotie in Nederland te regelen. Aart, een betere "regelneef" als jij had ik niet kunnen treffen. I want to thank Simon Livings for all the fruitful discussions we had and that he wants to accompany me to present my thesis.

Tenslotte wil ik Manja bedanken. Zij was degene die me steeds weer aanspoorde om 's avonds na het werk weer achter de computer te gaan zitten om "het boekje" af te ronden. Manja, je bent m'n steun en toeverlaat en ik bedank je voor het geduld dat je de afgelopen periode met me hebt gehad. Ik hou van je.

CONTENTS

CONTENTS

INTRODUCTION

1.1. GENERAL INTRODUCTION

Foam is a dispersion of gas in liquid that can be generated by for instance agitation at the gas liquid interface, leading gas through a glass sinter or a grit with very small holes in it, by the nucleation of gas bubbles when the liquid is supersaturated with gas or by excessive pressure gradients in the liquid. Foaming is mainly a physical phenomenon in which the chemical composition of the system plays an important role. The lifetime of the foam is for different reasons of great importance. Unwanted foam can create many problems, ranging from occasional annoyance to major disruption of operations. For example, foam can interfere with process instruments, sensors, pumps and filters, slow down drying of products as a result of the slower drainage of the liquid to be removed from the product, create bubbles in coatings or separation and segregation of process ingredients. On the other hand controlling the instability of foam is a functional part in production processes as for instance textile printing, distillation processes and gas washing, or in products as beer and champagne. In order to understand the control of foams, one must first be aware of the factors that contribute to foam stability. The thin liquid films between the gas bubbles play a crucial role in the stability of the foam. In the stability of the thin liquid films the surface properties play an important role. Foaming is a dynamical process and not all the physical parameters in a foam are in complete equilibrium. This means that the relation between foaming behaviour and the surface properties of the foaming liquid can only be found if the dynamic surface properties are taken into account.

The three main physical processes that contribute to foam stability are drainage, disproportionation and coalescence. These processes are interrelated and occur simultaneously in a foam. They are determined by the surface and bulk properties of the foaming system. Amongst others, temperature, pH and surfactant concentration all influence the properties of the liquid surfaces of the films in a foam and therefore affect foam stability.

1.2. DRAINAGE

The stability of foams is often related to the drainage process. Although drainage can be used as a measure for foam stability it has to be considered that the stability is determined by the interrelated effects of all the individual physical processes. As a result of drainage the foam becomes dryer because the Plateau borders and liquid films become thinner. A distinction can be made between two drainage processes. 1) Drainage that mainly takes place through the Plateau borders and which is governed by gravity and capillary forces, and 2) drainage of the thin liquid films in a foam in which in addition to gravity forces the Plateau border suction is the driving force for viscous flow through the interior of the film. In this way film drainage is also indirectly related to the gravity forces because they act on the liquid in the Plateau border.

The presence of particles (i.e. Pickering stabilization), high film elasticity, a high surface dilational viscosity, a high bulk viscosity, electrostatic double layer repulsion (i.e. ionic surfactants) or entropic repulsion (i.e. nonionic macromolecular surfactants and proteins) function as foam-stabilizing factors by acting in the thin liquid films between the bubbles in a foam. These physical properties slow down or even stop the film thinning process caused by drainage. This way the liquid films stay thicker and will be more stable against rupture compared to thinner ones.

The ability of the bubble walls to recover from an applied force is determined by the film and surface elasticity. Electrical double layer repulsion describes the electrical forces that stabilize the liquid films between bubbles when the distance between the film surfaces is small. Entropic repulsion is found in the liquid films of polymer solutions and describes the tendency to keep the film surfaces from approaching one another too closely, in accordancy with entropic principles.

A high bulk viscosity results in a deceleration of the drainage of liquid from the foam. This is due to the tangential shear stress performed by the moving liquid on the liquid surface containing surfactant resulting in a surface tension gradient which is responsible for this deceleration. A high surface dilational viscosity is responsible for a

high surface tension in expansion and a low surface tension in compression which can slow down the rate of drainage.

1.3. DISPROPORTIONATION

When an aqueous foam is made with a gas that is well soluble in the water phase one of the main foam coarsening processes is disproportionation or Ostwald ripening of the bubbles. This process refers to the interbubble gas diffusion as a result of gas pressure differences between bubbles. The rate of disproportionation increases with decreasing film thickness and increasing surface tension and is therefore related to drainage. On the other hand disproportionation has a positive effect on foam drainage as a result of the disappearance of bubbles, i.e. liquid films and Plateau borders, leading consequently to an excess liquid that drains. Furthermore, a coarser foam is draining faster than a finer foam. The reason for this phenomenon can be found in the surface properties. If the surfaces of the bubbles in a foam are motionless during drainage, which is the case with small bubbles, the drainage will be decelerated to the maximum which is possible. When the bubbles become bigger there is a threshold value beyond which the surface tension gradient is not able to keep the bubble surface motionless resulting in a faster drainage.

1.4. COALESCENCE

Coalescence is another important foam coarsening process. It is the merge of two bubbles as a result of the rupture of the film between the bubbles. To obtain more understanding of the physical processes that take place during coalescence, investigations have to be focused on the behaviour of thin liquid films.

The thin liquid films between the bubbles are the most fragile structures in a foam. As a result of drainage and in the absence of a disjoining pressure the films can become very thin without resistance. A disjoining pressure can be developed when

electrostatic repulsion or steric hindrance are present within the liquid film opposing the two film surfaces in approaching each other during drainage. When the films become thin Van der Waals attractive forces between the two film surfaces become more and more pronounced and may lead to an enhanced film thinning by squeezing the liquid out of the thin film towards the Plateau borders. When a liquid film reaches the so called critical thickness it may rupture spontaneously due to thermal or mechanical disturbances. Therefore, a disjoining pressure that is high enough may prevent film rupture due to this mechanism.

In practice foaming liquids often contain particles. When particles are present in the system the following mechanisms that can result in destabilization of a foam can be distinguished: the "hydrophobic particle mechanism" and the "spreading particle mechanism". The particles either originate from the foaming liquid itself or are introduced in the foam from outside.

Amongst others, Garret (1980), Dippenaar (1982) and Aronson (1986) described the "hydrophobic particle mechanism". The main condition in the hydrophobic particle mechanism is that the particles have to bridge the two surfaces of the thin liquid film in order to induce film rupture. Therefore the particles must have the size of the order of magnitude of the film thickness.

Ross (1950), Ross et al. (1953), Prins (1986, 1988, 1989) and Ronteltap (1989) described the "spreading particle mechanism". This mechanism involves the spreading of surface active material from particles present in the liquid surface. Compared to the hydrophobic particle mechanism the particles in the spreading particle mechanism may have a size that is much smaller than the film thickness in order to induce film rupture. Spreading particles could therefore be more effective in causing coalescence in a foam than hydrophobic particles. Although many mechanisms have been proposed to describe film rupture (i.e. coalescence) due to the spreading particle mechanism, none of them was conclusive.

Ross et al. (1953) described that the desorption of the originally film stabilizing surface active material from the film surface due to the introduction of spreading material as a

possible mechanism of film rupture. Furthermore, Ross et al. (1953) described that antifoaming agents that cause a decrease of the Gibbs film elasticity when they spread over the film surfaces give rise to an increased drainage rate of the liquid films. In combination with a pronounced weakening effect on the liquid films by for example reducing the disjoining pressure these agents could cause destabilization of the liquid films in a foam resulting in foam coarsening. The process of entering of particles out of the film liquid into the film surface is accompanied with a mechanical shock is another explanation for film rupture as is suggested by Lucassen (1992). Furthermore, the viscous drag of film liquid along with the moving surface during spreading resulting in local thinning of the liquid film is given as a responsible mechanism for film rupture by Bikerman (1973), Kruglyakov (1989), Prins (1986, 1988, 1989) and Ronteltap (1989). Both the hydrophobic and the spreading particle mechanism are more effective when the liquid films are thinner and therefore their performance depends on the rate of film drainage. On the other hand by assuming a certain concentration of particles to be present in the foaming liquid and by considering the volume of foaming liquid present in the film between the bubbles, the chance a particle to be present in the liquid film is smaller when the film is thinner and the bubbles are smaller. In general it may be assumed that the more time it takes for film thinning the longer the film destabilization due to the mentioned processes can be postponed.

The rate of drainage is increasing with an increasing extent of coalescence in a foam. This is due to the same reasons mentioned earlier. The merge of the bubbles results in the disappearance of Plateau borders and films and the resulting excess of liquid has to drain. Furthermore, a fine foam drains slower than a coarser foam and therefore coalescence (i.e. foam coarsening) will result in an increased rate of drainage. Due to coalescence the number of thin liquid films will decrease compared to the number of particles present in the foaming liquid. Additionally, the surface areas of the thin liquid films between the bubbles will increase due to coarsening and drainage of the foam. The films between larger bubbles have larger surface areas than

the films between smaller bubbles and drainage results in transformation of a spherical foam in a polyhedric foam which consequently leads to the formation of larger liquid films between the bubbles. For these reasons the chance of a particle to be present in a liquid film will increase. In this view it may be expected that a foam with small bubbles, i.e. a high number of thin liquid films with small surface areas in relation to the limited number of particles in the foaming liquid will be more stable than a foam which consists of larger bubbles.

1.5. AIM OF THIS STUDY

It was the aim of this study to be able to predict the rupture of a thin liquid film when a particle of known composition and size spreads over a thin liquid aqueous film with known physical properties. The study is focusing on the physical events that take place when a particle spreads over a thin liquid film. The foam destabilizing effect of spreading particles is also an example of a dynamic process and consequently it is to be expected that also in this process dynamic surface properties have to be taken into account.

1.6. CONTENTS OF THIS THESIS

The main physical processes that occur in a foam, i.e. drainage, disproportionation and coalescence will be reviewed in Chapter 2. In more detail the literature discussing coalescence initiated by the spreading particle mechanism which is subject of this study will be reviewed. The physical processes involved in the spreading particle mechanism, i.e. dewetting and spreading of particles, and the theories developed up till now to describe film rupture due to this mechanism will be discussed. In Chapter 3 the theory that is developed in this study to describe film rupture due to the spreading particle mechanism will be discussed. The theory focuses on the physical events, especially the hydrodynamics that occur when a lipid droplet containing surface active

components is entering into the film surface followed by the spreading over the film surface resulting in film thinning and eventually in film rupture and coalescence of bubbles. In Chapter 4 the experimental devices used to measure the physical parameters of importance in the spreading particle mechanism will be discussed and elucidated. Additionally the model systems used in this study will be discussed. The results of the experimental work will be presented in Chapter 5. Furthermore, in this chapter there will be a discussion of the effect of the dewetting process, the spreading velocity, the available surface area for spreading, the film thickness, the composition and size of the spreading particle and the surface and interfacial rheological behaviour of the film surface and the spreading particle on film rupture. The experimental results will be compared to the developed theories. Chapter 6 contains the final conclusions that can be drawn from the presented work.

REFERENCES CHAPTER 1.

Aronson, M.P., Langmuir, **2**:653 (1986).

Bikerman, J.J., "Foams", pp. 243-244 (1973), Springer Verlag, Berlin-Heidelberg-New York.

Dippenaar, A., Int. J. Mineral Process, **9(1)**:15 (1982).

Garret, J.; Coll. Interf. Sci.; **76(2)**:587 (1980).

Kruglyakov, P.M., "Equilibrium Properties of Free Film and Stability of Foams and Emulsions." In: Thin Liquid Films. Ed. I.B. Ivanov, pp. 767 (1989).

Lucassen, J., Coll. Surf., **65**:131 (1992).

Prins, A., "Theory and Practice of Formation and Stability of Food Foams." In: Food Emulsions and Foams, pp. 30 (1986); Ed E. Dickinson, Roy Soc. of Chem., Leeds.

Prins, A.; "Principles of Foam Stability." In: Food Emulsions and Foams, pp. 91 (1988), Ed. E. Dickinson and G. Stainsby.

Prins A., "Foam Stability as affected by the presence of small spreading particles." In: Surfactants in Solution, Vol. 10, pp. 91 (1989), Ed. K.L. Mittal.

Ronteltap, A.D., PhD Thesis, Agricultural University Wageningen (1989).

Ross, S., Phys. Coll. Chem., **54**:429 (1950).

Ross, S., Hughes, A.F., Kennedy, M.L. Mardoian, A.R., J. Phys. Chem., **57**:684 (1953).

FOAM BEHAVIOUR

2.1. INTRODUCTION

Foam is a dispersion of gas in liquid. It is a non-equilibrium system due to several mechanical disturbances of different origin. During foam formation the liquid films between the bubbles are continuously expanded and compressed. After foam formation the liquid structures in the foam, i.e. liquid films and Plateau borders are exposed to stresses as a result of physical processes taking place. For this reason the study on foam behaviour has to be focused on the surface rheological properties of the foam liquid under different dynamic conditions.

The three main physical processes determining foam stability are drainage, disproportionation and coalescence. These processes are responsible for an increase of the gas fraction, coarsening of the foam and foam collapse and are, therefore, responsible for a change in the bubble-size distribution. Since these processes are interrelated, as will be explained later, it is important to know by which mechanisms they are governed.

The subject of this study is coalescence which is the merge of two bubbles as a result of the rupture of the film between the two bubbles.

The thickness of the film is an important parameter in this mechanism. In general it is assumed that the thinner the films the more sensitive they become for rupture. Therefore, coalescence depends to a large extent on the drainage of liquid out of the foam resulting in film thinning. On the other hand, re-orientation of Plateau-borders and films during disproportionation and coalescence may give rise to film rupture. In a polyhedral foam, three films meet each other in one Plateau-border at an angle of 120°. In the case of disproportionation a small bubble disappears and an unstable situation arises in which four films meet each other in one Plateau-border. This unstable situation changes over into a stable one by forming a new film between two Plateau-borders. This process is accompanied by a large and instant increase of the surface area of the new film resulting consequently in a temporary increased surface

tension. This makes the film more sensitive to rupture. This process will be discussed in more detail in §2.3.

In the case of coalescence the rupture of a film between two bubbles results in a situation in which two films join in a Plateau-border which is also an unstable situation resulting in a reorientation of the foam structure. Furthermore the film rupture is accompanied by a mechanical shock wave which can destabilize the neighbouring films.

Hydrophobic or spreading particles present in the foam liquid or introduced from outside may induce coalescence due to respectively the so-called 'hydrophobic particle mechanism' or the 'spreading particle mechanism'.

The three main physical processes determining foam behaviour, i.e. drainage, disproportionation and coalescence, will be discussed in §2.2, §2.3 and §2.4 respectively. Coalescence initiated by particles present in the foam is subject of this study. In this process the particles must be in contact with the film surface and for this reason it is essential that they are poorly wetted by the film liquid. This dewetting process and its crucial parameters will discussed in §2.4.1. Film rupture due to the hydrophobic particle mechanism or due to the spreading of particles over the film surface will be discussed in detail in respectively §2.4.2. and §2.4.3. Finally the aim of this study is elucidated in more detail in §2.5.

2.2. DRAINAGE

Drainage is the liquid flow from a foam as a result of in general pressure differences caused by gravity and capillary forces. However, it has to be mentioned that the capillary forces are indirectly generated by the gravity forces as will be discussed later in more detail.

Due to drainage the liquid films and Plateau-borders in a foam become thinner and consequently the foam becomes dryer and the bubbles become deformed. The

events that take place during drainage by which the foam transforms gradually from a foam with spherical bubbles into a polyhedral structured foam are described by Ivanov and Jain (1979), Wasan and Malhotra (1986) and Ivanov and Dimitrov (1989).

In describing liquid flow from a polyhedral foam, a distinction can be made between the drainage through the Plateau-borders and through the thin liquid films.

Scheludko (1957) stated that in a polyhedral foam the Plateau-border suction contributes in addition to the gravity force as a driving force for film drainage. The gravity force is acting as the driving force for film drainage in two different ways. Directly on the liquid in a film which is not horizontal and indirectly through suction by the Plateau-border.

Van Havenbergh et al. (1984) described the Plateau-border suction in a free falling liquid film. Under the condition that the film is not an equilibrium film, the pressure inside the Plateau-border is lower than inside the plane film due to the curvature of the Plateau-border. For this reason there will be a liquid flow from the plane film towards the Plateau-borders as a result of this capillary suction. Through these Plateau-borders which are relatively thick the liquid will drain relatively easy as a result of gravity force.

Reynolds (1886) already formulated a law for the radial liquid flow if the surfaces of the film can be described as two circular plane parallel motionless plates as presented in eq. (2.1):

$$-\frac{d\theta_f}{dt} = \frac{2\theta_f^3 \Delta P}{3\eta r^2} \qquad (2.1),$$

where θ_f is the film thickness, ΔP is the driving pressure, t is time, η is the viscosity of the film liquid and r is the radius of a circular plane parallel film. Eq. (2.1) can be used to calculate the rate of drainage out of a liquid film with rigid surfaces with relatively good accuracy. It can be seen in eq. (2.1) that slow drainage is the result of

a high bulk viscosity η and even more pronounced as a result of a small film thickness θ_f.

A surface tension gradient is developed as a result of the liquid motion through the vertical films which is described by Djabbarah and Wasan (1985) and Prins (1988). The liquid motion along a liquid surface exerts a tangential shear stress on that surface leading to surface expansion and compression. In a vertical film up-stream the surface is expanded and down-stream the surface is compressed a surface tension gradient will be developed resulting in a surface motion opposing the liquid flow. Some time after drainage has started, a steady state is reached and the shear stress is in mechanical equilibrium with the surface tension gradient $d\gamma/dx$ along the surface as described by eq. (2.2):

$$\sigma = \eta \left(\frac{dv_x}{dz} \right)_{z=0} = -\frac{d\gamma}{dx} \qquad (2.2),$$

where σ is the shear stress, η is the viscosity of the liquid, v_x is the velocity in the liquid, z is the distance from a point in the liquid film perpendicular to the film surface and x is the lateral distance along the film surface where x=0 at the top of the vertical film. Due to this phenomenon the surface tension at the top of the film is increased and at the bottom decreased. When relatively thick films are considered, the extent to which the film surface has a lower velocity than the moving liquid depends on the stiffness of the surface as expressed by the value of the surface dilational viscosity (η_s^d) which gives the relation between the relative surface expansion rate $d\ln A/dt$ and the excess surface tension $\Delta\gamma = |\gamma_{dyn.} - \gamma_{eq}|$ in expansion (or compression) as in eq. (2.3):

$$\eta_s^d = \frac{|\gamma_{dyn} - \gamma_{eq}|}{\frac{d\ln A}{dt}} \qquad (2.3).$$

Gibbs (1961), Prins and Van den Tempel (1969) and Rao et al. (1982) elucidated that in the case of a thin enough film which is stabilized by surfactant the viscous flow through a vertical film takes place in such a way that the two film surfaces remain motionless. The property of the thin liquid film that is responsible for this phenomenon is called the Gibbs film elasticity. Under these conditions the liquid moves as if it were between two plane parallel solid walls and by assuming the film surfaces to be rigid and the films to be small, i.e. in the absence of marginal regeneration, the amount of liquid (Φ) flowing out of a vertical film per unit of time and per unit of width of the film can be described by eq. (2.4):

$$\Phi = \frac{\rho g \theta_f^3}{12\eta} \qquad (2.4),$$

where ρ is the density of the film liquid and g is the acceleration due to gravity. The motionless surface thus decelerates the drainage rate especially when the film becomes thin. Using eq. (2.4) it can be calculated that the time needed for a vertical film of initial thickness $\theta_{f,0}$ to reach a thickness θ_f is given by good approximation by eq. (2.5):

$$t = \frac{6\eta L}{\rho g \theta_f^2} \qquad (2.5),$$

where L is the film height.

In a vertical surfactant film of thickness θ_f mechanical equilibrium is established: the weight of the film is compensated by a surface tension gradient along the height x of the film as expressed in eq. (2.6):

$$2\frac{d\gamma}{dx} = \rho g \theta_f \qquad (2.6)$$

wherein the factor 2 accounts for the two surfaces of the film.

Malysa et al. (1980) presented a calculation for the drainage time of a plane parallel film to reach the critical film thickness of rupture that can be described with the Reynolds eq. (2.7):

$$t_c = \frac{3\eta A}{4\pi \theta_c^2 \Delta P} \qquad (2.7),$$

where t_c is the drainage time to reach the critical film thickness θ_c and A is the surface area of the plane parallel film. The driving force ΔP in eq. (2.7) can not be described in simple terms. For the exceptional case of horizontal plane parallel films in a polyhedral foam the driving force for drainage may assumed to be Plateau-border suction and ΔP will then be equal to the capillary suction (P_c). However, it has to be mentioned that most films in a foam are not orientated in a horizontal position.

When the film becomes thinner the Van der Waals attractive force between the two film surfaces starts to contribute as a driving force for drainage by squeezing the liquid out of the film.

Additionally a more important counteracting pressure called disjoining pressure as described by amongst others Derjaguin and Landau (1941), can be present when the film thickness decreases. The disjoining pressure refers to either electrostatic repulsion or steric repulsion, with the latter mostly found in liquid films of solutions of polymer molecules like proteins. This latter effect occurs much earlier than the Van der Waals attraction where the film thickness must be very small. Therefore, in the case of protein foams in which the equilibrium films are relatively thick the effect of Van der Waals attraction may be neglected. When taking into account the disjoining pressure, the driving pressure for film drainage can be described with eq. (2.8):

$$\Delta P = P_c - \Pi \qquad (2.8),$$

where P_c is the capillary pressure and Π is the disjoining pressure. Assume that ΔP is equal to γ_P / R_P, where γ_P and R_P are respectively the surface tension and the radius of curvature of the Plateau border. Furthermore, assume that the surface area A of

the plane parallel film can be replaced by R_F^2, where R_F is the radius of the plane parallel film. Substitution of ΔP of eq. (2.8) and A into eq. (2.7) gives eq. (2.9) with which the critical drainage time can be estimated:

$$t_c = \frac{3\eta R_F^2}{4\theta_c^2\left(\frac{\gamma_P}{R_P} - \Pi\right)} \qquad (2.9).$$

It can be seen that the critical drainage time for film rupture depends strongly on both the radius of curvature of the plane parallel film and the critical film thickness.

During drainage the films become thinner, therefore the disjoining pressure increases and the ΔP decreases resulting in a deceleration of film thinning. On the other hand it has to be considered that the Plateau-borders become also thinner due to drainage resulting in a smaller radius of curvature of their surfaces. This will consequently lead to an increase of the capillary suction that would accelerate film drainage. In practice when a foam is draining due to gravity the drainage rate is decreasing the further the drainage process has proceeded until an equilibrium situation is reached. This is due to the increased effect of the developed surface tension gradients, disjoining pressure and capillary suction on the deceleration of the viscous flow through the thinning films and Plateau borders during drainage.

When the disjoining pressure is equal to the capillary pressure the film can be stabilized if no evaporation takes place. The conditions for this equilibrium film is formulated by Scheludko (1962) in eq. (2.10):

$$\frac{dP_c}{d\theta_f} = \frac{d\Pi}{d\theta_f} \qquad (2.10).$$

Under practical conditions films may collapse when they are thicker than the equilibrium thickness. This critical thickness of films stabilized by high molecular weight material as for example proteins, is mostly larger than the equilibrium thickness. This could be a result of lipid impurities that are often present in protein

samples. These lipid impurities may rupture liquid films as will be discussed later. The films of solutions of low molecular weight material may become so thin that so-called Newton black spots appear as described by, amongst others, Scheludko (1967). Radoev et al. (1983) mentioned that the local thickness of a horizontal film at these spots determines whether or not these films rupture.

As is mentioned earlier the drainage of liquid from a foam will mainly take place through the Plateau-borders. Initially the Plateau-borders in a foam will contain too much liquid. Part of the liquid must drain before an equilibrium state is reached. The surfaces of the Plateau-borders are curved into a cylindrical shape, which enables them to retain liquid by means of capillary suction P_c. When the capillary suction equals the hydrostatic pressure of the liquid, the drainage through the Plateau-borders stops. At this equilibrium state at a certain height in a polyhedral foam, when the films are also in equilibrium, the radius of curvature of the Plateau-border surface satisfies eq. (2.11):

$$\rho g H = \frac{\gamma_P}{R_P} = \Pi \qquad (2.11),$$

where H is the hydrostatic height.

Kann (1984) and Kann and Feklistov (1985) mentioned that for the same reasons as the surface of a thin liquid film, the surfaces of Plateau-borders may become immobile but as a result of the high volume-surface ratio of the Plateau-borders this phenomenon is not as pronounced as in the case of the viscous liquid flow from thin liquid films. According to Mendelson (1967) and later in more detail discussed by Prins and Van 't Riet (1987), for a bubble smaller than approximately 10^{-3} m rising through an aqueous protein solution, the bubble surface is almost motionless. Therefore, during drainage the Plateau-border surfaces in a protein-stabilized foam having bubbles of about 10^{-3} m diameter can also be essentially motionless. Furthermore, Jackson et al. (1980) found experimentally that the rate of drainage of beer foam, (i.e. more or less a protein foam) is inversely proportional to the viscosity of the liquid. This

observation gives rise to the idea that the Plateau-border surfaces must apply a resistance force to the liquid flow. Therefore, after drainage from a foam has proceeded a certain time resulting in thinning of the Plateau-border, drainage through a Plateau-border can be decelerated if the surface tension gradient over the Plateau-border surfaces is high enough. This results in a much slower increase of Plateau-border suction during drainage because the Plateau-border radii of curvatures remain larger for a longer time and consequently result in a smaller thinning rate of the thin liquid films. This would postpone spontaneous film rupture and film rupture by the hydrophobic particle mechanism or by the spreading particle mechanism as will be discussed later.

2.3. DISPROPORTIONATION

Disproportionation is a foam coarsening process in which smaller bubbles become smaller in favour of the larger ones that will become bigger. Eventually the smaller bubbles disappear which causes the coarsening of the foam without, in this case, the rupture of a single film between the bubbles. The process enhances the rate of drainage. Disproportionation, also called isothermal distillation or Ostwald ripening is the interbubble gas diffusion as a result of a gas pressure difference between bubbles. If the gas composition and the surface tension are uniform throughout the foam this pressure difference is only a result of a difference in the bubble radii. The pressure difference is also determined by the surface tensions of the individual bubbles because, according to the law of Laplace, the pressure difference between two spherical bubbles of different sizes is presented in eq. (2.12):

$$\Delta P_{tot} = \Delta P_1 - \Delta P_2 = \frac{2\gamma_1}{r_1} - \frac{2\gamma_2}{r_2} \qquad (2.12),$$

where ΔP_{tot} is the total pressure difference, and ΔP_1 and ΔP_2 are the Laplace pressure differences of the individual bubbles and γ_1 and γ_2 are the surface tensions of the bubbles respectively with radii r_1 and r_2.

According to Henry's law there is a concentration gradient of the gas in the liquid between the smaller and larger bubbles as depicted schematically in Fig 2.1.

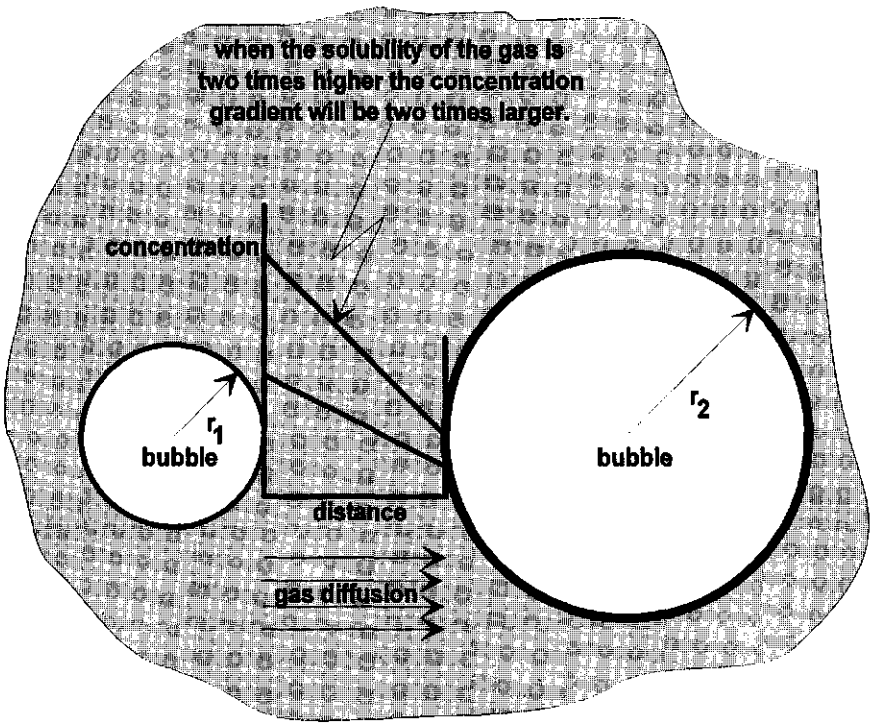

Fig 2.1: ***A schematic representation of the concentration gradient of the gas in the liquid between two bubbles with different radii. It is assumed that there is a single gas present in the bubble.***

The disproportionation process is described by several authors as De Vries (1958), De Vries (1972), Lifshitz and Slyosov (1961), Wagner (1951), Radanive and Lemlich (1971), Monsalve and Schechter (1984), Cheng and Lemlich (1985), Rieser and Lemlich (1988), Ramchadran et al. (1981), Markworth (1985), Stavans and Glazier (1989) and Ronteltap (1989). From these studies it can be concluded that the composition of the gas in the bubbles, the bubble-size distribution of the initial foam and the solubility of the individual gases in the aqueous phase determine the rate of disproportionation in the foam.

The disproportionation process in beer foam is described by Ronteltap (1989). He confirmed that the rate of gas diffusion in beer like foams depends mainly on a difference in partial gas pressures and gas solubilities. In the case of a carbondioxide (CO_2) foam the gas composition inside the bubbles differs from the gas composition outside the bubbles when they are in contact with the atmosphere in which the main gas is nitrogen (N_2). As a result rapid gas diffusion of CO_2 out of the bubbles occurs. the other hand N_2 will diffuse into the bubbles, but with a flux that is 50 times smaller compared to CO_2 as a consequence of the 50 times lesser solubility of N_2 in the aqueous phase. The system is pursuing thermodynamic equilibrium and therefore gas diffusion will continue until the gas compositions in- and outside the bubbles become almost identical. As a result of the different transport rates of CO_2 and N_2 these bubbles will shrink and eventually disappear and the foam height will decrease.

In the case of uniform gas composition that is found within the bulk of a foam, the Laplace pressure difference is the only driving force for gas diffusion as described by eq. (2.12). When the surface tension decreases far enough as a result of the compression of the bubble surface of the shrinking bubble, the driving force may become very low. This dynamic surface tension existing under surface compression conditions, is determined by the surface rheological properties of the bubble surface. Important parameters determining the dynamic surface tension described in literature are the surface dilational viscosity, the surface compression rate, the history of the

bubble surface and the extent of compression that are mentioned by Ronteltap (1989), and the surface elasticity as is described by Lucassen (1981).

According to Ronteltap (1989) a high surface dilational viscosity of the surface results in a very low dynamic surface tension during compression and in a high surface tension during expansion of the bubble surface. Furthermore the decrease of the surface tension depends strongly on the compression rate, because of the time dependency of visco-elastic surfaces as a consequence of relaxation processes. Ronteltap (1989) estimated the decrease of surface tension by using a powerlaw to describe the surface rheological behaviour of the shrinking bubble under steady-state compression conditions. This powerlaw, however, does not account for the absolute value of compression and the history of the bubble. Nevertheless, Ronteltap (1989) concluded that gas diffusion from bubbles can be slowed down considerably by the rheological behaviour of the bubble surface in terms of the surface dilational viscosity and that the rate of disproportionation is mainly determined by the geometry of the bubbles, the gas composition and the surface rheological behaviour of the liquid.

Lucassen (1981) described that when the elastic modulus E of the surface is larger than half of the surface tension the disproportionation process would stop when the surfactant causing the area dependence of the surface tension behaves purely elastic. In most cases, however, the surface tension after compression or expansion will relax towards the equilibrium value and the above mentioned condition is no longer valid. The result is that the disproportionation process will proceed. The elastic modulus depends, in that case, on the frequency of area changes, i.e. almost zero for very small rates and a constant value for high rates. Furthermore, there will be an upper limit on the rate at which the disproportionation process will take place because as soon as the elastic modulus $E = \gamma/2$, the rate of disproportionation will go down. In foodstuffs, Lucassen (1981) and Lucassen (1992) described that, for instance the introduction of small particles in the surface, which increase the elastic modulus, was found to reduce the disproportionation process.

Assuming no exchange of gas of the bubbles in the outer layers of the foam with the atmosphere, disproportionation results in coarsening of the foam but not in a considerable decrease of the foam volume.

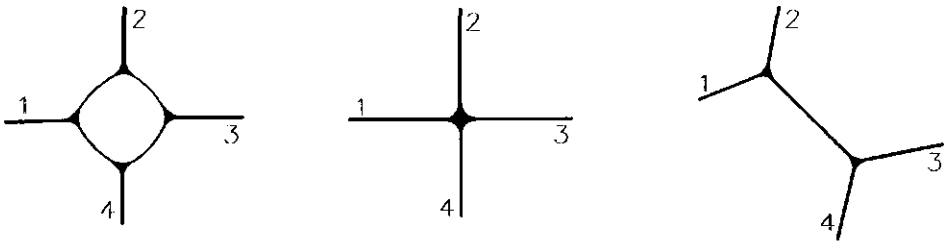

Fig 2.2: ***A schematic drawing of the events during reorientation of films and Plateau borders in a foam during the disproportionation process. (After Prins (1989)).***

In a well drained polyhedral foam that is in equilibrium three films meet each other in one Plateau-border at an angle of 120° as is illustrated schematically in Fig 2.2. Due to the disappearance of the smaller bubbles as a result of disproportionation an unstable situation may arise in which four films meet each other in one Plateau-border (see Fig 2.2). This unstable conformation will change into a stable one by the formation of a new film between two Plateau-borders and by a re-orientation of the Plateau-borders and films (see Fig 2.2). This new conformation consists of two Plateau-borders in which in each Plateau-border three films meet each other again at an angle of 120°. This change in conformation is accompanied by a large and rapid increase of the surface area of especially the new created film which results in, at least temporarily, an increased surface tension of this film. For this reason the film becomes more sensitive for rupture and therefore the process may result in coalescence. Since bubbles disappear in the disproportionation process, liquid films and Plateau-borders disappear, the gas fraction in the foam will increase and the rate of drainage will increase due to coarsening of the foam.

Durian et al. (1991) and Glazier (1992) presented mathematical approaches to describe coarsening as a result of only disproportionation in a two dimensional foam fitted between two glass plates. They made many assumptions in order to be able to perform mathematics but they came to the conclusion that the surface-number averaged diameter may increase proportionally with time (i.e. ageing of the foam). The experimental results they presented confirm this idea. The mathematical model is not compared to the change in bubble-size distribution in a three dimensional foam where disproportionation is the only foam coarsening process. Therefore it is unknown if the model is applicable to the three dimensional foams as found in practice.

2.4. COALESCENCE

Coalescence is the merge of two bubbles as a result of the rupture of the film between the bubbles. The result of this process is that the foam becomes coarser and the total number of bubbles decreases. The mechanisms for coalescence that have been proposed so far have in common that coalescence occurs preferentially when the thickness of the liquid film is small. Coalescence is, according to literature, often related to drainage. As a result of drainage the liquid films become thinner and may reach an equilibrium thickness. Considering optimal conditions such as a constant temperature, the absence of mechanical disturbances like vibrations and equilibrium vapor pressures in the surrounding atmosphere, these films can persist over a very long period of time. When the liquid of these equilibrium films evaporates or when for instance thermal disturbances occur, resulting in pressure gradients in the film liquid or surface tension gradients acting on the film liquid, these films may rupture.
A critical film thickness for rupture that is larger than the equilibrium film thickness is mentioned by Vrij and Overbeek (1968) and Vrij et al. (1970). They give a possible mechanism for film rupture at the critical film thickness as a result of spontaneous fluctuations in the film thickness. When the film becomes thin enough the film may rupture due to thermal motion of the film. Furthermore, re-orientation of films due to

disproportionation may give rise to film rupture. The absence or a low level of steric and electrostatic repulsion between the two film surfaces, better known as the absence of disjoining pressure, results in thinning of the film to very small thickness which promotes film rupture. Evaporation of film liquid, condensation out of the gas phase on the film surface may also initiate film rupture. In practice foams are already coarsening as a result of coalescence before the films in the foam drain to critical or even equilibrium thickness. The mechanisms described so far in which particles are involved are the "hydrophobic particle mechanism" and the "spreading particle mechanism" in which the particles responsible for film rupture are considered to be present in the film liquid. In practice the particles can be present in different ways as depicted schematically in Fig 2.3.

The position of the particle can either be in the film or in the gas phase (see Fig 2.3.A). When the particle is in the gas phase it depends on the wetting properties if the particle is not, partly or fully covered with film liquid. Furthermore, the particle can contain an amount of liquid (see Fig 2.3.B). When the particles are present in the film liquid they first have to make contact with the film surface in order to be able to spread over the latter or to initiate the hydrophobic particle mechanism. This is called the dewetting process. The dewetting process does not have to take place when the particles are not covered with film liquid and when they make contact with the film surface coming from the outer gas phase. It is important to know which physical properties the particles must have in order to become dewetted or remain wetted when they are making contact with the film. In this context the drainage of the liquid film separating the particle from the liquid surface and the wetting properties of the particle are important parameters and will be discussed in §2.4.1.

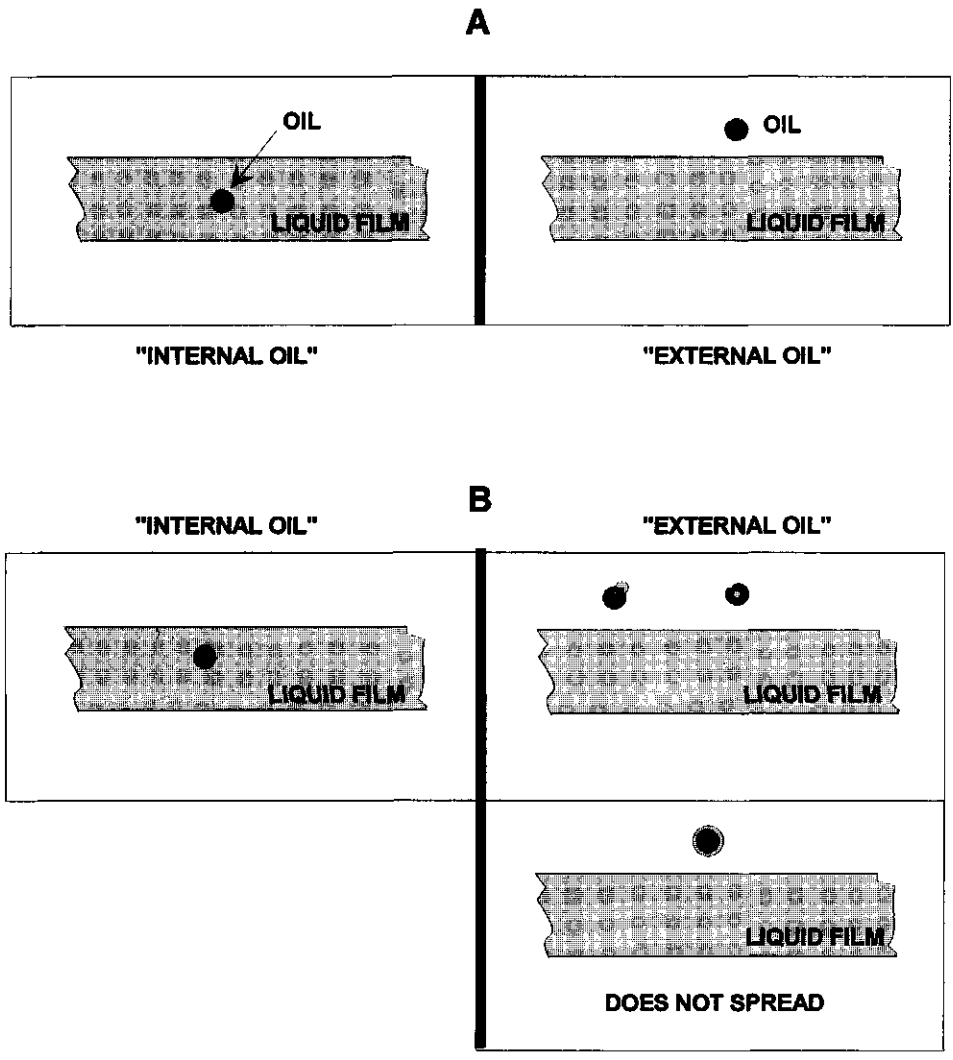

Fig 2.3: ***A representation of the possibilities an oil particle can be present in a system. The descriptions of the different configurations are mentioned in the text.***

If a solid hydrophobic particle is able to make contact with both liquid film surfaces the film may rupture due to the hydrophobic particle mechanism which will be discussed in §2.4.2. The explanations given for film rupture due to the spreading particle mechanism in which the particle must be able to make contact with at least one of the liquid film surfaces will be discussed in §2.4.3.

2.4.1. THE DEWETTING PROCESS

Garret (1979), Garret (1980), Dippenaar (1982) and Aronson (1986) described the hydrophobic particle mechanism. They considered that an insoluble hydrophobic oil droplet or particle in thin air-liquid-air films could result in the collapse of these films. Thinning of such a liquid film as a result of drainage leads to a certain point at which the oil drop can dewet at both air-liquid interfaces. Dombrowski and Fraser (1954) found that this point is reached when the oil drop has the size of the order of the thickness of the film and the particle is not wetted by the aqueous phase. In order to adopt such a bridging configuration the particle must dewet but is not allowed to spread.

If a particle encounters the liquid surface, a layer of liquid separates the particle from the air as a result of hydrodynamic resistance. Thinning and rupture of this layer precedes the formation of a three phase contact perimeter. Scheludko (1963) made calculations of the time required for thinning of the layer until rupture occurs. This time can be explained in a quantitative way by defining the critical drainage time that refers to the time needed for a plane parallel film to reach the critical film thickness for rupture. This critical drainage time is proportional to the surface area of the film and inversely proportional to the driving pressure ΔP with constant film thickness and with a rigid oil-liquid interface, as described by the Reynolds eq. (2.7). In a horizontal film the density difference between a particle and the film liquid causes a relatively small

buoyancy force that is pressing the particle against the surface of the liquid film resulting in bulging of film surface.

Another pressing force of the particle against the film surface can be due to expansion of the film surface. In that case the velocity component (v_z) perpendicular to the film surface can be described by eq. (2.13) which can be derived from the continuity equations:

$$v_z = z\frac{\mathrm{d}\ln A}{\mathrm{d}t} \qquad (2.13),$$

where z is the distance from a point in the film to the film surface and $\mathrm{d}\ln A/\mathrm{d}t$ is the relative surface expansion rate.

The resulting velocity component of the liquid flow perpendicular to film surface results in a force acting on the particle pressing it against the film surface. According to the Stokes equation this force (F_S) can be described by eq. (2.14):

$$F_S = 6\pi\eta R_p v_z \qquad (2.14),$$

where η is the viscosity of the liquid and R_P is the radius of the particle. Combining eq. (2.13) and eq. (2.14) and assuming that the particle is situated at a distance R_P from the surface ($z = R_P$ in eq. (2.13)) results in eq. (2.15) in which can be seen that the force is proportional to the surface area of the particle:

$$F_S = 6\pi\eta R_p^2\frac{\mathrm{d}\ln A}{\mathrm{d}t} \qquad (2.15).$$

Furthermore, entrapment of the particle between the two surfaces of a thinning film will also cause bulging of the film surface when the film becomes thinner than the particle diameter as depicted in Fig 2.4. By assuming that the driving force for drainage of the liquid is a Laplace pressure difference ΔP as a result of the curvature of the film covering the droplet due to bulging, ΔP equals $2\gamma_f/R_p$, with γ_f the surface tension of

the liquid film and R_P the radius of the particle. By assuming that the surface area of the film that is separating the particle from the film surface equals the surface area of a

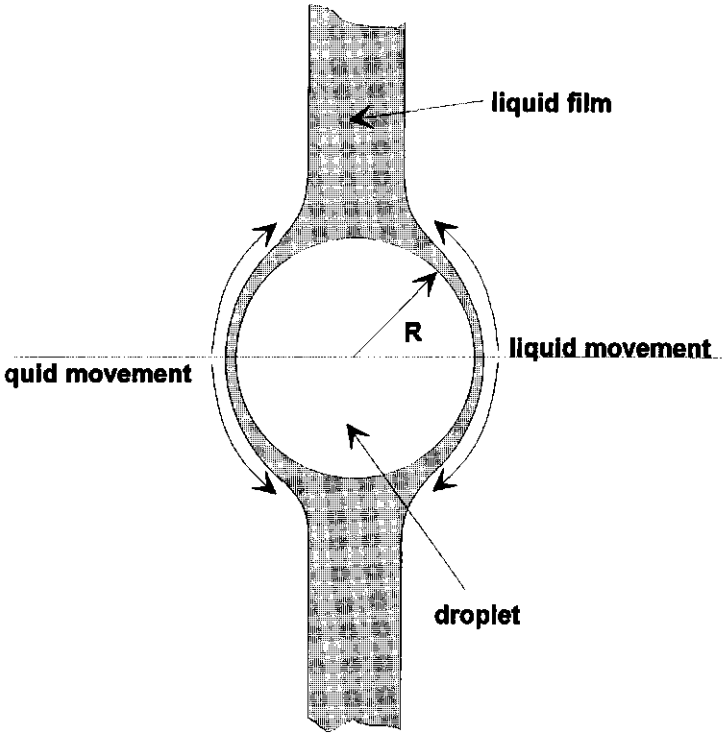

Fig 2.4: ***A schematic representation of a spherical particle squeezed between the two surfaces of a thin liquid film.***

spherical segment, i.e. $2\pi R_p h$, with h the height of the bulge with respect to the level of the plane of the film surface eq. (2.7) becomes:

$$t_c = \frac{3\eta R_p^2 h}{4\theta_c^2 \gamma_f} \qquad (2.16).$$

From eq. (2.16) it becomes clear that the critical drainage time for rupture depends strongly on both the radius of the particle and the critical film thickness for rupture. Scheludko et al. (1970) also described this drainage process and the measurement of the critical thickness for rupture of the layer is reported by Schulze (1975). In these investigations the meniscus of the liquid was pressed against a planar solid surface. This corresponds to the interaction of a large particle with a liquid-air surface because it can be assumed that these surfaces are both planar. The critical drainage time depends to a large extent on the surface area of that film because the viscous flow out of that film may be opposed by a surface tension gradient over that surface. The hydrodynamic resistance diminishes with a decreasing particle size as a result of the decrease of the surface area of the film separating the particle from the surface. Therefore, they assumed that in the case of a particle with a radius that is much smaller compared to the bubble size the latter can be assumed as a planar surface and the contact of that particle with a planar surface occurs with no hydrodynamic resistance. This means that when a small particle approaches the surface of a foam film between two much larger bubbles, the contact with the film surface takes place instantaneously.

Ronteltap (1989) reported results obtained by studying hole formation in a free falling film as a function of the size of potentially dewetting and spreading oil droplets. He found that if the droplet size is increased, at a certain size the droplets do not come into contact with the surface of the film. He gave as an explanation that at this size the drainage time to reach the critical film thickness for rupture exceeds the falling time of the liquid film in his device.

Scheludko et al. (1975) described the dewetting process in more detail. He introduced another rate determining barrier for dewetting by assuming a solid spherical particle floating in a horizontal plane liquid surface. As the spherical particle makes contact with the liquid-air surface the three phase contact grows from a point and passes through extremely small radii of the wetting perimeter. He introduced a central angle

α_c which defines the position of the particle with respect to the undisturbed liquid surface and which is also the angle between the solid surface and the plane containing the wetting perimeter as presented in Fig 2.5.

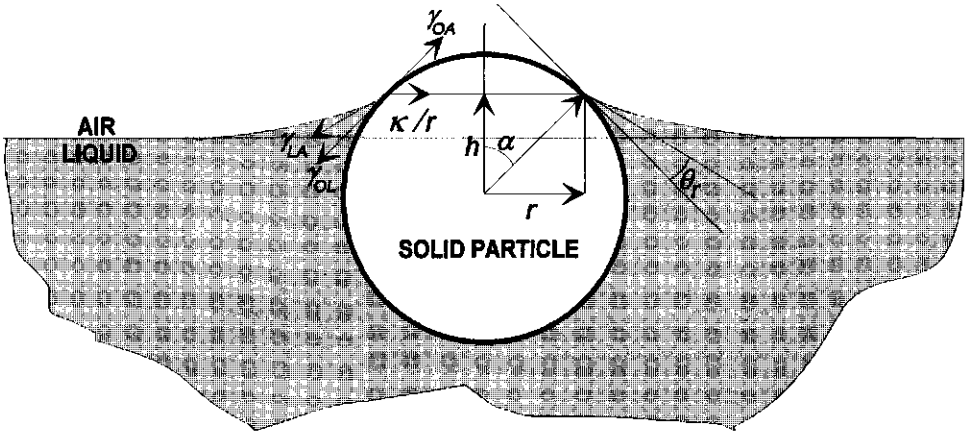

Fig 2.5: ***A solid spherical particle floating in mechanical equilibrium at the liquid surface as a result of the wetting properties, the surface and interfacial tensions and the radius of the particle. (After Scheludko (1975)).***

In cases of the type as in Fig 2.5 the equilibrium of the forces tangential to the surface of the sphere is expressed by eq. (2.17):

$$\gamma_{OA} - \gamma_{OL} = \gamma_{LA}\cos(\theta_r) - \frac{\kappa}{r}\cos(\alpha) \qquad (2.17).$$

where θ_r is the wetting angle for a perimeter of radius r and κ/r is the line tension of the wetting perimeter that is defined as the force directed towards the centre of radius of curvature r of the perimeter. If α is smaller than a critical value α_c, three phase

contact cannot occur spontaneously. If the value of α is larger than the critical value ($\alpha > \alpha_c$) the wetting perimeter will grow spontaneously. This critical value of α_c is given by eq. (2.18):

$$\cot(\alpha_c) = \frac{R\gamma_{LA}}{\kappa}(1 - \cos(\theta_r)) \qquad (2.18),$$

where R is the radius of the sphere, and θ_r is the wetting angle. The wetting perimeter for $\alpha = \alpha_c$ is regarded as the nucleus of a new particle-air surface and a three phase contact perimeter. In the case of a particle in a thin liquid film there is a resistance to the formation of this nucleus. To overcome this resistance the particle has to apply a pressing force on the liquid surface $G \geq f_c$ or an energy $U \geq A_c$, where f_c is the maximum resistance force and A_c is the work of reversible isothermal formation of this nucleus. Nutt (1960) and later Scheludko et al. (1975) derived an equation for f_c, knowing $\alpha = \alpha_c$ and $\theta_r = 0$ as presented in eq. (2.19):

$$f_c = \frac{2\pi R\gamma_{LA}}{1 + \left(\frac{R\gamma_{LA}}{\kappa}(1 - \cos(\theta_r))\right)^2} \qquad (2.19).$$

For given values of γ, κ and θ_r the force f_c has a maximum value $f_{c,max}$ of:

$$f_{c,\max} = \pi R_m \gamma_{LA} \quad for \quad R_m = \frac{\kappa}{\gamma_{LA}(1 - \cos(\theta_r))} \qquad (2.20).$$

The formation of a three phase contact is the most difficult for particles having the radius $R = R_m$. Introducing R_m from eq. (2.20) into eq. (2.18) gives:

$$\cot(\alpha_c) = \frac{R}{R_m} \qquad (2.21).$$

and eq. (2.19) becomes:

$$f_c = \frac{2\pi R \gamma_{LA}}{1 + \left(\frac{R}{R_m}\right)^2} \qquad (2.22).$$

This equation is analogous to the energy kT necessary for hole formation in a thin liquid film. Furthermore Scheludko (1975) states that the elementary work of expansion of a three phase contact can be expressed in the form:

$$dA = 2\pi r\left(\frac{\kappa}{r} - \gamma_{LA}(1 - \cos(\theta_r))\right)dr \qquad (2.23),$$

where A the surface area of the new formed surface. The value of A goes through a maximum (A_c) at $r = r_c$, thus by integrating equation (2.23) between the limits $r = 0$ and $r = r_c$ gives the work of formation of a two-dimensional nucleus as presented in equation (2.24):

$$A_c = \pi r_c \kappa = \frac{\pi \kappa^2}{\gamma_{LA}(1 - \cos(\theta_r))} \qquad (2.24).$$

Additionally the particle will apply a pressing force to the liquid-air surface as a result of the density difference between the aqueous phase and the particle if the liquid film is considered to be oriented more or less horizontal. This force stimulates the formation of a nucleus by increasing the value for the pressing force on the surface and in this way promotion of the dewetting process of the particle. In a vertical liquid film the resistance force of the two film surfaces to deformation as a result of the presence of a particle with a diameter larger than the film thickness, is a measure for the pressing force against the film surface. This theory could be considered also to be valid for small liquid particles which can, due to their relatively high Laplace pressure, not be deformed and are therefore comparable to solid particles.

The conditions for dewetting of a liquid particle are described by Ross and McBain (1944) and Robinson and Woods (1948). They introduced an "entering coefficient"

(E_c) that can be calculated when knowing the surface tensions of the liquid-air surface (γ_{LA}), the particle-air (in our case oil-air) surface (γ_{OA}) and the interfacial tension of the particle-liquid (in our case oil-liquid) interface (γ_{OL}). The three phase contact lines made by the droplet at the film surfaces are assumed to satisfy Neumann's triangle of surface tension forces. The oil drop will dewet when the surface tensions and the interfacial tension forces satisfy eq. (2.25):

$$\gamma_{LA} > \gamma_{OA} - \gamma_{OL} \qquad (2.25).$$

Eq. (2.25) looks similar to eq. (2.17) Scheludko et al. (1975) derived for solid spherical particles. However, in contrast to eq. (2.17) which is valid for solid particles, eq. (2.25) is valid for liquid particles which will change their shape until mechanical equilibrium is established and Neumann's triangle of forces is satisfied. The entering coefficient E_c can now be defined as in eq. (2.26):

$$E_c = \gamma_{LA} + \gamma_{OL} - \gamma_{OA} \qquad (2.26).$$

A droplet can only enter the liquid-air surface if $E_c > 0$. If $E_c < 0$ a droplet will remain wetted if by chance a small area of a new oil-air surface is formed when the droplet makes contact with the liquid surface. This results according to eq. (2.26) in an unstable situation and the new formed oil-air surface has only a short life-time because this surface immediately becomes wetted again by the liquid.

As a small spot of the droplet becomes dewetted the system is not yet in mechanical equilibrium resulting in a line tension that is equal to the entering coefficient. The droplet will adopt such a position and shape in the liquid surface, i.e. a lens with certain contact angles and radii of curvature, that the entering coefficient becomes zero and mechanical equilibrium as depicted in Fig 2.6 is established.

The entering coefficient presented in eq. (2.26) can be defined in more detail by considering the droplets to be present in the foaming liquid. Harkins and Feldman (1922) and Ross (1950) defined three different conditions which can be valid when a droplet reaches the liquid surface from the liquid bulk, named the initial, semi-initial

and final entering coefficient. In this context the entering coefficient in eq. (2.26) refers to the surface and interfacial tensions of the pure liquids.

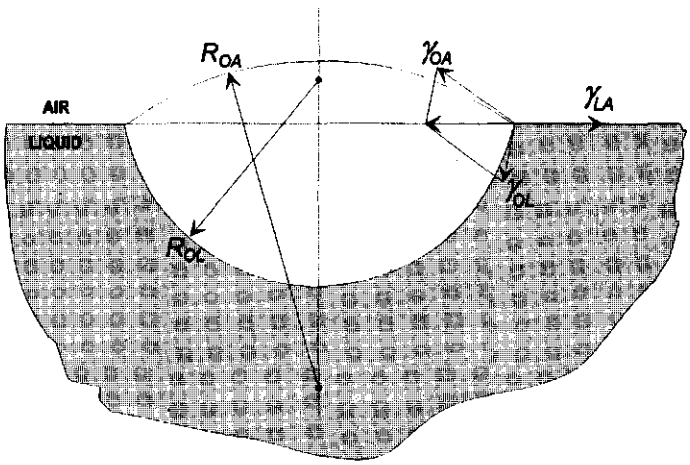

Fig 2.6: ***A liquid particle present in the surface of another liquid. There exists mechanical equilibrium and the Neumann's triangle of forces is satisfied.***

The initial coefficient refers to those cases in which the droplet is not complete in equilibrium with the surrounding solution due to a short residence time. Equilibrium of all components between the aqueous phase and the oil phase may not be established for some reason. Especially when surface active components have to redistribute over both phases the surface and interfacial tensions become a function of time. For instance the foaming liquid will dissolve during longer contact times in the poor soluble droplets until equilibrium, which may lead to a change of the properties of the oil-air surface due to the adsorption of surface active components at the oil-air surface at the moment the droplet arrives in the liquid surface. This is described by the semi-initial entering coefficient. At longer time scales the droplet and the foaming liquid in the

vicinity of the droplet will be in equilibrium. At this stage the final entering coefficient is defined. The three different entering coefficients are summarized in eq. (2.27) in which the primes refer to each liquid saturated with the other:

$$\begin{aligned} E_{c,(OL)} &= \gamma_{LA} + \gamma_{O'L'} - \gamma_{OA} \quad \textbf{(pure liquids, well defined)} \\ E_{c,(O'L)} &= \gamma_{LA} + \gamma_{O'L'} - \gamma_{O'A} \quad \textbf{(non equilibrium, poor defined)} \\ E_{c,(O'L')} &= \gamma_{L'A} + \gamma_{O'L'} - \gamma_{O'A} \quad \textbf{(equilibrium, well defined)} \end{aligned} \qquad (2.27).$$

Another point of concern is that the surface tensions presented by these authors are equilibrium surface tensions but in the case of film surfaces in foams it has to be considered that these systems are not in equilibrium due to mechanical disturbances and dynamic surface tensions have to be used.

Harkins and Feldman (1922) and Lucassen (1992) proposed that the rupture of the layer separating the oil droplet from the liquid-air surface would cause such a shock that this could rupture the entire liquid film, but they presented no theoretical calculations or experimental results. The dewetting process may take place in both the hydrophobic particle mechanism and the spreading particle mechanism and is therefore important when describing the mechanism of film rupture where particles are involved.

2.4.2. HYDROPHOBIC PARTICLE MECHANISM

Garret (1980), Dippenaar (1982) and Aronson (1986) described the hydrophobic particle mechanism acting in a thin liquid film. Garret (1980) described the destabilization of a plane-parallel symmetrical horizontal aqueous film by a hydrophobic oil droplet bridging the two liquid-air surfaces. Roberts et al. (1977) presented results of foam destabilization and made a proposition that this occurred by the dewetting of droplets followed by receding of the film from the droplet. The latter is unlikely since liquid droplets are not acting as solid particles and will deform in order to establish mechanical equilibrium.

When considering mechanical equilibrium Garret (1980) came to the conclusion that with one exception all configurations of an oil droplet bridging a plane-parallel liquid film must involve a curved air-liquid surface in the vicinity of the drop. Consequently Laplace pressure gradients are present in the liquid film and a state of mechanical equilibrium can therefore not exist. In the state depicted schematically in Fig 2.7 the Laplace pressure jump across the air-liquid surface is zero because the surfaces of the film are plane-parallel everywhere. Equilibrium will therefore be established when

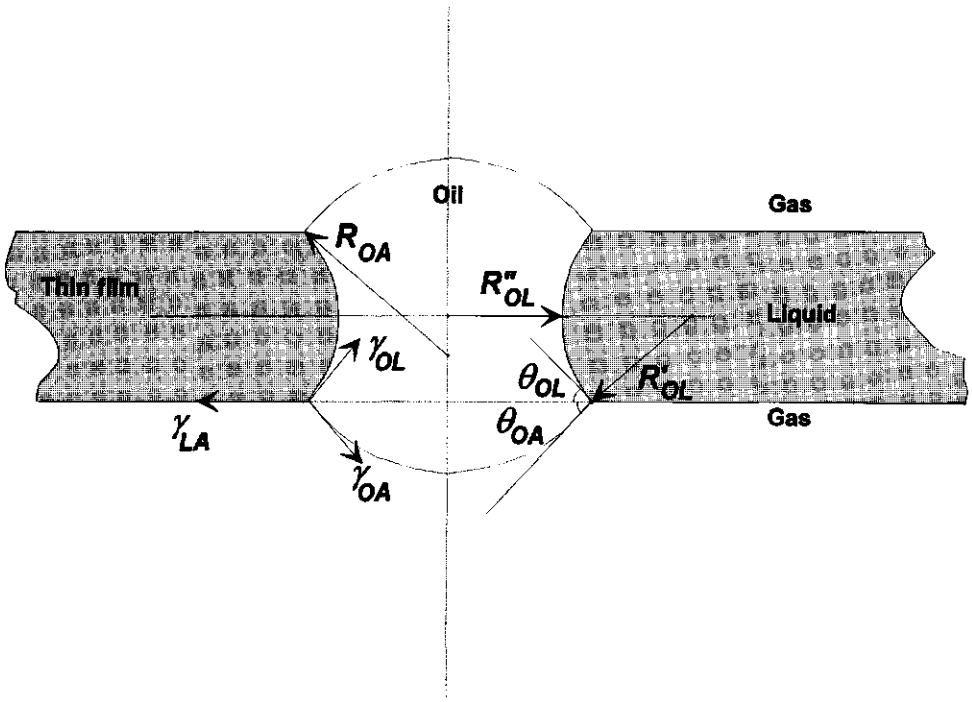

Fig 2.7: A schematic presentation of a liquid hydrophobic particle bridging the two surfaces of a liquid film. (After Garret (1980)).

the Laplace pressure jump across the oil-liquid interface ΔP_{OL} is equal to that across the air-oil interface ΔP_{OA} and can be calculated using eq. (2.28):

$$\Delta P_{OA} = \frac{2\gamma_{OA}}{R_{OA}} = \gamma_{OL}\left(\frac{1}{R''_{OL}} - \frac{1}{R'_{OL}}\right) = \Delta P_{OL} \qquad (2.28),$$

where the meaning of the symbols can be derived from Fig 2.7. Taking into account the Neumann angles θ_{OA} and θ_{OL} made by the oil-air and oil-liquid interfaces at the three-phase contact lines, he came to the conclusion that mechanical equilibrium can only exist for an oil droplet bridging a film if the oil-liquid interface is a spherical segment. The only possibility for this condition is if $\theta_{OL} > \pi/2$ for an unique film thickness which depends on γ_{AL}, γ_{OA} and γ_{OL} and on the planar radius of the oil lens and therefore on the volume of the oil droplet. However, this situation is unrealistic when considering a hydrophobic oil droplet with consequently poor wetting properties and therefore a wetting angle $\theta_{OL} < \pi/2$. Droplets which satisfy the criterion $\theta_{OL} < \pi/2$, as presented in Fig 2.7, can attain in a certain case a condition of mechanical equilibrium if they bridge a plane-parallel liquid film. Depending on the radius of the droplet compared to the film thickness and furthermore on the tension of the oil-air surface and the tension of the oil-liquid interface, a configuration can be obtained in which ΔP_{OA} is equal to ΔP_{OL} which is in mechanical equilibrium. This was confirmed by experiments which will be presented in Chapter 5. This is in contrast with the theory of Garret (1980) in which he came to the conclusion that the configuration presented Fig 2.7 is never stable due to non-equilibrium of pressures, i.e. $\Delta P_{OA} > \Delta P_{OL}$. In the case of film thinning it is possible that the oil drop is expanded to a thin film itself replacing the liquid film, and therefore also the properties of this thin oil film have to be considered with respect to the film stability. The response of this oil film besides the remaining liquid film to mechanical or thermal disturbances will then determine the stability of the entire film.

When a solid hydrophobic particle is present in the film and is dewetted at both film surfaces resulting in a bridging configuration, the liquid-air surface will be curved as a consequence of the poor wetting properties, as soon as the particle becomes

dewetted. Therefore the Laplace pressure in the film next to the droplet can be higher than in the gas phase and the plane part of the liquid film. In that case a pressure gradient in the film initiates liquid flow radially and in the plane of the film away from the droplet. The Laplace pressure depends on two radii of curvature. Considering a spherical solid particle the curvature of the film surface next to the particle may, depending on the wetting properties and the film thickness, be compensated by the curvature in the plane of the film. In that case only there is pressure equilibrium throughout the film and coalescence will not occur. However, there is drainage of liquid out of the film caused by Plateau-border suction resulting in a thinning of the film and consequently in a change of curvature of the liquid surface of the film. As a result pressure equilibrium is no longer established and the film may collapse due to receding of the film liquid as a result of the higher Laplace pressure near the particle. This theory was confirmed by experimental results of Frye and Berg (1988). In the case of anisometric solid particles there is a very small chance that there exists mechanical equilibrium and compensation of curvatures (*i.e.* pressure equilibrium) in the film attached to the solid particle. Therefore these particles have a larger potential to destabilize liquid films compared to spherical particles.

As a result of the liquid motion in the film induced by the receding liquid film from the particle a surface tension gradient will arise that opposes the liquid motion. This mechanism is known as the Marangoni effect. The surface viscosity will slow down the liquid motion. However, the rupture of the film can not be prevented by a surface tension gradient that opposes the film thinning process. It can only slow down the film drainage and postpone film rupture due to this mechanism. The film thinning process will continue due to Plateau border suction and furthermore, the surface tension in the vicinity of the particle will increase due to the surface expansion driven by the liquid motion radially away from the particle in the plane of the film. Consequently the local Laplace pressure will increase and the liquid flow will be enhanced resulting in a faster film thinning process. This results in a self inducing mechanism of film rupture caused by a locally thinning of the liquid film in the vicinity of the film bridged by a hydrophobic

solid particle. Therefore it depends to a large extent on the surface dilational properties up to which level the Marangoni effects can diminish the increased surface tension and therefore slow down the film thinning process.

The presented theories of the hydrophobic particle mechanism indicate that it is essential that these particles bridge the two surfaces of the film in order to initiate film rupture. For this reason the particles must have a diameter in the order of the film thickness. The other film rupturing mechanism where particles are involved and which is discussed many times in literature is the spreading particle mechanism. In this mechanism it is not a priori necessary that the particles bridge the two film surfaces, dewetting and spreading over one of the surfaces may already initiate film rupture. This mechanism will be discussed in the next section.

2.4.3. THE SPREADING PARTICLE MECHANISM

The second mechanism described in literature and which is subject of investigation in this study is the "spreading particle mechanism". Raleigh (1887) was the first who described the spreading of oleic acid on water. Later Harkins and Feldman (1922) defined the spreading coefficient (S_c). If a drop of liquid B (for example oil) is placed on the surface of a liquid A (for instance an aqueous solution), spreading may occur. Consequently a surface area of liquid A (*LA*) is replaced by an equal area of interface AB (*OL*) and an equal area of surface B (*OA*) provided that the surface B and interface AB keep their identity. The spreading coefficient may be developed by thermodynamic reasoning. Since only large scale motion is of importance in spreading only the surface free energies are involved. The decrease in Gibbs free energy S_c which occurs in spreading can therefore be given by eq. (2.29):

$$S_c = \gamma_{LA} - (\gamma_{OA} + \gamma_{OL}) \qquad (2.29),$$

where S_c is defined as the spreading coefficient. In literature the spreading coefficient may also be called the spreading pressure. Analogue to the entering coefficient, the spreading coefficient S_c is defined to be equal to a line tension since the system is pursuing mechanical equilibrium at which the line tension becomes zero. As soon as S_c, i.e. the line tension becomes zero the spreading process will stop.

When the droplet enters the liquid surface from the gas phase there will be disappearance of the surfaces liquid-air and oil-air and appearance of the interface oil-liquid. The work of adhesion W_A, i.e. the work necessary to expand the oil-liquid interface by 1 unit of area, can be given by the equation of Dupré in eq. (2.30):

$$\frac{W_A}{A} = \gamma_{LA} + \gamma_{OA} - \gamma_{OL} \qquad (2.30),$$

where A is the surface area. This equation may be illustrated physically as follows. Suppose that the oil and liquid phase are initially in contact in a column of cross-section 1 m^2. The interfacial energy of the system being γ_{OL}. Per unit surface area. They are now separated by a direct pull with air allowed to enter between them and the energy of the interfacial system becomes $\gamma_{LA} + \gamma_{OA}$. The work required to effect the separation of the liquids is defined as W_A which can, therefore, be calculated by using eq. (2.30). In the case when droplets present in the film liquid are entering, dewetting and spreading over the liquid surface there is disappearance of the liquid-air surface and appearance of the oil-air surface and the oil-liquid interface. In this case eq. (2.31) becomes valid:

$$\frac{W_A}{A} = \gamma_{OA} + \gamma_{OL} - \gamma_{LA} \qquad (2.31).$$

The work of cohesion W_C, is the work necessary to create inside a liquid two surfaces of each 1 unit of area. By breaking apart a bar an area A of oil, W_C is given by:

$$\frac{W_C}{A} = 2\gamma_{OL} \qquad (2.32),$$

where the 2 stands for the formation of two equal interfaces. It has to be mentioned that the work of cohesion depends on the way the new surface is created. When a new oil surface is created while the oil is surrounded by the liquid eq. (2.32) is valid. When the new oil surface is created while the oil is surrounded by air, γ_{OL} in eq. (2.32) must be replaced by γ_{OA}. The latter case is valid when for instance an oil droplet makes contact with the liquid surface when coming out of the gas phase.

A combination of eq. (2.29), eq. (2.30) or eq. (2.31) and eq. (2.32) delivers eq. (2.33):

$$S_c = \frac{W_A}{A} - \frac{W_C}{A} \qquad (2.33),$$

which says that spreading occurs if the adhesion between the two liquids is larger than the cohesion of the liquid to spread (i.e. oil), and spreading does not occur if the cohesion (W_C) is larger than the adhesion (W_A). Therefore, as mentioned earlier, a positive value of the spreading coefficient S_c refers to spreading of the oil droplet on the liquid and a negative value to not spreading. By considering out of which phase the particle makes contact with the liquid surface and by using the appropriate equations for the adhesion and cohesion under these conditions, eq. (2.33) delivers always an equation similar to eq. (2.29). Therefore, the spreading coefficient depends not on the phase, i.e. gas or liquid, out of which the particle makes contact with the liquid surface. Nevertheless there is a significant difference out of which phase the particle makes contact with the surface. When the particle comes out of the gas phase the dewetting process does not have to take place. This is in contrast with a particle coming out of the liquid phase. In this case the process of dewetting have to take place before the particle enters the liquid surface.

In eq. (2.29) it can be seen that a high surface tension of the liquid and low surface and interfacial tensions of the oil droplet are in favour of spreading of the droplet over the liquid surface. Harkins and Feldman (1922) divided the liquids in three different classes with reference to the way they spread on water. 1) Liquids which spread to a more or less uniform permanent sheet, but not a monomolecular layer. 2) Liquids

which spread to form a monomolecular layer, with any excess oil remaining in the form of a lens or lenses. 3) Liquids which are either volatile or more or less soluble in water and thus leave no lenses after spreading. They either do, or do not, go through the Newtonian color stage, and finally disappear by evaporation or dissolution. Furthermore they stated that the spreading liquid has to be more or less soluble in the liquid on which it is spreading, since spreading can only occur if a part of the spreading molecules is soluble in the liquid, i.e. surface active. Corresponding with this statement it is found that all non-spreading liquids are practically insoluble. Hardy (1913) showed that surface active impurities in a non-spreading liquid, may cause it to spread. On the other hand Raleigh (1890) observed that liquids which ordinarily spread on water may not do so if a surface active impurity is present in the water surface. Harkins and Feldman (1922) found that if the spreading coefficient has a low positive value the spreading of the liquid occurs into a permanent sheet that often exhibit Newtonian colors (i.e. approximately to 1000 molecules thick). Spreading into a monomolecular film mostly corresponds to a high spreading coefficient and polar groups present in the molecules of the spreading liquid. However, these groups seem not to be essential for the formation of a monomolecular layer as reported by Harkins and Feldman (1922). Washburn and Keim (1940) and Keim and Washburn (1940) reported that the spreading of different volatile organic liquids on water and the spreading of binary mixtures of volatile organic liquids on water were in good agreement with the spreading condition defined by Harkins and Feldman (1922). Furthermore Harkins (1941) defined analogous to the entering coefficient described in eq. (2.27) an initial, semi initial and final spreading coefficient as summarized in eq. (2.34), in which the primes refer to each liquid saturated with the other:

$$\begin{aligned} S_{c,(OL)} &= \gamma_{LA} - \gamma_{O'L'} - \gamma_{OA} \\ S_{c,(O'L)} &= \gamma_{LA} - \gamma_{O'L'} - \gamma_{O'A} \\ S_{c,(O'L')} &= \gamma_{L'A} - \gamma_{O'L'} - \gamma_{O'A} \end{aligned} \qquad (2.34).$$

Harkins (1922) has demonstrated that, sometimes, the spreading films are unstable and after a time will gather into a liquid lens in equilibrium with a monolayer. The time required for this transformation is that taken for the initial spreading coefficient to change to the final spreading coefficient, i.e., the time required for mutual equilibration of the two liquids. The value of the final spreading coefficient is zero or negative because mutual equilibration of the involved surfaces and interface diminishes the driving force for spreading.

Entering, i.e., dewetting is essential for the droplets to result in a condition in which the droplets have the possibility to spread. The relation between entering and spreading coefficient is obtained by combining eq. (2.27) and eq. (2.34) in eq. (2.35):

$$\begin{aligned} \mathbf{E}_{c,(OL)} &= 2\gamma_{O'L'} + \mathbf{S}_{c,(OL)} \\ \mathbf{E}_{c,(O'L)} &= 2\gamma_{O'L'} + \mathbf{S}_{c,(O'L)} \\ \mathbf{E}_{c,(O'L')} &= 2\gamma_{O'L'} + \mathbf{S}_{c,(O'L')} \end{aligned} \qquad (2.35).$$

Ross (1950) mentioned that three combinations of values of the entering coefficient and the spreading coefficient are possible (see Fig 2.8).

1) $E_c < 0$ and $S_c < 0$: refers to a droplet to remain wetted and not be able to spread. 2) $E_c > 0$ and $S_c < 0$: refers to a droplet that can enter the liquid surface (i.e. dewet) but will not spread over the liquid surface. These particles are considered to destabilize the foam as described by the hydrophobic particle mechanism. 3) $E_c > 0$ and $S_c < 0$: refers to a droplet that can enter the liquid surface and then starts to spread over the surface. From eq. (2.23), eq. (2.26) and eq. (2.31) it can be seen that droplets with an $E_c < 0$ and a $S_c > 0$ do not exist. The three kinds of behaviour can be translated into a phase-behaviour diagram by choosing a single oil to fix γ_{OA}, and then plotting γ_{OL} versus γ_{LA}. This is presented in Fig 2.8, in which both E_c and S_c increase toward the right hand side of the diagram. Ross's three regions of behaviour can be distinguished by solving eq. (2.23) and eq. (2.26) for the conditions $E_c = 0$ and $S_c = 0$.

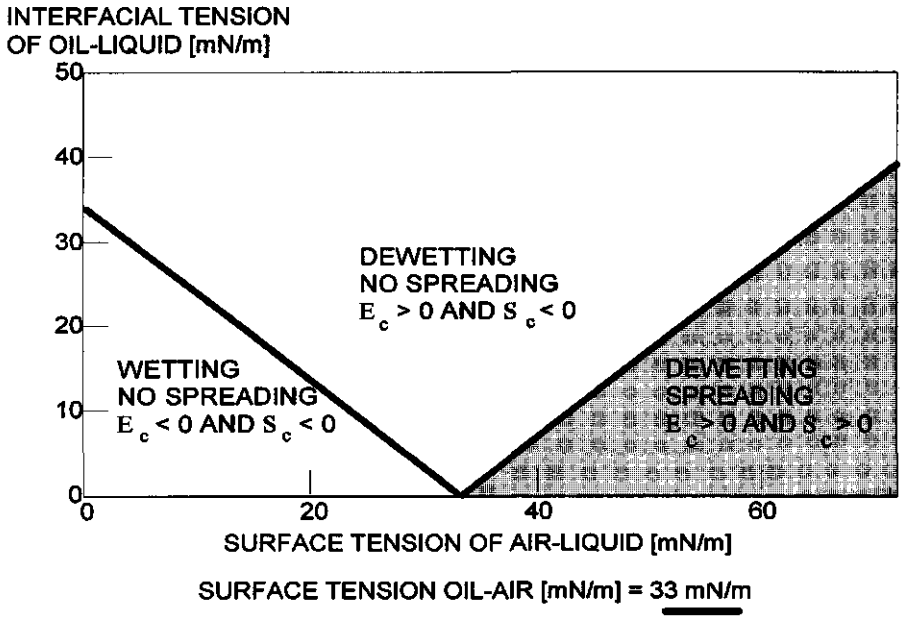

Fig 2.8: ***A plot of the interfacial tension versus the surface tension of the air-liquid surface. The parameter is the surface tension of the oil-air surface. The three possible combinations of E_c and S_c are indicated and divide the graph in three regions.***

This produces the two lines indicating the boundaries between the regions shown in Fig 2.8.

The values plotted in Fig 2.8 are arbitrary, but in agreement with the order of magnitude of the surface tensions of an oil phase and an aqueous solution. The mechanism for coalescence in foam initiated by the spreading from particles or droplets was first mentioned by Ross (1950) and Ross et al. (1953) and discussed by Bikerman (1973) and Kruglyakov (1989).

The spreading mechanism is presented schematically in Fig 2.9. As the spreading liquid, oil is chosen and a small droplet of this oil may come to the surface of an aqueous film in a foam (Fig 2.9: 1, 2 and 3). When the droplet encounters the film

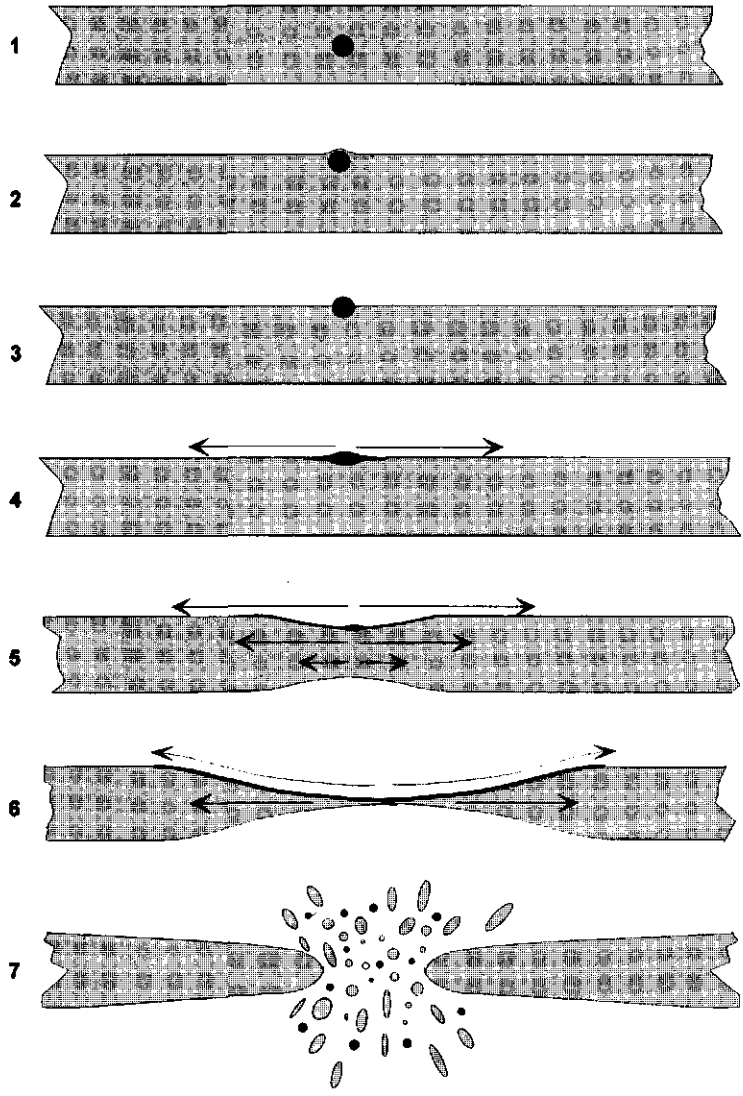

Fig 2.9: ***A schematic presentation of the series of events that take place when a particle enters the surface of a liquid film followed by spreading which is causing local thinning of the film and eventually film rupture.***

surface it is still separated from the gas phase by a film of liquid (Fig 2.9: 2).This film has to drain to the critical thickness for rupture. The time needed for drainage can be estimated using eq. (2.16) with R the droplet radius. If the entering coefficient E_c is positive the droplet will dewet and come into the surface. In order to spread, the spreading coefficient S_c must be positive (Fig 2.9: 4). The spreading coefficient S_c is positive if the surface tension of the foam liquid γ_{LA} is higher than the sum of the surface tension of the droplet γ_{OA} and the interfacial tension between the film liquid and the droplet γ_{OL}. Due to the shearing force exerted by the moving surface on the liquid in the film, this liquid is dragged along radially in the direction away from the spreading particle (Fig 2.9: 5-6). When the spreading proceeds far enough a thin spot in the film is formed and may result in film rupture due to thermal motion and consequently in coalescence of the bubbles that were separated by this film (Fig 2.9:7) Because here the interfacial and surface properties are important, the composition of the droplet is important. On the other hand the surface rheological properties of the film liquid are important and since the spreading process is a dynamic event the dynamic surface properties of the spreading layer and film surface are important.

Harkins and Feldman (1922) and Ross et al. (1953) stated that spreading predominantly occurs if the surface tension of the film liquid is high and the surface tension of the oil droplet and the interfacial tension of the oil-liquid interface are low. In a foam an increased surface tension is developed during drainage of the film as a result of gravity forces and Plateau border suction.

Ross (1950) and Ross et al. (1953) and later Prins (1989) and Ronteltap (1989) proposed a possible mechanism for film rupture induced by spreading of material over the film surface. Ross (1950) and Ross et al. (1953) reported foam destabilization caused by spreading of droplets and gave two different mechanisms depending on the properties of the spreading material.

Ross (1950) and Ross et al. (1953) stated that the spreading of material could change the surface rheological properties of the liquid film resulting in a reduction of the

surface dilational viscosity and consequently in a decrease of the surface tension gradient developed by the liquid flow along the film surface which is opposing drainage. Therefore an increase of the rate of thinning of the liquid film occurs after the material has spread over the film surface. In this view the surface rheological properties of a spread layer is of importance. Another mechanism he proposed was the local thinning of the liquid film in the area where the droplet is spreading resulting in film rupture, but he did not give a conclusive explanation.

Prins (1986, 1988, 1989) was the first who made an attempt to describe the thinning process of the liquid film in a more quantitative way. He assumed that the spreading phenomenon can be described by the propagation of a longitudinal wave over the film surface and the liquid dragged along with the spreading material can be estimated. The longitudinal wave theory was described by Joos and Pintens (1977). Using this theory the time needed for the wave to travel over a certain distance ξ is given by eq. (2.36):

$$t_\xi = \frac{(\eta\rho)^{\frac{1}{3}}\,\xi^{\frac{4}{3}}}{(\Delta\gamma)^{\frac{2}{3}}} \qquad (2.36),$$

where t_ξ is time, η is the viscosity of the film liquid, ρ is the density of the film liquid, ξ is the distance and $\Delta\gamma$ is the difference in surface tension over the wave which is assumed to be equal to the spreading coefficient defined in eq. (2.36). Prins states that the velocity of the front of the spreading material equals the velocity of the longitudinal wave by assuming a monolayer of surface active material to spread over the film surface. The surfactant has to spread long enough out of the droplet in order to establish a displacement of liquid in the film that results in a local thinning which may result in film rupture. This time is consequently related to the amount of surfactant in the droplet and the available surface area for spreading which is related to the bubble size. For the estimation of displacement of film liquid Prins (1989) used a combination of the penetration theory described by Lucassen (1968) and the

longitudinal wave theory of Joos and Pintens (1977). For the calculation of the distance (P) the liquid motion is penetrating into the film at the centre of spreading as a function of the spreading distance of the monolayer Prins (1977) used eq. (2.37):

$$P = \left(\frac{\eta^2 \xi^2}{\rho \Delta\gamma} \right)^{\frac{1}{3}} \qquad (2.37).$$

Prins assumed that the degree of film thinning is proportional to the penetration of surface motion into the film liquid and therefore he came to the conclusion that the film will rupture when the penetration equals the film thickness. Regarding eq. (2.37), it can be concluded that the larger the value of P and the smaller the film thickness the larger the chance that the film will rupture. Also a higher viscosity and smaller density of the film liquid are in favour for film rupture. Furthermore, according to eq. (2.37) a small value of $\Delta\gamma \rightarrow 0$ results in an, theoretically, infinite penetration depth P. However, according to eq. (2.36) the duration of the spreading time will in this case be infinite too. Therefore, it is to be expected that there exists an optimum between the $\Delta\gamma$ and the chance of film rupture.

The results reported by Ronteltap (1989) performed in a free falling liquid film confirm the positive effect of the viscosity of the film liquid on rupture when the droplets are spreading and, more important, the thicker the film the smaller the chance of film rupture. Additionally Ronteltap (1989) found an effect of the droplet size in relation to the viscosity of the film liquid and the possibility to induce film rupture. Small droplets were found to spread over a free falling liquid film but were not able to cause film rupture. This spreading phenomenon caused an optical effect. In the light of a stroboscope a twinkling of small light spots all over the film was observed. The spreading layer reflects light in a different way than the surrounding film. Hole formation does not take place because the film thinning process can not proceed far enough due to a deficiency of spreading material. Therefore, the time of spreading is too short compared to the time needed to thin the film far enough.

When the same amount of droplets was added to the foaming liquid but the viscosity of the film liquid was increased and film thickness was kept equal this lead to an increase of the number of holes. Ronteltap (1989) stated that this was the result of an increase of the number of droplets in the droplet-size distribution added to the film liquid that have the potential to induce film rupture. At a higher viscosity of the film forming liquid the minimum droplet size to rupture the film decreases according to the theory of Prins (1989). Prins (1989) and Ronteltap (1989) also assumed that the film will rupture when the penetration depth equals the initial film thickness.

In order to understand the liquid flow in a thin liquid film caused by the spreading of material over one surface, it is necessary to discuss the hydrodynamics in more detail. Keulegan (1951) reported that as a result of the application of a surface tension gradient to the liquid surface in an open channel, a surface flow is produced and due to mechanical equilibrium this surface flow is balanced by return flow within the liquid. In his experiments he brought a spreading material (i.e. a liquid) on the liquid surface in the middle of the channel. This resulted in a constant spreading of material towards both ends of the channel. Due to the moving surface, underlying liquid is dragged along with the surface resulting in a hydrostatic pressure difference increasing from the centre of spreading towards the outer ends of the channel. This hydrostatic pressure difference will cause the return flow observed by Keulegan (1951). In this view it could be expected that in addition to hydrostatic pressure gradients as a result of Laplace pressure differences in the film, - due to curvature of the surfaces developed during spreading -, an additional liquid flow towards the centre of spreading occurs. The results of Mansfield (1959), Ahmad and Hansen (1971), Ruckenstein et al. (1970) and O'Brien et al. (1975), who did experiments to measure and describe the spreading rate of a monolayer on a liquid surface in a trough, give rise to the idea that this process of return flow of liquid may also occur in a liquid film. If this is the case, the decrease in film thickness caused by the viscous drag of the film liquid by the moving surface would be decelerated.

On the other hand it may be possible that in the case of spreading over one film surface the opposite film surface is curved in agreement with the pressure decrease in the region of the film where it is thinning. This would implicate that instead of a penetration depth equal to the film thickness already a penetration depth of say half the film thickness would be enough to result in film rupture.

Finally, the Reynolds number of the flow within a thin liquid film is very small (i.e. 0.1 when the film thickness is 10^{-6}m, the spreading velocity is 0.1 $m \cdot s^{-1}$, the density of the film liquid is 1000 $kg \cdot m^{-3}$ and the viscosity is 0.001 $N \cdot s \cdot m^{-2}$) and therefore no pressure induced flow towards the centre of spreading, which is the opposite direction of the liquid flow induced by viscous dragging, has to be expected.

The shear stress applied by the spreading surface on the liquid is of importance. Prins (1989) predicts that a lower spreading velocity is in favour of film thinning and rupture. He states that a higher spreading coefficient results in a smaller penetration depth and consequently to a smaller chance for film rupture. Nevertheless, it has to be considered that at very low spreading velocities, i.e. $\Delta\gamma$ goes to zero, the time scale of viscous drag of film liquid along with the moving surface could have the same order of magnitude as the time scale for restoration of the film to the initial thickness. Furthermore, it can be assumed that a very large part of the energy exerted on the film liquid by the moving surface is dissipated as heat. In that case the film will not rupture due to a locally film thinning.

So far, the geometry of the environment where spreading takes place was not a point of consideration. However, it plays serious role as will appear in the following.

The spreading distance and consequently the spreading time is limited not only by the limited amount of spreading material in the droplet but also by the limited surface area available for spreading. At very high spreading velocities and a small surface area available for spreading, which is the case with small bubbles, the time scale of spreading will be very short because the possible spreading distance is small. This will result in a smaller penetration of the surface motion into the film liquid and may

therefore not lead to film rupture. Analogous to this is the spreading of a very small particle which will be finished within a very short time scale because the spreading material is limited. Therefore, it depends on the geometrical conditions of the droplet and the environment by which factor the spreading time will be limited. It is to be expected that there is an optimum in film rupture as a function of the spreading velocity. This hypothesis implicates that very small bubbles are more stable against coalescence as a result of the spreading mechanism than in the case where bigger bubbles are involved.

Since the spreading of material from a small particle over a liquid surface can be considered as a dilational process, it is to be expected that the surface dilational modulus has effect on this process. Prins (1989) states that the propagation speed of the longitudinal wave depends on the surface dilational modulus E which is a measure of the resistance of a liquid surface against a dilational disturbance. The surface dilational modulus is defined by Lucassen (1968) in eq. (2.38):

$$E = \frac{d\gamma}{d\ln A} \qquad (2.38),$$

where A is the surface area of the liquid. The velocity of the longitudinal wave also depends on the frequency of the wave ω and the relation between the wave velocity v_f, the modulus E and frequency has been described by Lucassen (1968) in eq. (2.39):

$$v_f = E^{\frac{1}{2}}\left(\frac{\omega}{\rho\eta}\right)^{\frac{1}{4}} \qquad (2.39).$$

By assuming that the value of ω is given by $1/t_\xi$ Prins (1989) introduced this theory in eq. (2.36) in which the expression for t_ξ becomes:

$$t_\xi = \frac{\xi^{\frac{4}{3}}(\rho\eta)^{\frac{1}{3}}}{E^{\frac{2}{3}}} \qquad (2.40).$$

Introduction of eq. (2.40) in eq. (2.37) results in:

$$P = \left(\frac{\eta^2 \xi^2}{E\rho} \right)^{\frac{1}{3}} \qquad (2.41).$$

Eq. (2.41) can be derived directly from eq. (2.37) by replacing $\Delta\gamma$ with E. This equation implies that a film surface with a high surface dilation modulus is more stable against rupture caused by of the spreading of a particle.

Curvature of the film surfaces as a result of the viscous drag exerted on the film liquid by the surface motion, could give rise to capillary pressures which counteract spreading. Therefore, it is to be expected that a pressure gradient should be accounted for in the hydrodynamic theories; this will be discussed in Chapter 3. Prins (1989) assumed also that the droplet completely spreads into a layer with a certain thickness, but it is possible that only a part of the droplet have to spread from a lens in the centre of spreading in order to establish film rupture. Furthermore, as mentioned earlier a monolayer of surface active components may spread in front of the spreading liquid layer. For this reason it has to be considered that the spreading velocity of the monolayer determines the duration of spreading.

Besides using the longitudinal wave theory to calculate the spreading velocity, others have calculated the spreading velocity in a different way. Mansfield (1959) calculated the velocity of a spreading monolayer considering the hydrodynamic resistance to spreading. He presented for spreading at constant velocity an equation for the surface velocity that depends on the shear stress imposed on the section of liquid that is already covered with spreading material. This relation is modified to meet the conditions of a liquid film as presented in eq. (2.42):

$$v_\xi = \frac{\Delta\gamma\, \theta_f}{4\eta\xi} \qquad (2.42),$$

where θ_f is the film thickness, $\Delta\gamma$ the spreading pressure and ξ the distance of spreading. In this derivation it is assumed that the opposite surface does not deform in any direction.

Ahmad and Hansen (1971) performed experiments by spreading a monolayer on thin liquid films in a trough and found good results by applying eq. (2.43) to describe the velocity of the front of the monolayer:

$$v_t = \left(\frac{2\theta_f \Delta\gamma}{\eta t}\right)^{\frac{1}{2}} \qquad (2.43),$$

where t is the time after the start of spreading. They also assumed that the opposite surface is motionless. Plotting the square of v_t versus reciprocal of the time resulted in strait lines which slopes increased with increasing thickness of the liquid film. O'Brien et al. (1975) reported spreading velocities of oleic acid on water up to 0.3 ms^{-1}, and velocity profiles of the underlying liquid (i.e. water). They found that the penetration depths were inversely proportional to the spreading velocity. In their experiments they found a decrease of the spreading velocity as a function of the spreading time and consequently a steeper increase of the penetration depth as expected with constant spreading velocity.

Davies and Rideal (1963) reported the spreading velocities of oils on water and found a first period during spreading in which the spreading velocity decreases rapidly, followed by a period of nearly constant spreading velocity and finally another decrease to zero as a result of the depletion of the spreading liquid. Considering the theory of Prins (1989) the initially relatively high spreading velocity is expected to have a small effect on the film destabilization but the longer period of constant spreading velocity would be of importance due to it's larger penetration. Davies and Rideal (1963) correlated the spreading velocities by using eq. (2.44):

$$v_\xi = K' \frac{S_c}{\eta} \qquad (2.44),$$

where K' is a constant and S_c is Harkins' initial spreading coefficient and η is the viscosity of the liquid. They mentioned that although some correlation can be found, the quotient S_c/η must be taken as a rough measure (it neglects amongst other parameters the viscosity of the spreading material) of the factors controlling the rate of spreading.

Ruckenstein et al. (1970) presented a complete analysis of the spreading process. Their final result is, however, very complicated and involves numerical integration. Suciu et al. (1970) and Suciu et al. (1967) give a lot of experimental data of the spreading velocities of alcohols over water surfaces, but made no theoretical considerations about the physical process of spreading.

Leviton and Leighton (1935), Ross and McBain (1944), Robinson and Woods (1948), Ross (1950), Schramm and Novosad (1989), Prins (1988), Prins (1989) and Ronteltap (1989) related the foam destabilization with the spreading of droplets over the films between the bubbles. All authors concluded that spreading material can have a detrimental effect on foam stability. It is the aim of this study to describe the coalescence in foams induced by spreading droplets in more detail. Considering the possibilities depicted in Fig 2.3 for the droplets to enter the liquid surface and the theories and observations of other investigators presented here, it becomes clear that the spreading phenomenon can induce coalescence just a short period of time after foam production. According to Prins (1989) theory droplets with a diameter of about one order of magnitude smaller than the film thickness can induce the film to rupture. Therefore this mechanism is, compared to the hydrophobic particle mechanism, much more pronounced as far as the droplet size is concerned. Considering a certain film thickness the hydrophobic particle mechanism works if the droplet has a size in the order of the film thickness and provided the particles are solid. The spreading particle mechanism gives rise to film rupture when the droplets are much smaller.

In the case of lipid particles present in foodstuffs or on the consumers lips, they mostly contain surface active impurities that are in favour of the spreading particle mechanism

because they may lower the interfacial and surface tension of the droplet and spread into a monolayer in front of the spreading droplet.

Although the rupture of the liquid film separating a droplet from the gas phase is accompanied with a mechanical shock, which is reported to be a possible mechanism for coalescence, in practice the oil droplets can also be introduced from out of the gas phase and the dewetting process is not taking place.

In this study the theory of Prins (1989) will be tested and the hydrodynamics of the liquid flow in the film induced by surface movement resulting in thinning, will be investigated. Since none of the authors discussing the spreading mechanism, take into account the spreading of the droplet itself as the cause for film rupture, this will be investigated. At first view it can be expected that due to the bulk rheological properties of the oil drop (i.e. viscosity) the spreading velocity of the droplet into a thin film will take place at much lower velocities than are found during the spreading of monolayers. Considering the theory of Prins (1989) this would result in a longer spreading time and a much more effective viscous drag of the underlying film liquid resulting in local thinning of the film.

Another parameter that was not investigated in the past is the effect of the surface area available for spreading since the surface areas of the bubbles in a foam are finite. Spreading of material would result in a decrease of the initial liquid-air surface of the bubble causing compression of the remaining liquid-air surface by the spreading layer. Ronteltap (1989) found a relatively large decrease in surface tension of beer surfaces in compression. This may result in a decrease of the spreading coefficient to eventually negative values at which the spreading would stop. In this context a high surface dilational viscosity and foams with small bubbles are conditions that stabilize foams against the detrimental effect of spreading particles. Furthermore, the surface properties of the foaming liquid and the oil droplets under investigation in relation to the chance of film rupture due to spreading are investigated.

2.5. AIM OF THE STUDY

The aim of the present research is to describe the local thinning of a free liquid film caused by the spreading of a particle over one of the film surfaces in a quantitative way. In this study advantage is taken from the knowledge obtained with the overflowing cylinder technique in which hydrodynamic coupling between bulk and surface motion is described quantitatively. The new theories developed by Bergink-Martens (1993) and Bergink-Martens et al. (1994) to describe the overflowing cylinder and the relation between the flow in the bulk liquid due to surface motion as a result of a surface tension gradient, are used in this study. The analogy is used to describe the hydrodynamics of film thinning due to the surface motion as a result of spreading.

REFERENCES CHAPTER 2

Ahmad, J., and Hansen, R.S., J. Coll. Int. Sci., **38**:601 (1972).

Aronson, M.P., Langmuir, **2**:653 (1986).

Bergink-Martens, D.J.M., Bos, H.J., Prins, A., Schulte, B.C., J. Coll. Int. Sci., **138**:1 (1990).

Bergink-Martens, D.J.M., "Interface dilation, the overflowing cylinder technique", PhD Thesis, Agricultural University Wageningen (1993).

Bergink-Martens, D.J.M., Bos, H.J., Prins, A., J. Coll. Int. Sci., 165:221 (1994).

Bikerman, J.J., "Foams", Springer Verlag, Berlin-Heidelberg-New York, pp. 243-244 (1973).

Cheng, H.C., Lemlich, R., Ind. Eng. Chem. Fundam., **24**:44 (1985).

Davies, J.T., Rideal, E.K., "Interfacial Phenomena", Academic Press, New York and London, pp. 25-28 (1963).

Derjaguin, B.V., Landau, L.D., Acta Physicochimica USSR, **14**:633 (1941).

De Vries, A.J., Rec. Trav. Chim., **77**:383 (1958).

De Vries, A.J., "Morphology, Coalescence and Size Distributions of Foam Bubbles." In: Adsorptive bubble separation techniques, Ed. R. Lemlich, Acad. Press., New York, London, pp. 7 (1972).

Dippenaar, A., Int. J. Mineral Process., **9(1)**:15 (1982).

Djabbarah, N.F., Wasan, D.T., A.I.Ch.E. J., **31(6)**:1041 (1985).

Dombrowski, N., Fraser, R.P., Phil. Trans. Roy. Soc., **247**:13 (1954).

Durian et al., Science, **252**:686 (1991).

Frye, G.C., Berg, J.C., J. Coll. Int. Sci., **130(1)**:54 (1980).

Garret, J. Coll. Interf. Sci., **69(1)**:107 (1979).

Garret, J. Coll. Interf. Sci., **76(2)**:587 (1980).

Gibbs, J.W., Collected works, Dover Publications, New York, Vol 1 pp.301 (1961).

Glazier, J.A., Weaire, D., J. Phys. Condens Matter, **4**:1867 (1992).

Hardy, Proc. Roy. Soc., **88A**:313 (1913).

Harkins, W.D., Feldman, A., J. Amer. Chem. Soc., **44**:2665 (1922).

Harkins, J. Chem Phys., **9**:52 (1941).

Ivanov, I.B., Dimitrov, D.S., "Thin film drainage." In: Thin Liquid Films. Ed. I.B. Ivanov, pp. 379 (1989).

Ivanov, I.B., Jain, R.K., "Dynamics and Instability of Fluid Interfaces." In: Lecture Notes in Physics, Ed. T.S. Sorensen, Springer Verlag, New York, pp. 121 (1979).

Jackson, G., Roberts, R.T., Wainwright, T., J. Inst. Brewing, **86**:34 (1980).

Joos, P., Pintens, J., J. Coll. Int. Sci., **60(3)**:507 (1977).

Joos, P., De Keyzer, P., "The Overflowing Funnel as a Method for Measuring Surface Dilational Properties.", Levich Birthday Conference, Madrid (1980).

Kann, K.B., Colloid J., **46(3)**:508 (1984).

Kann, K.B., Feklistov, V.N., Colloid J. USSR, **46**:1052 (1985).

Keim, C.P., Washburn, E.R., J. Amer Chem. Soc., **62**:2318 (1940).

Keuligan, G.H., J. Res. Nat. Bur. Stand. Wash., **46**:358 (1951).

Kruglyakov, P.M., "Equilibrium Properties of Free Film and Stability of Foams and Emulsions." In: Thin Liquid Films. Ed. I.B. Ivanov. pp. 767 (1989).

Leviton, A., Leighton, A., J. Dairy Sci., **18**:105 (1935).

Lifshitz, I.M., I.M., Slyosov, V.V., J. Phys. Chem., Solids, **19**:35 (1961).

Lucassen, J., Trans. Faraday Soc., **64**:2221 (1968).

Lucassen, J., "Dynamic Properties of Free Liquid Films and Foams." In: Anionic Surfactants. Ed. E.H. Lucassen-Reynders. Marcel Dekker, pp. 259 (1981).

Lucassen, J., Coll. Surf., **65**:131 (1992).

Malysa, K., Cohen, R., Exerowa, D., Romianowski, A., J. Int. Sci., **80(1)**:1 (1980).

Mansfield, W.W., Aust. J. Chem., **12**:382 (1959).

Markworth, A.J., J. Coll. Int. Sci., **107(2)**:569 (1985).

Mendelson, J.D., A.I.Ch.E.J., **13**:250 (1967).

Monsalve, A., Schechter, R.S., J. Coll. Int. Sci., **107(2)**:327 (1984).

Nutt, C.W., Chem. Eng. Sci., **12**:133 (1960).

O'Brien, R.N., Fehler, A.I., and Leja, J., J. Coll. Int. Sci., **51**:366 (1975).

Prins, A., Van den Tempel, M., J. Phys Chem., **73**:2828 (1969).

Prins, A., "Theory and Practice of Formation and Stability of Food Foams." In: Food Emulsions and Foams., Ed E. Dickinson, Roy Soc. of Chem., Leeds, pp. 30 (1986).

Prins, A., Van 't Riet, K., Trends in Biotechnology, **5(11)**:296 (1987).

Prins, A., "Principles of Foam Stability." In: Food Emulsions and Foams, Ed. E. Dickinson and G. Stainsby, pp. 91 (1988).

Prins A., "Foam Stability as affected by the presence of small spreading particles." In: Surfactants in Solution, Vol. 10, Ed. K.L. Mittal, pp. 91 (1989).

Radanive, A.Y., Lemlich, R., J. Coll. Int. Sci., **70(2)**:329 (1979).

Radoev, P.B., Scheludko, A., Manev, E.D., J. Coll. Int. Sci., **95(1)**:254 (1983).

Raleigh, "Scientific Papers ", **92(3)**:351 (1887-1890).

Ramchadran, N., Didwania, A.K., Sirkar, K.K., J. Coll. Int. Sci., **83(1)**:94 (1981).

Rao, A.A., Wasan, D.T., Manev, E.D., Chem. Eng. Commun., **15**:63 (1982).

Reynolds, O., Phil. Trans. Roy Soc. London, **a177**:157 (1886).

Rieser, L.A., Lemlich, R., J. Coll. Int. Sci., **123(1)**:299 (1988).

Roberts, K., Axberg, C., Osterlund, R., J. Colloid and Interface Sci., **62**:264 (1977).

Robinson and Woods, J. Soc. Chem. Ind., **67**:361 (1948).

Ronteltap, A.D., PhD Thesis, Agricultural University Wageningen (1989).

Ross and Mc Bain, Ind. Eng. Chem., **36**:570 (1944).

Ross, S., Phys. Coll. Chem., **54**:429 (1950).

Ross, S., Hughes, A.F., Kennedy, M.L. Mardoian, A.R., J. Phys. Chem., **57**:684 (1953).

Ruckenstein, E., Smigelschi, O., Suciu, D.G., Chem. Eng. Sci., **25**:1249 (1970).

Scheludko, A., Kolloid Z., **155**:39 (1957).

Scheludko, A., Proc. Kon. Ned. Acad. Wetenschappen, **B65**:87 (1962).

Scheludko, A., Kolloid Z., **191**:52 (1963).

Scheludko, A., Adv. Coll. Int. Sci., **1**:391 (1967).

Scheludko, A., Tschaljowska, S., Fabrikant, A., Faraday Spec. Disc., **1**:112 (1970).

Scheludko, A., Toshev., B.V., and Bojadjev, D.T., J. Chem. Soc. Faraday I, **72**:2815 (1975).

Schramm, L.L., Novosad, J.J., Coll. and Surf., **46**:21 (1990).

Schulze, H.I., Coll. & Pol. Sci., (1975).

Stavans, J., Glazier, J.A., Phys. Rev. Lett., **62**:1318 (1989).

Suciu, D.G., Smigelschi, O., Ruckenstein, E., A.I.Chem.Eng.J., **13**:1120 (1967).

Suciu, D.G., Smigelschi, O., and Ruckenstein, E., J. Coll. Int. Sci., **33**:520 (1970).

Van Havenbergh, J., Bussmann, H., Joos, P., J. Colloid and Interface Sci., **101(2)**:462 (1984).

Vrij, A., Overbeek, J.Th.G., J. Am. Chem. Soc. **90(12)**:3074 (1968).

Vrij, A., Hesselink, F.Th., Lucassen, J., van den Tempel, M., Proc. Kon. Ned. Akad. Wetensch. **B73**:124 (1970).

Wagner, C., Z. Electrochem., **65**:581 (1951).

Wasan, D.T., Malhotra, A.K., A.I.Ch.E. Symp. Ser., **82(252)**:5 (1986).

Washburn, E.R., Keim, C.P., J. Amer Chem. Soc., **62**:1747 (1940).

THEORY

3.1. INTRODUCTION

The process of film rupture initiated by the spreading of a particle over one of the surfaces of the film was described qualitatively in the previous chapter. The developed theory is analogous to the theory developed by Bergink-Martens (1994) to describe the working of the overflowing cylinder. The similarity between the overflowing cylinder and a spreading particle is that the surface motion is: 1) driven by a surface tension gradient and 2) geometrically radial symmetric. Thus it is assumed that a particle will spread due to the driving force of a surface tension difference between the clean liquid surface and the surface and interfacial tensions of the liquid particle as was first mentioned by Harkins and Feldman (1922) in a radial symmetric way. From liquid particles containing surface active components a monolayer of the latter will spread preceding the spreading liquid particle. The spreading process is then driven by a surface tension gradient developed at the front of the spreading monolayer. It is this spreading process, which includes the spreading of a monolayer in front of a spreading droplet inducing surface motion, that causes drag of underlying liquid which will cause film thinning and eventually film rupture. The spreading process and the, consequently, thinning of the liquid film due to shear forces exerted on the underlying liquid will be explained theoretically.

In this theory a liquid particle is considered to be present in the surface of a thin liquid film as was already presented schematically in Fig 2.9. If the spreading coefficient S_c is positive the particle will start to spread in a pure radial way. This spreading of material from a small particle over a liquid surface can be considered as a dilational process. The geometry and the dilational properties of the process are analogue to the overflowing cylinder technique described by Bergink-Martens (1993). Therefore, a theory was developed which is based on the theory applied by Bergink-Martens to describe the overflowing cylinder but where the liquid drag due to surface motion is translated into the thinning process of a thin liquid film. The result is a theory which describes the film thinning process and eventual film rupture due to spreading droplets

by using the parameters film thickness, droplet radius, liquid bulk viscosity, liquid bulk density, the surface tension of the film, the surface- and interfacial tension of the droplet, surface tension gradients, surface dilational viscosity and the surface dilational modulus. These parameters determine whether or not the film will rupture.

3.2. DESCRIPTION OF THE PROBLEM

Consider a small, potentially spreading, liquid particle in the surface of a thin liquid film with thickness δ. The co-ordinate system is chosen in such a way that the centre of spreading corresponds to the intersection of z- and ξ-axis which position is at the surface of a thin liquid film as presented in Fig 3.1.

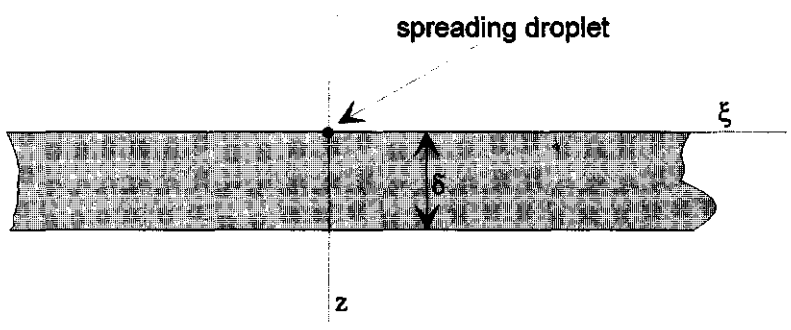

Fig 3.1: ***The co-ordinate system in which the theoretical calculations are based on. The intersection of the two axes is in the centre of spreading. In this figure the situation at the start of the spreading process is presented.***

According to the theory of Bergink-Martens (1993) that was applied to the overflowing cylinder a cylindrical co-ordinate system is used. The origin of this co-ordinate system coincides with the intersection point of the free top surface and the vertical axis of symmetry. The vertical axis represents distance z which is zero at the plane surface

where the particle is present and points downward (in the direction of gravity). The horizontal axis parallel to the free surface represents the radial spreading distance ξ which is zero at the centre of the spreading oil droplet. In this study we assume that the spreading process can be described in these cylindrical co-ordinates. The starting point for analysis of the flow of film liquid underlying the spreading particle are the Navier Stokes equations which are in cylindrical co-ordinates described by the eq. (3.1), eq. (3.2) and eq. (3.3).

$$v_\xi \frac{\partial v_\xi}{\partial \xi} + v_z \frac{\partial v_\xi}{\partial z} = -\frac{1}{\rho}\frac{\partial P}{\partial \xi} + \nu\left[\frac{\partial^2 v_\xi}{\partial \xi^2} + \frac{1}{\xi}\frac{\partial v_\xi}{\partial \xi} - \frac{v_\xi}{\xi^2} + \frac{\partial^2 v_\xi}{\partial z^2}\right] \tag{3.1},$$

$$v_\xi \frac{\partial v_z}{\partial \xi} + v_z \frac{\partial v_z}{\partial z} = -\frac{1}{\rho}\frac{\partial P}{\partial z} + \nu\left[\frac{\partial^2 v_z}{\partial \xi^2} + \frac{1}{\xi}\frac{\partial v_z}{\partial \xi} + \frac{\partial^2 v_z}{\partial z^2}\right] + g \tag{3.2},$$

$$\frac{\partial v_\xi}{\partial \xi} + \frac{\partial v_z}{\partial z} + \frac{v_\xi}{\xi} = 0 \tag{3.3},$$

where, v_ξ and v_z are respectively the radial and vertical velocity components, P is the pressure, ν is the kinematic viscosity, ρ the fluid density and g is the acceleration due to gravity. Similar to Bergink-Martens (1993), due to the lack of characteristic length scales self similar solutions are sought. An a priori unknown time scale $t^* = a^{-1}$ is introduced were a is the constant of proportionality in the velocity distribution. This time scale was related to the relative surface expansion rate, $d\ln A/dt$. A combination of the time scale t^* and the kinematic viscosity ν introduces a diffusion length scale $l^* = \sqrt{(\nu / a)}$ which may be related to the penetration depth of liquid motion. In order to obtain a similarity solution the vertical co-ordinate z is non-dimensionalized by this 'penetration depth'. Hence a new co-ordinate σ is introduced which is defined by $\sigma = z\sqrt{a/\nu}$. Also a stream function $f(\sigma)$ is introduced and the radial and vertical velocity components are related to $f(\sigma)$ in such a way that the continuity eq (3.3) is identically satisfied. This resulted in the eqs. (3.4) and (3.5) in which the velocity components are related to a stream function:

$$v_\xi = a\xi \frac{df}{d\sigma} \tag{3.4},$$

$$v_z = -2\sqrt{av} \bullet f(\sigma) \tag{3.5}.$$

In these equations a represents the constant of proportionality in the velocity distribution and is described by eq. (3.6):

$$a = \frac{1}{2}\frac{d\ln A}{dt} = \frac{v_f}{\xi} = C(t) \tag{3.6},$$

where, $d\ln A/dt$ is the relative surface expansion rate and v_f is the velocity of the front of the expanding monolayer.

As Bergink-Martens (1993) already stated is the relative surface expansion rate of a radial expanding surface in an overflowing cylinder at steady state conditions constant over most of the distance r, i.e. the radius of the cylinder. In the case of a spreading particle the relative expansion rate is a function of both the spreading distance ξ and the time of spreading t. The film thinning process is caused by spreading process which induces a vertical velocity component in the film liquid towards the moving film surface. The closer to the surface the horizontal velocity component parallel to the film surface increases to maximum at the surface and the vertical velocity component becomes smaller to zero at the film surface. With the vertical velocity component liquid is streaming towards the moving surface and the horizontal velocity component transports it along with the surface. This explains the drag of film liquid by the moving surface. The evolution of this process depends on the spreading velocity v_ξ which determines the relative surface expansion rate as described in eq. (3.6). Furthermore, the spreading velocity changes with time t but also with spreading distance ξ. Therefore eq. (3.5) was rewritten by introduction of eq. (3.6) in eq.(3.5) which can be seen in eq. (3.7) and eq. (3.8). With the distance dependency eq. (3.8) is rewritten as eq. (3.9) in which v_z becomes a function of ξ and t:

$$v_z(t) = -2\sqrt{\frac{1}{2}\frac{d\ln A}{dt} v} f(\sigma) \tag{3.7},$$

$$v_z(t) = -2\sqrt{C(t)v} f(\sigma) \tag{3.8},$$

$$v_z(\xi,t) = -2\sqrt{C(\xi,t)\,\nu}\,f(\sigma) \qquad (3.9).$$

However, in contrast to the situation in the overflowing cylinder where a stationary rotational symmetric flow upwards through the cylinder exists. In the case of a spreading droplet the boundary conditions in the surface are not uniform and not stationary. For this reason eq. (3.9) does not identically satisfy eq. (3.3) because eq. (3.4) contains also the constant $C(t)$. Although this implicates that the starting point of this theory is not completely justified it is possible to satisfy by approximation eq. (3.3) when:

$$\xi \frac{\partial}{\partial \xi}\left(\frac{\mathbf{d}\ln A}{\mathbf{d}t}\right) << C(t) \qquad (3.10).$$

This would mean that:

$$x \frac{\partial}{\partial x}\left(\frac{\mathbf{d}\ln A}{\mathbf{d}t}\right) << \frac{\mathbf{d}\ln A}{\mathbf{d}t} \qquad (3.11).$$

which is, as will be seen later in this Chapter and in Chapter 5, a reasonable assumption.

To obtain the film thinning process the displacement of the film surface due to the spreading of the particle has to be defined. This displacement S can be described by eq. (3.12) which is a function of the vertical velocity component that is responsible for the supply of film liquid to the expanding surface which will drag the liquid away from the centre of spreading:

$$S = \int_0^{\tau} v_z \mathbf{d}t \qquad (3.12).$$

Here, τ is the time scale at a distance where the front of the spreading layer has passed. It has to be mentioned that this time scale differs with the distance. In other words, the longest spreading time at the surface is found near the centre of spreading whereas a spreading time equal to zero exists at the front of the spreading layer. The vertical velocity component defined in eq. (3.7) to eq. (3.9) can be introduced in eq. (3.12) what results in eq. (3.13):

$$S(\xi,t) = -2f(\sigma)\sqrt{\nu}\int_0^t \sqrt{C(\xi,t)}\,dt \qquad (3.13).$$

Using eq. (3.13) the displacement of the film surface in the z-direction is described as a function of time. To obtain the relation with the distance ξ of spreading the equation of Bergink-Martens (1993) was used. This equation describes the relation between a surface tension gradient and the relative surface expansion rate in a pure dilational expansion process. Bergink-Martens (1993) derived the following eq. (3.14) that describes the spreading distance as a function of time t and the surface tension gradient $d\gamma/d\xi$:

$$\frac{d\gamma}{d\xi} = 0.415\,\xi(\eta\rho)^{\frac{1}{2}}\left(\frac{d\ln A}{dt}\right)^{\frac{3}{2}} \qquad (3.14).$$

Bergink-Martens (1993) also mentioned that the relative surface expansion rate is related to the radial velocity in the way as shown in eq. (3.15):

$$\frac{d\ln A}{dt} = \frac{2v_r}{r} \qquad (3.15).$$

Hence, if $v_r=v_\xi$ and $r=\xi$ eq. (3.14) can be rewritten as eq. (3.16):

$$v_\xi = \frac{1}{2}\left(0.415\,(\eta\rho)^{\frac{1}{2}}\right)^{-\frac{2}{3}}\left(\frac{d\gamma}{d\xi}\right)^{\frac{2}{3}}\xi^{\frac{1}{3}} \qquad (3.16).$$

Here the velocity of the front of the monolayer v_ξ is a function of the spreading distance ξ. In the case of an oil droplet the spreading process starts with the spreading of the droplet itself. For this situation we defined the surface tension gradient as the spreading coefficient S_c devided by the spreading distance:

$$\frac{d\gamma}{d\xi} = \frac{\gamma_{LA}-\gamma_{OA}-\gamma_{OL}}{\xi} = \frac{S_c}{\xi} \qquad (3.17),$$

We want to have the displacement of the film surface as a function of ξ and t and therefore we say that $v_\xi=d\xi/dt$ and introduce this together with eq. (3.17) in eq. (3.16):

$$\frac{d\xi}{dt} = \frac{1}{2}\left(0.415\,(\eta\rho)^{\frac{1}{2}}\right)^{-\frac{2}{3}} S_c^{\frac{2}{3}}\xi^{-\frac{1}{3}} \qquad (3.18).$$

When solving this differential we can write the spreading distance ξ as a function of t as is done in eq. (3.19):

$$\xi = \int_0^t v_f \mathrm{d}t = \left(\frac{3}{2}\right)^{\frac{3}{4}} S_c^{\frac{1}{2}} \left(0.415(\eta\rho)^{\frac{1}{2}}\right)^{-\frac{1}{2}} t^{\frac{3}{4}} \tag{3.19}.$$

In eq. (3.19) it is assumed that at time t=0 the spreading distance ξ=0. This is, however, not correct. In the case a particle enters the liquid surface it is assumed that, at t=0, the spreading distance equals already ξ=R This distance corresponds to a certain spreading time that must be excluded in eq. (3.19). Therefore, in the case of a particle entering the surface as a sphere the excluded time ζ can be defined. To obtain ζ we rewrite eq. (3.19) into spreading time as a function of spreading distance and we introduce for the spreading distance ξ the particle radius R:

$$\zeta = \frac{3}{2}\left(0.415(\eta\rho)^{\frac{1}{2}}\right)^{\frac{2}{3}} S_c^{-\frac{2}{3}} R^{\frac{4}{3}} \tag{3.20}.$$

Now eq. (3.19) can be rewritten by introducing ζ:

$$\xi = \int_0^t v_f \mathrm{d}t = \left(\frac{3}{2}\right)^{\frac{3}{4}} S_c^{\frac{1}{2}} \left(0.415(\eta\rho)^{\frac{1}{2}}\right)^{-\frac{1}{2}} (t+\zeta)^{\frac{3}{4}} \tag{3.21}.$$

We can eliminate ξ in eq. (3.18) and write v_ξ as a function of time t:

$$v_\xi = \frac{1}{2}\left(\frac{3}{2}\right)^{\frac{1}{4}} S_c^{\frac{1}{2}} \left(0.415(\eta\rho)^{\frac{1}{2}}\right)^{-\frac{1}{2}} (t+\zeta)^{-\frac{1}{4}} \tag{3.22}.$$

To be able to use these equations in eq. (3.7) to eq. (3.9) we defined the relative surface expansion rate of the spreading oil droplet as in eq. (3.23):

$$\frac{\mathrm{d}\ln A}{\mathrm{d}t} = \frac{2v_\xi}{\xi} = \left(0.415\,(\eta\rho)^{\frac{1}{2}}\right)^{-\frac{2}{3}} S_c^{\frac{2}{3}} \xi^{-\frac{4}{3}} \tag{3.23}.$$

Substitution of eq. (3.21) in eq. (3.23) delivers eq. (3.24) which describes the relative surface expansion rate as a function of time as was mentioned in eq. (3.6):

$$a = C(t) = \frac{3}{4(t+\zeta)} \tag{3.24}.$$

Upon substituting eq. (3.24) into eq. (3.7) we obtain eq. (3.25) which describes the vertical velocity component v_z as a function of time t:

$$v_z(t) = -2f(\sigma)\sqrt{\frac{3\nu}{4(t+\zeta)}} \tag{3.25}.$$

The displacement S of the film surface is a function of both the distance $r<\xi$ and the time t. The displacement increases from zero at the front of the spreading oil droplet to a maximum at the centre of spreading. To calculate this displacement for every distance, i.e. from the centre of spreading to a distance $r<\xi$, r has to be defined in terms of the velocity v_ξ by integrating eq. (3.22) between $t=0$ and $t=\tau$:

$$r = \int_0^\tau v_\xi \, dt = \left(\frac{3}{2}\right)^{-\frac{3}{4}} \left(0.415\,(\eta\rho)^{\frac{1}{2}}\right)^{-\frac{1}{2}} S_c^{\frac{1}{2}} (\tau+\zeta)^{\frac{3}{4}} - R \tag{3.26}.$$

The time τ can now be expressed as a function of r:

$$\tau = \frac{3}{2}\left(0.415\,(\eta\rho)^{\frac{1}{2}}\right)^{\frac{2}{3}} \Delta\gamma^{-\frac{2}{3}} (r+R)^{\frac{4}{3}} - \zeta \tag{3.27}.$$

The displacement of the film surface in the z-direction at distance r from the centre of spreading can be described by eq. (3.28):

$$S(r,t) = \int_\tau^t v_z \, dt = -2f(\sigma)\left(\frac{3\nu}{4}\right)^{\frac{1}{2}} \int_\tau^t (t+\zeta)^{-\frac{1}{2}} dt = -2f(\sigma)\left(\frac{3\nu}{4}\right)^{\frac{1}{2}} \cdot 2\left(\sqrt{t+\zeta} - \sqrt{\tau+\zeta}\right) \tag{3.28}.$$

By substituting eq. (3.27) into eq. (3.28) the displacement $S(r,t)$ can be described as a function of r and t as presented in eq. (3.29):

$$S(r,t) = -4f(\sigma)\sqrt{\frac{3\nu}{4}}\sqrt{t+\zeta} + 4f(\sigma)\sqrt{\frac{3\nu}{4}}\sqrt{\left(\frac{3}{2}\right)\left(0.415(\eta\rho)^{\frac{1}{2}}\right)^{\frac{2}{3}} S_c^{-\frac{2}{3}} (r+R)^{\frac{4}{3}}} \tag{3.29}.$$

By solving the numerical constants this equation becomes eq. (3.30):

$$S(r,t) \approx -3.4641 f(\sigma)\sqrt{\nu}\sqrt{t+\zeta} + 3.4641 f(\sigma)\sqrt{\nu}\sqrt{\frac{3}{2}\left(0.415(\eta\rho)^{\frac{1}{2}}\right)^{\frac{2}{3}} \Delta\gamma^{-\frac{2}{3}} (r+R)^{\frac{4}{3}}} \tag{3.30}.$$

Eq. (3.30) can be used to calculate the downward displacement of the film surface at distance r from the centre of spreading. The validity of eq. (3.30) is limited to the boundary condition $r<\xi$ where $S(r,t)=0$, which is described by eq. (3.31):

$$3.4641 f(\sigma)\sqrt{\nu}\sqrt{t+\zeta} = 3.4641 f(\sigma)\sqrt{\nu}\sqrt{\frac{3}{2}\left(0.415(\eta\rho)^{\frac{1}{2}}\right)^{\frac{2}{3}} S_c^{-\frac{2}{3}}(r+R)^{\frac{4}{3}}} \qquad (3.31).$$

By solving eq. (3.31) the conditions at which eq. (3.30) is valid are now described by condition (3.32):

$$r < \left(\frac{2}{3}\right)^{\frac{3}{4}}\left(0.415(\eta\rho)^{\frac{1}{2}}\right)^{-\frac{1}{2}} \Delta\gamma^{\frac{1}{2}}(t+\zeta)^{\frac{3}{4}} - R \qquad (3.32).$$

There will be a limit of the distance the particle will spread into a thin layer. Long ago Franklin (1765) mentioned that olive oil spreads over water into a layer with a thickness of 25 Å before it breaks up into small droplets which will, probably, be in equilibrium with a surrounding monolayer. Later Rayleigh (1899) reported a minimum layer thickness of 14 Å for castor oil. We took in this study for order of magnitude calculations a minimum layer thickness of 20 Å. The distance the droplet will spread is then defined by:

$$R_l = \sqrt{\frac{4R^3}{3h}} \qquad (3.33),$$

where, R_l is the spreading distance and h is the layer thickness. The validity of the equations mentioned before are then up to a spreading distance R_l. We assume that the monolayer spreading starts after breaking up of the oil layer which consists at that point of oil droplets surrounded and in equilibrium with monolayer. At that moment the spreading coefficient is no longer valid and we estimate the surface tension gradient similar to eq. (3.17) with eq. (3.34):

$$\frac{d\gamma}{d\xi} = \frac{\gamma_0 - \gamma_1}{\xi} = \frac{\Delta\gamma}{\xi} \qquad (3.34),$$

where, γ_0 the surface tension of the 'clean' surface in front of the monolayer and γ_1 is the surface tension of the monolayer at x=0 which is in the middle of the surface area

with radius R_l. The assumption of a uniform surface tension gradient is only an approximation. Experimental evidence in favor of this assumption is given by Ahmad and Hansen (1972) and later by Joos and Pintens (1977). From this point the spreading coefficient is substituted by the surface tension difference $\Delta\gamma$.

To this end, a new excluded time has to be defined. The time ζ' the droplet needed to spread into a layer with radius R_l is defined by eq. (3.35):

$$\zeta' = \frac{3}{2}\left(0.415(\eta\rho)^{\frac{1}{2}}\right)^{\frac{2}{3}} S_c^{-\frac{2}{3}} R_l^{\frac{4}{3}} + \zeta \qquad (3.35),$$

and the equations mentioned before can be rewritten by substituting ζ with ζ' and R with R_l.

When the spreading of a particle into a monolayer proceeds far enough we assume that the thin liquid film ruptures when the displacement $S(r,t)$ at r=0 equals the film thickness δ. This condition is described by eq. (3.36):

$$S(0,t) = -\delta = -3.4641 f(\sigma)\sqrt{\nu}\sqrt{t+\zeta} + 3.4641 f(\sigma)\sqrt{\nu}\sqrt{\zeta} \qquad (3.36),$$

or by eq. (3.37) when spreading of only the droplet is not enough to induce film rupture:

$$S(0,t) = -\delta = -3.4641 f(\sigma)\sqrt{\nu}\sqrt{t+\zeta'} + 3.4641 f(\sigma)\sqrt{\nu}\sqrt{\zeta'} \qquad (3.37),$$

The time needed for spreading of the particle until film rupture is initiated can be described by eq. (3.38) in which δ is written as function of $t_{rupture}$:

$$t_{rupture} = \left(\frac{\delta}{3.4641 f(\sigma)\sqrt{\nu}} + \sqrt{\zeta}\right)^2 - \zeta \qquad (3.38).$$

Substituting $t_{rupture}$ of eq. (3.38) in eq. (3.21) delivers eq. (3.39) which gives the minimum spreading distance $\xi_{rupture}$ causing film rupture:

$$\xi_{rupture} = \left(\frac{2}{3}\right)^{\frac{3}{4}} S_c^{\frac{1}{2}} \left(0.415(\eta\rho)^{\frac{1}{2}}\right)^{-\frac{1}{2}} \left(t_{rupture} + \zeta\right)^{\frac{3}{4}} \qquad (3.39).$$

With eq. (3.35) the minimum bubble size can be estimated if a certain film thickness at the centre of spreading is assumed. Also in these eq. (3.38) and eq. (3.39) ζ and S_e may have to be substituted by ζ' and $\Delta\gamma$ respectively.

For the value of the stream function $f(\sigma)$ the graph presented by Bergink-Martens (1992) was used. From this graph the value of 0.8 for $f(\sigma)$ was extracted and used in the calculations to illustrate the theory explained above in a more numerical way. These calculations will be presented later in this Chapter.

The theoretical approach mentioned above is valid for a radially symmetric spreading particle in two dimensions. However, as will be explained in Chapter 4, experiments were carried out in a rectangular geometry in one dimension (direction). In order to be able to verify the measured spreading velocities with the theory the above mentioned theoretical approach was adapted to a rectangular spreading geometry. The Navier Stokes equations for this one dimensional co-ordinate system are described by eq. (3.40), eq. (3.41) and eq. (3.42):

$$v_\xi \frac{\partial v_\xi}{\partial \xi} + v_z \frac{\partial v_\xi}{\partial z} = -\frac{1}{\rho}\frac{\partial P}{\partial \xi} + \nu\left[\frac{\partial^2 v_\xi}{\partial \xi^2} + \frac{\partial^2 v_\xi}{\partial z^2}\right] \qquad (3.40),$$

$$v_\xi \frac{\partial v_z}{\partial \xi} + v_z \frac{\partial v_z}{\partial z} = -\frac{1}{\rho}\frac{\partial P}{\partial z} + \nu\left[\frac{\partial^2 v_z}{\partial \xi^2} + \frac{\partial^2 v_z}{\partial z^2}\right] \qquad (3.41),$$

$$\frac{\partial v_\xi}{\partial \xi} + \frac{\partial v_z}{\partial z} = 0 \qquad (3.42),$$

where, v_ξ and v_z are respectively the horizontal and vertical velocity components, P is the pressure, ν is the kinematic viscosity, ρ is the fluid density and g is the acceleration due to gravity. The ξ-axis is chosen in the plane of the liquid surface and the z-axis goes into the direction of gravity. Similar to what was described for the radial geometry we can use here the equations Bergink-Martens derived for the horizontal and vertical velocity components that are related to a stream function $f(\sigma)$ in which $\sigma = z\sqrt{a/\nu}$:

$$v_\xi = a\xi \frac{df}{d\sigma} \qquad (3.43),$$

$$v_z = -2\sqrt{av} \bullet f(\sigma) \tag{3.44}$$

In these equations a represents again the constant of proportionality in the velocity distribution and is described by eq. (3.45):

$$a = \frac{\partial \ln A}{\partial t} = \frac{\partial v_\xi}{\partial \xi} \tag{3.45}$$

The next step is to express the Navier Stokes equations and the boundary conditions in terms of $f(\sigma)$ and its derivatives, and to solve the equations. Upon substitution of the relations v_ξ and $v_{z,}$, i.e. eq. (3.43) and eq. (3.44), into the Navier Stokes equation for lateral momentum flux, i.e. eq. (3.40), the following expression is obtained:

$$\left[\frac{\partial f}{\partial \sigma}\right]^2 - f(\sigma)\frac{\partial^2 f}{\partial \sigma^2} = \frac{\partial^3 f}{\partial \sigma^3} \tag{3.46}$$

Eq. (3.46) is a differential equation for $f(\sigma)$ which can be solved by numerical techniques if sufficient boundary conditions are specified. By solving $f(\sigma)$ the corresponding velocity distribution can be found with eq. (3.43) and eq. (3.44). Considering that at the free surface σ=0 and combining eq.(3.41) and eq. (3.43), the relative surface expansion rate equals:

$$\frac{\partial \ln A}{\partial t} = \frac{\partial v_\xi}{\partial \xi} = a\left(\frac{\mathrm{d}f}{\mathrm{d}\sigma}\right)_{\sigma=0} \tag{3.47}$$

Since a is a constant of proportionality, without loss of generality, the boundary condition for $\mathrm{d}f/\mathrm{d}\sigma$ can be chosen:

$$\left(\frac{\mathrm{d}f(\sigma)}{\mathrm{d}\sigma}\right)_{\sigma=0} = 1 \tag{3.48}$$

Furthermore, the vertical velocity v_z=0 at the free surface and, therefore, an additional boundary condition for $f(\sigma)$ is:

$$f(0) = 0 \tag{3.49}$$

To integrate the third order differential eq. (3.46) a third boundary condition must be specified. For that reason it is assumed that a surface tension gradient influences a thin layer on top of the bulk flow. The third boundary condition is then obtained by a

matching condition at the bottom of the layer where the thin layer matches the bulk flow.

A surface tension gradient developed at the free surface generates a tangential shear stress in the surface which is balanced by the viscous shear stress. By applying eq. (3.43) the shear stress φ is expressed by:

$$\frac{\partial \gamma}{\partial \xi} = \varphi = -\eta\left(\frac{\partial v_\xi}{\partial z}\right)_{\sigma=0} = -\eta a \xi \left(\frac{\partial^2 f}{\partial \sigma^2}\right)_{\sigma=0} \sqrt{\frac{a}{\nu}} = -a\xi\sqrt{a\eta\rho}\left(\frac{\partial^2 f}{\partial \sigma^2}(0)\right) \qquad (3.50),$$

where, η (= $\rho\nu$) is the dynamic viscosity of the bulk fluid. To calculate the surface tension gradient the value of $f''(\sigma=0)$ has to be known. This was done by solving eq. (3.46) numerically by means of a 4th order Runga-Kutta scheme, in which $f''(\sigma=0)$ is adjusted till the boundary condition at the bottom of the surface layer is satisfied. The numerical calculation showed:

$$\frac{\partial^2 f}{\partial \sigma^2}(0) = 1 \qquad (3.51).$$

With:

$$\frac{\mathrm{d}\ln A}{\mathrm{d}t} = a \qquad (3.52),$$

eq. (3.50) becomes:

$$\frac{\mathrm{d}\gamma}{\mathrm{d}\xi} = \left(\frac{\mathrm{d}\ln A}{\mathrm{d}t}\right)^{\frac{3}{2}} \xi\sqrt{\eta\rho} \qquad (3.53).$$

If we assume, as we did already above in the theoretical approach for a radially expanding droplet, that only spreading of the droplet occurs, the surface tension gradient can be estimated by:

$$\frac{\mathrm{d}\gamma}{\mathrm{d}\xi} = \frac{\gamma_{LA} - \gamma_{OL} - \gamma_{OA}}{\xi} = \frac{S_c}{\xi} \qquad (3.54).$$

Similar to the procedure elucidated for radial spreading eq. (3.55) can be derived for the spreading distance as a function of spreading time:

$$\xi = 4^{\frac{3}{4}} S_c^{\frac{1}{2}} t^{\frac{3}{4}} \qquad (3.55).$$

The spreading velocity can than be expressed as a function of spreading distance or spreading time:

$$v_\xi = 3S_c^{\frac{2}{3}}\xi^{-\frac{1}{3}} = 3 \bullet 4^{-\frac{1}{4}} S_c^{\frac{1}{2}} t^{-\frac{1}{4}} \qquad (3.56).$$

This theoretical approach for a rectangular geometry was used for the comparison of measured spreading velocities with calculated velocities in a rectangular geometry. The used measurement device, i.e. the overflowing canal technique, will be explained in Chapter 4.

3.3. THEORETICAL RESULTS AND DISCUSSIONS

In the theoretical calculations we have assumed, for the sake of simplicity, that the spreading coefficient S_c equals the surface tension difference $\Delta\gamma$ which is in reality not necessarily the case, but the calculations are only made to investigate the effect of parameters such as droplet size, surface tension difference, liquid viscosity and film thickness on the spreading process and, eventually, the collapse of the film. For these calculations the equations for radial spreading were used.

In fig (3.2) an example of the evolution of the spreading velocity is plotted as a function of the spreading distance.

It can be seen in this figure that the velocity decreases rapidly during the first period of spreading. This is due to the increasing surface area covered by the spreading particle. Therefore, the total shear stress exerted on the underlying liquid will increase and the surface tension gradient will decrease resulting in a decrease of the spreading velocity.

In fig (3.3) the displacement perpendicular to the film surface and the spreading distance is plotted as a function of time. It can be seen that the displacement velocity is the largest at the beginning of spreading which is in conformity with the evolution of the relative surface expansion rate according to eq. (3.24).

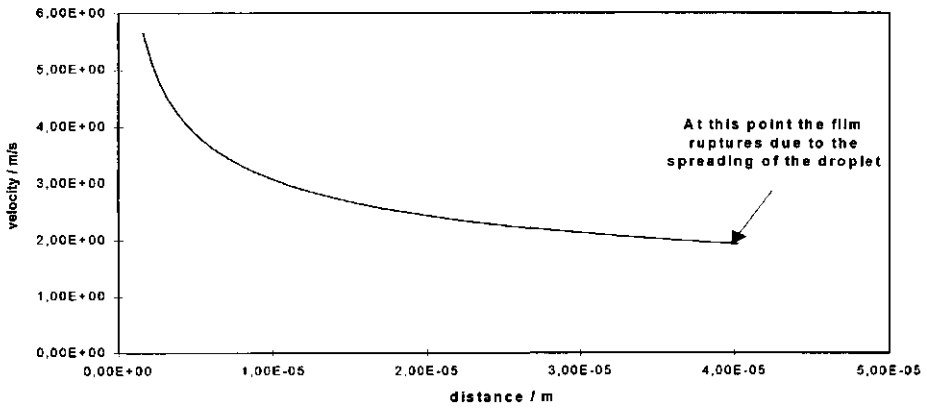

Fig 3.2: ***The evolution of the spreading velocity of a particle with radius 1 μm as a function of the spreading distance according to eq. (3.22) over a film with thickness 10 μm. The spreading coefficient was assumed to be 0.02 Nm^{-1}.***

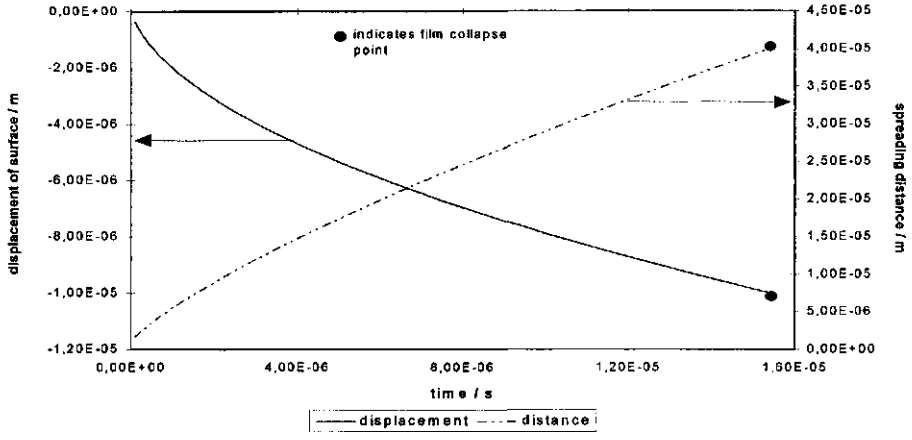

Fig 3.3: ***The displacement perpendicular to the film surface and the spreading distance according to respectively eq. (3.31) and eq. (3.21). The droplet radius was 1 μm, the film thickness 10 μm and the spreading coefficient 0.02 Nm^{-1}.***

In reality it is expected that there is pressure equilibrium over the whole film. This would result in a curvature of also the bottom film. If we assume that this takes place in the same way as the top surface the displacements of the two surfaces would contribute each half of the total displacement plotted in Fig (3.3).

This is not justified considering the higher surface tension of the bottom surface. This results, according to the law of Laplace, in a larger radius of curvature of the bottom surface compared to the top surface. However, to illustrate in an order of magnitude the effect the displacements as a function of distance according to eq. (3.30) are plotted in Fig (3.4).

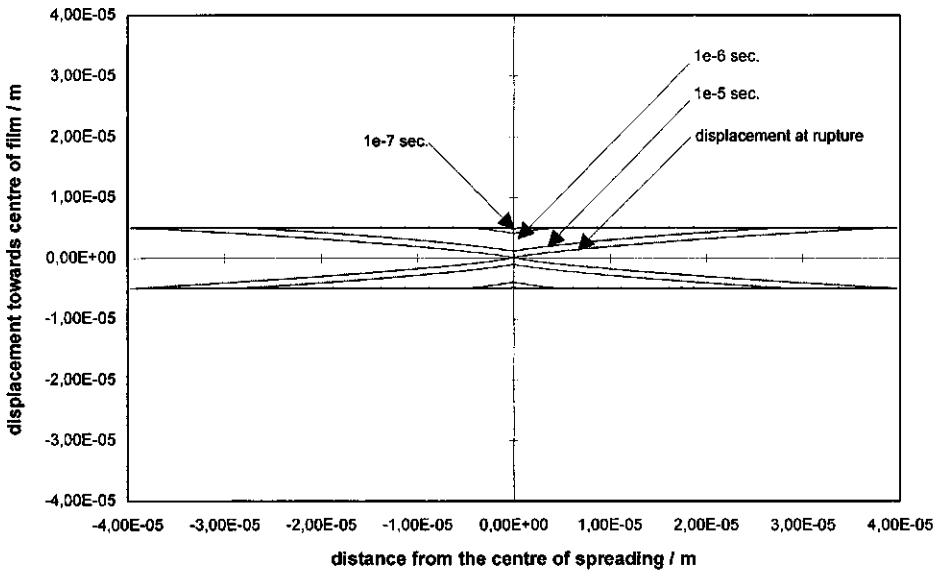

Fig 3.4: ***The displacements of the top and bottom surfaces, i.e. constriction of the film, as a function of spreading distance and spreading time according to eq. (3.29). The film thickness is 10 μm and the spreading coefficient 0.02 Nm^{-1}.***

The two axes coincide in the middle of the film at the centre of spreading. In Fig (3.4) it can be seen that relative to the centre of the film the film surface is concave at the centre of spreading and becomes immediately convex further away from the centre of spreading. This implicates suction at the centre of spreading due to a negative Laplace pressure and an overpressure in the regions surrounding the centre of spreading due to a positive Laplace pressure. This would in favour of the presence of a driving force opposing the film thinning process. The importance of this driving force will be discussed later. The radii of curvature of both the concave and convex regions increase with spreading distance and spreading time. From the theory it can be concluded that there is an effect of the surface tension difference on the spreading. To illustrate the effect of an increasing surface tension difference on the minimum spreading distance to induce film rupture these parameters are plotted in Fig (3.5).

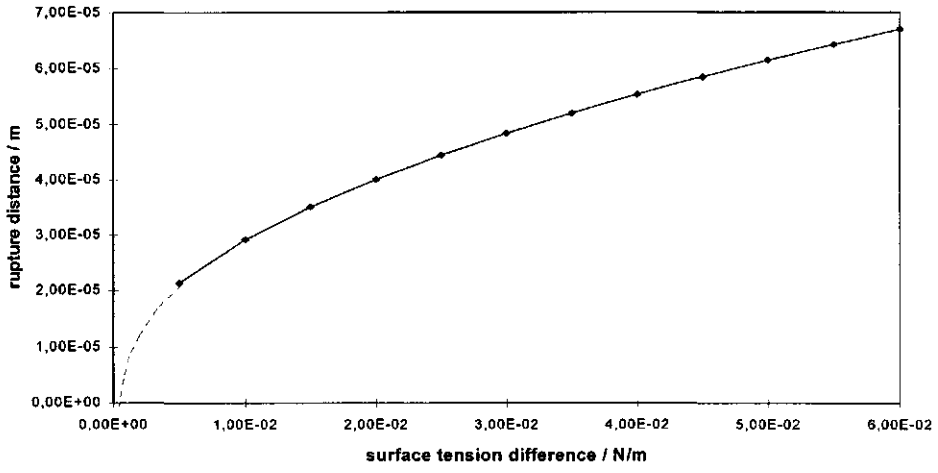

Fig (3.5): The minimum spreading distance to induce film rupture as a function of the surface tension difference according to eq. (3.35). The droplet radius is assumed 1 μm and the film thickness 10 μm.

It can be seen that an increasing surface tension results in an increasing minimum spreading distance. This effect is due to the fact that with higher surface tension differences the spreading velocity is higher and, therefore, the spreading distance at the moment of film rupture will be larger. The time scale plays a role in such a way that the penetration of the movement of liquid into the film takes time. Therefore, high spreading velocities result in smaller penetration distances of the surface motion into the film liquid. Furthermore, from the theory it is clear that the displacement is not proportional to the spreading distance which explaines the flattening of the curve in Fig (3.5).

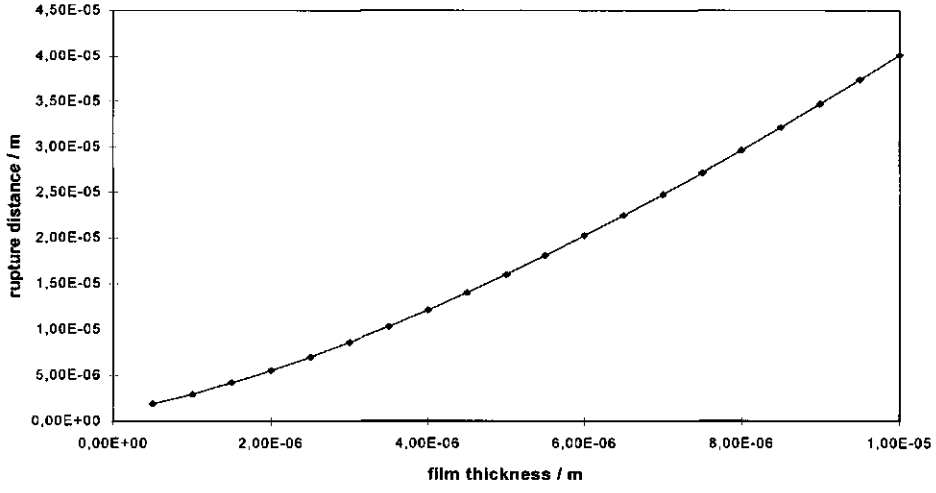

Fig (3.6): ***The minimum spreading distance to induce film rupture as a function of the film thickness according to eq. (3.35). The droplet radius was assumed to be 1 μm and the spreading coefficient 0.02 Nm^{-1}.***

In Fig (3.6) the minimum rupture distance to induce film rupture is plotted as a function of the film thickness. It can be seen that this spreading distance increases more than

proportional with the film thickness. Hence the thicker the film the further the spreading distance to rupture the film must be. From eq. (3.35) it can also be seen that the viscosity of the film liquid has not a large effect on the minimum spreading distance ($\eta^{1/3}$). When the minimum spreading distance to induce film rupture is plotted as a function of the viscosity this suggestion is confirmed.

In Fig (3.7) can be seen that an increase of the viscosity of the film liquid results in a small decrease of the minimum spreading distance. Finally, a spreading droplet without any surfactant is considered. This means that the droplet would spread into a thin layer which breaks up into small droplets as the thickness of the spreading film reaches a critical thickness. Then the maximum film thickness that can be ruptured by this droplet is restricted to the maximum spreading distance that can be obtained by a droplet with certain size. If we assume a critical thickness of the spreading layer 20 Å we can calculate the maximum spreading distance.

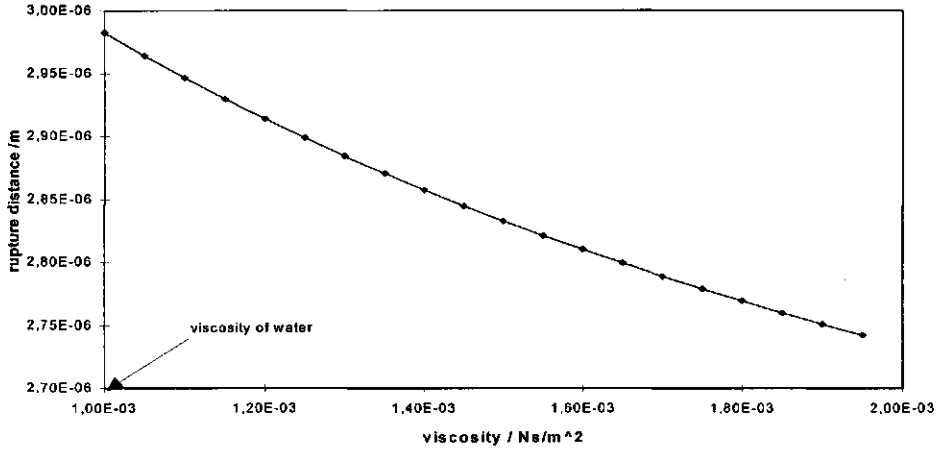

Fig 3.7: ***The effect of the viscosity of the film liquid on the minimum spreading distance to cause film rupture according to eq. (3.39). The droplet radius was assumed 0.1 μm, the spreading coefficient 0.02 Nm^{-1} and the film thickness 1 μm.***

In Fig (3.8) this distance is plotted as a function of the droplet radius. It can be seen that the maximum spreading distance increases relatively to the droplet radius. By using eq. (3.38) and eq. (3.39) the resulting maximum film thickness that can be ruptured can be calculated. The maximum film thickness as a function of the droplet radius is plotted in Fig (3.9). In Fig (3.9) can be seen that the maximum film thickness increases proportional to the droplet radius. If, however, the ratio film thickness / droplet radius is regarded, it increases much in the beginning and flattens of to about 4 or to about 8.7 depending on the spreading coefficient. This can be explained by the spreading velocities of the large droplets. These velocities decrease to a, more or less, constant value which was already observed in Fig (3.2). Consequently, the maximum film thickness that can be ruptured will not increase anymore with increasing droplet radius. However, the value of the spreading coefficient has a large impact on

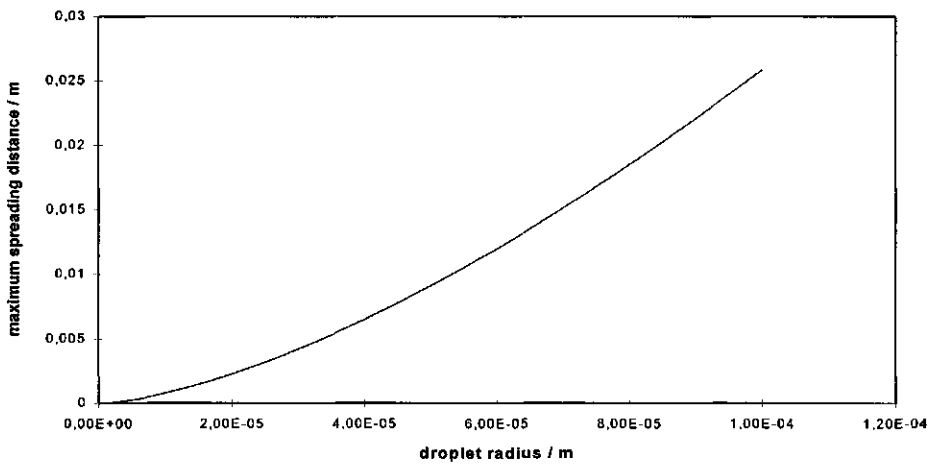

*Fig (3.8): **The maximum spreading distance, before breaking up into small droplets, as a function of the droplet radius according to eq. (3.33).***

the maximum film thickness that can be ruptured. The closer this value is to zero, the larger, the film thickness that can be ruptured, provided the spreading distance is reached and the same droplet radius is assumed. For the sake of clearity, when the spreading coefficient is close to zero still reasonable spreading velocities are developed due to the remaining large surface tension gradient when the droplets are small.

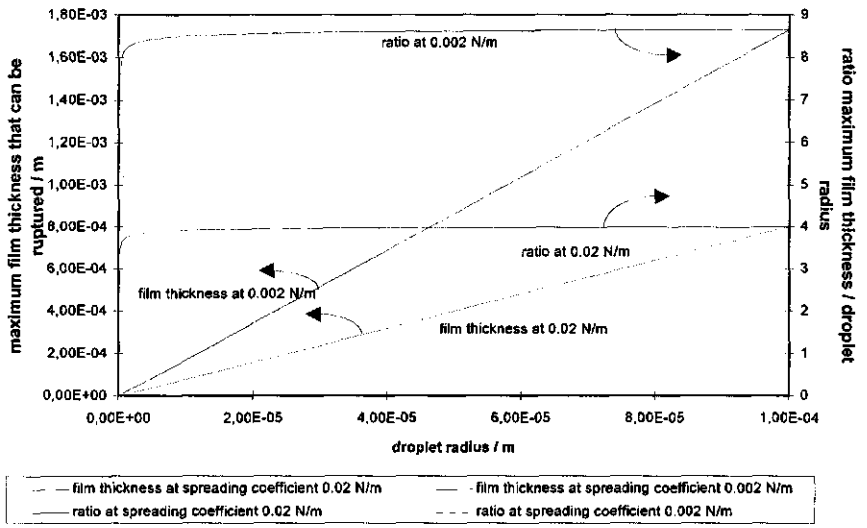

Fig (3.9): The maximum film thickness that can be ruptured and ratio film thickness / droplet diameter as a function of the droplet radius. The spreading coefficient was 0.02 Nm^{-1} and 0.002 Nm^{-1}.

3.4. DISCUSSIONS OF THE THEORY

In the theory presented here it is assumed that the surface tension difference $\gamma_0 - \gamma_1$ is constant. This assumption may not be justified since the surface load Γ_S decreases with spreading distance due to the increasing surface area at the front of the

monolayer. However, if we assume enough supply of surface active components from the spreading particle we can say that γ_0 will be constant. The surface area available for spreading is in the case of a bubble, always finite. This would mean that the 'clean' surface in front of the monolayer is compressed during the spreading process. Hence, due to the presence of surface-active impurities, the 'clean' surface yields, due to the surface compression, a lower surface tension γ_l which would slow down the rate of spreading. Therefore, the surface rheological behaviour of the 'clean' surface in front of the monolayer may be important for the proceeding of the monolayer. In the case of a very stiff clean surface, i.e. a high surface dilational modulus $E = \mathrm{d}\gamma/\mathrm{dln}A$, the surface tension would decrease rapidly and the driving force for spreading, i.e. the surface tension gradient as defined in eq. (3.17), would become smaller. This results in a decreasing spreading velocity that may even becomes zero or negative. The latter would result in a receding monolayer.

On the other hand, if we take the theory suggested by Prins (1989) that the spreading process can be considered as the propagation of a longitudinal wave, the limited surface area could result in a reflection of the wave when it approaches itself at the opposite side of the bubble surface. This may lead to damping of the wave and, consequently, stop further propagation of the spreading process.

The spreading process, taking place at the top film surface, introduces also expansion of the surface area at the bottom side of the film due to the curvature that is developed. This results in a surface tension gradient which would trigger surface motion towards the centre of spreading. The connected shear stress exerted by this moving surface on the adjoining liquid results in liquid movement towards the centre of spreading which would oppose the thinning process. There are at least three reasons to believe that this will have only a minor contribution.

1) If we look to the theoretically calculated displacement of the film surfaces in Fig 3.4, we can see that at the centre of spreading the radius of curvature is very small. As was mentioned before, due to the curved surface at the centre of spreading the Laplace pressure will be lower compared to the region below the

moving surface further away from the centre of spreading and the still planar region of the film where the spreading material did not arrive yet. This results additionaly in a liquid flow towards the centre. On the other hand, there is a good reason to believe that at the centre of spreading, which is the stagnation point of liquid flow, the radius of curvature will not be that small and the Laplace pressure difference effect is smaller. However, if we speculate that the shear stress exerted by the spreading surface on the underlying liquid is bigger than the effect of the pressure difference on return flow of liquid towards the centre of spreading, the final result will still be a thinning of the film and, eventually, rupture and coalescence of the two bubbles separated by this film.

2) The relative surface expansion rate of the top surface is, certainly in the beginning of the spreading, much higher than the relative surface expansion rate of the bottom surface. Therefore, the liquid drag away from the centre of spreading is expected to be much higher than the induced liquid flow towards the centre of spreading at the bottom surface.
3) The bottom surface will also be supplied by film surfactant which will decrease the surface tension gradient resulting in a decreased effect of the Laplace pressure difference within the film as was suggested in 1).
4) Due to the dimensions of the film, i.e. film thickness, liquid flow away from the centre near the moving surface and return flow near the opposite film surface will be more difficult the further the penetration of motion of film liquid proceeds from the moving surface into the film. Considering the very low Reynolds numbers, as already mentioned in Chapter 2, this would not be possible.

This theory does not account for hydrostatic and capillary pressures which are developed because the surface does not remain flat during the spreading process. Ahmad and Hansen (1972) already drew attention to this feature which would counteract the spreading process. Since we are dealing with very thin liquid films we assume no significant effect of gravity or inertia on the film thinning process. Furthermore, as was already mentioned in Chapter 2, the Reynolds number of flow in

films with these thicknesses, i.e. around 1 μm, is very small, i.e. in the order of magnitude of 0.1. Consequently, no return flow within the film has to be expected. However, the displaced volume of liquid must stay somewhere. Borgas and Grotberg (1988) and Gaver and Grotberg (1992) payed attention to this fact. Their theory suggests that the displaced volume of liquid is build up gradually towards the front of the spreading. They found evidence to this by analyzing photographs of spreading monolayers. However, their analysis was valid for monolayer spreading on viscous thin films supported by a solid wall where the streaming profile is completely different. Furthermore, the front of spreading is expanded during the spreading process. This may level out the build up of displaced liquid. Further hydrodynamic analysis would be necessary to include better the conservation of mass during the spreading process, i.e. displacement of liquid resulting in film thinning.

Another assumption is that the surface active component of the monolayer is not, or hardly soluble in the underlying liquid. In the case of diffusion of surface active material from the monolayer to the bulk liquid, the actual spreading pressure would decrease resulting in a lower spreading velocity. The decrease of the propagation speed of the expanding monolayer due to diffusion exchange with the bulk liquid is related to the dilational surface viscosity of the expanding monolayer. A somewhat similar situation was investigated by van Voorst Vader et al. (1964) but this has not been taken into account in the present study.

REFERENCES CHAPTER 3.

Ahmad, J. and Hansen, R.S., J. Colloid and Interface Science, **38**:601 (1972).

Bergink-Martens, D.J.M., Bos, H.J., Prins, A., J. Colloid and Interface Science, **165**:221 (1994).

Bergink-Martens, D.J.M., "Interface dilation, the overflowing cylinder technique", PhD Thesis, Agricultural University Wageningen (1993).

Borgas, M.S., Grotberg, J.B., J. Fluid Mech., **193**:151 (1988).

Gaver, D.P., Grotberg, J.B., J. Fluid Mech., **235**:399 (1992).

Harkins, W.D., Feldman, A., J. Amer. Chem. Soc., **44**:2665 (1922).

Joos, P., Pintens, J., J. Coll. Int. Sci., **60(3)**:507 (1977).

van Voorst Vader, F., Erkelens, Th.F., van den Tempel, M., Trans. Faraday Soc., **60**:1170 (1964).

EXPERIMENTAL TECHNIQUES

4.1. INTRODUCTION

The most fragile structures (for rupture) in a foam are the thin liquid films between the bubbles. Therefore, the physical structure in a foam on which this study focusses is the thin liquid film. The spreading behaviour of oil droplets and the mechanism of film thinning and eventually film rupture due to the spreading of droplets over the surface of the films between the bubbles in a foam, is subject of investigation in this study.
It will be attempted to describe the local thinning of a liquid film when, due to spreading of surface active material out of a particle over the film surface, film liquid is dragged away from the center of spreading to such an extent that the film ruptures. This implicates that the hydrodynamic processes, that take place in the film during spreading, have to be quantified. It is the aim to predict under what circumstances of spreading and properties of the spreading phase and the film liquid the film will rupture.
The following steps in the whole process can be distinguished: 1) transport of the particle to the film surface, 2) dewetting of the particle ensuring physical contact between the particle surface and the film surface, 3) spreading of the particle over the film surface and 4) movement of the film bulk liquid induced by the surface movement due to spreading material.
The experiments were performed to characterize the spreading process in terms of dewetting, spreading, spreading velocity and film rupture. However, it is very difficult to determine the spreading behaviour of very small droplets (i.e. a radius of 1-100 μm) over thin liquid films and therefore experiments were done to investigate the spreading behaviour of relatively large oil droplets (i.e. a radius of 0.5-1 mm) over the surfaces of liquid bulk systems instead of thin liquid films. It was assumed that this kind of spreading behaviour provides usefull information to be used to describe the spreading behaviour of very small droplets over the surface of thin liquid films. The 'model' systems used in this study have some properties in common with systems existing in practice (§4.2). The surface properties as the equilibrium and dynamic surface and

interfacial tensions were measured using an overflowing cylinder technique (§4.3). Another surface property called the surface dilational modulus was investigated using a recently developed ring-trough technique (§4.4). The relation between the droplet size and the thickness of the thin liquid film that can be ruptured due to the spreading of this droplet, was investigated using a free falling liquid film technique (§4.5). In order to be able to measure the spreading velocity of a monolayer out of a spreading oil droplet an overflowing canal technique was developed (§4.6). The spreading velocity of an oil droplet into a relatively thick layer was measured by applying an image analysis technique on video pictures of a spreading oil droplet on the expanding surface of an overflowing cylinder (§4.7). The spreading behaviour was investigated as a function of the available film surface and the mechanism responsible for the rupture of a model film with a finite surface, i.e. the dewetting process, the hydrophobic mechanism or spreading mechanism, was investigated (§4.8). Some additional rheological techniques were used to measure, for example, the bulk viscosities (§4.9).

4.2. THE SYSTEMS USED IN THIS STUDY

Since foodstuffs are all complex systems the experiments were performed using commercial edible soya oil (ARO) as the surface entering material (i.e. oil particles). Although it is a 'dirty' system implicating it may contain surface active components, Ronteltap (1989) reported that it does not even spread on pure water.

Harkins and Feldman (1922) and Harkins (1941) mentioned the positive effect of surface active impurities on the spreading behaviour of liquids. Therefore, the emulsifier Tween 80 (i.e. polyoxy-ethylene-(20)sorbitan-monooleate, Merck-Schuchardt) was added in different aliquots ranging from 10^{-4} % w/w up to 20 % w/w to the soya oil in order to introduce surface active impurities in the oil phase. The molar weight of the Tween 80 was $1309.7*10^{-3}$ kg·mol^{-1}.

The aqueous phases used in this study were Teepol (RECA TP) solutions containing various concentrations of Teepol, or lager beer degassed by stirring during at least 5

hours. Teepol is a commercial available anionic detergent which has to be diluted for use. The main components are alkarysulfonate, alcoholethersulfate and alcoholethoxylate. The amount of active components is about 15%.

The surface rheological properties as for example the surface tension in expansion or compression and the surface dilational modulus of Teepol solutions and beer (i.e. more or less a protein solution) are expected to be different. For this reason it is expected that the spreading behaviour of material over the surfaces of these aqueous solutions wil be different as is discussed in Chapter 2 and Chapter 3.

In some experiments an emulsion was made by emulsifying an amount of soya oil (2-40% w/w) in the liquid using a laboratory scale homogenizer (Rannie) at various pressures ranging from 0.5 to 5 bar or an Ultra Turrax mixer (Janke & Kunkel KG). The droplet-size distributions were measured using a light scattering technique as described by Walstra (1968) or the size of single droplets was determined by using a microscope.

4.3. THE OVERFLOWING CYLINDER TECHNIQUE

A radially expanding liquid surface as is found during the spreading of surface active material from a particle or a droplet is pure dilational. In order to investigate the surface properties during steady state surface expansion of the aqueous solutions and the oil, an overflowing cylinder technique as described by Piccardi and Ferroni (1951, 1953), Padday (1957), Joos and De Keyser (1980), Bergink-Martens et al. (1990) and Bergink-Martens (1993) was used. With this device a pure dilational expanding liquid surface or interface is created.

The surface and interfacial tensions were always measured by using a Wilhelmy plate technique. Sometimes use was made of roughened glass plates and at other times roughened glass cylinders as described by Bergink-Martens et al. (1992). There was no difference between the measured tensions using glass plates or glass cylinders.

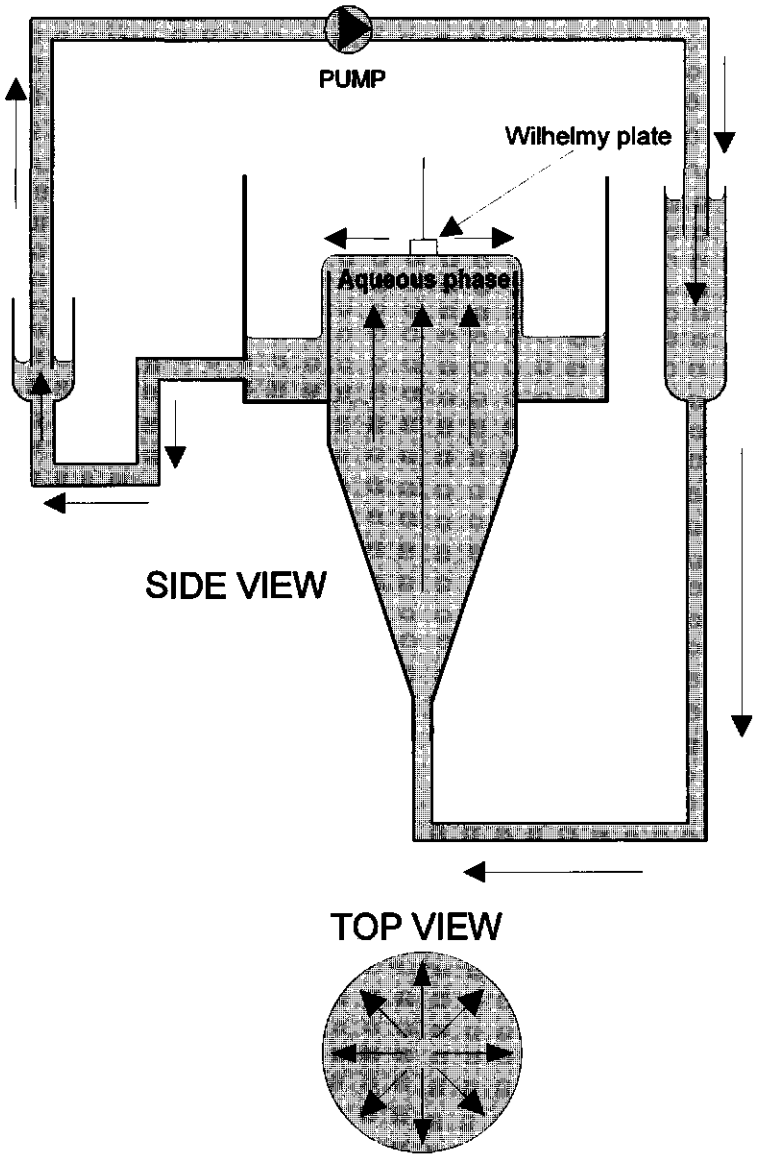
PUMP
Wilhelmy plate
Aqueous phase
SIDE VIEW
TOP VIEW

A schematic representation of the device to measure surface tensions under steady state expansion is presented in Fig 4.1. The experiments have been carried out on a temperature controlled metal cylinder with a diameter of 0.08 m, a height of 0.8 m and a wall thickness of 0.001 m. The flow rate could be adjusted by using a needle valve and a flow meter.

To avoid pumping vibrations that can disturb the horizontal top surface of the overflowing liquid, the pump was uncoupled from the overflowing cylinder as can be seen in Fig 4.1. While the experiment is running the pump continuously sucks liquid out of the smaller vessel, which is closely connected to the overflowing cylinder, into the larger vessel. This way a constant hydrostatic pressure difference between the liquid level in the larger vessel and the surface of the overflowing cylinder is established. The liquid flows from the larger vessel through the cylinder up to the top of the cylinder were the liquid is allowed to flow over the rim of the vertical inner cylinder forming a wetting film on the outside of the inner cylinder. The wide conical shape (1:10) of the instrument before it becomes cylindrical provides a laminar flow field of the liquid in the cylinder. From the outer cylinder the liquid flows into the smaller vessel out of which the liquid is pumped to the larger one again. The closed system contains about 4 liters of liquid. When the cylinder is positioned in a perfect vertical position, a pure axially symmetric velocity distribution with zero velocity in the centre of the circular meniscus is created. A thorough discussion of the device is given by Bergink-Martens (1993).

Bergink-Martens (1993) derived a relation between the relative surface expansion rate ($d\ln A/dt$) and the velocity (v_R) as a function of the distance (R) from the centre of the circular meniscus in the overflowing cylinder. In the vicinity of the centre the radial velocity appears to be linearly dependent on R and the relation between the $d\ln A/dt$ and v_R is given by eq. (4.1):

$$\frac{d\ln A}{dt} = \frac{v_R}{R} + \frac{\partial v_R}{\partial R} = \frac{2v_R}{R} \qquad (4.1).$$

To obtain the relative surface expansion rate the velocity of the radially expanding liquid surface was measured by using a differential Laser Doppler Anemometry technique (LDA). This technique is widely used for the measurement of the flow velocity of bulk liquids and gases and some practical instruments are mentioned by Watrasiewicz and Rudd (1976), Durst et al. (1981), Drain (1980) and Wiedemann (1984). A detailed description of the theory of differential Laser Doppler Anemometry is reported amongst others by Drain (1980) and Durst et al. (1981). The first application of this technique to measure interfacial velocities of two non mixing liquids in a channel is described by Ollenik (1983). In the present study this technique was used to measure the velocity of a liquid-gas interface.

One of the main characteristics of a LDA setup is the intersection of two coherent linearly polarized laser light beams to form a probe volume where the velocity has to be measured. It is essential that there are light scattering particles in the liquid or in the gas in which the velocity has to be measured, and that these particles have the same velocity as the liquid or gas, the liquid-gas surface or the liquid-liquid interface. There are several measurement methods that make use of the Doppler characteristics. The present method is analyzing the light scattered by the particles that are going through the probe volume and can be compared with the so called Fringe model as reported in literature by, amongst others, Drain (1980) and Durst et al. (1981).

Due to the polarization of the laser light beams an interference pattern in the probe volume is obtained at the point where the beams intersect. The bright (maximum light intensity) and dark (minimum light intensity) fringes of the interference pattern are a result of the electromagnetic waves of the light which are exactly in phase where the bright fringes are found, and which are 180° out of phase where the dark fringes are found. The direction of the fringes is parrallel to the bisector of the direction of the beams. The distance (d) between either the bright fringes or the dark fringes are related to the wavelength of the laser light (λ) and the angle (θ_B) with which the laser beams intersect. This relation is given in eq. (4.2):

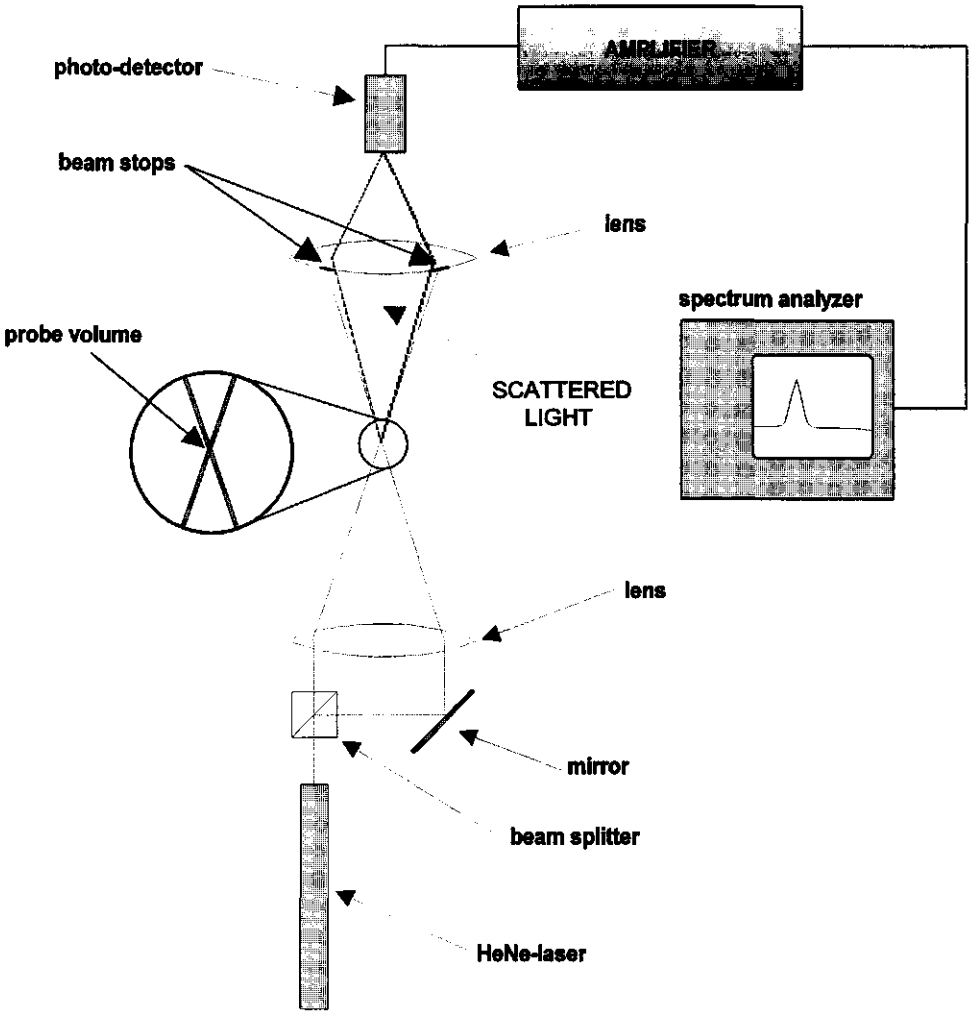

Fig 4.2: Representation of the experimental LDA setup used to measure the surface velocity in the overflowing cylinder.

$$d = \frac{\lambda}{2\sin\left(\frac{\theta_B}{2}\right)} \qquad (4.2).$$

A particle that moves with a velocity (v_P) perpendicular to the direction of the fringe pattern in the probe volume will scatter light in all directions with fluctuations in the intensity as a result of the bright and dark fringes. The frequency (f_D) of the intensity fluctuations is described by eq. (4.3):

$$f_D = \frac{1}{t} = \frac{v_P}{d} = \frac{2 v_P \sin\left(\frac{\theta_B}{2}\right)}{\lambda} \qquad (4.3),$$

where t is the time a particle needs to travel from fringe to fringe. Eq. (4.3) shows that by measuring the frequency of the fluctuations in the intensity of the scattered light the velocity of the particles can be calculated. The frequency obtained by using this model is equal to the Doppler frequency that is found by measuring the frequency shift between the scattered light and the laser beams as described by Drain (1980) and Durst et al. (1981).

When particles intersect the probe volume with an angle ϕ_P that is different from 90° compared to the direction of the light fringes in the probe volume, eq. (4.3) is also valid if v_P is substituted by $v_P \sin \phi_P$.

In this method the measured frequency is independent of the position where the scattered light is detected because the frequency of the intensity fluctuations of the scattered light is equal in all directions.

The total setup of the device used in this study is drawn schematically in Fig 4.2. The device consists of a linearly polarized light beam from a Helium-Neon laser (Melles Griot, λ = 632.8 nm, 5 mW) which is divided into two coherent light beams with equal intensity by means of an (50-50%) optical beam splitter. The beams are directed parallel to a positive lens with a focal length f=16 cm by using a mirror. By this lens the two laser beams are crossed at the surface of which the velocity has to be

measured. For reasons that will be explained later the angle of incidence was chosen in such a way that maximum reflection and detection of the light is obtained. Part of the forward scattered light is focussed on a photo-detector (HLD,TAM) by a second lens with a focal length f = 7 cm. The reflected laser beams are stopped by two beam stops on the lens because impact of the two laser beams on the detector would cause an extreme large noise signal due to the extreme high intensity of the laser beams compared to the intensity fluctuations of the scattered light.

The intensity fluctuations of the scattered light are detected by the photo-detector and are transformed by the latter into voltage fluctuations in the generated electronic signal. This electronic signal is analyzed by using a Fast Fourier Transform spectrum analyzer (Stanford SR 760 FFT) which determines the frequency spectrum of the voltage fluctuations in the electronic signal. The spectrum analyzer relates the found frequencies with the amplitudes corresponding to the voltage fluctuations in the electronic signal. In this way the frequencies of large amplitude fluctuations in the signal are assigned to be more significant than frequencies of small amplitude fluctuations. Therefore, the distinction is made between frequencies due to the intensity fluctuations in the scattered light, which has a high intensity and the frequencies due to noise in the electronic signal either originating from the electronic hardware or from other light sources.

The system was tested by using a horizontal rotating Aluminum disk on which the two laser beams were projected as presented schematically in Fig 4.3. The direction of the fringes in the interference pattern was perpendicular to the direction of the angular velocity of the disk. The roughness of the disk provided enough light scattering for detection. The frequency of the intensity fluctuations of the scattered light was measured at different angular velocities of the disk. This was done by projection of the probe volume at different distances from the centre of the disk. The angle ϕ_B between the two laser beams was 23.4°. The frequencies of the voltage fluctuations in the electronic signal coming from the photo-detector were measured by the spectrum

analyzer over a period of 20 seconds. During this period an averaged frequency spectrum was obtained..

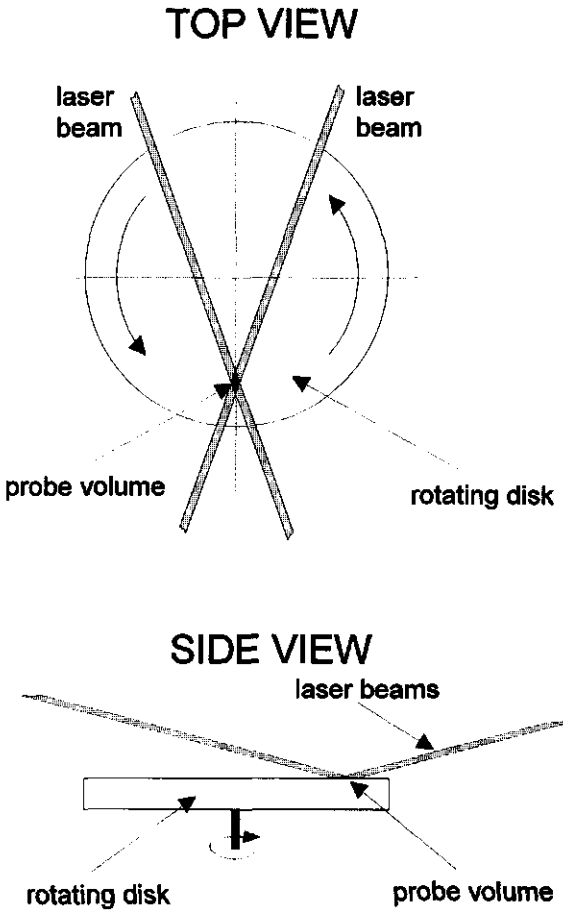

Fig 4.3: A presentation of the setup to calibrate the LDA technique.

A plot of the measured frequencies versus the surface velocity (v_A) at positions at different distances from the centre of the rotating disk is presented in Fig 4.4. By using linear regression a line can be fitted through the measurement points. The slope of

this line was $6.4 \cdot 10^5$ m^{-1} (R^2=0.998). The theoretical slope (ψ) can be calculated using eq. (4.4):

$$\psi = \frac{f_D}{v_A} = \frac{2 \sin\left(\frac{\theta_B}{2}\right)}{\lambda} \qquad (4.4).$$

Using eq. (4.4) and the applied angle between the laser beams of 23.4° a theoretical slope of $6.41 \cdot 10^5$ m^{-1} was calculated. The values of the theoretical and the experimental slopes were in good agreement and from these results it was concluded

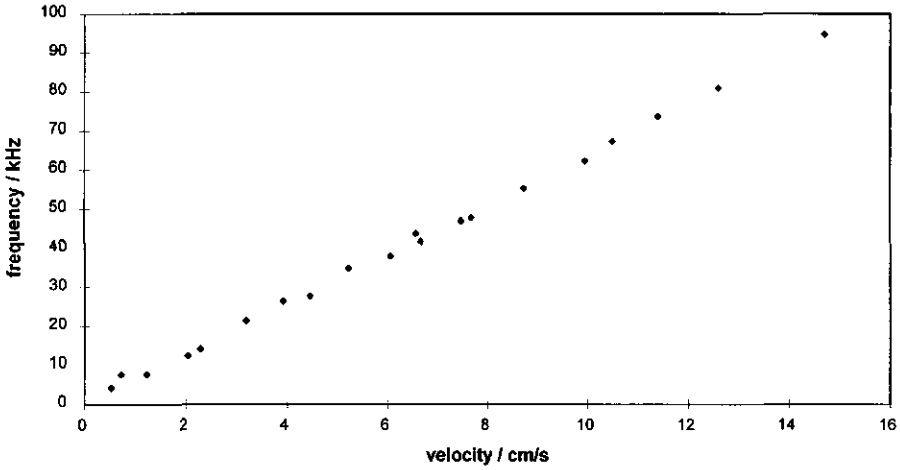

Fig 4.4: ***The results of the frequency measurement, using the LDA-technique, on a rotating aluminum disk. The frequency is plotted as a function of the angular velocity of the disk.***

that the relation between the velocity of the scattering surface and the measured frequency of the intensity fluctuations of the scattered light is described by eq. (4.3).
In order to test the equipment on a liquid surface a petri dish filled with clean water was placed on the rotating disk. Since clean water does not contain particles that are

able to scatter light, talcum powder (Talcum Ph. Eur. from OPG Farma) was sprinkled on the liquid surface. Talcum powder is experienced to give very good scattering of the laser light. The particle-size distribution of the talcum powder was determined by sifting. The diameter of about 90% of the particles was smaller than 70 μm and 40% of the particles was even smaller than 30 μm. The used talc powder was tested on its effect on the surface tension of the liquid. When sprinkling talcum powder on the clean surface of water (i.e. having a surface tension of 72 $mN \cdot m^{-1}$) this did not result in a decrease of the surface tension of the water. This indicates that the talcum does not contain surface active components. Furthermore, the talcum powder particles have very good floating properties. When particles were brought on Teepol-solutions with very low surface tensions (i.e. 27 $mN \cdot m^{-1}$) they were not wetted by the liquid and therefore did not sink into the liquid bulk within a time period of 30 minutes.

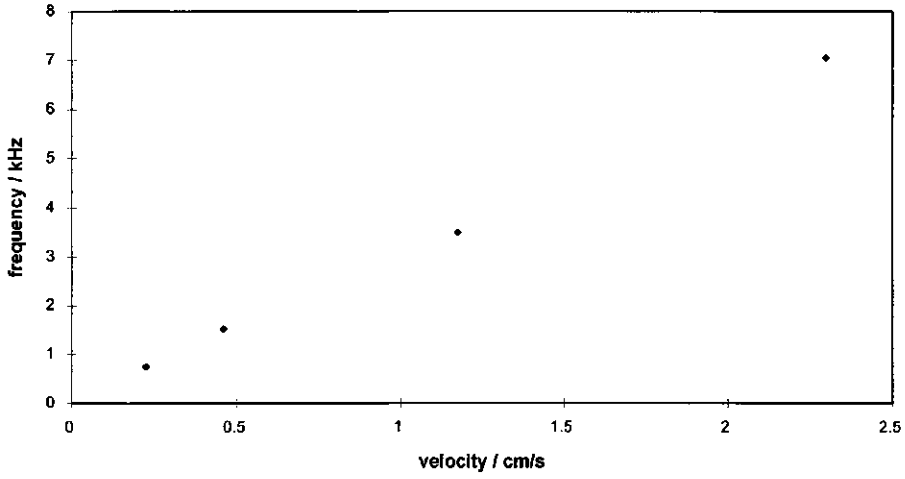

Fig 4.5: ***Surface velocities measured at a water surface containing Talcum powder in a rotating Petri dish at different distances from the centre of rotation.***

The measured frequencies of the intensity fluctuations in the electronic signal coming from the photo-detector are plotted in Fig 4.5 versus the surface velocities measured at different distances from the centre of rotation of a water surface containing talcum powder particles.

In these experiments the angle θ_B between the laser beams was 10.7°. Similar to what is done in Fig 4.4, a line was fitted through the measurement points using linear regression. The slope of this line was $3.07 \cdot 10^5$ m^{-1} (R^2=0.9999). The theoretical slope calculated using eq. (4.4) was $2.95 \cdot 10^5$ m^{-1}. The small difference between the experimental value and the theoretical value of the slope is not significant and the conclusion was drawn that the velocity of a liquid surface containing talcum powder particles can be measured accurately by using the present technique.

This technique was applied to the overflowing cylinder in the way depicted in Fig 4.6. In the method used in this study the two laser beams are placed in reflection on the expanding surface of the overflowing cylinder in such a way that the probe volume is positioned exactly in the air-liquid interface as is also described by Ollenik (1983) for a liquid-liquid interface.

The bisector of the beam directions, which is the direction of the fringes in the interference pattern, is perpendicular to the direction of the surface velocity as can be seen in Fig 4.6. The angle of incidence of the laser beams with the planar liquid surface, as depicted in Fig 4.6, appeared not to influence the measured frequency of the intensity fluctuations of the scattered light coming from the aluminum disk or the water surface containing talcum particles. However, in the case of the surface of the overflowing cylinder the angle of incidence of the beams with the planar liquid surface was chosen in such a way that maximum reflection and detection of the light is obtained. The advantage of placing the laser beams this way in reflection on the surface is that only information from the surface is obtained and not from the underlying subsurface layers in the liquid.

This is of crucial importance in the measurement of the surface velocity because the decrease of the radial velocity in the subsurface layers in the liquid is very large as

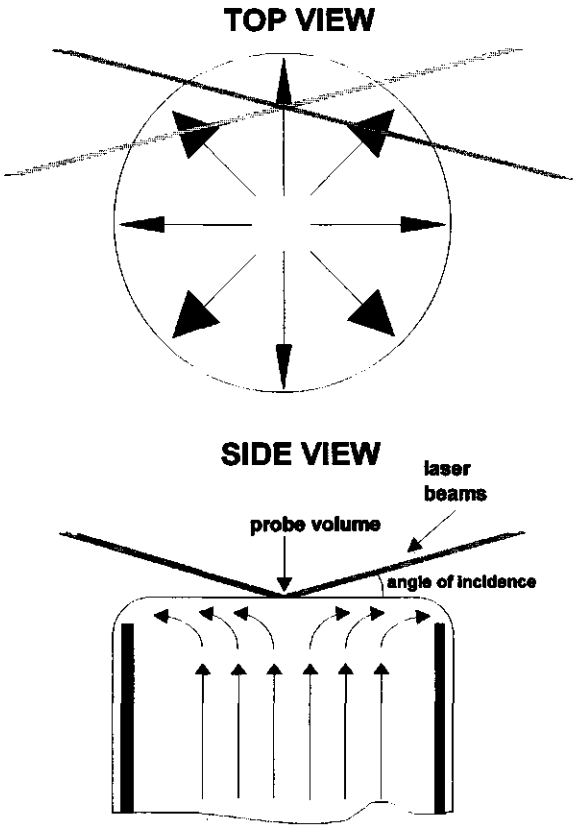

*Fig 4.6: **Positioning of the laser beams on the surface of the overflowing cylinder.***

described by Bergink-Martens (1993). When also light scattered by particles present in the subsurface layers was detected, the frequency spectrum of the intensity fluctuations in the scattered light was much wider having additional low frequencies due to the lower velocity of these particles. This was found during experiments in which the angle of incidence was increased to approximately 40°. Furthermore, to obtain maximum reflection the plane of the polarization of the laser light was always horizontal.

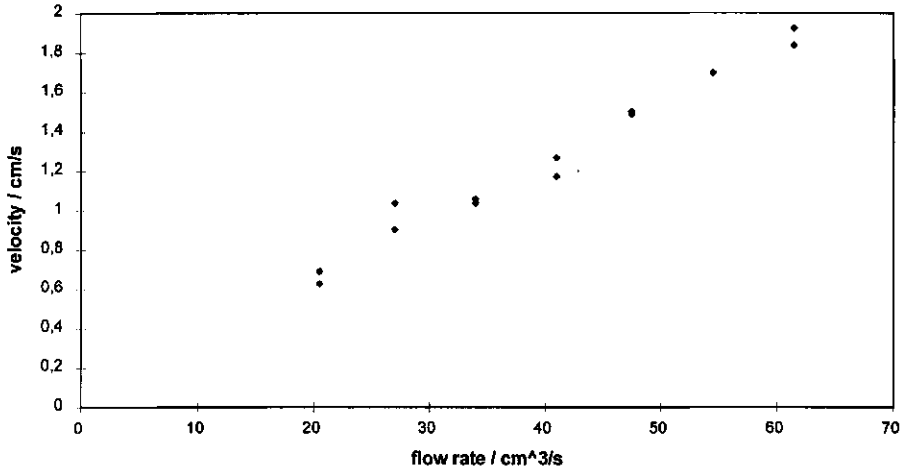

Fig 4.7: The surface velocity of an expanding water surface in the overflowing cylinder.

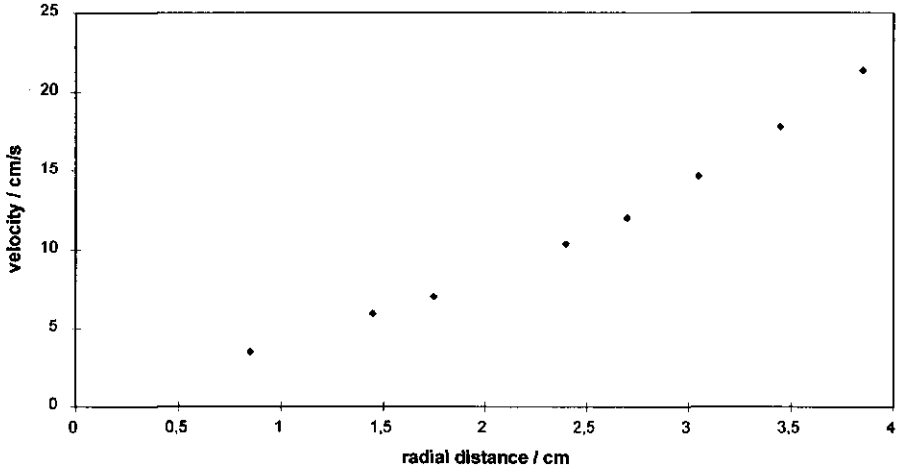

Fig 4.8: The results of velocity measurements on a Teepol-solution in the overflowing cylinder as a function of the radial distance by using the LDA-technique.

By applying eq. (4.3) to the expanding surface in the overflowing cylinder the value of v_R in eq. (4.1) can directly be measured as v_P. By moving the probe volume over a line radially from the centre of the meniscus, the dependency of v_R on the radial distance from the centre can be measured. The talcum powder particles were brought on the circular surface of the overflowing cylinder by means of a vibrating gutter. To ensure that enough particles pass through the measurement probe the particles were brought on the surface at a position 2 cm in the upstream direction from the interference pattern of the probe volume. Bergink-Martens (1993) concluded that at this distance the particles have more than enough time to accelerate until they have obtained the surface velocity. From model calculations performed by Bergink-Martens (1993) she concluded that especially for surfactant solutions as investigated in this study the velocity of the talcum powder particles is equal to the velocity of the overflowing liquid surface. Bergink-Martens (1993) developed a theory which describes the surface velocity of a liquid in an overflowing cylinder. By applying this theory to pure water she came to the conclusion that the surface velocity of the expanding water surface is more or less proportional to the flow rate of the water in the system. In Fig 4.7 the measured velocity at a radial distance of 2.95 cm from the centre of the expanding circular water surface is presented as a function of the flow rate. The angle θ_B between the laser beams was 11°. The measured values are in good agreement with the experimental values obtained by using a photographic technique and the theory of Bergink-Martens (1993) who found a surface velocity v_r = 1.3 $cm \cdot s^{-1}$ at this radial distance from the centre and at a flow rate of 33.3 $cm^3 \cdot s^{-1}$.

In Fig 4.8 the measured surface velocities of a 0.3 % v/v Teepol solution are presented as a function of the radial distance. The flow rate was 33.3 $cm^3 \cdot s^{-1}$ and the angle θ_B between the laser beams was 11°. The measured velocities are also in good agreement with the values reported by Bergink-Martens (1993).

Additionally, the velocity profile of an expanding beer surface in the overflowing cylinder is depicted in Fig 4.9. In this experiment the applied flow rate was also 33.3 $cm^3 \cdot s^{-1}$ and the angle θ_B between the laser beams was again 11°. By comparing Fig

4.7, Fig 4.8 and Fig 4.9 it can be seen that the Teepol solution developes a much higher surface velocity than the water, and that the beer developes only a small increase in the surface velocity. According to Bergink-Martens (1993) this is due to the surface tension gradient that can be developed by the various liquids in the overflowing cylinder. The larger the surface tension gradient the higher the surface velocity that is found. In the case of pure water there exists no gradient and the surface velocity is governed hydrodynamically as Bergink-Martens (1993) discussed in detail.

The reproducebility was very good for all solutions investigated in this study. A maximum variation of 500 Hz which corresponds to an accuracy of 0.1 $cm \cdot s^{-1}$ in the surface velocity was found.

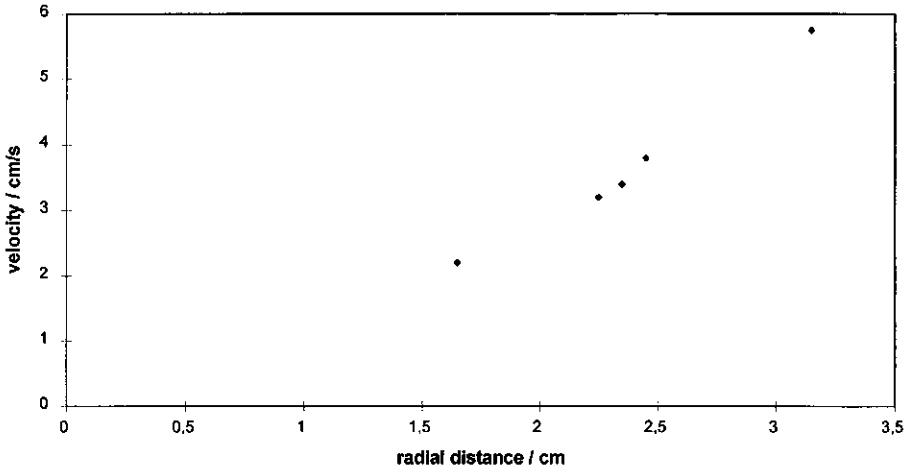

Fig 4.9: ***The surface velocity of beer in the overflowing cylinder as a function of radial distance.***

The conclusion was drawn that the calculated velocity using eq. (4.3) equals the velocity of the particles moving on the surface of the overflowing cylinder. By using

this measuring technique the velocity of the expanding surface could be measured and used in the interpretation of the spreading velocity of oil droplets over that surface as will be discussed later.

A modified overflowing cylinder made out of glass, with a diameter of 0.06 m, a height of 0.5 m and a wall thickness of 0.0033 m was used to measure the tensions of the oil-liquid interfaces in expansion as described by Bergink-Martens (1993). A schematic representation of the device is given in Fig 4.10. The aqueous solution is pumped upwards through the inner cylinder. The outer glass cylinder with a diameter of 9.5 cm is higher than the inner cylinder. This way it is possible to pump the aqueous solution against an oil phase.

When starting up an experiment the system is filled with the aqueous solution till above the rim of the inner cylinder and oil is poured gently on top of the aqueous phase avoiding mixing of the two phases. After this procedure the flow is started. By reducing the volume of aqueous solution and by adding oil, a wetting aqueous film is formed on the outside of the inner cylinder. The flow rate of the aqueous phase could be adjusted using a needle valve and a flow meter. The flow rate had to be relatively high to prevent the outside of the overflowing cylinder being wetted by the oil phase due to rupture of the thin aqueous film. A flow rate that was too high, however, resulted in spontaneous emulsification of the oil phase in the aqueous phase due to instabilities over the interface of the wetting film.

The closed system contains about 4 litres aqueous solution and about 400 ml of oil. The length of the wetting film could be adjusted by changing the amounts of oil and aqueous solution. The expanding water-oil interface has the same steady state velocity profile as the air-water overflowing cylinder discussed previously and which is measured and discussed by Bergink-Martens (1993).

In the present investigations the velocity of the expanding oil-water interface was not measured. The interfacial tension in expansion was measured using a Wilhelmy plate technique with a roughened glass plate. The height of the oil layer on top of the overflowing liquid was chosen in such a way that during calibration and the experiment

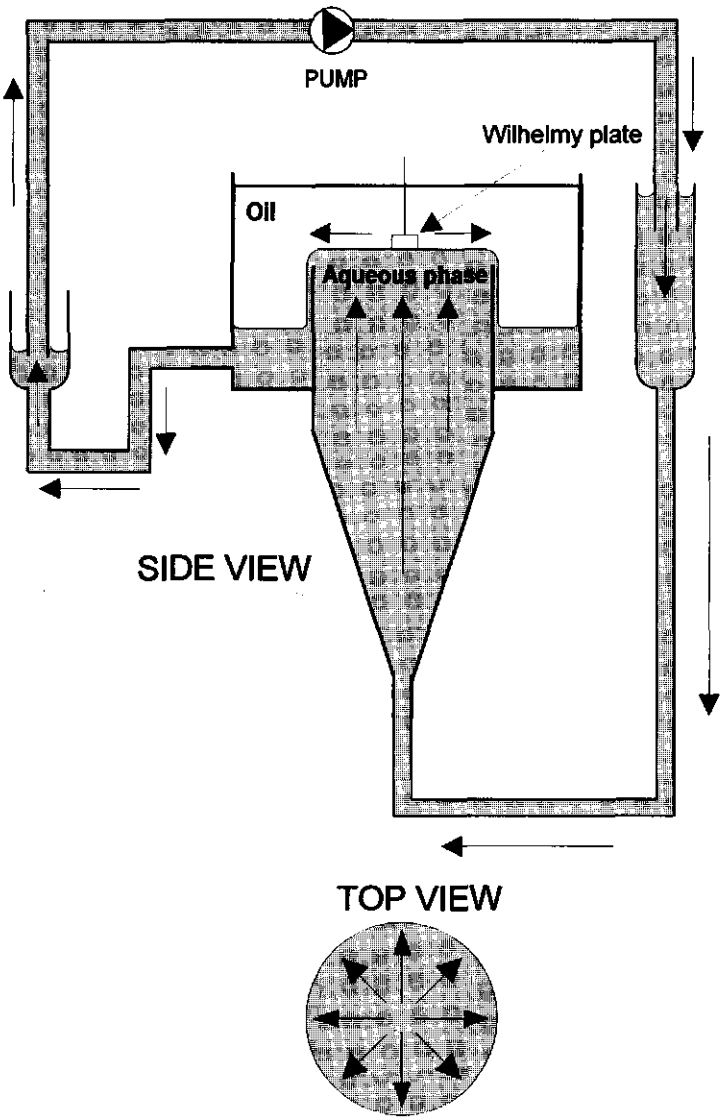

Fig 4.10: ***A schematic drawing of the modified overflowing cylinder that is used for the measurement of the dynamic interfacial tensions of oil-water interfaces.***

the Wilhelmy plate was immersed in the oil phase. This way the measured value of the interfacial tension was corrected for the buoyancy force by the oil phase acting on the Wilhelmy plate. The equilibrium interfacial tension was measured with the same Wilhelmy plate technique in a beaker filled with the aqueous solution with an oil layer on top. A more thorough discussion of the measurement of the tension under expansion and equilibrium of interfaces of soy oil-water and soy oil-Teepol solutions is reported by Bergink-Martens (1993).

4.4. THE RING-TROUGH METHOD

Prins (1989) suggested that the surface dilational modulus E effects the propagation speed of the longitudinal wave which he assumed to be equal to the spreading velocity of the monolayer in front of the spreading droplet (see Chapter 2). The surface dilational moduli of the investigated solutions were measured using the ring-trough method developed by Kokelaar et al. (1991) and makes use of a completely wetted cylindrical ring placed vertically in the liquid surface. The ring is moved vertically in a sinusoidal way which results in a periodical change in the surface area inside the ring. A schematic representation of the measuring technique is given in Fig 4.11. According to Lucassen and Van den Tempel the surface dilational modulus E of a liquid is defined as the ratio between the infinitesimal change in surface tension $\mathrm{d}\gamma$ and the infinitesimal relative change in surface area $\mathrm{d}\ln A = \mathrm{d}A/A$ as is given in eq. (4.5):

$$E = \frac{\mathrm{d}\gamma}{\mathrm{d}\ln A} \qquad (4.5).$$

If an oscillatory experiment is applied to a liquid surface the dilational modulus can be determined using eq. (4.6):

$$E = |E|\cos(\theta_E) + i|E|\sin(\theta_E) \qquad (4.6),$$

where $|E|$ is the amplitude of the ratio between the surface tension and surface deformation and θ_E is the loss angle of the modulus. Eq. (4.6) is build up of two parts. The first part is a real part of the modulus that is be considered to be the storage modulus E_d that can be defined as in eq. (4.7):

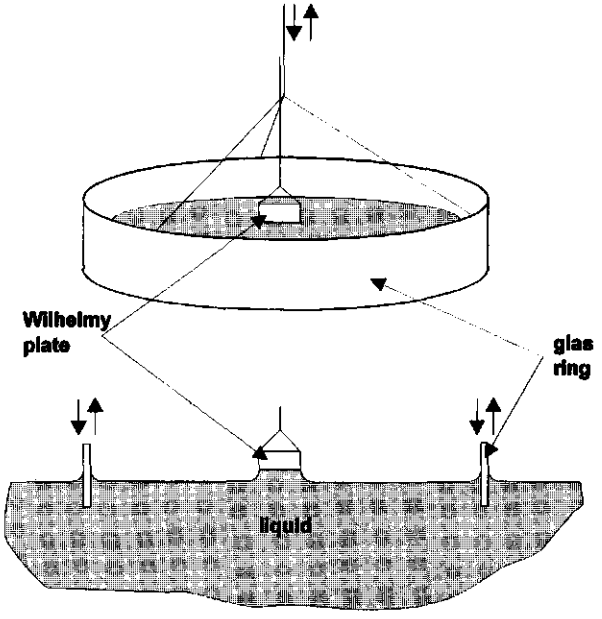

Fig 4.11: ***A schematic presentation of the experimental setup of the ring-trough (after Kokelaar (1991)).***

$$E_d = |E|\cos(\theta_E) \qquad (4.7).$$

The second part of eq. (4.6) is the imaginary part of the modulus and is related to the product of the radial frequency ω and the surface dilational viscosity η_d^s as presented in eq. (4.8):

$$\eta_d^s \omega = |E|\sin(\theta_E) \qquad (4.8),$$

in which the product $\eta_s''\omega$ can considered to be the loss modulus. The advantages of this new method are no leakage of the surface that is subjected to a sinusoidal change in surface area, and an almost pure dilational change of the surface indicating that shear is almost absent. The most important part of the measurement method is a cylindrical ring placed vertically in the liquid surface and can be seen in Fig 4.12.

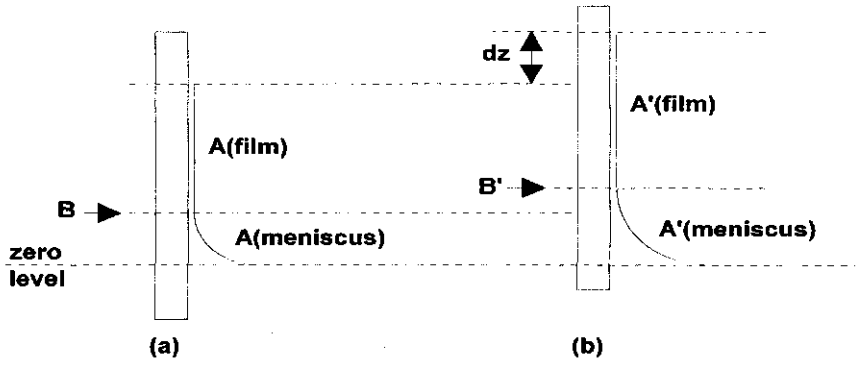

Fig 4.12: ***A schematic representation of the events taking place when moving the glass ring in a vertical direction (after Kokelaar (1991)).***

When the contact angle of the meniscus against the inner wall of the ring is 0°, the surface area of the liquid inside the ring can be changed in a controled manner by applying an up and downwards movement to the ring. The resulting change of the surface tension can be measured using a Wilhelmy plate technique in the centre of the circular liquid surface. Due to the vertical sinusoidal movement of the ring the area of the liquid film adhering to the inner wall of the ring is being enlarged and diminished.
To obtain complete wetting of the inner wall of the ring by the liquid, this wall was roughened which resulted in the adherence of a thin vertical liquid film to the wall. The height of this film depends on the surface tension of the liquid because the capillary rise of the liquid against the wall ($h_{capillary}$) depends on the surface tension of the liquid in a way as expressed in eq. (4.9):

$$h_{capillary} = \sqrt{\frac{2\gamma}{\rho g}} \qquad (4.9).$$

When a surfactant is present the surface tension will increase when the ring is moved upwards resulting in a decrease of the length of the film. The reverse will occur when the ring is moved downwards. The displaced volume of liquid by moving the ring up and down is compensated by moving a solid cylinder with the same horizontal cross-sectional area as the ring, opposite to the movement of the ring in the liquid surface. This way variations of the height of the liquid surface which would have a serious effect on the measurement of the surface tension (i.e. a decrease of the liquid height results in an increase of the measured surface tension due to the buoyancy effect) is brought to a minimum. By performing numerical mathematics as described by Kokelaar et al. (1991) the values of A and dA are obtained from the vertical displacement of the ring. Kokelaar et al. (1991) corrected the dA by using a table that indicates how the area of the meniscus depends on the surface tension of the liquid. By means of a computer program and by using the measured parameters, i.e. the surface tension as a function of time, the amplitude and frequency of the sinusoidal movement of the ring and the radius of the ring, together with the table needed for the corrections, the values of the dilational modulus E the storage modulus and the loss modulus were calculated. A detailed technical description of the device is given by Kokelaar et al. (1991). The values of E were used to explain the differences in spreading velocity of an oil droplet over the various aqueous solutions investigated in this study.

4.5. THE FREE FALLING LIQUID FILM TECHNIQUE

The free falling film can be used to study hole formation in the film, as a result of the spreading of an individual oil droplet, in a quantitative way. Droplets of known size and composition can be brought in the film and whether hole formation takes place or not follows from simple observation. In addition the place in the film where hole

formation takes place and the local film thickness can be determined in a quantitative way.

The setup of the apparatus is presented schematically in Fig 4.13. A thin sheet of liquid is produced by using a container with a slit at the bottom side. The liquid sheet falls free as a result of gravity and is guided by two wires on each side into a vessel from which the liquid is pumped back to the container again.

The film is relatively thick compared to the films in a foam. Nevertheless, the device can be used to study film rupture due to the spreading of particles over the film surface.

Van Havenberg and Joos (1983, 1984) described the behaviour of the falling film quantitatively and came to the conclusion that the falling velocity of the film is determined by the flow rate of the liquid and the gravity force. When the width of the slit (θ_0), the flow rate (Q) and the slit length (l) are known the initial velocity (v_0) of the film when it leaves the slit in the container can be calculated. Furthermore, Brown (1961) and later Bergink-Martens et al. (1992) described that by assuming that the flow rate is constant and that the film falls by obeying the law of gravitation, the film thickness (θ_x) and the falling velocity (v_x) at every distance from the slit can be calculated using eq. (4.10):

$$Q = v_0 \theta_0 l = v_x \theta_x l \qquad (4.10),$$

and eq. (4.11):

$$v_x^2 = v_0^2 + 2gx = (v_0 + g t_x)^2 \qquad (4.11),$$

where g is the acceleration due to gravity, x is distance from the slit and t_x is the time needed for a film element to fall down to a distance x from the slit of the container.

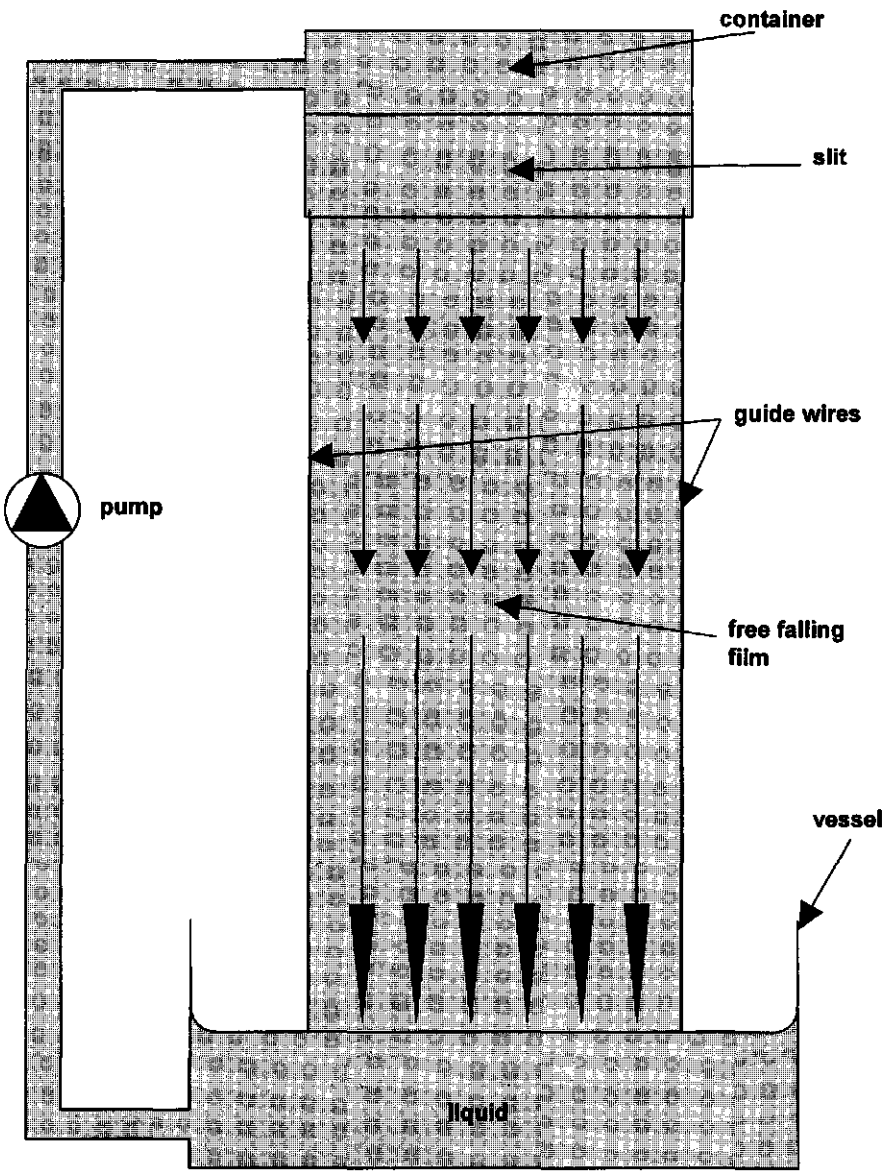

Fig 4.13: A schematic drawing of the free falling film apparatus.

Rearranging eq. (4.10) results in eq. (4.12) which can be used to calculate the initial velocity of the film at the slit:

$$v_0 = \frac{Q}{\theta_0 l} \qquad (4.12).$$

The falling velocity of the film at distance x from the slit can be calculated using eq. (4.13) which is easily derived from eq. (4.11):

$$v_x = (v_0^2 + 2gx)^{\frac{1}{2}} = v_0 + g t_x \qquad (4.13).$$

By combining eq. (4.10) and eq. (4.13) the film thickness at a distance x from the slit can be calculated using equation (4.14):

$$\theta_x = \frac{\theta_0 v_0}{v_x} = \frac{\theta_0 v_0}{(v_0^2 + 2gx)^{\frac{1}{2}}} = \frac{\theta_0 v_0}{v_0 + gt} \qquad (4.14).$$

Van Havenberg and Joos (1983) showed that the viscosity of the film liquid has only a minor effect on the velocity of the film if the film liquid is a low viscosity aqueous solution. Therefore the effect of the bulk viscosity of the film liquid was neglected.

Culick (1960) introduced a theory by which the surface tension at a distance x from the slit can be calculated. When the free falling film is disturbed by putting an obstruction in the film, a V-shaped edge called the Mach wave appears. The Mach wave is determined by a combination of the falling velocity (v_x) of the film and the bursting velocity (v_B). If an object, for instance a thin needle, is obstructing the falling film two situations can arise: 1) the film remains stable showing a V-shaped bow-wave generated from the needle and 2) the film tears due to the presence of the needle showing a tear angle which has the same value as the angle of the bow-wave. This fact demonstrates that both phenomena can be explained by the same physical law: the propagation of a shock-wave or Mach-wave. The bursting velocity is the velocity of the rim of an expanding hole in the film. After a negligible short period of time the

bursting velocity has reached a maximum that can be described by the Culick equation (4.15):

$$v_B = \left(\frac{2\gamma_x}{\rho\theta_x}\right)^{\frac{1}{2}} \qquad (4,15),$$

where γ_x is the surface tension of the film surface at distance x from the slit. The bursting velocity is related to the falling velocity according to eq. (4.16):

$$v_B = v_x \sin(\alpha) \qquad (4.16),$$

where α is the Mach angle of the V-shaped edge. By combining eq. (4.15) and eq. (4.16) the Brown's relation is obtained with which the surface tension of the film at distance x from the slit where the disturbance is located, can be calculated:

$$\gamma_x = \frac{1}{2}\rho\theta_x v_x^2 \sin^2(\alpha) \qquad (4.17).$$

Therefore, when measuring the Mach angle and knowing the film thickness the surface tension can be calculated. Experimental verification of the relation of the Mach angle with the local surface tension was reported by, amongst others, Antoniades et al. (1980) and Lin and Roberts (1981). However, Bergink-Martens et al. (1992) presented a direct method to measure the surface tension along the height of the free falling film using a modified Wilhelmy plate technique. By comparing the overflowing cylinder technique with the free falling liquid film technique they came to the conclusion that both techniques generated the same dynamic surface tension in expansion. Furthermore, they proved by calculations that the effect of the measured surface tension gradient with a typical value of 0.1 $N \cdot m^{-2}$ on the falling velocity of the film can be neglected and eq. (4.10) and eq. (4.11) of Van Havenberg and Joos (1983) are valid.

The excess surface tension of the expanding (or compressed) surface is according to Boussinesq (1913) proportional to the relative surface expansion (or compression)

rate. The constant of proportionality is specified by the surface dilational viscosity η_d^s and the relation is given in eq. (4.18):

$$\gamma_{dyn} - \gamma_{eq} = \eta_d^s \frac{\mathrm{d}\ln A}{\mathrm{d}t} \qquad (4.18),$$

where γ_{dyn} is the dynamic surface tension in expansion (or compression), γ_{eq} is the equilibrium surface tension and $\mathrm{d}\ln A/\mathrm{d}t$ is the relative surface expansion (or compression) rate. As can be seen in eq. (4.18) the dynamic surface tension is directly related to the relative surface expansion rate. The relative surface expansion rate at a distance x from the slit of the falling liquid film apparatus can be calculated using eq. (4.19):

$$\left(\frac{\mathrm{d}\ln A}{\mathrm{d}t}\right)_x = \frac{\mathrm{d}v_x}{\mathrm{d}x} = \frac{g}{(v_0^2 + 2gx)^{\frac{1}{2}}} = \frac{g}{v_0 + g\,t_x} \qquad (4.19),$$

as follows from eq. (4.13).

When a particle is introduced in the falling liquid film, this particle will apparently move in the direction of the surface due to a velocity component perpendicular to the film surface. The value of this velocity component depends on the distance x from the slit where the particle is present in the film.

Van Voorst Vader (1964) derived a relation to describe the convective diffusion of surfactant to an expanding liquid surface by applying continuity equations of the velocity parallel and perpendicular to the liquid surface. This relation describes the evolution of the velocity component in the liquid perpendicular to an expanding liquid surface as a function of the relative surface expansion rate and the distance between a position in the liquid to the liquid surface. This relation is given in eq. (4.20):

$$v_z = z\left(\frac{\mathrm{d}\ln A}{\mathrm{d}t}\right)_{z=0} \qquad (4.20),$$

where v_z is the velocity component perpendicular to the liquid surface and z is the distance from a point in the liquid to the liquid surface. This relation implicates that v_z = 0 when z = 0 (i.e. the liquid surface). Eq. (4.20) was also applied to describe the velocity of a particle perpendicular to and in the direction of, the expanding surface of the falling liquid film. By applying calculation on the falling film the conclusion was drawn that by combining eq. (4.20) with eq. (4.19) the velocity component perpendicular to the expanding film surface v_z is given by eq. (4.21):

$$v_z = \frac{zg}{v_0 + g t_x} \qquad (4.21),$$

When a particle with radius R_P is introduced in the film at a distance α_P from the centre of the film as illustrated by Fig 4.14 it will encounter the film surface when eq. (4.22) is satisfied:

$$\frac{1}{2}\theta_t = \frac{1}{2}\frac{\theta_0 v_0}{v_0 + g t_e} = \alpha_P + \beta_P R_P + R_P \qquad (4.22),$$

where t_e is the time a film element must fall to satisfy the condition on the right hand side of eq. (4.22) and the dimensionless factor β_P is describing the thickness of the film separating the particle from the film surface. By rearranging eq. (4.22) the time t_e is given by eq. (4.23):

$$t_e = \frac{v_0}{g}\left(\frac{\theta_0}{2(\alpha_P + \beta_P R_P + R_P)} - 1\right) \qquad (4.23).$$

Due to the velocity component perpendicular to the film surface, the particle is pressed against that surface.

At the moment a particle encounters the expanding liquid surface of the falling film it will be pressed against that surface with a force (F_S) that can be described by the Stokes equation (4.24):

$$F_S = 6\pi\eta R_P v_z \qquad (4.24).$$

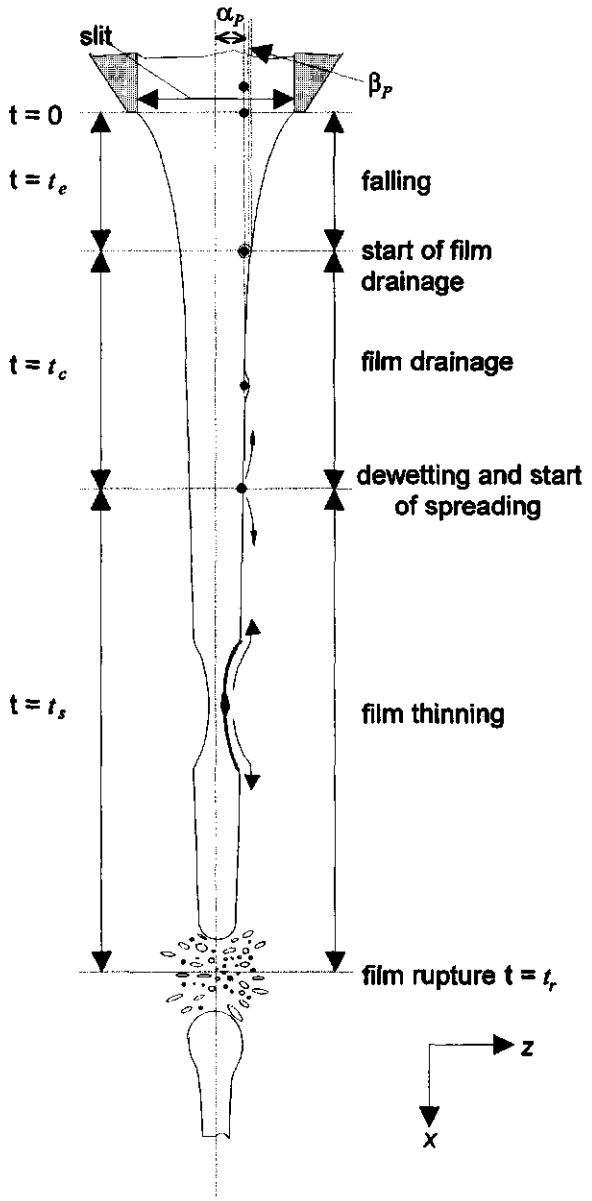

Fig 4.14: A representation of the events after introducing a spreading droplet in the free falling film.

This pressing force will be in equilibrium with a counteracting force (F_c) as a result of the Laplace pressure of the bulging film surface acting on a part of the surface area of the particle with radius R_P. This force F_c is described by eq. (4.25):

$$F_c = \Delta P A_P = \frac{2\gamma_{dyn}}{R_P} A_P \qquad (4.25),$$

where ΔP is the pressure and A_P is the surface area on which this pressure is acting. Here the dynamic surface tension (γ_{dyn}) must be used because the falling film developes an expanding surface and therefore a non-equilibrium surface tension. In eq. (4.25) the particle radius R_P is used by assuming that the curvature of the bulge in the film surface is given by the particle radius. The thickness of the thin liquid film separating the particle from the film surface is relatively small compared to the radius of the particle.

It is expected that the particle will cause bulging of the film surface. For this reason eq. (4.24) has to be corrected for the height h of the bulge with respect to the planar surface of the film, caused by a particle pressing against that surface at a distance x from the slit. The Stokes equation eq. (4.24) now becomes:

$$F_S = 6\pi\eta R_P \left(\left(\frac{\mathrm{d}\ln A}{\mathrm{d}t} \right)_x (R_P - h) \right) = \frac{6\pi\eta R_P g(R_P - h)}{v_0 + g t_x} \qquad (4.26),$$

and A_P in eq. (4.25) becomes the surface area of the spherical segment of the bulge with height h that equals the spherical segment of the particle as is presented in eq. (4.27):

$$F_c = \frac{2\gamma_{dyn}}{R_P} 2\pi R_P h = 4\pi\gamma_{dyn} h \qquad (4.27).$$

Equalization of eq. (4.26) and eq. (4.27) gives the height of the bulge that is described by eq. (4.28):

$$h = \frac{R_P^2}{\left(\frac{4\gamma_{dyn}}{6\eta\left(\frac{d\ln A}{dt}\right)_x} + R_P\right)} = \frac{R_P^2}{\left(\frac{4\gamma_{dyn}(v_0 + g t_x)}{6g\eta} + R_P\right)} \quad (4.28).$$

Malysa et al. (1980) presented a calculation for the drainage time of a plane parallel film to reach the critical film thickness of rupture that can be described with the Reynolds equation:

$$t_c = \frac{3\eta A}{4\pi\theta_c^2 \Delta P} \quad (4.29),$$

where t_c is the drainage time to reach the critical film thickness θ_c for rupture, η is the dynamic viscosity of the film liquid, A is the surface area of the plane parallel film and ΔP is the pressure difference due to Plateau border suction. By assuming that the particle interface is rigid and the driving force for drainage of the liquid is a Laplace pressure difference ΔP as a result of the curvature of the film covering the particle, i.e. in that case ΔP equals $2\gamma_{dyn}/R_P$, with R_P is the radius of the particle and furthermore, by introducing the surface area $A = 2\pi R_P h$ of a spherical segment representing the bulge in the surface due to the pressing particle, eq. (4.29) can be rewritten as eq. (4.30):

$$t_c = \frac{3\eta R_P^2 h}{4\theta_c^2 \gamma_{dyn}} \quad (4.30).$$

Introduction of h as described by eq. (4.28) leads to eq. (4.31) with which the critical drainage time for rupture can be estimated:

$$t_c = \frac{3\eta R_P^2}{4\theta_c^2 \gamma_{dyn}\left(\frac{4\gamma_{dyn}}{6\eta\left(\frac{d\ln A}{dt}\right)_x} + R_P\right)} = \frac{9\eta^2 g R_P^2}{4\theta_c^2 \gamma_{dyn}(v_0 + g t_x)\left(2\gamma_{dyn} + \frac{3\eta g R_P}{v_0 + g t_x}\right)} \quad (4.31).$$

Rupture of the thin liquid film separating the particle from the film surface results in entering of the particle into the film surface.

When the particle spreads over the surface of the free falling liquid film this will result in thinning of the film as described theoretically in Chapter 3. When the film thinning process proceeds long enough it may result in film rupture and hole formation. The total time t_r needed for a particle with radius R_P to encounter the film surface (t_e), to become dewetted and consequently enter the film surface (t_c), followed by spreading resulting in thinning and finally rupture of the film (t_s) can be described by eq. (4.32):

$$t_r = t_e + t_c + t_s \qquad (4.32),$$

where t_s is the time of spreading needed to result in such a local thinning of the film that it will rupture. Combining eq. (4.23) and eq. (4.31), and introduction of t_s into eq. (4.32) results in eq. (4.33) with which the distance where the film will rupture can be predicted:

$$x_r = \frac{v_0^2}{2g}\left(\left(\frac{\theta_0}{2(\alpha_P + \beta_P R_P + R_P)} + \frac{9\eta^2 g^2 R_P^4}{4v_0\gamma_{dyn}\theta_c^2(v_0 + gt_x)\left(2\gamma_{dyn} + \left(\frac{3\eta g R_P}{v_0 + gt_x}\right)\right)} + \frac{gt_s}{v_0}\right)^2 - 1\right) \qquad (4.33),$$

where x_r is the distance from the slit where the film will rupture.

From eq. (4.33) it becomes clear that the distance from the slit where the film will rupture depends to a large extent on the adjustable parameters α_P and β_P. In our experiments β_P was arbitrarily chosen to be 0.1 and for α_P it was assumed that it had a fixed value as will be explained in the following section. Furthermore, the radius of the particle has a large influence on the drainage time of the film separating the particle from the film surface.

To measure the distance of film rupture x_r induced by the introduction of spreading particles, a free falling film apparatus with a film length of 1.2 m, a split length of 0.1275 m and a split width of $0.75 \cdot 10^{-3}$ m was used. To prevent bending of the nylon

guide wires as a result of the surface tension of the film a weight of 0.96 kg was attached at the bottom end of the wires. During the experiments the system was thermostatted at 25°C. The closed system contained during experiments an amount of film liquid with a total volume of 5 litres.

The film liquids used in these experiments were degassed lager beer or a 0.15% v/v Teepol (RECA TP) solution. At this Teepol concentration the falling film was stable over the complete length of 1.2 m. At lower concentrations the film was not stable over the total length.

Surface Tension [$mN \cdot m^{-1}$]	Experimental (Avg. of 10 exp.)	After Bergink-Martens (1993)*
Equilibrium	25.3 ± 0.2 $mN \cdot m^{-1}$	26 $mN \cdot m^{-1}$
Dynamic**	63.9 ± 0.2 $mN \cdot m^{-1}$	62 $mN \cdot m^{-1}$

*** Graphically intrapolated**
**** Overflowing cylinder (flow rate: $2.64 \cdot 10^{-5}$ $m^3 \cdot s^{-1}$)**

Table 4.1: Equilibrium and dynamic surface tensions of 0.15% v/v Teepol solutions.

Bergink-Martens et al. (1992) mentioned that the overflowing cylinder and the free falling film generate the same dynamic surface tension in expansion. Therefore, to obtain the dynamic surface tension of the liquid when it is falling free as a thin film, it was measured by using the overflowing cylinder technique. The values of the measured equilibrium and the dynamic surface tensions are presented in table 4.1 and compared to the values Bergink-Martens (1993) measured.

From table 4.1 it becomes clear that, although different batches of Teepol are used, the values measured in this study are in good comparison with the values measured

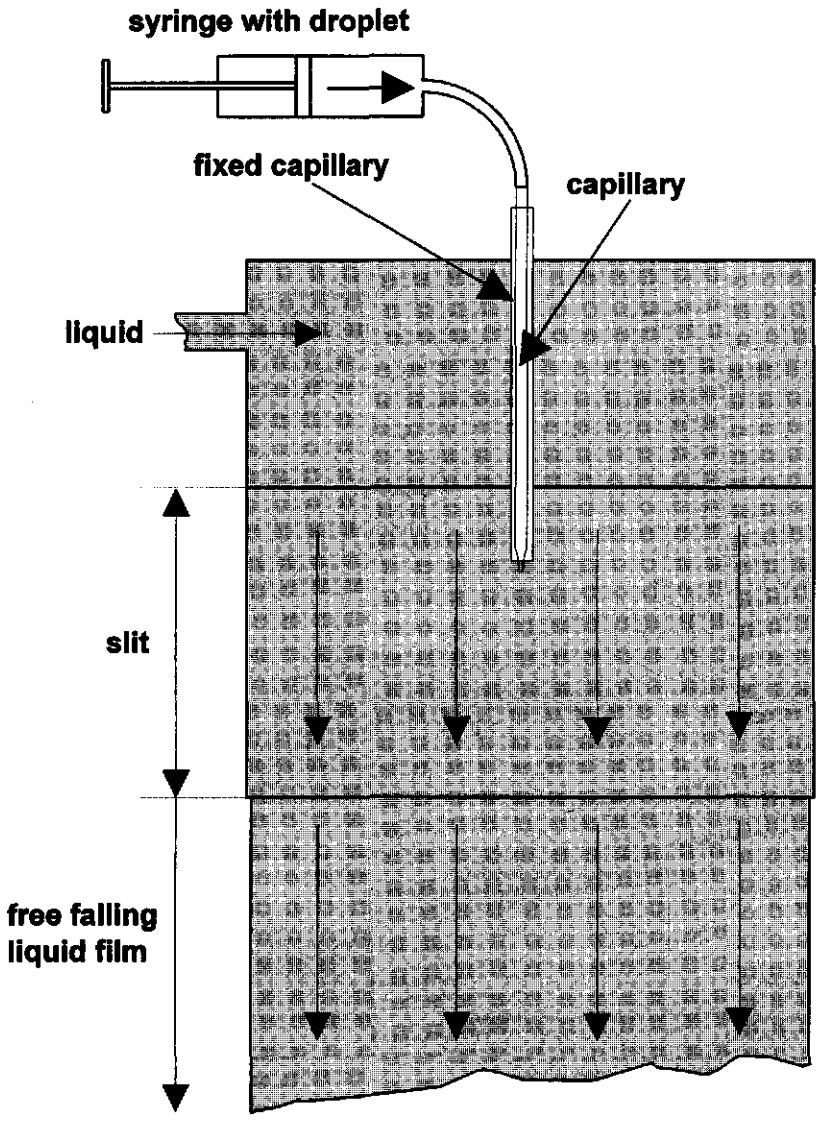

Fig 4.15: Drawing of the way the lipid particles are introduced into the free falling liquid film.

by Bergink-Martens (1993). The equilibrium and dynamic surface tension in expansion of the degassed lager beer were 42 $mN \cdot m^{-1}$ and 52 $mN \cdot m^{-1}$ respectively. Soy oil particles of different sizes with or without 2% w/w Tween 80 added to the oil phase were introduced in the free falling liquid film and their effect on the film stability was investigated. The selection and size determination of the soy oil particles was done by using a microscope. The separate oil particles were selected out of a soy oil-Teepol (0.15% v/v Teepol) emulsion by using a capillary with an inner diameter of $2 \cdot 10^{-4}$ m on a syringe with which a single oil particle was sucked together with some aqueous phase of the emulsion into the capillary. In the container with the slit of the free falling film apparatus a second capillary with an inner diameter of $3 \cdot 10^{-4}$ m was present from which the bottom end was brought into the thin slit, as presented in Fig 4.15, to a position where it was fixed during all experiments. The smaller capillary containing one oil droplet was brought through the larger capillary until the bottom end of this capillary was reached and where the droplet was introduced in the liquid stream that formed a thin liquid film at the bottom end of the slit. Therefore, the distance α_p from the centre of the film was assumed to have the same value during all experiments. The distance from the slit where the film ruptured was measured by eye using a spring ruler mounted along the side of the free falling film. The number of performed independent experiments per film liquid used in the apparatus are presented in table 4.2.

Experiment			number of
film liquid	soy oil	flow $[m^3 \cdot s^{-1}]$	experiments
0.15% Teepol	+ 2% w/w Tween	$2.71 \cdot 10^{-5}$	31
0.15% Teepol	+ 2% w/w Tween	$2.05 \cdot 10^{-5}$	14
0.15% Teepol	pure	$2.71 \cdot 10^{-5}$	13
degassed lager beer	+ 2% w/w Tween	$2.71 \cdot 10^{-5}$	12

Table 4.2: The conditions during the performed experiments

In each experiment several oil particles with different sizes were introduced in the film and observations were made whether or not these particles caused film rupture after introduction in the film. The distance from the slit where the film eventually ruptured was measured. The variations in the experiments were the composition of the film liquid, the composition of the soy oil and the flow rate of the film liquid (i.e. the thickness of the film).

4.6. THE OVERFLOWING CANAL TECHNIQUE

The surface motion due to the spreading of a monolayer of surfactant in front of a spreading droplet was measured using an overflowing canal. A schematic drawing of the device is presented in Fig 4.16.

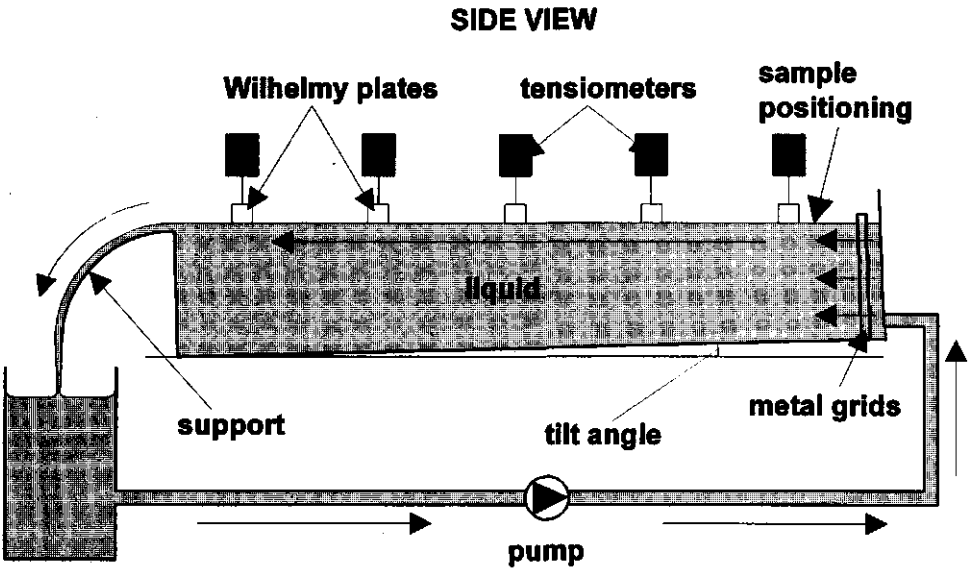

Fig 4.16: A schematic drawing of the overflowing canal technique.

The liquid in the canal was allowed to flow over the rim on one side of the canal in order to simulate 1) a very large surface area which is found when a small oil droplet is spreading over the relatively large surface of a bubble in a foam, and 2) to create an increased surface tension due to expansion which is also the case in a draining thin liquid film as is discussed in Chapter 2. The canal was made of stainless steel and had a length of 140 cm, a width of 22 cm and a depth of 15 cm. The liquid was flowing over the rim at one side of the canal and was recycled using a pump. To improve the stability of the falling liquid film the latter was supported by a wall as can be seen in Fig 4.16. This way an expanding liquid surface comparable to the expanding liquid surface in the overflowing cylinder was created. The metal grids at the beginning of the canal transforms the turbulent flow of the incoming liquid into a lamilar flow. During experiments the closed system consists of 50 liters aqueous solution. By means of five tensiometers distributed over the length of the canal the surface tension and surface tension gradients developed along the liquid surface can be measured.

When using a surfactant solution the surface tension gradient generated in this device is, in analogy with the overflowing cylinder, dependent on the height of the falling liquid film at one end of the canal. Due to the increased surface tension of the falling film there is a surface tension gradient operating over the total length of the liquid surface in the canal which is increasing towards the rim where the liquid is overflowing. Therefore, it may be assumed that the surface velocity of the liquid in the canal is, in analogy, dependent on the surface tension gradient as Bergink-Martens (1993) described for the overflowing cylinder. In Fig 4.17 the surface tension measured in the overflowing canal is plotted versus the distance from the beginning of the canal at the side were the liquid is flowing in. As can be seen the surface tension is increasing towards the rim where the liquid is allowed to overflow. Through the measured surface tensions a polynomial (>0.99 confidence interval) was fitted to be able to calculate the surface tension as a function of distance. The result is presented in Fig 4.18. The surface tension gradient at every distance can be calculated by differentiating the fitted polynomial from Fig 4.18. The surface tension gradient as a

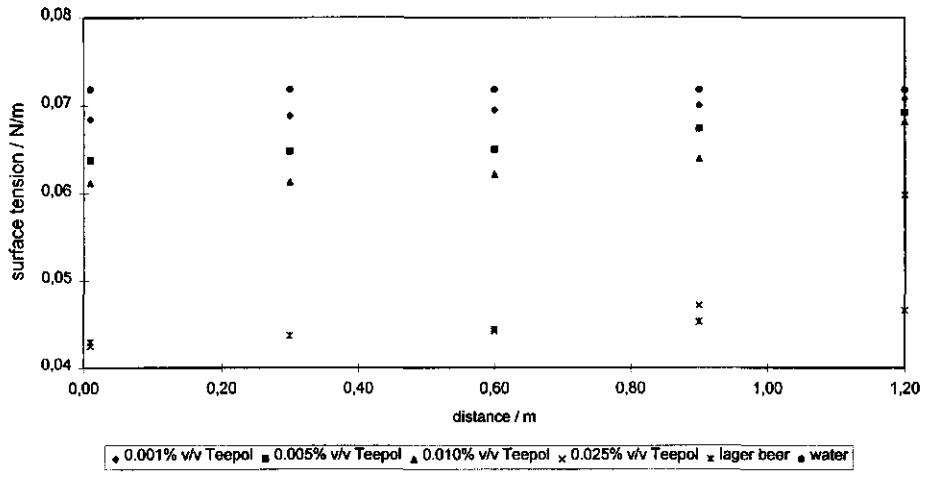

Fig 4.17: The measured surface tension as a function of the distance from the entrance in the overflowing canal.

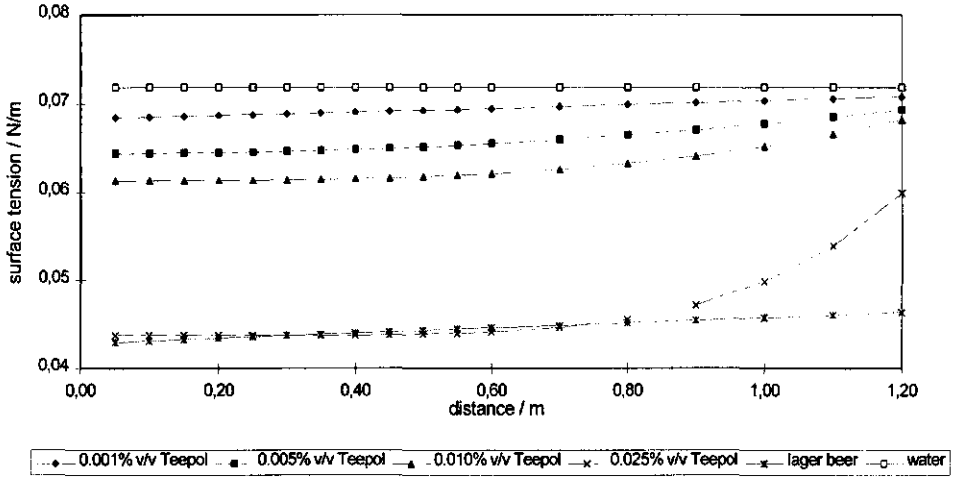

Fig 4.18: The result of the fitted polynomial through the measured surface tensions presented in Fig 4.17.

function of the distance in the overflowing canal is presented in Fig 4.19. In Fig 4.19 can be seen that the surface tension gradient is increasing towards the rim. This is in agreement with the results reported and described for the overflowing cylinder by Bergink-Martens (1993). According to Bergink-Martens (1993) the surface velocity is directly related to the surface tension gradient over that surface: an increasing surface tension gradient results in an increasing surface velocity.

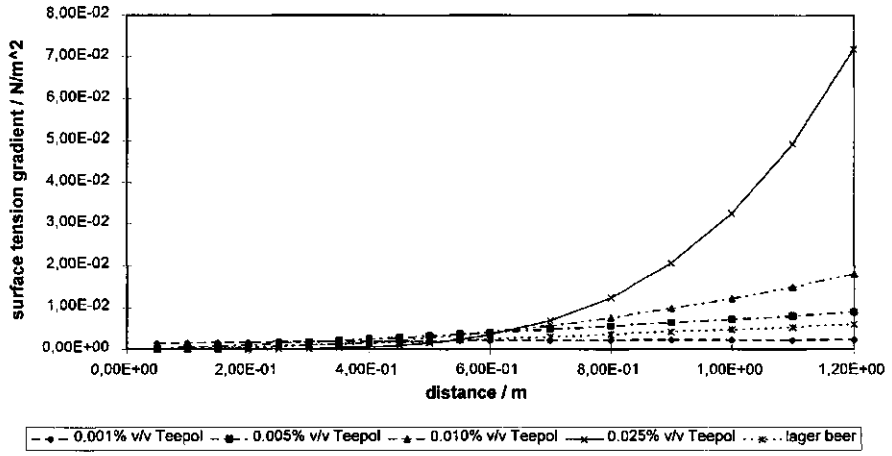

Fig 4.19: The surface tension gradient as a function of the distance in the overflowing canal.

In analogy with Bergink-Martens (1993) the surface velocity of the overflowing aqueous solution in the canal was measured by bringing a polyethylene particle on the surface at the position near the metal grids opposite to the rim where the liquid was allowed to overflow. The time the particle needed to travel on the surface in the direction of the falling film was measured by using a stop-watch. At consecutive distances from the beginning of the canal, where the particle was brought on the surface, the elapsed time was registred. This way the surface velocity profile could be

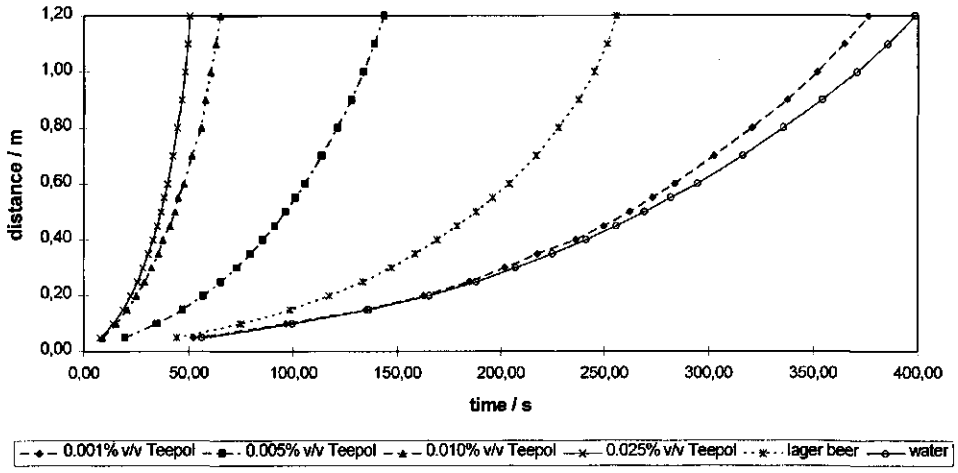

Fig 4.20: ***The propagation distance of Talcum particles placed on the surface in the overflowing canal as a function of time.***

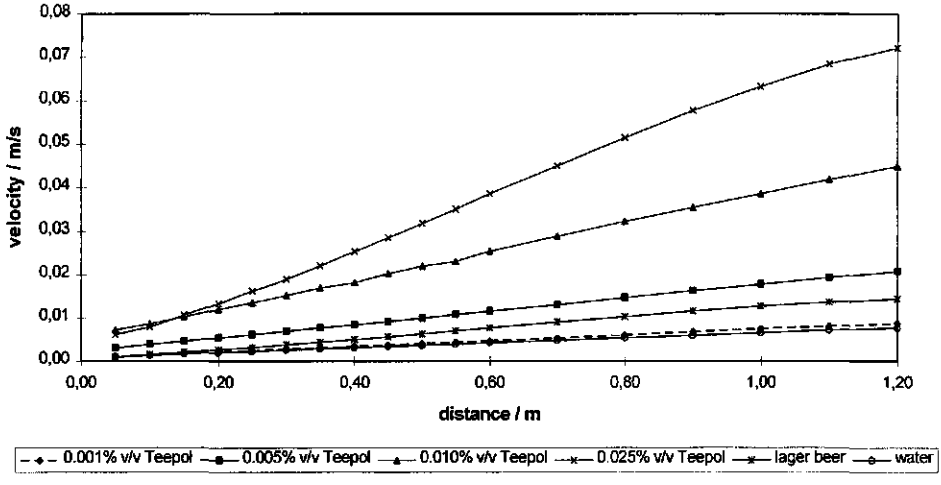

Fig 4.21: ***The velocity of the surface in the overflowing canal as a function of distance.***

determined and was used for the correction of the propagation speed of the monolayer as will be discussed below. In Fig 4.20 the position of the particles plotted as the average of triple measurements is presented as a function of time for the different investigated liquids. These data are used to calculate the surface velocity as a function of the distance. This was done by fitting the curve with an exponential (type: $y = a + b\ \mathrm{EXP}(-x/c)$), having a confidence interval >0.99, followed by differentiating the equation of the fitted exponential.

A plot of the obtained velocity profile as a function of distance is presented in Fig 4.21. In this figure can be seen that the surface velocity increases from the beginning of the canal and the acceleration increases during the first half of the distance in the canal in the direction of the rim where the liquid is overflowing. This implicates that also in the canal exists a surface expansion that, in analogy to the free falling liquid film and the overflowing cylinder is driven by a surface tension gradient. However, due to the geometry of the system this surface expansion is one-dimensional which is in analogy with the free falling liquid film that was discussed in §4.5.

The relative surface expansion rate $\mathrm{d}\ln A/\mathrm{d}t$ as a function of the distance is, for this one-dimensional expansion defined by eq. (4.34):

$$\frac{\mathrm{d}\ln A}{\mathrm{d}t} = \frac{\mathrm{d}v_x}{\mathrm{d}x} \qquad (4.34).$$

From eq. (4.34) It can be concluded that the $\mathrm{d}\ln A/\mathrm{d}t$ can be calculated by differentiating again the equation describing the velocity profile. The obtained curves are presented in Fig 4.22.

The relative surface expansion rate is also increasing towards the rim of the canal which is also in agreement with the theory applied to the overflowing cylinder by Bergink-Martens (1993). Here is, due to the one dimensional surface expansion, a somewhat different behaviour of the $\mathrm{d}\ln A/\mathrm{d}t$ found. However, the theory which was applied to the overflowing cylinder, i.e. a two-dimensional expansion, was rewritten by

Bos (see Chapter 3) for a one-dimensional expansion as is found in the overflowing canal. The obtained equation is shown in eq. (4.35):

$$\frac{d\gamma}{dx} = \left(\frac{d\ln A}{dt}\right)^{\frac{3}{2}} x\sqrt{\eta\rho} \qquad (4.35).$$

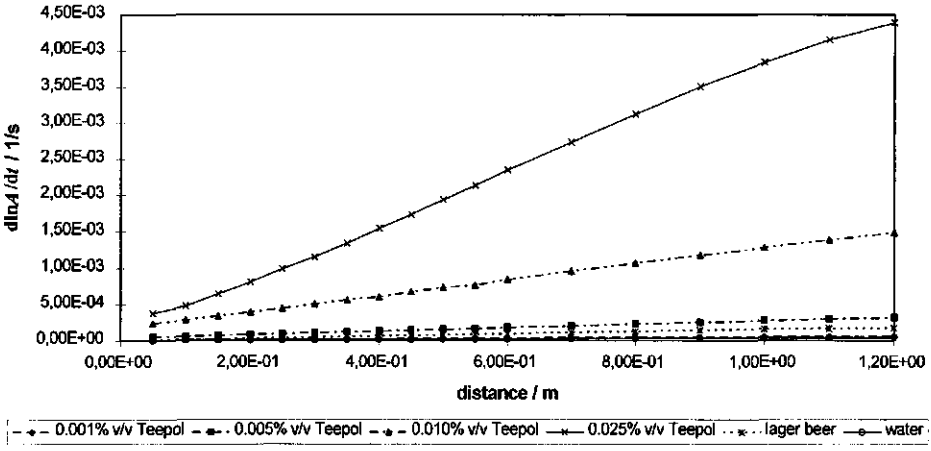

Fig 4.22: ***The relative surface expansion rate $d\ln A/dt$ as a function of the distance in the overflowing canal.***

The results of the calculated velocities are too high compared to the measured velocities as can be seen in Fig 4.23. The calculated values differ up to more than 14 times the measured velocity. However, it is out of the scope of this work to describe the found velocity profiles and surface tension gradient profiles physically. This would need a thorough hydrodynamic study of the fluid dynamics existing in the canal. However, possible hypothesis can be mentioned. The tilted position of the canal (see Fig 4.16) would result in a decreasing liquid flow towards the overflowing rim. In this direction the surface area through which liquid is flowing increases resulting in a decreased volume flow per surface area. Nevertheless, as mentioned earlier this

technique was used to simulate a semi infinite liquid surface with an increased surface tension in expansion as exists when a small particle spreads over the surface of a large bubble, i.e. film in a foam where drainage takes place. Therefore, only the physical behaviour of a spreading droplet over a liquid surface will be described.

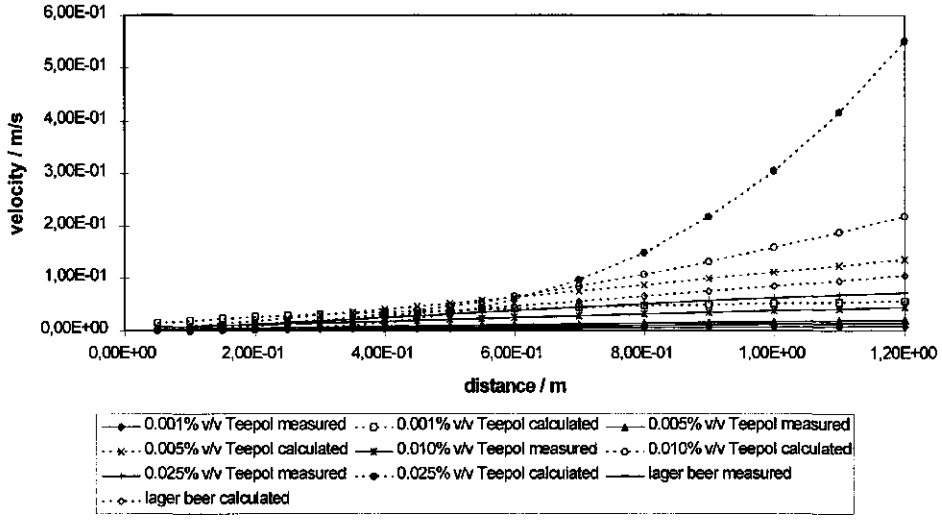

Fig 4.23: The measured and, according to eq. (4.35), calculated velocities of the surface in the overflowing canal.

Before bringing a droplet on the surface the five recorders that are connected to the devices to measure the surface tension, are started simultaneously in order to obtain a starting point which is equal for all recorders. The spreading material was brought on the liquid surface at the opposite side of the rim of the canal where the liquid was overflowing. The surface tension was measured simultaneously using Wilhelmy plates at different distances from the point where spreading started. The spreading material was brought on the surface by means of a syringe that produced droplets with a volume of 5 μl. The syringe with an oil droplet hanging at the end of it, was lowered

towards the liquid surface by using a micro-screw. At the moment the droplet made contact with the liquid surface it started to spread or not depending on the balance of surface tension forces as described by the spreading coefficient S_c which is discussed in Chapter 2. Care was taken that the droplet did not drop off the syringe on the surface before the droplet was allowed to make contact with the liquid surface. The result could be that the droplet would fall through the surface into the liquid bulk which causes errors in the experiment because in that case only a part of the droplet will spread.

During preliminary experiments a modified method described by Trurnit (1960) was used to bring the droplets completely in contact with the liquid surface. This method consists of a roughened glass sphere present in the liquid surface. The sphere is supported by a glass rod standing on the bottom of the canal as presented in Fig 4.24. By bringing the droplet on the roughened glass sphere it could not fall through the liquid surface into the liquid bulk and furthermore, it allows the droplet to spread immediately over the liquid surface by way of the thin liquid film and the liquid meniscus wetting the roughened glass sphere. Both methods however, gave equal results and for the majority of the spreading experiments the Trurnit (1960) technique was not used.

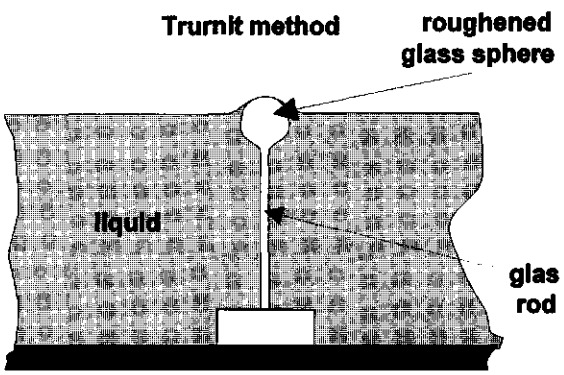

Fig 4.24: A presentation of the Trurnit method.

The first tensiometer was positioned at approximately 1 cm in the downstream direction from the position where the droplet was brought on the liquid surface. The distance between the tensiometers and the elapsed time between the start of the decrease of the surface tension measured with two consecutive tensiometers are used to calculate the propagation time of the monolayer over that distance. This is done by fitting a exponential with a confidence interval >0.99 through the data points of the distance versus the propagation time of the monolayer. By differentiating the obtained equation a velocity profile as a function of the distance was obtained. The results will be discussed in Chapter 5.

4.7. IMAGE ANALYSIS TO MEASURE THE SPREADING VELOCITY

The spreading velocity of the oil droplet itself into a relatively thick oil layer was measured using the device schematically presented in Fig 4.25. The device consists of an overflowing cylinder as described in §4.2, a video camera (Sony, CCD-V90E) and a syringe with a needle having an outer diameter of 0.083 cm.

A droplet of soy oil was brought on the liquid surface just beside the centre of the circular meniscus of the overflowing liquid on the radial line perpendicular to the observation line of the video camera. The droplets were brought on the surface in the same way as described in §4.4. Depending on the value of the spreading coefficient S_c the droplet started to spread while moving along with the overflowing liquid surface.

In order to obtain enough contrast between the thin spreading oil layer and the aqueous solution the video camera had to be placed with an angle as can be seen in Fig 4.25. The camera was thoroughly fixed to avoid changes in the distance between the camera and the spreading droplet. This way optical deformation of the pictures in the horizontal plane was minimized.

The picture frames coming from the video camera were collected by a computer (Estate 486, 33 MHz) using hardware and software (Iris Videodigitizer, Inside Technology) specially developed for this purpose. By using this technique up to a

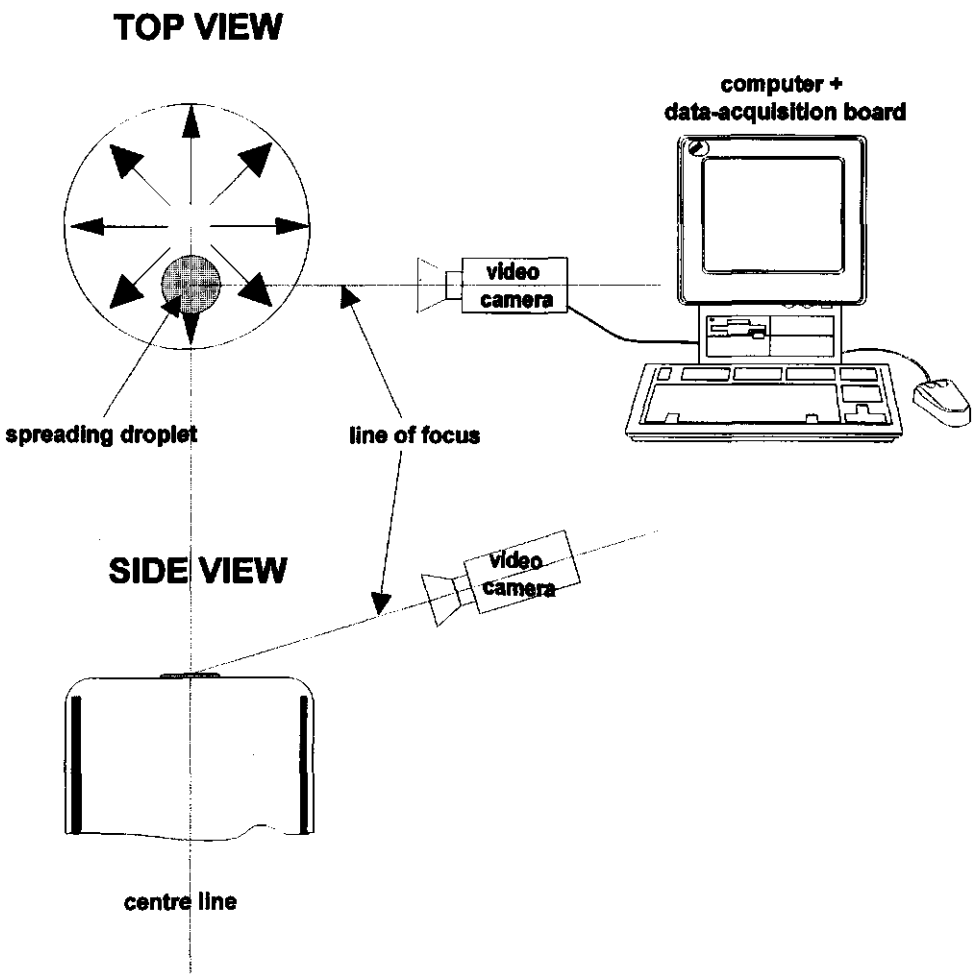

Fig 4.25: A schematic representation of the equipment used to measure the spreading velocity of an oil droplet on the expanding surface in the overflowing cylinder.

maximum speed of 25 pictures per second could be collected with a resolution of 192 times 192 pixels. Accordingly the time interval between two single video picture frames was found to be 0.04 s.

The analysis of the pictures was performed by using an Image Analyzer (Magiscan, Applied Imaging). By determining the coordinate of the front of the spreading droplet compared to the centre of spreading on the radial line perpendicular to the line of focus of the camera on consecutive video pictures, the spreading velocity of the droplet could be calculated. In this calculation it was assumed that the movement of the centre of the spreading droplet is equal to the surface velocity of the 'clean' aqueous phase in the cylinder which is measured using the LDA technique described in §4.2.

The centre of spreading was determined on the first picture frame containing the droplet just after bringing it on the surface. The centre of spreading was assumed to be the exact middle of the then still almost circular spreading oil layer. This assumption was justified since spreading had just started, i.e. there is a maximum elapsed time of 0.04 s between the two picture frames with and without a spreading droplet and the propagation distance of spreading was still very small. Furthermore, the velocity of the 'clean' surface in the vicinity of the centre of the circular expanding liquid surface where the droplet is brought on the surface, is relatively low. Therefore on the first picture frame it was assumed that the position of the droplet was equal to the position where the droplet was brought on the liquid surface.

The volume of the droplet that was brought on the liquid surface was found by the determination of the weight of a single droplet in twentyfold and the density of the soy oil sample used in these experiments. The measurement of the density of the soy oil was done by triple weighing a volume of 100 ml soy oil in a volumetric flask and was found to be 918.7 $kg \cdot m^{-3}$. The average diameter of the droplets was found to be 2.56 mm ± 0.04 mm.

4.8. ADDITIONAL EXPERIMENTAL TECHNIQUES

Technique I

To investigate the influence of oil droplets on the stability of a liquid film, experiments were performed in which use was made of rings made of a stainless steel wire with a diameter of 3 mm as depicted in Fig 4.26.

The diameter of the rings varied from 2 cm to 10 cm and the capillary tube had an inner diameter of 0.5 mm. The oil droplets were brought on the surface of the liquid film using the syringe method described in §4.4 or added in the film as an emulsion via a capillary tube into the Plateau border of the film as can be seen in Fig 4.19. By using the syringe, oil droplets with a volume of 5 μl were produced. A liquid film was produced in the ring by pulling the ring gently out of a vessel containing the film liquid under investigation. After that, the ring was brought in such a position that the film was horizontal when oil droplets were brought from outside on the film surface by means of the syringe. When emulsion droplets were introduced from inside the film the ring was positioned in a way that the liquid film was vertical and the capillary was at the top. This was done to allow the liquid film to drain which results in film thinning. After 30 second the frame was repositioned in the horizontal way as decribed earlier. Now the droplets present in the film could approach the upper surface of the film due to the density difference. In the case of appropriate conditions in terms of entering and spreading coefficient in addition to the available surface area for spreading a droplet could rupture the film. Care was taken to minimize vibrations and air flow around the system which could result in film instability and eventually film rupture. The film was assumed not to be destabilized after introduction of the oil droplets on or in the liquid film when it had a life time of at least 15 minutes.

Technique II

The dewetting and spreading properties were also observed on liquid surfaces which are in equilibrium when the liquid is in rest in a beaker. The oil droplets were brought from outside on the surface by means of the earlier mentioned syringe method.

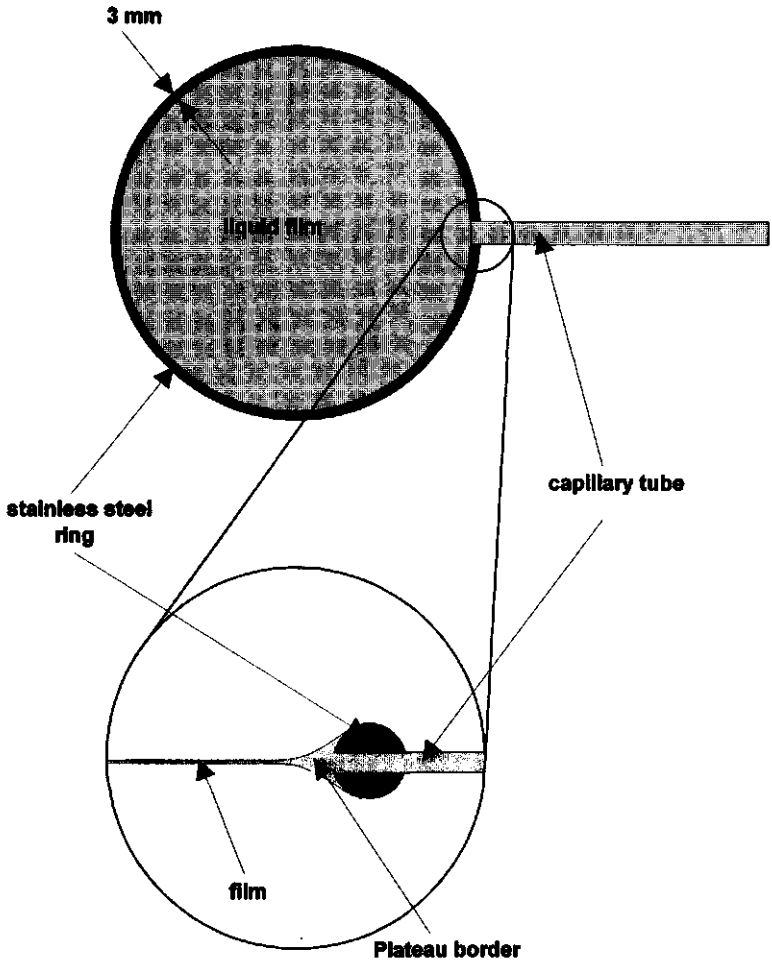

Fig 4.26: A schematic drawing of the equipment used to measure the effect of spreading particles on the stability of liquid films with different sizes.

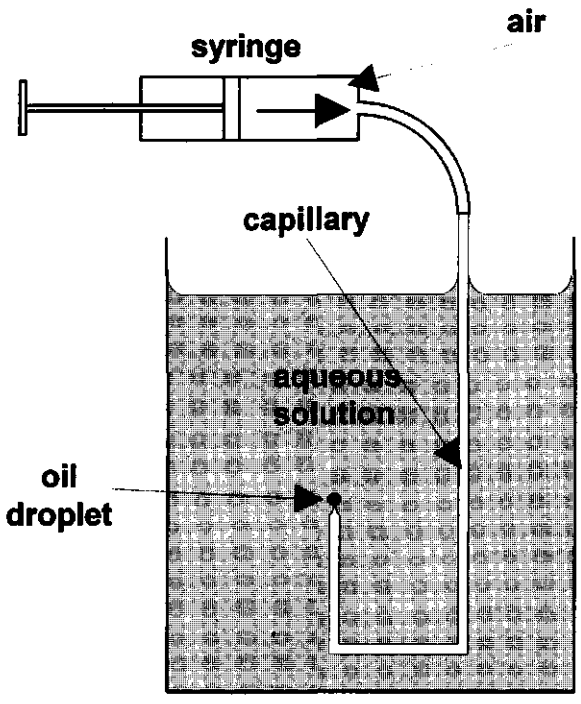

Fig 4.27: The experimental setup to observe the dewetting behaviour of particles.

The oil was also brought in contact with the liquid surface via the liquid using the syringe in a way presented in Fig 4.27.

The contact time of the droplet with the foaming liquid was elongated by varying the time of release from the syringe before the oil droplets were allowed to cream up to the liquid surface. Contact times of 1 hour were established and it was assumed that then the oil phase is in equilibrium with the aqueous phase and the conditions defined by the final entering and spreading coefficients are satisfied. When bringing the droplets on the liquid surface it is assumed that the initial entering and spreading coefficients are valid.

To relate the spreading behaviour to the surface area available for spreading, oil droplets were brought on in the middle of circular surfaces with different diameters varying from 2 cm to 10 cm, using the earlier mentioned syringe method. In these experiments the distinction was made between a monolayer spreading from the oil droplet that can be measured as a decrease of the surface tension and motion of talcum powder particles in front of the spreading monolayer, and the spreading of the oil droplet as a whole that can be observed by eye as the spreading of the oil lens into a relative thick oil layer sometimes exhibiting Newtonian colors.

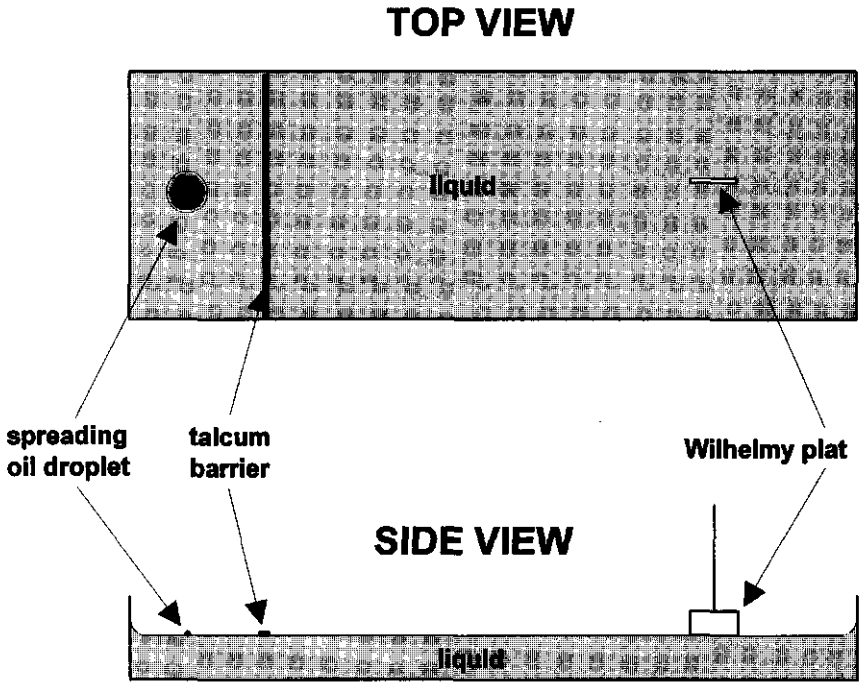

Fig 4.28: The experimental setup to observe the effect of surface tension on the spreading behaviour.

Technique III

The spreading behaviour of soy oil (ARO) was investigated as a function of the surface tension in a Langmuir trough. A droplet (0.85 μl) of soy oil containing 0% w/w, 0.1% w/w or 2.0% w/w Tween 80 was brought on the surface of a Teepol solution by using a micropipette (Socorex 841). With the Wilhelmy plate technique the changes in surface tension, due to the oil addition, were recorded during a period of at least 15 minutes. Before adding the droplet also a talcum 'barrier' was brought on the surface of the Teepol solution to visualize the propagation of a spreading monolayer or oil droplet. A schematic drawing of the experimental setup is shown in Fig 4.28. For the three types of oil samples the spreading behaviour was investigated at different surface tensions. The different surface tensions were attained by varying the Teepol concentrations of the continuous phase. The total volume of liquid present in the Langmuir trough varied between $1.6 \cdot 10^{-3}$ m^{-3} and $1.7 \cdot 10^{-3}$ m^3. The trough had a width of 19.0 cm, a length of 40.0 cm and a depth of 3.0 cm. All experiments were performed at ambient temperature.

4.9. MEASUREMENT OF ADDITIONAL PHYSICAL QUANTITIES

When a particle is spreading over the film surface of a bubble the film surface in front of the spreading particle is compressed resulting in a decrease of the surface tension. To investigate the surface rheological behaviour in compression of the aqueous solutions investigated in this study use was made of a Langmuir trough with a width of 19.0 cm, a length of 40.0 cm and a depth of 3.0 cm, equiped with a caterpillar belt as described by Prins (1986) and Ronteltap (1989) to perform single surface compression experiments. A schematic representation of the experimental set-up can be found in Fig 4.29. The caterpillar belt was equipped with a single barrier. With this configuration a surface area of 304 cm^2 was compressed to 61 cm^2 (i.e. 500% compression). In the compressed area the surface tension was measured with the Wilhelmy plate technique. For all experiments a constant compression speed of 2.67

$cm \cdot s^{-1}$ was used. The measurements were carried out at ambient temperature and solutions of Teepol (RECA TP) and degassed lager beer were investigated. In some experiments ethanol (pro analyse, Merck) was added to the beer samples up to a concentration of 5% v/v in order to determine the influence of the ethanol on this surface rheological behaviour of the beer.

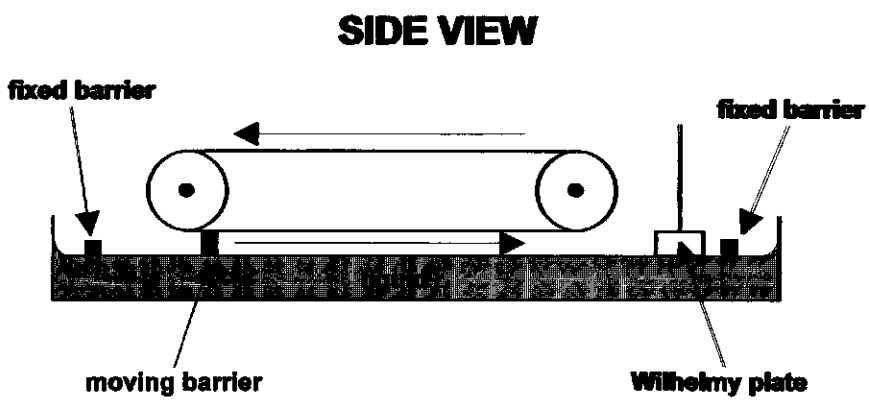

Fig 4.29: A schematic presentation of the caterpillar trough.

Since the viscosity of the oil can play an important role in the spreading velocity of the oil particle, the bulk viscosity of the oil phase was determined using an KPG-Ubbelohde viscometer. The value of the kinematic bulk viscosity (ν) followed from the measured efflux time (t_{eff}) and the capillary constant (c) of the viscometer as is given in eq. (4.36):

$$\nu = t_{eff} c \qquad (4.36).$$

The dynamic bulk viscosity can now be calculated using eq. (4.37):

$$\eta = \nu\rho \qquad (4.37),$$

where ρ is the density of the liquid. The measurements were carried out at three different temperatures. At each temperature triple measurements were done. The

influence of Tween 80 on the dynamic viscosity was investigated by measuring the viscosity of soy oil containing 2% w/w Tween 80.

REFERENCES CHAPTER 4

Antoniades, M.G., Godwin, R., Lin, S.P., J. Coll. Int. Sci., **77**:583 (1980).

Bergink-Martens, D.J.M., Bos, H.J., Prins, A., Schulte, B.C., J. Coll. Int. Sci., **138**:1 (1990).

Bergink-Martens, D.J.M., Bisperink, C.G.J., Bos, H.J., Prins, A., Zuidberg, A.F., Colloids and Surfaces, **65**:191 (1992).

Bergink-Martens, D.J.M., PhD Thesis, Agricultural University Wageningen (1993).

Brown, D.R., J. Fluid Mech., **10**:297 (1961).

Boussinesq, M.J., Ann. Chim. Phys., **29**:349 (1913).

Culick, F.E.C., J. Appl. Phys., **31**:1128 (1960).

Drain, L.E., The Laser Doppler Technique, John Wiley, Chichester, (1980).

Durst, F., Melling, A., Whitelaw, J.H., Principles and Practice of Laser-Doppler Anemometry, second edition, Academic Press, London, (1981).

Harkins, W.D., Feldman, A., J. Amer. Chem. Soc., **44**:2665 (1922).

Harkins, J. Chem Phys., **9**:52 (1941).

Van Havenberg, J., Joos, P., J. Coll. Int. Sci., **95**:172 (1983).

Van Havenberg, J., Bussmann, H., Joos, P., J. Coll. Int. Sci., **101**:462 (1984).

Joos, P., De Keyser, P., The Overflowing Funnel as a Method for Measuring Surface Dilational Properties, Levich Birthday Conference, Madrid, (1980).

Kokelaar, J.J., Prins, A., De Gee, M., J. Coll. Int. Sci., **146**:507 (1991).

Lin, S.P., Roberts, G., J. Fluid Mech., **112**:443 (1981).

Malysa, K., Cohen, R., Exerowa, D., Romianowski, A., J. Int. Sci., **80(1)**:1 (1980).

Ollenik, R., PhD Thesis, Technischen Universität München (1983).

Padday, J.F., Proc. Int. Congr. Surface Activity II, London, Butterworths, London, pp 1-6, (1957).

Piccardi, G., Ferroni, E., Ann. Chim. (Rome), **41**:3 (1951).

Piccardi, G., Ferroni, E., Ann. Chim. (Rome), **43**:328 (1953).

Prins, A., "Theory and Practice of Formation and Stability of Food Foams." In: Food Emulsions and Foams., Ed E. Dickinson, Roy Soc. of Chem., Leeds, pp. 30 (1986).

Prins A., "Foam Stability as affected by the presence of small spreading particles." In: Surfactants in Solution, Vol. 10, Ed. K.L. Mittal, pp. 91 (1989).

Ronteltap, A.D., PhD Thesis, Agricultural University Wageningen (1989).

Trurnit, H.J., J. Coll. Sci., **15**:1 (1960).

Van Voorst Vader, F., Erkens, Th.F., Van Den Tempel, M., Trans. Faraday Soc., **60**:1170 (1964).

Walstra, P., J. Coll. Int. Sci., **27**:493 (1968).

Watrasiewicz, B.M., Rudd, M.J., Laser Doppler Measurements, Butterworths, London, (1976).

Wiedemann, J., Laser Doppler Anemometrie, Springer Verlag, Berlin, (1984).

5 RESULTS AND DISCUSSIONS

5.1. INTRODUCTION

The aim of this study was to describe the process of film rupture due to the spreading of material over one of the film surfaces. In order to test the theory presented in Chapter 3 different measurements were done to evaluate the validity of the theory. In §5.2 the results of experiments performed in the overflowing cylinder are presented. In §5.3 results of the spreading experiments of Soy oil containing the surfactant Tween 80 in the overflowing canal are presented and explained by the developed theory. For that reason the theory presented in Chapter 3, i.e. a radial geometry, is adapted to the rectangular geometry found in the overflowing canal. The derivation of the equations describing rectangular spreading is also done in this paragraph. To collect quantitative information about the film thickness that can be ruptured by droplets of certain size in reality experiments were done with a free falling liquid film. Potentially spreading droplets with known size were introduced in the falling film and the distance from the origin, where they ruptured the film, was measured. The rupture distances predicted by the theory, discussed in Chapter 4, and measured rupture distances are compared and related to the film thickness. The results of these experiments are discussed in §5.4.

When droplets spread over limited bulk surfaces the surrounding surface of the aqueous phase is compressed. Therefore, single compression experiments in a Langmuir trough equipped with a caterpillar belt are evaluated and discussed in §5.5. In §5.6 the relation between the response of the surface tension of the aqueous surface upon spreading of a droplet and the final spreading distance is discussed. These results provide information about the effect of finite surfaces with different surface rheological behaviour on the spreading behaviour of droplets. Also qualitative experiments were done by introducing droplets on and in thin films with limited surfaces. The results verified the existence of a relation between surface area of the film, the surface rheological behaviour of the film, the spreading distance and the effect of the spreading process on the stability of the film.

5.2. THE EXPERIMENTS IN THE OVERFLOWING CYLINDER

The overflowing cylinder technique was used for three reasons. 1) To measure the dynamic and equilibrium surface tension of the air-liquid interface. This dynamic surface tension could be used to estimate the surface tension of a free falling liquid film as was discussed in Chapter 4. Furthermore, the dynamic and equilibrium surface tension of the oil-air interface were measured to obtain information to be used to calculate the spreading coefficient S_c. 2) To measure the dynamic and equilibrium interfacial tensions of the Soy oil with or without Tween 80 against the aqueous phase. This was done to be able to draw conclusions on the value of the spreading coefficient. 3) To measure the spreading velocity of the oil droplet on an expanding liquid surface to have an indication of the spreading velocity of the oil lens.

In table 5.1 the dynamic and equilibrium surface tension of different substrates are presented. It can be seen that an increasing Teepol concentration shows a decreasing equilibrium surface tension but only a minor decrease in the dynamic surface tension. This means that in equilibrium a large part of the decrease of the surface tension is due to the minor components present in the Teepol. In dynamic conditions with higher Teepol concentrations they will play a more important role besides the major components. This can be seen when comparing the dynamic and equilibrium surface tensions of the 1 % v/v Teepol solution which are equal. The values correspond to the values mentioned by Bergink-Martens (1993).

The lager beer used in these experiments show a small difference between the equilibrium and dynamic surface tension. This is not surprising since lager beer is known to be a very "dirty" system as was mentioned by Ronteltap (1989). Regarding the surface tensions of Soy oil with or without Tween 80 we may conclude that the Tween has no effect on the tensions of the oil-air surface. The Tween 80 molecule consists of a long hydrophobic chain with a hydrophilic head. Since the air phase may be seen as a hydrophobic phase, the Tween molecule

gains no energy profit by adsorbing at the oil-air surface. If the molecule would adsorb at the oil-air surface it would get into a lower entropy which is unfavourable. Furthermore, the conclusion can be drawn that the Soy oil does not contain impurities that lower the oil-air surface tension since the dynamic and equilibrium surface tensions are equal.

System	Dynamic surface tension	Equilibrium surface tension
Clean water	72.0	72.0
0.001% v/v Teepol	71.8	not measured
0.005% v/v Teepol	71.6	not measured
0.010% v/v Teepol	71.3	not measured
0.025% v/v Teepol	71.1	not measured
0.05% v/v Teepol	70.8	28.0
1% v/v Teepol	27.7	27.7
Lager beer	48.0	42.0
Pure Soy oil	32.5	32.5
Soy oil + 0.1% w/w Tween 80	32.5	32.5
Soy oil + 2% w/w Tween 80	32.5	32.5

Table 5.1: The values of the dynamic and equilibrium surface tensions measured with the overflowing cylinder technique.

In table 5.2 the dynamic and equilibrium interfacial tensions of Soy oil with or without Tween 80 additions against aqueous phases with different aliquots of Teepol, or lager beer are presented. From the values presented in this table it can be concluded that both Teepol and especially Tween 80 have a large effect on the dynamic interfacial tension. It can be seen that Teepol in the aqueous phase lowers the dynamic interfacial tension of pure Soy oil. If there is, however, 2% w/w Tween

80 present in the oil phase the dynamic interfacial tension decreases even more. When the Tween 80 adsorbs at the interface the system gains free energy which is favourable. The same reason counts for the soap molecules in the Teepol and the protein and other surface active components in the lager beer.

These large decreases of the interfacial tensions may have a large effect on the spreading coefficient and, probably, also on the spreading velocity of the droplet since the surface tension difference becomes much bigger when surfactants adsorb at the oil-liquid interface. Furthermore, the spreading process is a dynamic process and therefore especially the dynamic interfacial tensions are considered. The values presented in table 5.2. are used to calculate the spreading coefficient and the spreading velocity in §5.3.

The values of the dynamic interfacial tensions were well reproducible. The values of duplo measurements differed at the most 0.1 mNm^{-1} which is smaller than the accuracy of the measurement technique, i.e. 0.4 mNm^{-1}. The reproducibility of the equilibrium surface tensions is much smaller. The measured tensions depend much on the age of the surface/interface. To reach the state of equilibrium molecules must adsorb at the interface. This adsorption is diffusion dependent and it may, therefore, take a long period of time before state of equilibrium is reached. Especially solutions containing large surface active macromolecules, i.e. present in lager beer, need a longer time to reach equilibrium than solutions containing small surface active components.

Another important information that can be seen in table 5.2 is that the Soy oil does contain surface active components which adsorb at the oil-liquid interface because the dynamic interfacial tension is higher than the equilibrium. In the case of absence of surface active components these surface tensions should be equal.

Now the surface and interfacial tensions are known the spreading coefficients can be calculated. The calculated values together with the observations of eventual spreading are presented in table 5.3. The spreading behaviour was observed in the experimental set-up described in §4.8. During these experiments the oil droplets

Aqueous phase	Oil phase	Dynamic interfacial tension [mNm^{-1}]	Equilibrium interfacial tension [mNm^{-1}]
Clean water	Pure Soy oil	32.0	4.3
Clean water	Soy oil + 2% w/w Tween 80	25.6	2.8
0.001% v/v Teepol	Pure Soy oil	21.2	not measured
0.001% v/v Teepol	Soy oil + 2% w/w Tween 80	19.5	not measured
0.005% v/v Teepol	Pure Soy oil	19.8	not measured
0.005% v/v Teepol	Soy oil + 2% w/w Tween 80	12.0	not measured
0.010% v/v Teepol	Pure Soy oil	17.1	not measured
0.010% v/v Teepol	Soy oil + 2% w/w Tween 80	9.0	not measured
0.025% v/v Teepol	Pure Soy oil	13.6	not measured
0.025% v/v Teepol	Soy oil + 2% w/w Tween 80	5.2	not measured
0.050% v/v Teepol	Pure Soy oil	11.8	1.6
0.050% v/v Teepol	Soy oil + 2% w/w Tween 80	0.8	0.3
1% v/v Teepol	Pure Soy oil	1	0.9
1% v/v Teepol	Soy oil + 2% w/w Tween 80	≈0	≈0
Lager beer	Pure Soy oil	14.7	8.7
Lager beer	Soy oil + 2% w/w Tween 80	0.9	≈0

Table 5.2: ***The dynamic and equilibrium interfacial tensions of oil-aqueous solution interfaces. The composition of the aqueous phase and the oil phase was varied.***

were brought on an aqueous surface in equilibrium. When the droplet starts to spread the interfacial tension of the droplet may increase and the surface tension of the aqueous phase decrease, if the surface area of the latter is limited which is the case when using a trough as was done here. Therefore, additional experiments were done by bringing the droplets on an expanding aqueous surface in the overflowing cylinder. Here the dynamic surface tension of the aqueous phase exists and the surface area may considered to be infinite.

Both spreading behaviours on equilibrium and dynamic surfaces are reported in table 5.3.

Aqueous phase	Oil phase	Spreading coefficient [mNm^{-1}]		Yes/No spreading of droplet			
				theory		experimental	
		dyn.	eq.	dyn.	eq.	dyn.	eq.
water	Pure Soy oil	7.5	35.2	Y	Y	Y	Y
water	Soy oil + 2% w/w Tween 80	18.3	36.7	Y	Y	Y	Y
0.001% v/v Teepol	Pure Soy oil	18.1	-	Y	-	Y	-
0.001% v/v Teepol	Soy oil + 2% w/w Tween 80	19.8	-	Y	-	Y	-
0.005% v/v Teepol	Pure Soy oil	19.2	-	Y	-	Y	-
0.005% v/v Teepol	Soy oil + 2% w/w Tween 80	27.0	-	Y	-	Y	-
0.010% v/v Teepol	Pure Soy oil	21.7	-	Y	-	Y	-
0.010% v/v Teepol	Soy oil + 2% w/w Tween 80	29.8	-	Y	-	Y	-
0.025% v/v Teepol	Pure Soy oil	25.0	-	Y	-	Y	-
0.025% v/v Teepol	Soy oil + 2% w/w Tween 80	33.4	-	Y	-	Y	-
0.050% v/v Teepol	Pure Soy oil	26.5	-6.1	Y	N	Y	N
0.050% v/v Teepol	Soy oil + 2% w/w Tween 80	37.5	-4.8	Y	N	Y	N
1% v/v Teepol	Pure Soy oil	-5.8	-5.7	N	N	N	N
1% v/v Teepol	Soy oil + 2% w/w Tween 80	-4.8	-4.8	N	N	N	N
Lager beer	Pure Soy oil	0.5	0.9	Y	Y	Y	N
Lager beer	Soy oil + 2% w/w Tween 80	14.6	9.5	Y	Y	Y	Y

Table 5.3: The calculated spreading coefficient, the theoretical spreading behaviour and the observed spreading behaviour.

In table 5.3 can be seen that the spreading coefficient according to eq. (2.34) predicts very well the spreading behaviour in terms of Yes/No occurrence of spreading. However, the non-spreading of pure Soy oil on an equilibrium surface of lager beer was not predicted by the theory. Since the surface area is here finite and by taking into consideration that the spreading coefficient is close to zero, it is most probable that, due to the spreading process and the surface rheological behaviour of the beer surface in compression, the surface tension of the beer surface will decrease fast to a value at which the spreading coefficient becomes <0. This would stop the spreading process. When this happens in an early stage of spreading it may be possible that the spreading process is not observed before it stops. This phenomenon would be interesting considering the spreading of droplets over surfaces of small bubbles. Since the surface area of bubbles is finite the spreading process may stop in such an early stage that the spreading would not result in film rupture.

The spreading experiments on the expanding surface in the overflowing cylinder were evaluated by using the image analysis technique described in §4.7. Although analysis of the video pictures is complicated and inaccurate, an attempt was made to calculate in an order of magnitude the spreading velocity of the droplet. Spreading of pure Soy oil and Soy oil + 0.1% w/w Tween 80 on 0.4% and 0.5% v/v Teepol solutions was evaluated. From these experiments it was concluded that the spreading velocity increases with increasing Teepol concentration in the aqueous phase. This can be explained with the lower interfacial tension of the oil-liquid interface at higher Teepol concentrations which results in an increased spreading coefficient. Consequently the spreading velocity will be higher. Comparing the surface tensions of a 0.4% v/v and a 0.5% v/v Teepol solution the surface tension decreases from about 0.05 Nm^{-1} to about 0.04 Nm^{-1}. This explains, in combination with the lower tension of the oil-liquid interface, why the initial spreading velocity of a pure Soy oil droplet increased from 0.05 ms^{-1} to about 0.2 ms^{-1} when spreading on a 0.5% v/v or a 0.4% v/v Teepol solution respectively. Upon addition of 0.1% w/w

Tween 80 to the oil phase the spreading velocity on a 0.4% v/v Teepol solution increased to 0.25 ms^{-1} due to lowering of the interfacial tension. The number of measurements was restricted to the three mentioned above because of the big difficulties with the evaluation of the data. However, the examples give an order of magnitude indication of the spreading velocity of the oil droplets. It has to be noted here that the measured velocities are much lower than the velocities of droplets with sizes in the order of microns. Because the droplets used here are much larger the initial perimeter of the oil lens in contact with the liquid surface is much bigger. For this reason the starting velocity of spreading is, according to eq. 3.20 much smaller due to the larger lens radius. This parameter is called in Chapter 3 the excluded spreading time.

5.3. THE EXPERIMENTS IN THE OVERFLOWING CANAL

In Chapter 4 was already mentioned that the overflowing canal was used to simulate the spreading of a small droplet over a large surface area. Due to the overflow the surface area in the overflowing canal is assumed to be infinite. Additionally, the surface tension of the liquid present in the canal increases over the length of the canal. This is assumed to be comparable to the increased tension of the film surfaces in a draining foam. Nevertheless, there are some differences between the spreading of a droplet on a film surface and on the surface in the canal. The main difference has a geometric origin. The spreading process over a film is a two-dimensional spreading behaviour. The droplet is spreading in a radial way, i.e. first dimension, and due to the increasing perimeter at the front of the spreading material the surface area is additionally expanded in a circular way, i.e. second dimension. In the canal the spreading process is in one direction. Because of the walls there is no circular expansion possible. For this reason, the theoretical approach for a radial geometry was adapted to the one-dimensional spreading that is found in the overflowing canal. This adaptation was elucidated in Chapter 3. A second

difference is the spreading over a bulk surface in the case of the canal and over a thin liquid film in the case of a thin film in a foam. In both cases, however, mechanical and mass equilibrium are considered, i.e. surface tension gradient in equilibrium with viscous shear. In the case of the spreading over the liquid surface in the canal this results in an increased velocity of the surface and a thin bulk liquid layer underlying the moving surface. In the case of spreading over a thin liquid film this results in local thinning of the thin film in the centre of spreading. However, in both cases hydrodynamic behaviour is used to describe the spreading process and, therefore, it is possible to relate both theories that describe the two spreading processes and to apply the results of spreading measurements in the canal with the spreading process over the surface of a thin liquid film.

The oil droplets brought on the liquid surface had a volume of about 5 μl. When assuming this volume spreads into a layer with thickness 20 Å before it breaks up into small droplets the total spreading distance in the canal would have become 12.8 m. Since the device used here had a total length of 1.4 m the conclusion can be drawn that in these spreading experiments the spreading coefficient has to be used as the driving force for spreading and it is allowed to use eq. (3.56).

For the spreading experiments in the overflowing canal two arguments can be mentioned why no correction was made for the excluded time as was mentioned in Chapter 3. 1) The droplets are brought onto the surface by slowly lowering the syringe with a small oil droplet hanging at it. Therefore, as soon as the droplet touches the liquid surface, i.e. a diameter much smaller than the actual droplet diameter, the spreading already starts. 2) The time scale on which the propagation of spreading was measured in the overflowing canal was much larger than the time scale discussed in Chapter 3. When considering these two arguments we concluded that a correction for the excluded spreading time was not necessary.

Since both theoretical approaches, i.e. for a radial and rectangular geometry, derived in Chapter 3 are based on the same principle it was concluded that when the spreading velocities measured in the overflowing canal can be described with eq.

(3.56) the equations derived in Chapter 3 for a radial spreading droplet, i.e. a much smaller radial geometry, are also valid. However, as was already stated in Chapter 3 the spreading coefficient may not be constant. This is indeed the case when higher Teepol concentrations where used in the overflowing canal. In these solutions the surface tension increases towards the rim where the liquid was allowed to overflow as could be seen in Fig (4.18). Therefore, in the spreading coefficient, γ_{LA} was corrected with spreading distance in the overflowing canal by using the surface tension values as a function of distance obtained by fitting the measured values which were presented in Fig (4.19).

For the calculations of the spreading velocity as a function of the spreading distance the dynamic surface tension profile of the aqueous phase as a function of distance in the overflowing canal was used (see Fig (4.17) and Fig (4.18)). For the surface and interfacial tensions of the oil the values reported in tables 5.1 and 5.2 were used. With these data the spreading coefficients according to eq. (3.54) were calculated for the different systems of the aqueous and oil phase used in the experiments. In these calculations it is assumed that the surface and interfacial tensions of the Soy oil do not change during the spreading process. Evidence for these assumptions are found in the results of the measurements of the surface and interfacial tensions done in the overflowing cylinder. Furthermore, for a constant interfacial tension a very fast supply of surfactant out of the oil phase is necessary. This can be assumed to happen for two reasons: 1) The spreading oil layer becomes thinner with increasing spreading distance. Consequently the distance of transport of surfactant to the interface becomes smaller. This will secure the supply of surfactant to the interface. There is, however, a note to be made. When the oil layer becomes very thin the supply of surfactant will decrease due to depletion of surfactant but we think that this is not relevant in the spreading experiments performed here in the overflowing canal. This effect becomes more important when the droplet size decreases and the spreading velocities are much higher and the layer is thinning much faster. 2) Due to the spreading process a velocity component perpendicular to the interface is developed.

This velocity component secures also the supply of surfactant out of the aqueous phase.

The results for spreading of Soy oil + 2% w/w Tween 80 on surfaces of clean water, 0.001% v/v, 0.005% v/v, 0.01% v/v, 0.025% v/v Teepol and lager beer can be found in Fig (5.1) to Fig (5.6). The measured spreading velocities are corrected for the base velocity of the 'clean' surface which exists already. In these figures can be seen that the theory predicts rather well the spreading velocity as a function of spreading distance on surfaces of clean water, 0.001% v/v and 0.005% v/v Teepol. However on surfaces of 0.01% v/v and 0.025% v/v Teepol and lager beer the theoretical curves deviate from the measured curves. This could be due to errors in the extraction of the propagation time from the recorder chart.

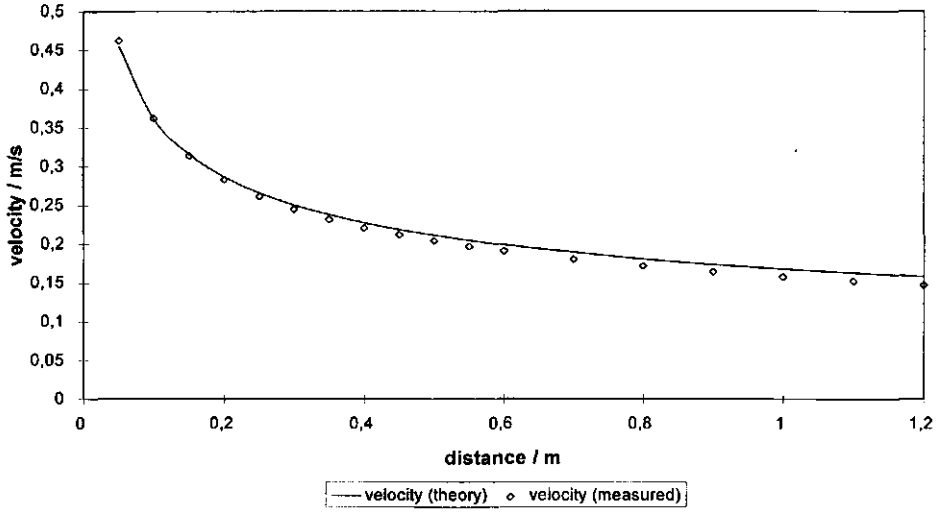

Fig 5.1: ***The spreading velocity of Soy oil + 2% w/w Tween 80 as a function of the spreading distance according to eq. (3.56) in the overflowing canal containing clean water.***

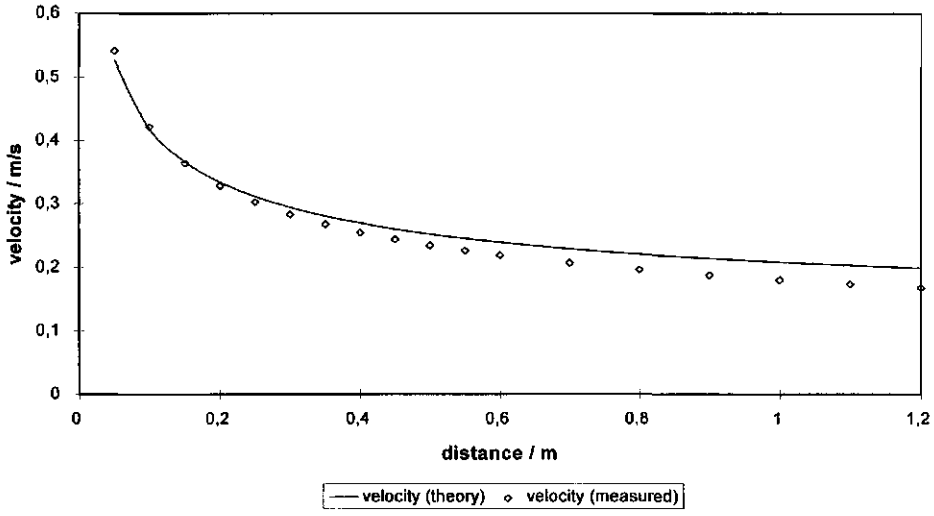

Fig 5.2: The spreading velocity of Soy oil + 2% w/w Tween 80 as a function of the spreading distance according to eq. (3.56) in the overflowing canal containing 0.001% v/v Teepol solution.

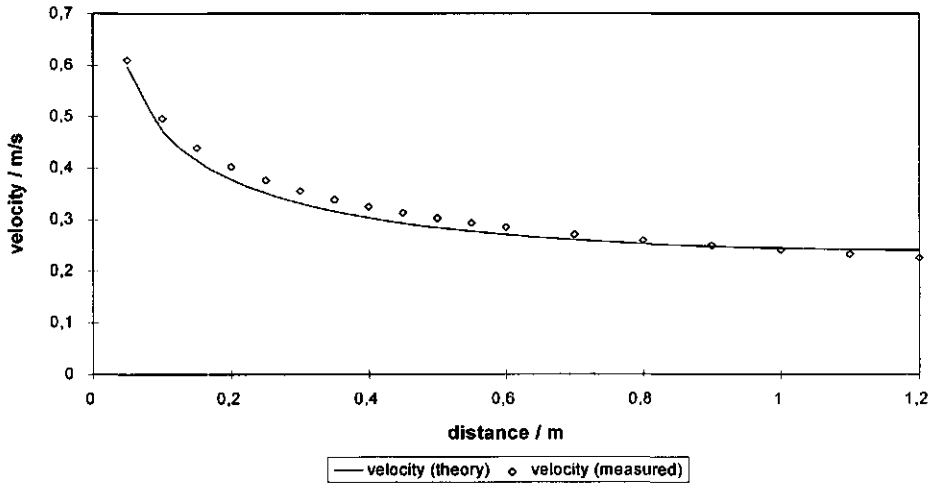

Fig 5.3: The spreading velocity of Soy oil + 2% w/w Tween 80 as a function of the spreading distance according to eq. (3.56) in the overflowing canal containing 0.005% v/v Teepol solution.

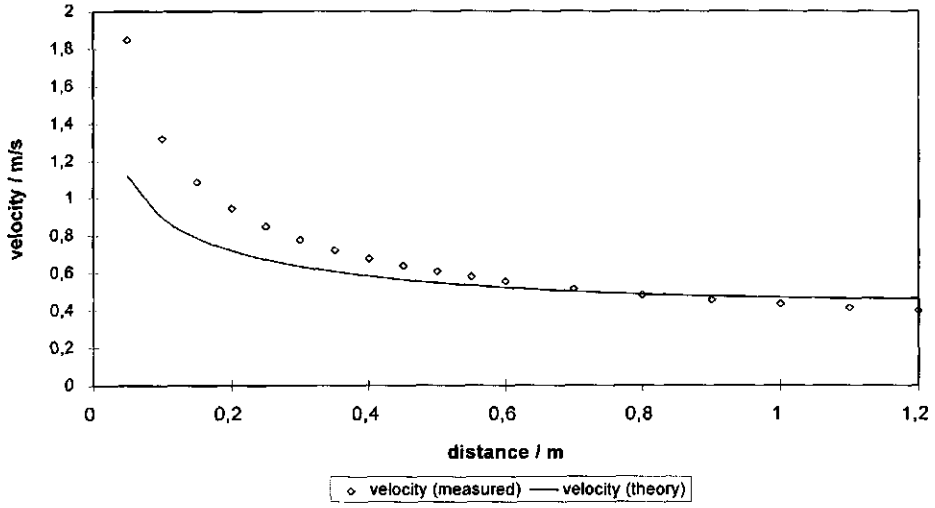

Fig 5.4: The spreading velocity of Soy oil + 2% w/w Tween 80 as a function of the spreading distance according to eq. (3.56) in the overflowing canal containing 0.01% v/v Teepol solution.

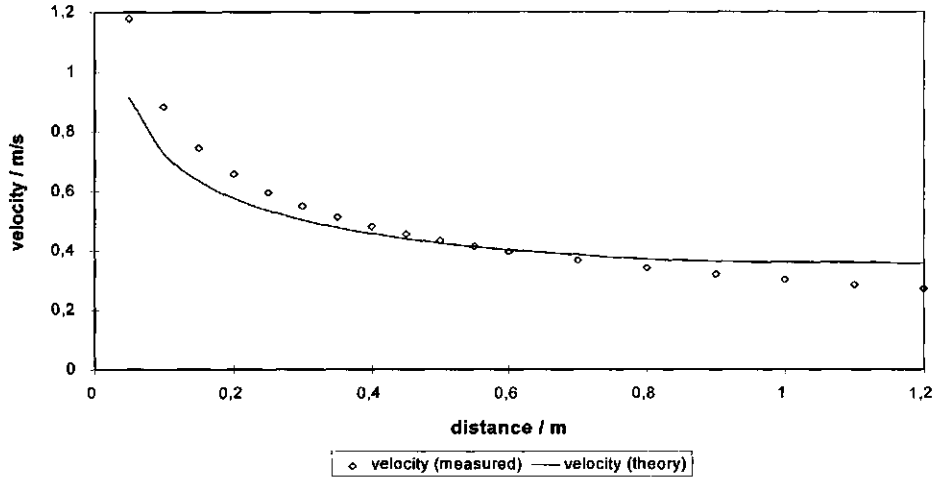

Fig 5.5: The spreading velocity of Soy oil + 2% w/w Tween 80 as a function of the spreading distance according to eq. (3.56) in the overflowing canal containing 0.025% v/v Teepol solution.

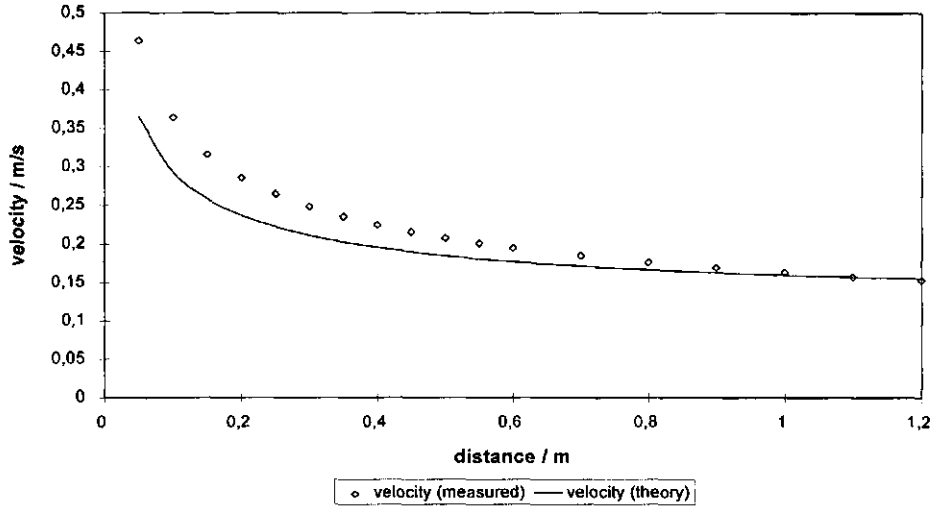

Fig 5.6: ***The spreading velocity of Soy oil + 2% w/w Tween 80 as a function of the spreading distance according to eq. (3.56) in the overflowing canal containing lager beer.***

Especially at higher Teepol concentration and beer it was difficult to choose the point where the surface tension starts to decrease because of the more gradual and smaller decrease of the surface tension. Faster and more accurate signal capturing, by for instance data acquisition by means of a computer, could have improved the validity of the measured data. Furthermore, the interfacial tension of the Soy oil could have been overestimated which has drastic consequences in the beginning of spreading, i.e. a lower spreading velocity, and these tension may, in reality, be closer to equilibrium. Due to the proceeding spreading process the interfacial tension may increase and become close to the values mentioned in table 5.2. Regarding these two assumptions the consequence for the calculated spreading velocity as a function of distance would be a higher velocity at the start of spreading approaching the measured values. In the theoretical curves can be seen that their values approach the

measured values at longer spreading distances. This would confirm the statement mentioned above.

In Fig (5.1) to Fig (5.6) can be seen that the spreading velocity increases up to a Teepol concentration of 0.01% w/w in the aqueous phase. Above this concentration, i.e. 0.025% w/w Teepol, the spreading velocity decreases again. Regarding the surface tensions of the aqueous phase mentioned in Fig (4.17) and Fig (4.18) this can be explained. In these figures it can be seen that the surface tension measured in the canal decreases drastically above the Teepol concentration 0.01% w/w. Furthermore, in Tables 5.1 and 5.2 it can be seen that the surface tension of the oil does not change as a function of the Teepol concentration and that the decrease of the interfacial tension between the 0.01% w/w and the 0.025% w/w is relatively small. Consequently, the spreading velocity will be lower. When looking to the values of the spreading coefficient in table 5.3 it is expected that the spreading velocity over a 0.025% w/w Teepol solution would be the highest. However, it has to be considered that these spreading coefficients are calculated with data obtained by measuring the surface and interfacial tensions in the overflowing cylinder. For the surface and interfacial tension of the oil this seems acceptable since the expansion rates during spreading are relatively high. For the surface tension of the aqueous phase, however, the used values are not justified.

In Fig (5.7) the equilibrium and dynamic surface tensions measured in the overflowing cylinder, the minimum dynamic surface tension measured at the beginning of the canal, and the maximum dynamic surface tension, measured near the overflowing rim in the overflowing canal are plotted as a function of the logarithm of the Teepol concentration. In this figure it can be seen that the surface tensions in the overflowing canal have values between the equilibrium surface tension and the dynamic surface tension measured in the overflowing cylinder. Apparently different surface expansion rates are developed in the overflowing canal resulting in lower dynamic surface tensions but still higher than the equilibrium surface tension.

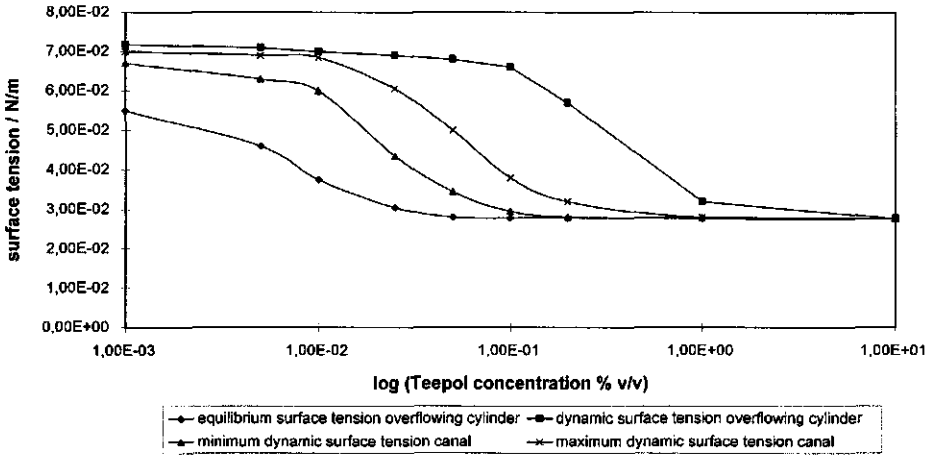

Fig 5.7: ***The equilibrium and dynamic surface tensions measured in the overflowing cylinder (after Bergink-Martens (1993)), the minimum and maximum dynamic surface tension measured in the overflowing canal as a function of the logarithm of the Teepol concentration.***

More important in this study is the steep decrease in the minimum surface tension measured in the overflowing canal. This surface tension determines the initial spreading velocity of the droplet. As spreading of the droplets in the overflowing canal proceeds the difference between the surface tensions of the various aqueous solutions become smaller. This was already illustrated in Fig (4.17) and Fig (4.18). Consequently, the spreading velocities go to almost equal values as can be seen in Fig (5.1) to Fig (5.6).

By calculating the spreading coefficient of a spreading droplet on the various aqueous solutions as a function of the spreading distance, as is done in Fig (5.8), it can be seen that the measured spreading velocities can be explained partly by the change in the value of the spreading coefficient as a function of spreading distance. For these spreading coefficients the interfacial and surface tensions of the oil droplet mentioned

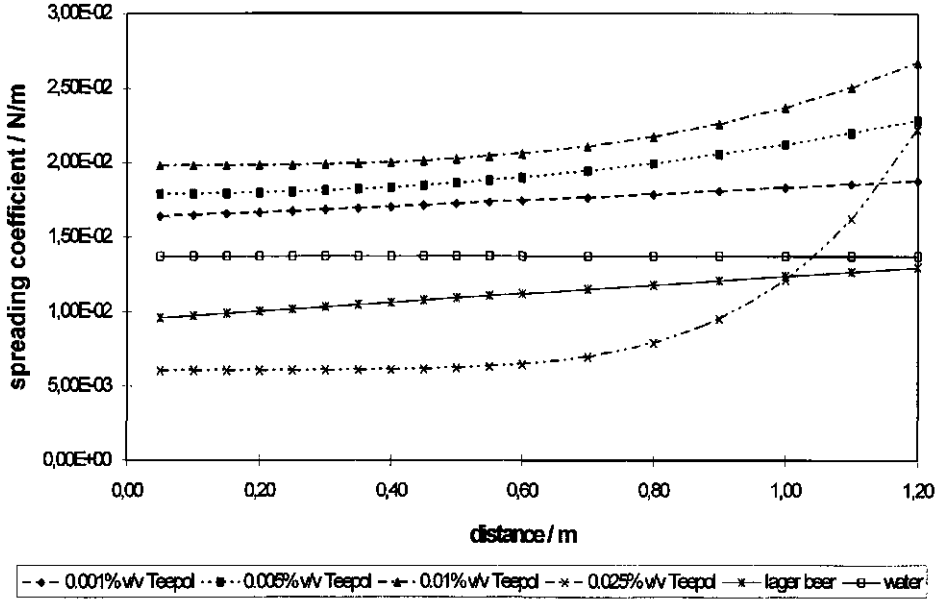

Fig 5.8: ***The spreading coefficients as a function of the spreading distance of a Soy oil + 2% w/w Tween droplet over aqueous surfaces of Teepol solutions with various concentrations which are mentioned in the text.***

in table 5.1 and 5.2 and the surface tensions plotted in Fig (4.17) and (4.18) are used. In Fig (5.8) a maximum in the initial spreading coefficient at a Teepol concentration of 0.01% w/w can be found which is in agreement with the measured spreading velocities. Although the calculated spreading coefficients are not proportional to the measured spreading velocities, it confirms the found evolutions of the spreading velocities as a function of the spreading distance. The spreading coefficients have approximately the same value for water and beer which explains the almost equal spreading behaviour over these two aqueous surfaces as can be seen in Fig (5.1) and Fig (5.6).

5.4. THE EXPERIMENTS IN THE FREE FALLING LIQUID FILM

The free falling liquid film was used to measure in a more quantitative way the effect of spreading droplets on the stability of a thin aqueous film. The experimental device was explained in §4.5.

Compared to the thickness of the films found in a foam, the thickness of this free falling liquid film is rather large. Nevertheless, the measurements were done with relatively large oil droplets and, therefore, rupture of the film should be possible. Additionally, information is gathered about the order of magnitude thickness of a film that can be ruptured by a droplet with certain size.

For each individual experiment a fresh Soy oil (with or without Tween 80 addition) in Teepol (0.15% w/w) emulsion was prepared by using an Ultra Turrax. For experiments to determine the effect of spreading droplets on the stability of a beer film the spreading droplets were also prepared in a Teepol solution instead of beer. This was done because emulsification of Soy oil in beer was difficult due to instability of the emulsion. It is assumed that the very small volume of Teepol solution, accompanying the droplet when it is introduced in the slit, has no effect on the film stability. When a volume of Teepol solution, without droplet was introduced in a beer film, no film destabilisation could be observed. Another assumption is that the droplet adapts to the conditions in beer almost spontaneously.

By using a microscope one droplet, with desired size, was sucked into a capillary. The size of the droplet was measured by using a graduated scale in the microscope. The accuracy of this size-measurement was ± 1.25 μm. The droplet was then injected into the slit of the falling film device as was explained in §4.5. In Fig (5.9) the distances from the slit where a Soy oil + 2% w/w Tween 80 droplets ruptured the film immediately after injection is plotted as a function of the droplet radius. Also the predicted distance calculated with eq. (4.33) is plotted. In this equation can be seen that the rupture distance is mainly determined by the time the droplet encounters the

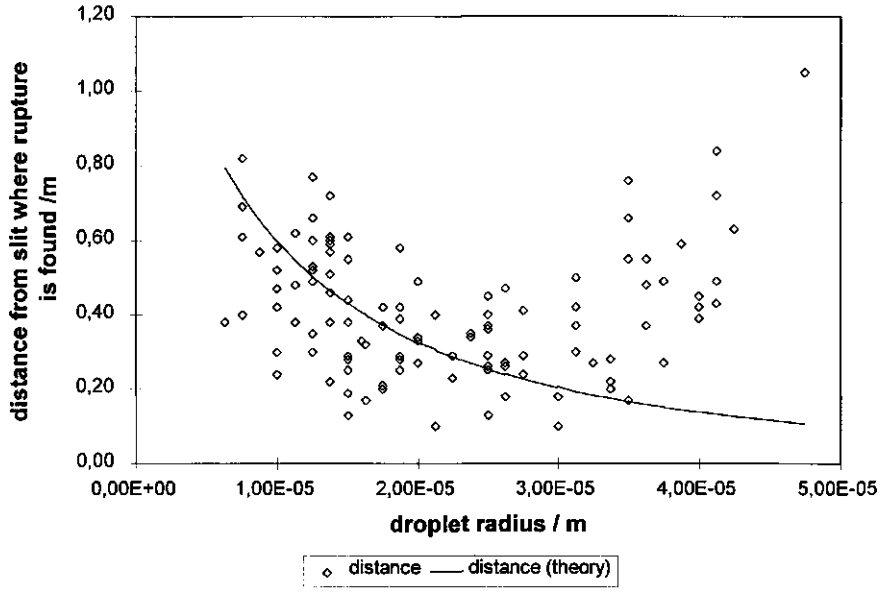

Fig (5.9): ***The distance from the slit where droplets ruptured the film as a function of the radius of Soy oil + 2% w/w Tween 80 droplets. The flow rate was 2.71E-5 m^3s^{-1}***

surface and the drainage time of the thin film separating the droplet from the surface. Although the scattering of the distances is big, the theoretical curve confirms the tendency at smaller droplet radii. However, for larger droplets the theory does not predict the rupture distance. This is due to the fact that for the adjustable parameter α_P (see Fig (4.14) always the same value is used. This value was determined by averaging the calculated values that are needed to predict the measured rupture distances. These values are plotted in Fig (5.10). The average value of α_P appeared to be 20 μm and this value was used in all calculations. When using this value for α_P eq. (4.33) predicts smaller rupture distances when larger droplets are introduced into the film. However, at droplet radii larger than about 20 μm the rupture distance is increasing regarding the measured distances in Fig (5.9).

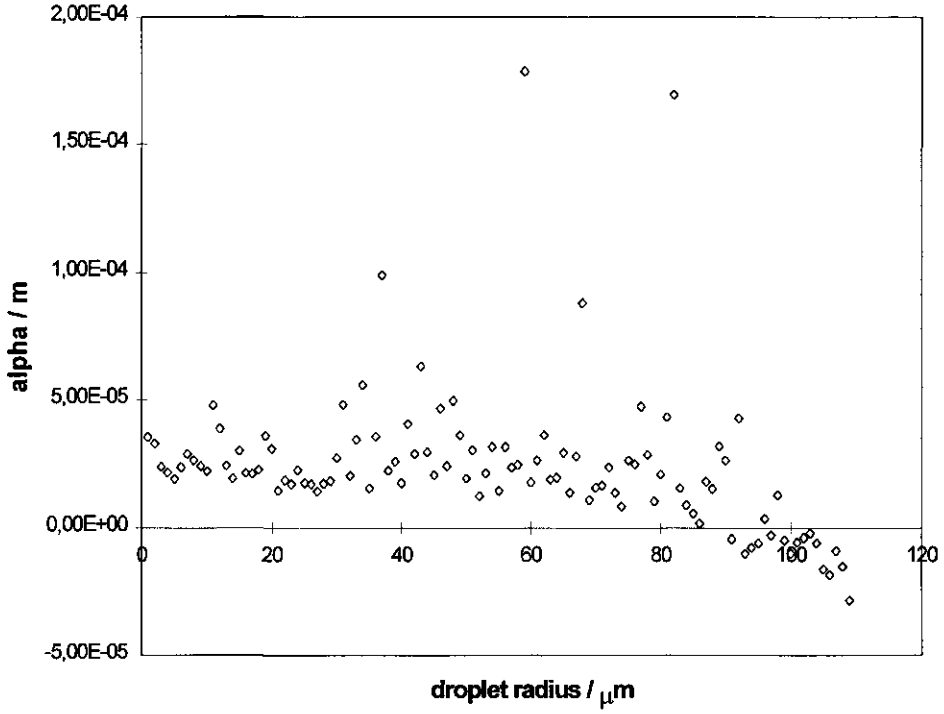

Fig (5.10): The calculated α based on the measured rupture distance of Soy oil + 2% w/w Tween 80 droplets in a 0.15% v/v Teepol film.

This may be explained by the fact that deformation of the droplet is not included in the theory. At smaller droplet sizes this deformation will not be big due to the higher Laplace pressure. However at larger droplet sizes this factor will become more important. In Fig (5.11) the half film thickness, the droplet diameter and the ratio half film thickness / droplet diameter were plotted as a function of the distance from the slit where the droplet encounters the film according to eq. (4.22).

It can be seen that the droplets with a diameter bigger than about 46 μm encounters the film surface at a point where the half film thickness is smaller than the droplet diameter. If we assume that the space wherein a droplet has to fit is limited to half

the film thickness, the droplet should have been deformed. This assumption can be explained by the fact that at the centre, due to symmetry, the velocity component

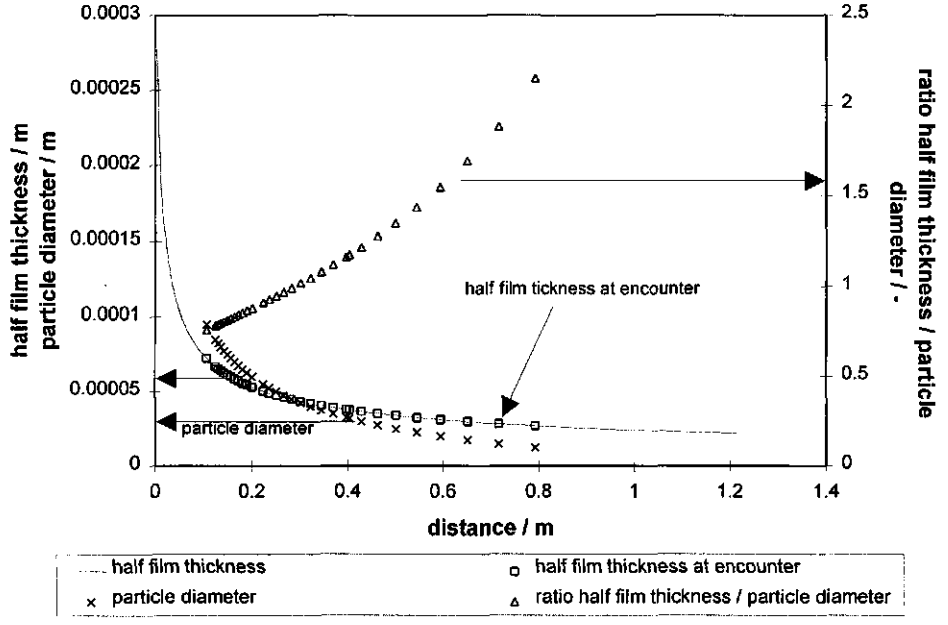

Fig (5.11): The half film thickness, the film thickness when the droplet encounters the surface according to eq. (4.22), the droplet diameter and the ratio half film thickness / droplet diameter.

perpendicular to the film surface is zero. However, close to the centre of the film the velocity component perpendicular to the film surface is the highest. Therefore a droplet with a diameter bigger than 46 μm will be dragged to the film half where most of the droplet is already present. Then eq. (4.23) changes into:

$$t_e = \frac{v_0}{g}\left(\frac{\theta_0}{4.2R_P} - 1\right) \qquad (5.1).$$

From this point on the droplet will be squeezed into half the film thickness. We may assume that the droplet takes an ellipsoidal shape, i.e. like a bulged pancake, with the large radius of curvature a=c acting along the circumference of the pancake and the smallest radius b acting perpendicular to the film surface, b equals about half the thickness of the pancake. The radii of curvature of the top and bottom surface of the pancake are left out of consideration.

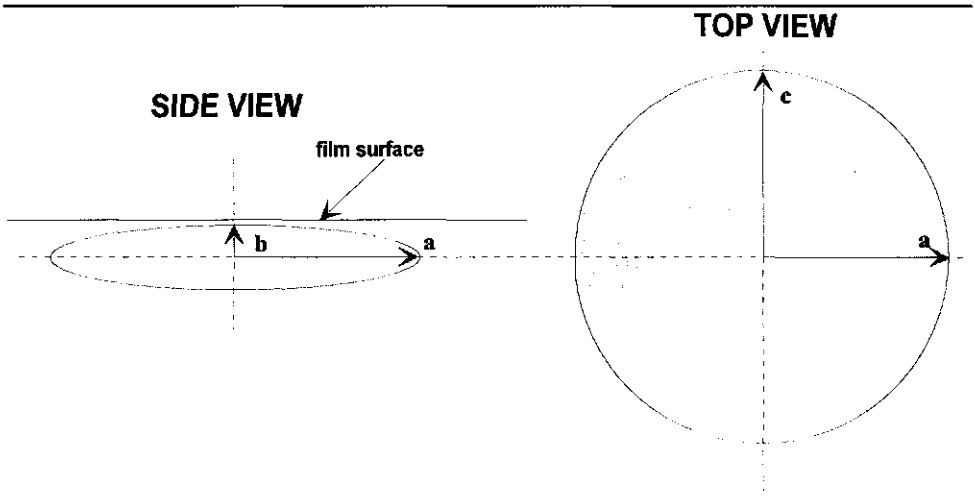

Fig (5.12): A schematic drawing of the droplet deformation squeezed into half the film thickness of the free falling film.

The surface area of the thin film separating the droplet from the surface of the free falling film will increase due to the deformation. If we consider conservation of mass of the droplet we can write this surface area as a function of the film thickness:

$$A = \frac{4\pi R_P{}^3}{\theta_x}$$

(5.2),

where the pancake thickness b=$1/4\theta_x$. We can see in this equation that the surface area is inversely proportional to the film thickness. Taking into consideration the facts that:

1) Larger droplets encounter the film surface at smaller distances from the slit where the decrease of the film thickness is faster and consequently the surface area increase is larger.
2) The radius of curvature of the thin film increases due to the flattening of the droplet.
3) Consequently, the surface area will increase and the pressure difference between the film separating the droplet from the film surface and the pressure in the flat free falling liquid film will decrease due to the increased radius of curvature of the flattening droplet.

Therefore, the draining time according to eq. (4.31) will increase drastically. For this reason the distance where the droplet arrives in the film surface will increase. Consequently, the rupture distance increases with larger droplet radii. Since the change of the radius of curvature was not known, the pressure difference could not be calculated and, therefore, this was not implemented in the theory.

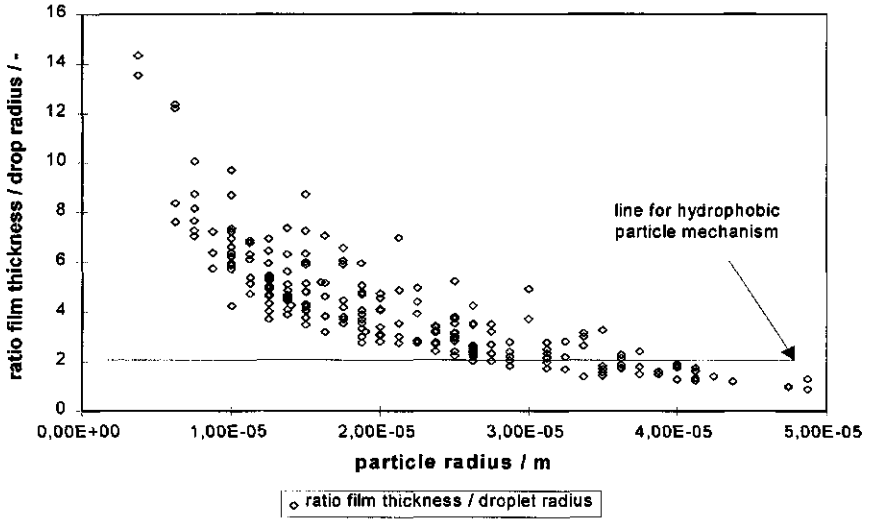

Fig (5.13): The ratio film thickness at rupture / droplet radius as a function of the droplet radius.

It was, however, not the aim of this study to describe this mechanism completely but some interesting conclusions can be drawn from the results. When the ratio: (film thickness at the point of film rupture) / (droplet radius) is plotted as a function of the droplet radius as in Fig (5.13) it can be seen that, especially, the smaller droplets ruptured a film thickness up to more than 14 times the droplet radius. The values in Fig (5.13) are the results from all measurements. These experiments were pure Soy oil or Soy oil + 2% w/w Tween 80 in a 0.15% v/v Teepol film at flow rates 2.71E-5 m^3s^{-1} and 2.05E-5 m^3s^{-1}. Soy oil + 2% w/w Tween 80 in a lager beer film at a flow rate 2.71E-5 m^3s^{-1}. This would implicate that spreading droplets are able to rupture films with a thickness much larger than their own diameter. For that reason we may conclude that once they are spreading over a film surface, they have a much larger film rupturing effect than droplets that cause film rupture according to the hydrophobic droplet mechanism. In the latter mechanism the droplets suppose to rupture a film when the droplet diameter equals the film thickness.

The droplets that ruptured the films with a thickness of 14 times the droplet radius were Soy oil droplets with a radius of 3.75 μm spreading over the surface of a 0.15% v/v Teepol. The spreading coefficient was assumed to be equal to the one presented in table 5.2 for Soy oil on 0.05% Teepol, i.e. 0.0265 Nm^{-1}. According to the theory a maximum film thickness of 26.3 μm can be ruptured by these droplets. However, the falling film is over the whole falling distance thicker than that. The thickness of the film at the rupture distance from the slit was 53.8 μm. Apparently the droplet could rupture a film with twice the thickness as was predicted to be the maximum. This difference can be explained by considering the spreading velocity in relation to the rheological behaviour of the interface. These small droplets have a very high spreading velocity. Consequently the relative surface expansion rate of the interface will be high. The response of the interfacial tension will be a very steep increase towards the values found for a Soy oil-water interface. If we assume that this occurs, the spreading coefficient will decrease to app. 0.0025 Nm^{-1}. When we use this value in the theory a maximum film thickness of 58 μm can be ruptured when

the droplet spreads into a thin layer until it reaches a thickness of 20 Å. Therefore, the conclusion was drawn that, especially with small droplet sizes, the rheological behaviour of the oil-liquid interface at high expansion rates becomes important. According to the theory droplets with radii in the order of magnitude of 1-10 μm spread with velocities of approx. 5 ms^{-1}. Consequently, the relative expansion rates of the oil-liquid interface are approx. 10 s^{-1}.

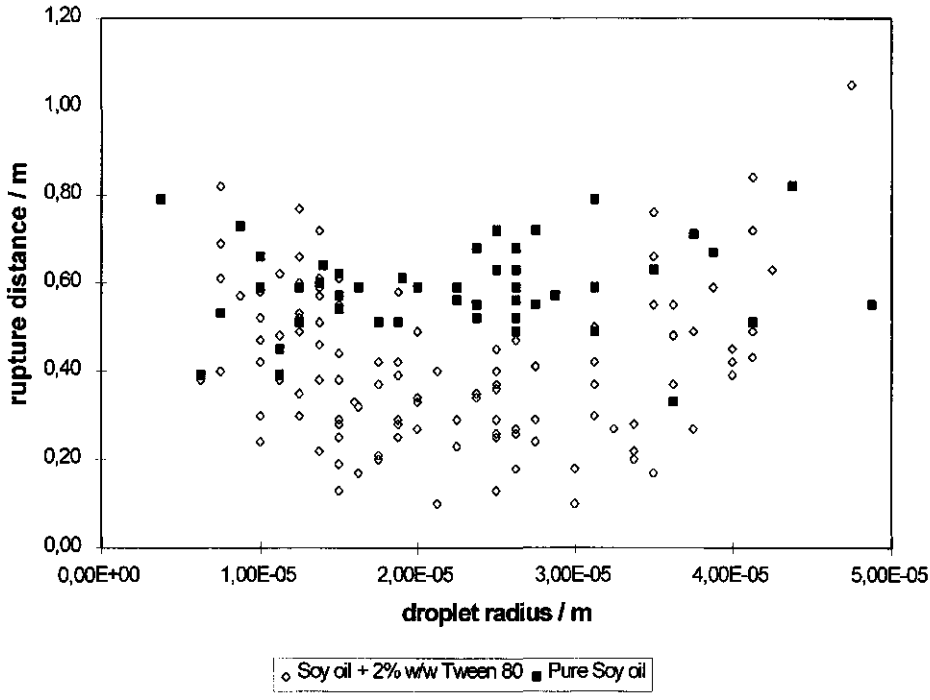

Fig (5.14): The rupture distances of pure Soy oil and Soy oil + 2% w/w Tween 80 as a function of the droplet radius.

Due to the high viscosity of the oil phase these values are not reached in the overflowing cylinder and, therefore, the interfacial tensions measured with this technique are underestimated compared to the values that are probably reached

during spreading of these small droplets. Measurement of the interfacial tension as a function of the expansion rate would have given additional information. This was, unfortunately, not possible with the existing device. For droplets spreading on the surface of the overflowing canal spreading velocities of 0.1-1 ms^{-1} were measured. The expansion rates are, therefore, 10-100 times smaller than found with small droplets. Consequently, in this case, the values of the interfacial tension are believed to be close to the values measured with the overflowing cylinder.

Compared to droplets containing Tween 80, droplets of pure Soy oil rupture the falling film at distances from the slit which are in general longer as can be seen in Fig (5.14). This can be explained by the fact that after these droplets have spread into a thin layer this layer breaks up into small droplets. Since there is hardly no surfactant Tween 80 present in the droplets the spreading does not continue. Therefore, there is a upper limit in film thickness that can be ruptured. Furthermore, due to the fact that the spreading coefficient for pure Soy oil droplets is smaller than for droplets containing Tween 80, the spreading velocity will be smaller and, consequently, the film has fallen further until the droplet displaced enough film liquid that it will rupture. For the larger droplet diameters the same explanation about the droplet deformation as mentioned before, accompanying the observations in Fig (5.14) is valid. In Fig (5.15) can be seen there was no influence of an increase of 32% of the flow rate on the rupture distance. This is due to the fact that the flow rate mainly affects the film thickness close to the slit. Since the droplets are assumed to be introduced near the middle of the film the distance from the slit where they encounter the surface will not differ very much due to the relative small difference in flow rate. Therefore, they rupture the film at approximately the same distances from the slit where the films at both flow rates have approximately the same thickness.

In Fig (5.16) the rupture distances of Soy oil + 2% w/w Tween 80 droplets are plotted as a function of the droplet radius and composition of the free falling film.

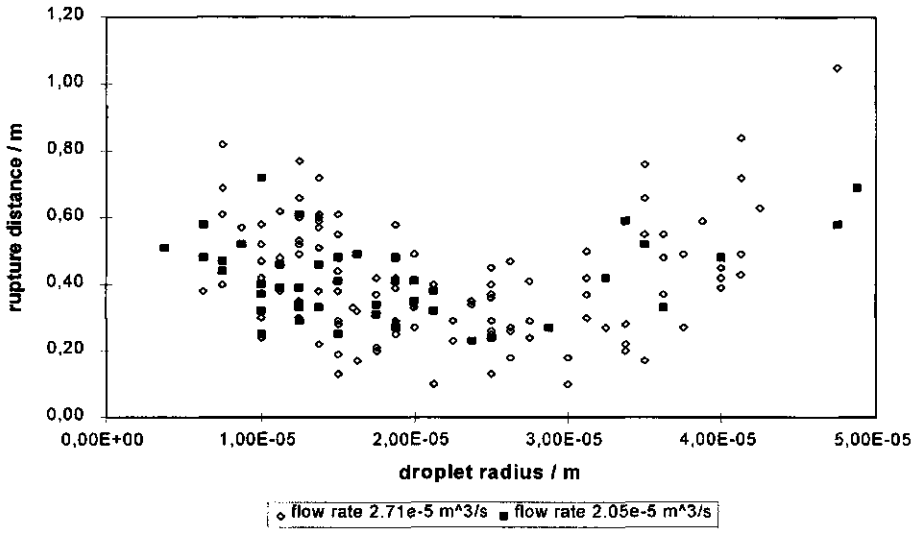

Fig (5.15): The rupture distance of Soy oil + 2% w/w Tween 80 as a function of the droplet radius and the flow rate.

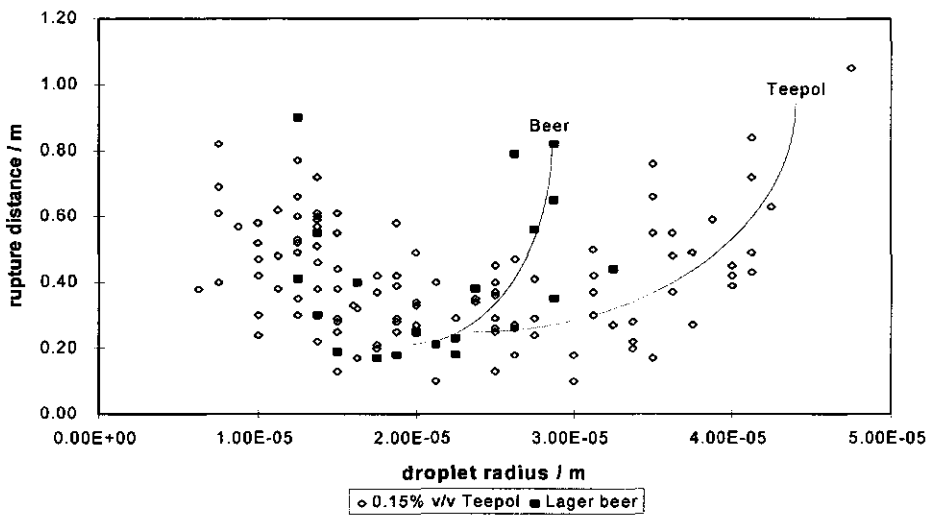

Fig (5.16): The rupture distance as function of the droplet radius and the composition of the film liquid.

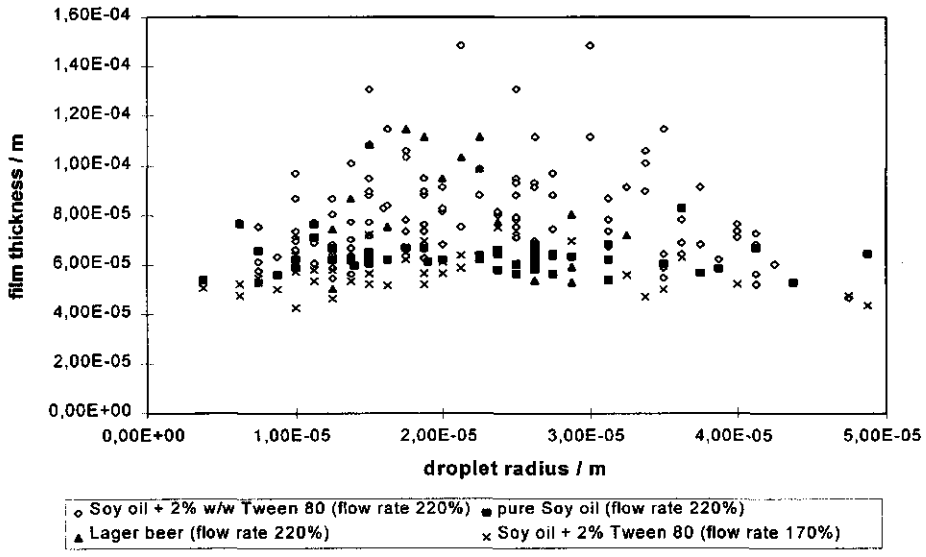

Fig (5.17): The film thickness at rupture as a function of the droplet radius for different Soy oil compositions, film compositions and flow rates.

Comparing the rupture behaviour of droplets of Soy oil + 2% w/w Tween 80 in Teepol or lager beer films the conclusion can be drawn that at small droplet sizes they show the same behaviour. Nevertheless the rupture distance for larger droplets increases much steeper in lager beer than in Teepol. This can be explained by the larger deformation of the droplets in beer due to the lower interfacial tension. For this reason the drainage time of the film that separates the droplet from the film surface, increases and the droplets enter the surface at longer distances from the slit. Furthermore, the dynamic surface tension of lager beer is much lower than the surface tension of the 0.15% v/v Teepol solution, i.e. 48.0 and 67.8 mNm^{-1} respectively (see Table 5.1). Consequently the spreading coefficient will be smaller for beer and the spreading velocity lower. Therefore, the time needed to rupture a certain film thickness will be longer resulting in film rupture at larger distances from

the slit. This effect has a larger impact on larger droplets because of the lower initial spreading velocity. When plotting the film thickness at the point of rupture as a function of the droplet radius, as in Fig (5.17) there appears to be a lower limit of about 47 μm. This is due to the fact that the minimum film thickness at the bottom of the free falling film, i.e. 1.4 m is 43 μm and this observation is an artefact due to the experimental set-up. The maximum distance where film rupture was accepted to be caused by the introduced droplet was around 1 m. Above this distance the free falling film became less stable and spontaneous instability of the film and rupture by spreading droplets could no longer be distinguished. At about 1 m the film thickness is about 47 μm which corresponds to the lower limit found in Fig (5.17).

Surface tension [mNm^{-1}]	Twinkling	Film rupture
43.3	NO	NO
52.5	NO	NO
61.5	NO	NO
64.1	NO	NO
66.8	NO	NO
67.1	YES	NO
67.5	YES	NO
67.9	YES	NO
68.0	YES	YES
68.3	YES	YES
69.1	YES	YES

Table 5.4: The observations on free falling films with varying surface tensions when emulsion droplets are introduced in the film liquid.

Ronteltap (1989) observed twinkling in the film when an emulsion of spreading particles was introduced in the film liquid. He explained this by the fact that the droplets would spread over the film surface but due to the small size they would not

rupture the film. Furthermore, large particle would not come to the surface due to long drainage times of the film separating the droplet from the film surface. In this study a small volume of an emulsion of Soy oil + 2% w/w Tween 80 in 0.15% v/v Teepol separately prepared from the solution in the falling film was introduced in films with different surface tensions (i.e. different Teepol concentrations). The results are presented in table 5.4.

In table 5.4 it can be seen that at surface tensions above 66.8 mNm^{-1} the emulsion droplets initiate twinkling but no film rupture. From surface tensions of 68.0 mNm^{-1} and higher both occurs. If it is assumed that the interfacial tension of the droplets increases during spreading towards pure Soy oil against water a surface tension of the film larger than 65 mNm^{-1} is needed to initiate spreading. For this reason, in a film with a surface tension close to 65 mNm^{-1} no twinkling could be observed. Between 66.8 and 68 mNm^{-1} only twinkling could be observed. There are reasons to believe that the curvature of the film towards the centre of spreading is responsible for the optical effect that is called twinkling. It is also possible that a difference in refractive index between the aqueous phase and the oil layer causes different reflection of the stroboscopic light. After spreading stops the film will restore itself again and the flat film surface after restoration will provide no optical effect. In this way twinkling of light flashes can be explained. Only during the short period of spreading time this optical effect occurs. This can be explained by the droplet size according to Ronteltap (1989). He measured the droplet size distribution in the emulsion he introduced into the falling film. He suggested that smaller droplets may spread but do not induce film rupture due to the insufficient spreading distance. In that case the film would become thinner at the centre of spreading but will not reach the critical thickness for rupture because the spreading process did not proceed far enough. Considering the theory postulated in Chapter 3 this is not very reasonable since this theory predicts already film rupture at small droplet radii. This was also confirmed by the results from the experiments done with single droplets. A more reasonable explanation would be that multiple droplets

spread almost simultaneously over the film surface. Consequently they spread towards each other and the surface tension of the 'clean' aqueous surface between the spreading droplets will decrease due to compression. As soon as it decreases to 65 mNm^{-1} the spreading process will stop because the spreading coefficient has become zero. Therefore, spreading occurs without rupturing the film. Another speculative explanation would be the influence of the surface dilational viscosity. Bergink-Martens found a small increase of its value at lower Teepol concentrations. This would decrease the spreading velocity which diminishes the possibility of film rupture and 'twinkling' would remain as an observation after introduction of emulsion in the film.

At surface tensions above 68 mNm^{-1} besides twinkling also film rupture was observed. This can be explained by the spreading velocity. Due to the increased spreading coefficient at lower Teepol concentrations the spreading velocity will increase. Consequently, within a certain time interval more surface area will be covered by the spreading particle. It is impossible for the emulsion droplets that are still in the film liquid to come to the surface area covered with a spreading droplet because then the entering coefficient would be equal or even smaller than the value necessary for a droplet to enter the film surface. This is due to the lower surface tension as a result of spreading material. Therefore, in combination with the increased spreading velocity, the chance that a droplet can spread far enough to induce film rupture increases. Apparently at surface tensions above 68 mNm^{-1} this is the case. Theoretically, it is expected that, at low droplet concentrations, twinkling and film rupture would take place simultaneously. It could be possible that the droplet concentration was too high. Unfortunately, the effect of droplet concentration on the observations in the film was not investigated. However, it has to be noted that the very small surface tension difference of the falling film where only twinkling or both twinkling and film rupture could be observed, i.e. 0.9 mNm^{-1}, could be a measurement error. Additionally, the surface tensions were measured using the overflowing cylinder technique and not directly in the free falling film itself which may

have introduced an error although this would be contradictive to the theory elucidated in Chapter 4.

The possible influence, of exchange of components between Soy oil droplets containing 2% w/w Tween 80 and the used 0.15% Teepol solutions, during the preparation of the droplets, on the spreading behaviour of the soy oil was tested. Samples of Soy oil were kept in contact with the Teepol solution during 24 hours by using the method described in §4.8. After this period of time the spreading ability of the oil was tested on an equilibrium surface of Teepol solutions with varying surface tensions. As a reference, the spreading behaviour of oil droplets that not have been in contact with the Teepol solution was tested. The results are presented in table 5.5.

Surface tension aqueous phase [mNm^{-1}]	Yes/No spreading of reference	Yes/No spreading after contact time
51.0	Y	Y
53.7	Y	Y
56.8	Y	Y
59.6	Y	Y
66.5	Y	Y

Table 5.5: The effect of contact time of droplets with the aqueous phase on their ability to spread.

From these results can be concluded that there is no effect of the contact time of the oil droplets with the Teepol solution on the spreading ability. An influence on the spreading velocity was not tested. It has to be mentioned that the spreading velocities, judged by eye, were relatively small. This would explain that no twinkling is observed when emulsions were introduced into the falling films with surface

tensions in he same range (see Table 5.4). Apparently, due to the low spreading velocity the droplets do not deform the falling film in such a way that a reflection effect occurs.

5.5. COMPRESSION EXPERIMENTS IN THE LANGMUIR TROUGH

Compression experiments were done in a Langmuir trough equipped with a caterpillar belt as described in §4.9. This was done to obtain information about the response of the surface tension upon compression. When droplets are spreading over the surfaces of bubbles the surface area in front of the spreading droplet is compressed because the bubble surface is finite. This may have consequences on the spreading coefficient because the surface tension of the aqueous phase may decrease to a value that the spreading coefficient becomes zero or even negative. Consequently the spreading process will stop and the displaced liquid within the film may restore the original film thickness and film rupture will not take place. This phenomenon is expected to take place when the bubbles are smaller and, therefore, this could be one of the reasons that foams with smaller bubbles are more stable against spreading droplets than coarser foams.

In Fig (5.18) the change in surface tension upon a single compression of a lager beer, 0.25% v/v Teepol and a 1% v/v Teepol solution are plotted as a function of the relative surface compression rate. It can be seen that the beer surface shows a steep decrease in surface tension but does not reach the low values of the Teepol solutions. Although the surface compression rates here are small compared to the compression rates that exist during spreading of small droplets over film surfaces of bubbles, these results indicate that the surface rheological behaviour of lager beer provides a larger inhibition of the spreading process due to the larger decrease in surface tension upon surface compression. On the other hand we can conclude that, due to the higher surface tension droplets with certain surface tension values may spread on this beer but not on the Teepol surfaces.

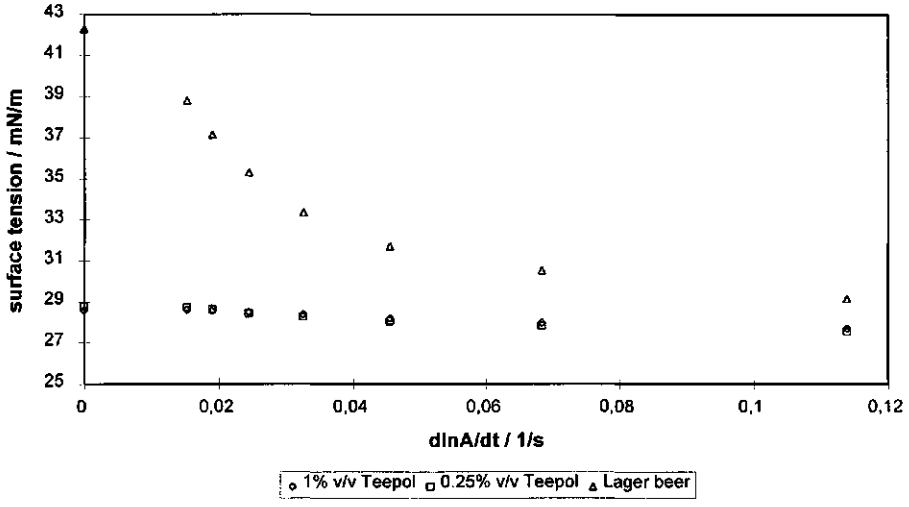

Fig (5.18): The surface tension as a function of the relative surface compression rate in a single compression experiment using a Langmuir trough equipped with a caterpillar belt.

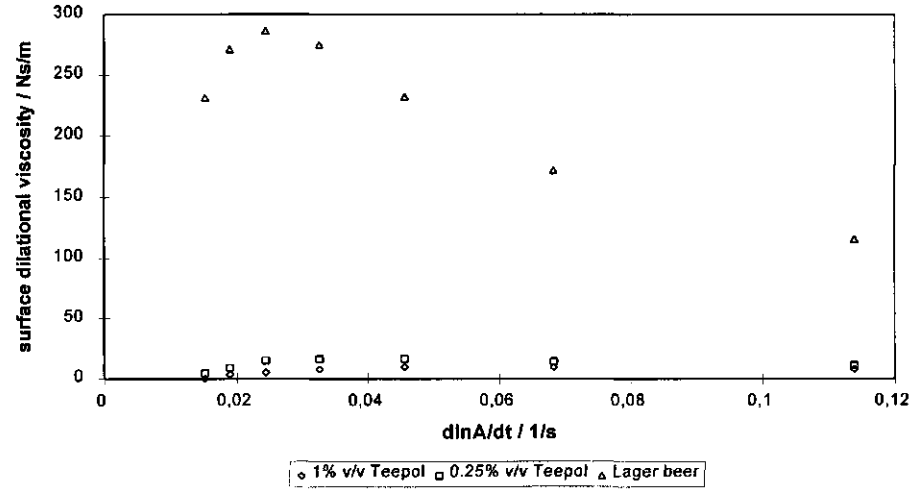

Fig (5.19): The surface dilational viscosity as a function of the relative surface compression rate during single compression experiments in a Langmuir trough equipped with a caterpillar belt.

Ronteltap (1989) stated that the decrease of the surface tension in compression is related to the surface dilational viscosity. A high surface dilational viscosity provides low surface tensions in compression. In Fig (5.19) the surface dilational viscosity is plotted as a function of the relative surface compression rate. It is clear that the surface dilational viscosity of the lager beer is much higher than for the Teepol solutions.

This confirms the values presented in Fig (5.18). It would provide a lot of information if the response of the aqueous surface upon compression could be measured at compression rates that are developed during spreading. However, these compression rates could not be established with the device used here. Nevertheless, the results indicate that the response of the aqueous surface may determine up to a large extent the spreading behaviour on finite surfaces as will be presented in the next paragraph; §5.6.

5.6. SPREADING EXPERIMENTS ON FINITE BULK SURFACES

In contrast to spreading experiments done on film surfaces that will be discussed in §5.7 spreading experiments were carried out over surfaces of bulk liquids. To test the effect of the surface tension upon spreading the displacement of Talcum particles due to spreading over an equilibrium surface in a Langmuir trough was measured. The equipment was discussed in §4.8 and a schematic representation of the experimental set-up can be found in Fig (4.28). Different equilibrium surface tensions were generated by using solutions with different concentrations of Teepol. The spreading droplets were pure Soy oil, Soy oil + 0.1% w/w Tween 80 and Soy oil + 2% w/w Tween 80.

In Fig (5.20) the displacement of the Talcum barrier is plotted as a function of the surface tension of the aqueous phase. A 100% displacement corresponds to displacement of the Talcum barrier up to the opposite wall of the trough. In other

words, the values give the percentage of the original aqueous surface that was compressed. In this figure it can be seen that the spreading distance increases for all spreading oils with increasing surface tension. It is known that, according to Bergink- Martens (1993), in these ranges of Teepol concentrations the surface dilational viscosity increases with higher surfactant concentrations. Therefore these measurements confirm the effect of the surface dilational viscosity on the spreading process because at higher Teepol concentrations the surface tension will decrease more rapidly and the spreading process stops in an earlier stage.

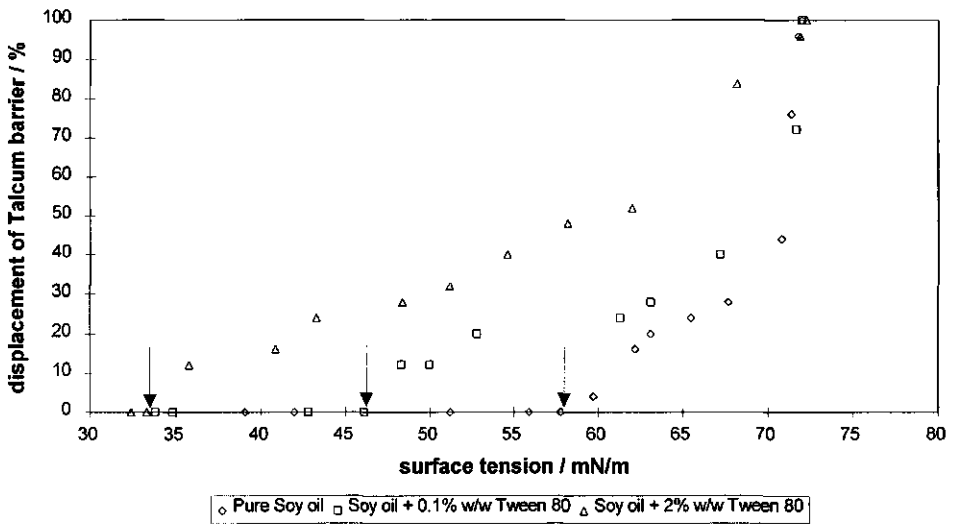

Fig 5.20: ***The displacement of a Talcum barrier as result of a spreading droplet on surfaces with different equilibrium surface tensions. The arrows indicate the surface tension were the droplets of Soy oil with different concentrations Tween 80 start to spread.***

The driving force for the spreading is the spreading coefficient or, in the case of a monolayer, the surface tension difference. We see in Fig (5.20) that the spreading

of the different Soy oil samples starts at different surface tensions. This can be explained by the value of the spreading coefficient. The value of the surface tension of the Soy oil did not change upon addition of Tween 80 as was mentioned in table 5.1. However, addition of Tween 80 to the Soy oil gives a decrease of the interfacial tension of the Soy oil. This decrease was bigger when more Tween 80 was added. The pure Soy oil starts to spread at about 58 mNm^{-1}. If we take a surface tension of 32.5 mNm^{-1} for Soy oil, the dynamic interfacial tension would be at the maximum 25.5 mNm^{-1}. This value is reasonable considering a value of 32.0 mNm^{-1} found for the dynamic surface tension of pure Soy oil against clean water. For the same reasons the other two Soy oil samples start to spread at lower surface tensions because of the decrease of the interfacial tension of the Soy oil due to increasing Tween 80 and Teepol concentrations. The values calculated for the interfacial tensions were 13.6 and 0.8 mNm^{-1} for 0.1% w/w and 2% w/w Tween 80 addition to the Soy oil. These values are in agreement with the order of magnitude of the values measured with the overflowing cylinder technique.

The increase of the spreading distance with decreasing Teepol concentrations can also be explained with the spreading velocity. The interfacial tension of the Soy oil increases due to lower Teepol concentrations. The effect is that the spreading velocity decreases and consequently the compression rate of the aqueous surface. Therefore, the surface tension of the aqueous phase decreases less due to a lower spreading velocity but also due to a larger effect of the relaxation processes. Hence the droplet can spread further until the spreading coefficient becomes zero. This is confirmed by the experimental results. Furthermore, in the concentration range used here, which was between 10^{-3} and 10^{-2} ml/l Teepol the surface dilational viscosity decreases with lower Teepol concentrations. At higher Teepol concentrations the surface dilational viscosity goes through a maximum as was reported by Bergink-Martens (1993). By combining this effect with the lower spreading velocity, the droplet may spread further until the surface tension has decreased far enough to stop the spreading process.

In Fig (5.20) a tendency can be observed that at higher Tween 80 concentrations in the Soy oil, the spreading distance increases less with increasing surface tensions of the aqueous phase. This can be explained with the surface dilational viscosity of the aqueous phase. We assume equal spreading coefficients, i.e. equal spreading velocities. For the Soy oil + 2% w/w Tween the condition of the same displacement of the Talcum barrier is satisfied at higher Teepol concentrations compared to the 0.1% w/w Tween 80 and the 0% w/w Tween 80 concentrations in the oil phase. At higher Teepol concentrations the surface dilational viscosity is higher. Consequently, the surface tension decrease will be larger and the spreading process will stop earlier.

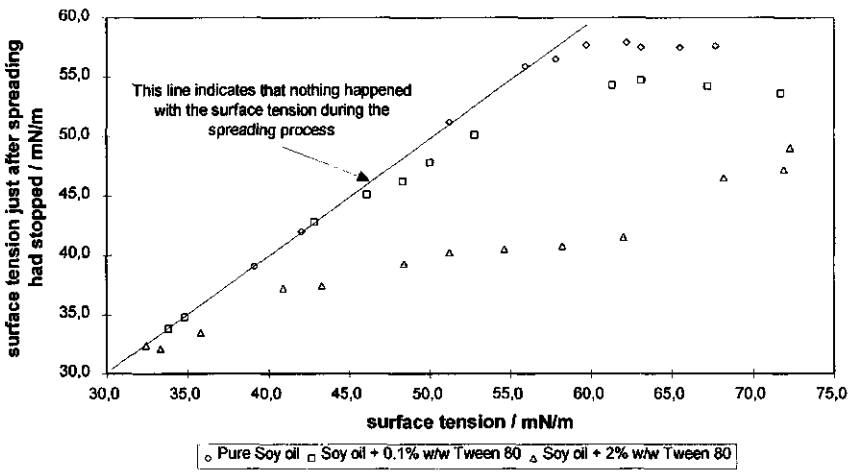

Fig (5.21): The surface tension of the aqueous solution measured near the opposite wall of the trough just after the spreading process had stopped as a function of the equilibrium surface tension of the aqueous phase before spreading.

In the case of clean water all displacements are 100%. This indicates also the effect of the surface dilational viscosity. In clean water a surface dilational viscosity is

zero. Therefore, the surface tension will not decrease and spreading can proceed to a 100% displacement of the Talcum barrier. In Fig (5.21) the surface tension measured near the opposite wall of the trough at the moment the spreading process had stopped is plotted as a function of the equilibrium surface tension before a droplet has spread. It can be seen that due to the higher spreading rate and the lower interfacial tension of the oil the surface tension must decrease more before the spreading stops when the Tween 80 concentration in the Soy oil is increased. Additionally the values appear to reach a plateau at low Teepol and Tween 80 concentrations. This Plateau is due to the fact that at these low Teepol concentrations there is no longer a decreasing effect of the Teepol on the interfacial tension. Only the effect of Tween 80 can be observed in the lower plateau value of the Soy oil + 0.1% Tween 80. The Soy oil + 2% Tween 80 does not reach a plateau since the interfacial tension of the oil phase is close to zero as was already measured with the overflowing cylinder technique.

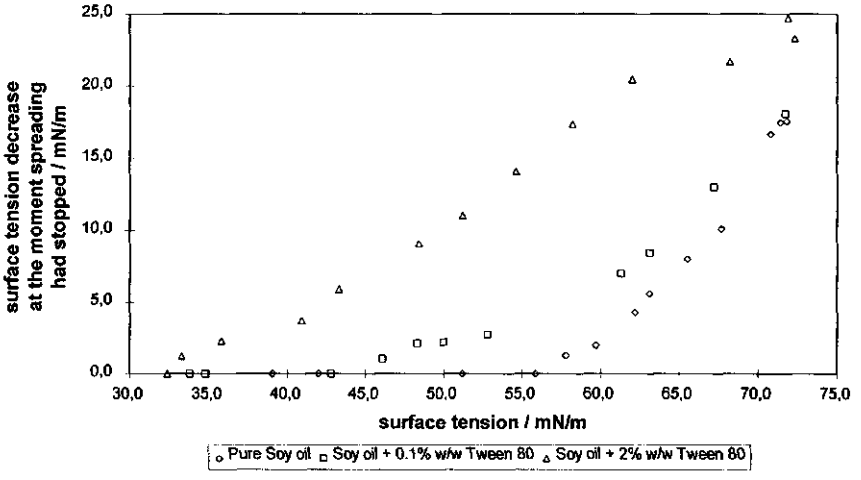

Fig (5.22): The decrease of the surface tension at the moment the spreading had stopped as a function of the equilibrium surface tension of the aqueous phase.

The surface tension decrease at the moment when the spreading had stopped, is plotted in Fig (5.22). This decrease is, in theory, equal to the spreading coefficient since at those moments the spreading coefficient has become zero. When evaluating the values presented in Fig (5.22) these values are in good agreement with the values mentioned in table 5.3 and it can be seen that the spreading coefficient increases with decreasing Teepol concentrations in the aqueous phase and with increasing Tween 80 concentrations in the oil phase. It is important to know that spreading experiments on equilibrium beer surfaces are not done because Soy oil does not, or very slowly (i.e. when Tween 80 was added to the oil phase), spread on these surfaces. This confirms the spreading behaviour listed in Table 5.3. The overall conclusion that can be drawn is that for the spreading on a finite surface the surface dilational viscosity is an important parameter. However, the aqueous surfaces in a foam are not in complete equilibrium and, therefore, the normally used definition for the surface dilational viscosity is not valid. To obtain information about the effect of the spreading process on an already expanding surface a technique should be developed with which an expanding aqueous surface is exposed to a spreading droplet with a relative expansion rate which is bigger than the relative surface expansion rate of the 'clean' aqueous surface. Furthermore, the compression rates should equal the compression rates found in practice during the spreading process. This technique was not available and, therefore, no data are available to be correlated to the spreading process.

Another important aspect is the presence of surfactant in the oil phase. Due to this surfactant the oil droplet can spread even over surfaces with low surface tensions. This means in practice that oil droplets containing surfactant destabilize the films in a foam over a wider range of surface tensions. Therefore, they can deteriorate a foam to a large extent.

5.7. EXPERIMENTS ON FINITE FILM SURFACES

These experiments were done to provide qualitative information about the influence of the surface area of a thin film on the effect of the presence of spreading droplets. The experimental set-up was discussed in §4.8 and a schematic presentation can be found in Fig (4.26). The oil droplets were introduced on and in the thin film with different diameters of 0.02, 0.04, 0.06, 0.08, or 0.1 m. The film liquid was a 0.15% or a 1% v/v Teepol solution and the composition of the oil phase was varied between pure Soy oil and Soy oil containing 2% w/w Tween 80. The droplets that were brought on the surface had a volume of about 5 μl. The droplets introduced in the film were prepared as an 0.05% w/w emulsion in the film liquid (a 0.15% or a 1% v/v Teepol solution) by using an Ultra Turrax. From these emulsions films were drawn in the frames as mentioned before and their film stability was monitored. In Table 5.5 the observations made for the different experiments are presented as Yes/No rupturing of the film. The results in Table 5.6 show, although they are qualitative and only in the case that droplets are brought on the film, that the surface area of a film has an effect on the film stability. When the droplets were brought on the film surface they ruptured the film of 0.15% v/v Teepol when it had a diameter larger than at least 0.04 m. Apparently, the surface areas of films with a diameter smaller than 0.04 m provide not enough spreading space to induce film rupture. It can be argued that the film elasticity plays a role in governing the spreading behaviour of a droplet and the effect of the latter on the film stability. This would be the case if transport of surfactant by means of diffusion from the compressed film surface in front of the spreading material to the opposite film surface is faster than the film thinning process. If this is the case an additional surface tension gradient at the opposite surface would be developed. This will result in movement of the opposite surface towards the centre of spreading. This surface motion exerts a shear stress on the film liquid which will start to move also towards the centre of spreading leading to a film thickening process at that region of the film.

Place of droplets	Aqueous phase	Oil phase	Ring diameter [m]				
			0.02	0.04	0.06	0.08	0.1
On big droplets	0.15% v/v Teepol	Pure Soy oil	N	N	Y	Y	Y
On big droplets	0.15% v/v Teepol	Soy oil + 2% w/w Tween 80	N	N	N	Y	Y
On big droplets	1% v/v Teepol	Pure Soy oil	N	N	N	N	N
On big droplets	1% V/V Teepol	Soy oil + 2% w/w Tween 80	N	N	N	N	N
In small droplets	0.15% v/v Teepol	Pure Soy oil	Y	Y	Y	Y	Y
In small droplets	0.15% v/v Teepol	Soy oil + 2% w/w Tween 80	Y	Y	Y	Y	Y
In small droplets	1% v/v Teepol	Pure Soy oil	N	N	N	N	N
In small droplets	1% v/v Teepol	Soy oil + 2% w/w Tween 80	N	N	N	N	N

Table 5.6: The effect of spreading droplets on the stability of thin liquid films with different diameters. The droplets are brought on and in the film which cause Yes or No film rupture.

A high enough film elasticity may, therefore, at least postpone or even prevent film rupture. The transport by means of diffusion can be described by the penetration theory which is described by eq. (5.2).

$$P^* = \sqrt{\pi D t} \qquad (5.2),$$

where P^* is the penetration depth, D is the diffusion coefficient and t is time. In our case the penetration depth equals the film thickness δ.

In Fig (5.23) the displacement of the surface at the centre of spreading, which follows the penetration of liquid motion according to eq. (3.36), and the penetration according to eq. (5.2) are plotted as a function of spreading time. On the Y-axis point zero indicates the initial level of the film surface before spreading has started.

It is clear that the penetration velocity of liquid motion into the film liquid is much higher than the penetration velocity of diffusion. Therefore, it can be concluded that the information of surface compression at one side of the film will never reach the other side of the film before the spreading droplet has ruptured the film. In other words, the effect of film elasticity has no time to be developed and the spreading process and the accompanied film thinning are only governed by viscous flow. For this reason the effect of the surface dilational viscosity has to be considered.

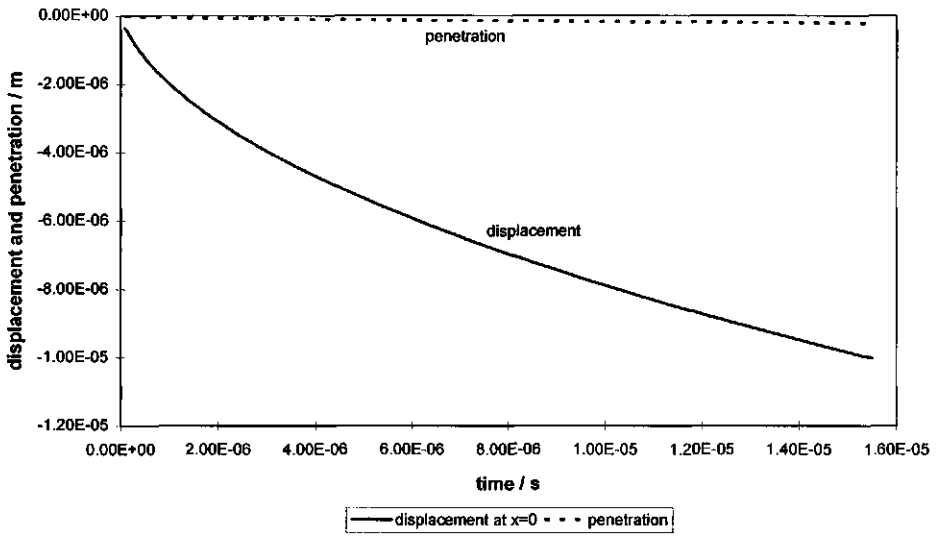

Fig 5.23: ***The penetration of liquid motion into the film liquid according to eq. (3.36) and the penetration according to the penetration theory (see eq. (5.2)) plotted as a function of the spreading time.***

As was mentioned in §5.7, the surface dilational viscosity can also influence the spreading behaviour. If a small diameter ring is used, the relative compression rate of the aqueous surface will be high due to the initial high spreading velocity. This will stop the spreading process earlier due to the steep decrease in surface tension

of the film. Bringing oil droplets on the surfaces of films made of 1% v/v Teepol, showed no effect on the stability. This is not surprising when regarding the spreading coefficient. Are the spreading coefficients 0.0263 and 0.0348 Nm^{-1} for pure Soy oil and Soy oil + 2% Tween 80 respectively on 0.15% v/v Teepol; on 1% v/v Teepol they are respectively -0.0058 and -0.0048 Nm^{-1}. This explains that oil droplets brought on the 1% v/v Teepol have no effect.

When attempts were made to produce films from emulsions, to study the effect of droplets in the film, this was not possible from the 0.15% v/v Teepol solution. However, from the 1% v/v Teepol solution stable films could be made. When regarding the spreading coefficients this difference is not surprising. There is an other argument that can be used to explain this difference. The entering coefficients for pure Soy oil and Soy oil + 2% w/w Tween 80 on 0.15% v/v Teepol are respectively 0.0437 and 0.0352 Nm^{-1}. For the 1% v/v Teepol they are respectively -0.0038 and 0.0048 Nm^{-1}. Therefore, the emulsion droplets in the 1% v/v Teepol solution do not even come into the surface. Interesting would be to test a situation with negative spreading coefficient and a positive entering coefficient. This is theoretically possible when lower Teepol concentrations are used and consequently the interfacial tension of the oil increases. However, in practice it is not possible to produce a stable film with these concentrations of Teepol. All the films made out of the 0.15% v/v solution were unstable. This is different from bringing droplets on the surface when considering the size of the droplets. In the emulsion are the droplets much smaller than when a droplet was brought on the surface. This has influence on the distance a droplet can spread. For emulsion droplets this is further because they are much smaller in relation to the available surface area of the film over which they can spread. The droplets brought on the surface by means of a syringe have already a diameter which only 10-100 times smaller than the film diameters. When these droplets are brought on the film they will cover the total film surface very fast by a monolayer due to their relatively large content of surfactant (i.e. Tween 80). This will inhibit further spreading of the droplet over the film surface. In contrast, the

emulsion droplets have diameters 10^4-10^5 times smaller than the diameters of the films. Due to their relatively small content of surfactant they do not cover the film surface instantaneously with monolayer and consequently they can proceed spreading resulting in, eventually, film rupture. Additionally, according to the theory discussed in Chapter 3, these smaller droplets will spread with a higher initial velocity which is in favour of the chance to rupture the thin liquid film. Although it has to be mentioned that this velocity must not be too high so that there is not time enough for the film thinning process.

5.8. MEASUREMENTS OF THE SURFACE DILATIONAL MODULUS

In Chapter 2 the possible effect of the surface dilational modulus was suggested. Prins (1989) derived an equation, see eq. (2.39), with which the influence of the surface dilational modulus on the spreading velocity of a monolayer is described. For that reason eq. (2.39) was rewritten to a velocity as a function of the spreading distance:

$$v_L = \frac{E^{\frac{2}{3}}}{\xi^{\frac{1}{3}}(\eta\rho)^{\frac{1}{3}}} \qquad (5.3),$$

where, v_L is the velocity according to the longitudinal wave theory.

A high surface dilational modulus would, according to eq. (5.3) increase the spreading velocity of the monolayer assuming the spreading velocity is equal to the propagation speed of a longitudinal wave. In this study we wanted to see if the same correlation can be found for the spreading of oil droplets. For that reason the surface dilational modulus was measured for the Teepol solutions used in the overflowing canal. The results are presented in Fig (5.24).

In Fig (5.24) it can be seen that the moduli increase with decreasing Teepol concentrations over the whole range of frequencies. This means that the

longitudinal wave would propagate with a higher velocity over the solutions with lower Teepol concentrations. The results presented in §5.3 showed, however, an increasing velocity at higher Teepol concentrations in the aqueous phase. Therefore, the conclusion can be drawn that the propagation speed of the front of a spreading oil droplet follows not the longitudinal wave theory. To illustrate this, the measured spreading velocity of Soy oil + 2% w/w Tween 80 on 0.001% v/v Teepol solution, the velocity calculated according to the theory presented in this study and the propagation speed according to eq. (5.3) of Prins (1989) and according to the theory of Joos and Pintens (1977) are plotted in Fig (5.25).

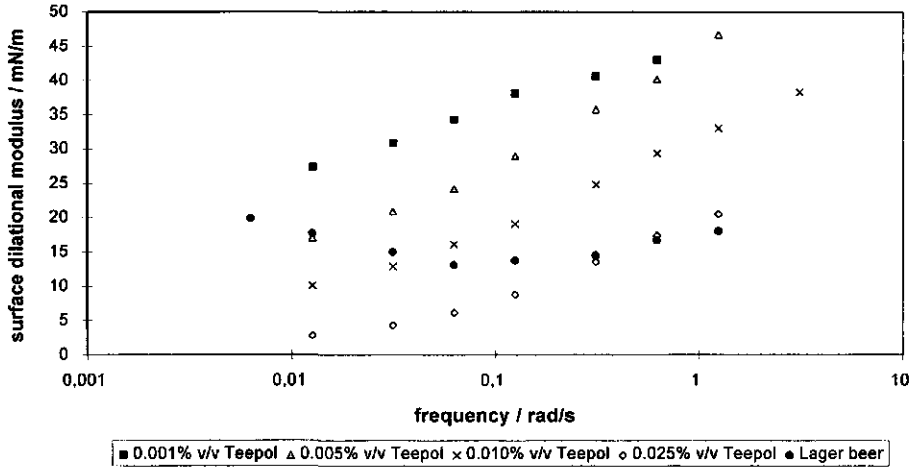

Fig (5.24): The surface dilational moduli as a function of different deformation frequencies for the Teepol solutions and lager beer used for the spreading experiments in the overflowing canal.

For the calculation of the velocity according to the longitudinal wave theory of Prins (1989) the highest measured modulus was chosen. In this case the modulus used in eq. (5.3) was 0.04 Nm^{-1} (see Fig 5.24) since the deformation rates during this spreading process are in the order of magnitude of 1 s^{-1}, i.e. the differential of the spreading velocity as a function of spreading distance. For the sake of clarity, the

deformation rates increase drastically towards smaller spreading distances due to the increasing spreading velocity as a result of the higher surface tension gradient (see Chapter 3). The theory of Prins (1989) underestimates the velocity but it can be seen that this theory delivers a line parallel to the measured velocities.

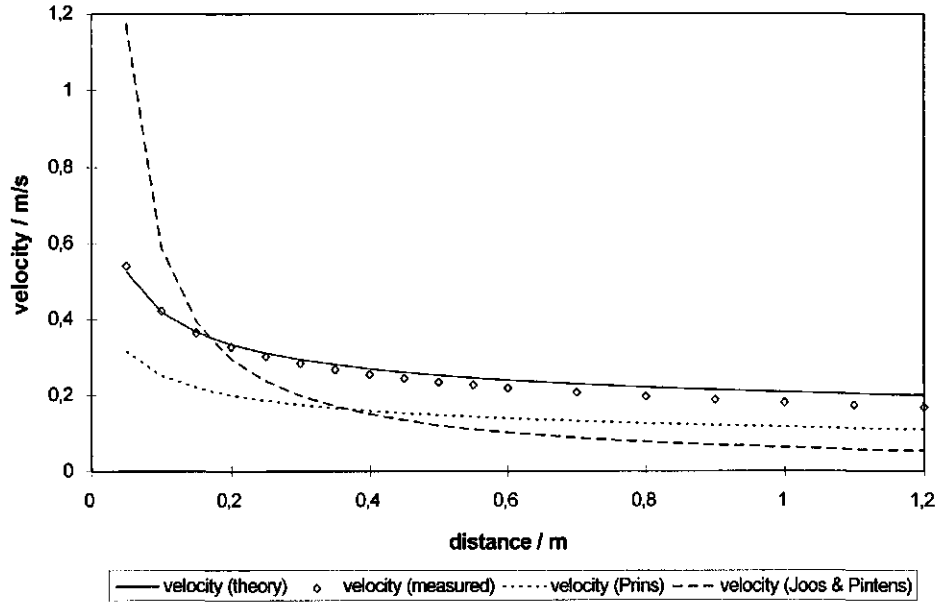

*Fig (5.25): **The spreading velocities that were measured, predicted by the theory presented here and predicted according to the longitudinal wave theory of Prins (1989), see eq. (5.3) and according to the theory of Joos and Pintens (1977) on the surface of an aqueous solution of 0.001% v/v Teepol in the overflowing canal.***

However, this difference will increase with increasing Teepol concentration since the surface dilational modulus decreases with increasing Teepol concentration and consequently the propagation speed will also decrease. However, in this study an increasing spreading velocity was found when the Teepol concentration was higher.

In Fig (5.25) can be seen that the velocity according to the longitudinal wave theory of Joos and Pintens (1977) is overestimating at smaller spreading distances and underestimating at longer distances compared to the velocities measured and predicted by the theory presented here. In the theory of Joos & Pintens (1977) the spreading coefficient was introduced for the surface tension difference. Therefore this kind of spreading velocity profile found here by applying the theory of Joos & Pintens (1977) will also be found at higher Teepol concentrations.

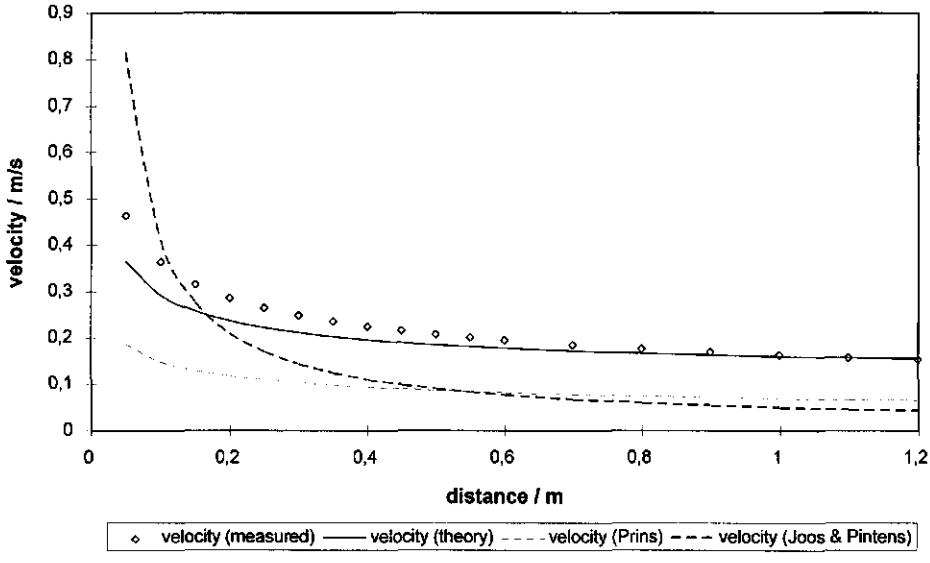

Fig (5.26): The spreading velocities according to the theory presented here, the measured values and the velocity predicted by the longitudinal wave theory of Joos & Pintens (1977) and Prins (1989), see eq. (5.3) on the surface of an aqueous solution of lager beer in the overflowing canal.

In the case of lager beer, which shows a different behaviour of the dilational modulus, we performed the same exercise and the result is presented in Fig (5.26).

Also in Fig (5.26) we can observe a much lower velocity predicted by Prins (1989) and overestimation at smaller spreading distances and an underestimation at longer distances when the theory of Joos & Pintens (1977) is used. The conclusion was drawn that the spreading of oil droplets, as far as we can see from the results presented here, does not follow the longitudinal wave theory.

5.9. GENERAL DISCUSSION AND FINAL CONCLUSIONS

This study was an attempt to describe the rupture of thin films in a foam due to the spreading of droplets over one of the surfaces of those films. This mechanism is important for several reasons. In practice foams are often destroyed when it is not desired or a foam must be destroyed but it is too stable and this becomes very difficult. In the case of beer foam undesired foam collapse is observed if small fat droplets are introduced. These droplets may originate from external sources as fatty consumers lips or the contamination is already present in the glass wherein the beer is poured or, in the worst case, the droplets are already present in the beer itself. Defoaming systems used in, for example, the chemical or food industry consist often of particles that can destroy the foam according to the hydrophobic particle mechanism. These systems are, especially in the case of foodstuffs, very limited in their concentration that is allowed to use. For instance, regurgitation that babies may suffer from after consumption of infant formula, appears to be due to foam formation in the babies stomach. It is, however, in most countries not allowed to add defoaming systems to the formula, that destroy or inhibit the foam formation during drinking.

Increased knowledge on the spreading mechanism allows to make, in one case, the foam more robust against it and, in the other case, to implement it as a product property. The latter can be achieved by changing the properties of an ingredient, i.e. the oil phase, in such a way that they become active spreading particles that will

inhibit foam formation. In any case, spreading particles can be found everywhere and their desired or undesired effect on foam has to be understood.

A theory, based on the theory developed to describe the overflowing cylinder technique, was used to describe the film thinning and film rupture on the size scale of droplets and films present in foams. The theory was tested with experiments done at a more macroscopic scale. The results of these experiments seemed to verify the validity of the theory. There was, however, an important difference between the theory and the practical experiments. The time scale valid for the theory appeared to be 20-200 times smaller than the time scale at which the practical experiments were done. This may have large consequences for the surface rheological behaviour of the involved surfaces and interfaces. On one hand the driving force, i.e. the spreading coefficient, may become a different value which has consequences for the maximum film thickness that can be ruptured. On the other hand we have to consider that the film surfaces on bubbles are finite. This may have a big impact on the spreading distance and, therefore, on the stability of the film. If the spreading distance is too short the film will remain intact. When the response of the finite aqueous surface upon compression is a very steep decrease in surface tension, the spreading process will stop in an early stage and film rupture will not be induced. The surface rheological behaviour was found to play an important role in the spreading behaviour, i.e. spreading distance. Also at macroscopic scales of droplet size and film size: an effect of the surface area could be distinguished. Films with small surface areas were found to be stable upon spreading of droplets of micro-litre size over one of their surfaces. It was, however, not possible to measure the surface rheological behaviour at time scales that exist during the spreading of small droplets on small surfaces. Nevertheless, the longer time scale experiments did show the important effect of rheological parameters as surface and interfacial tension and surface dilational viscosity during compression on the spreading behaviour and film rupture. It can be concluded that the theory describes the hydrodynamics of the spreading rather well but increased knowledge

of the surface rheological behaviour at smaller time scales would improve the applicability. Nevertheless, the theory consists of many assumptions and parameters such as acceleration and droplet viscosity were not taken into consideration. Regarding the size and time scales and the values of the driving forces, i.e. surface tension gradients, we concluded that these parameters may be neglected. There was, however, no experimental evidence for doing so.

The surface area of the bubble was found, as mentioned before, an important parameter that influences the spreading behaviour. In the case of small droplets spreading over large bubble surfaces the surface rheological behaviour of the bubble surface appeared to play a minor role. In the case of small bubble surfaces this parameter becomes much more important. This may be an explanation for the high stability of fine foams against spreading because the spreading distance becomes too short to rupture the film.

Another important parameter was found to be the interfacial tension of the droplet. In the systems investigated here the value of the interfacial tension decreased sometimes, depending on the composition of the droplet and the aqueous phase, to almost zero. However, the surface tension of the oil was not affected. Regarding these possibilities the surface tension of the aqueous phase will have a lower limit below which spreading will no longer occur. In practice foaming solutions of soap molecules or proteins may have a dynamic surface tension of <30 mNm^{-1}. Consequently, for spreading the surface tension of the oil must be lower than this value assuming the interfacial tension to be close to zero. Droplets of the system used in this study, i.e. Soy oil with or without Tween 80 addition, would not spread over surfaces with surface tension of that value because the spreading coefficient would be smaller than zero (i.e. surface tension oil-air 35 mN/m and interfacial tension oil-aqueous solution almost 0 mN/m). Consequently these droplets would not affect the foam stability due to spreading over and, eventually, rupturing of the foam films.

In this study the events that take place when one droplet spreads over a surface were investigated. In practice, however, the number of droplets present in the system can be very high. Considering that more than one droplet may spread over one surface simultaneously this can have a large effect on what will happen to the film. When more than one droplet spreads over the relatively small surface area of a bubble, the film surface will be compressed more because the droplets spread towards each other. Consequently the spreading of a number of droplets present in the film surface may stop in an early stage and the film remains stable. Furthermore, when a droplet, or more than one droplet has spread over the bubble surface without rupturing the film the properties of the film surface have changed in such a way that the entering and spreading coefficients have become negative. This means that once a film has survived a spreading process it will remain stable because it has become impossible for other droplets to reach the surface.

The developed theory predicts that the capability of droplets to induce film rupture increases when the spreading coefficient is small. A film thickness up to 14 times the droplet radius were found to be possible to be ruptured. For that reason spreading droplets are theoretically capable to rupture the films in a foam in an early stage of film drainage. In order to do that they have to arrive in the film surface. This may be complicated considering the conditions during drainage. From the theory described in Chapter 2 it is known that the liquid drag exerted on the film surface during drainage is in equilibrium with a surface tension gradient that is developed in the surface. This would implicate that the surface can be motionless and, consequently, a velocity component perpendicular to the film surface will be absent. The question rises what driving force is then moving droplets towards the film surface. This can only be density difference which can drive a droplet to the surface in the case of a close to vertical film.

Furthermore, in an early stage after foam formation the liquid films behave, more or less as free falling liquid films. Under these conditions parts of the surfaces of the films will expand. This results in a driving force, i.e. a velocity component

perpendicular to the film surface, by which droplets present in the film liquid may arrive at the film surface. However, the thickness of the films will still be large and the droplets in the system may not be able to rupture these films depending on the sizes of the droplets and the surface area of the films as discussed earlier. After drainage has proceeded some period of time viscous flow within the film becomes more and more important and the liquid velocity will decrease due to the fact that the film surface becomes more and more motionless. At that moment the droplets have a smaller chance to arrive in the film surface unless there is an other driving force that moves the droplets to the film surface. In the case of droplets present in a non-vertical film the density difference is a driving force. When at this moment droplets arrive in the film surface they can spread and rupture those films easier because they have become thinner.

In the case the droplets are introduced from outside the foam the situation is different. The droplets arrive in this situation directly in the film surface where they can spread and rupture the film. If we assume that the droplets break up into smaller ones upon film rupture, these droplets will also arrive directly in the surfaces of the films surrounding the ruptured film. Consequently, these droplets may rupture these films too provided the droplets are still large enough.

From the results of this study the main parameters that can be distinguished for the spreading mechanism are:

1) A droplet has to be dewetted at the film surface, i.e. entering coefficient bigger than zero. This is important in both the cases when the droplets are present in the film or when droplets come into the film surface out of the gas phase. In the latter case the dewetting process does not have to take place but it is a prerequisite that the entering coefficient is positive otherwise the droplet would be wetted immediately upon contact with the aqueous phase.
2) In order to spread the spreading coefficient must be bigger than zero. The interfacial tension of the oil phase is important because it determines up to a large extent the value of the spreading coefficient. Lower values of the interfacial

tension increase the capability of droplets to spread over surfaces of foaming liquids. On the other hand, a lower interfacial tension results in a larger spreading coefficient which decreases the maximum film thickness that can be ruptured. A favourable condition would be that the spreading coefficient during the spreading process is small. However, if the value is too small the time before the film is ruptured becomes too long and the film may restore the film thinning process already during the spreading process. This implicates that the surface and interface rheological behaviour will be different for individual foaming systems and droplets and with that also the effect of these droplets on film stability.

3) The place where the droplets are coming from, plays a role in the final effect on foam stability. Without experimental evidence it can be concluded that the chance of film rupture increases when the droplets arrive in the film surface out of the gas phase. In that case the droplets are not in equilibrium with the aqueous phase and, therefore, they can develop still the lowest possible interfacial tension which is in favour of the spreading process. Furthermore, there is no limiting step of dewetting from the droplet. The chance that in a foam film a droplet arrives out of the aqueous phase in the film surface is smaller. However, from the experimental results that are available (see table 5.6) it can be concluded that droplets in the film are more active to rupture the film. In this case clear notice has to be taken on the fact that the droplets brought on the thin liquid film were much bigger than the droplets that were introduced in the film. This has, as discussed before, also a big influence on the effect of the droplets on film rupture due to the different spreading distance and time.
4) In both points 1) and 2) the dynamic surface rheological properties of the involved interfaces play an important role. In the case of the dewetting process out of the film liquid the oil-air surface is expanded and the oil-aqueous interface is compressed. Are the droplets coming out of the gas phase, the situation is vice versa. Regarding the spreading process both the oil-air and the oil-aqueous

interfaces are expanded. Therefore, it is clear that study of the dynamic surface tensions of these interfaces in compression and expansion give information about the dewetting and spreading behaviour and not the equilibrium interfacial tensions. At the time scales of spreading these interfacial tensions may increase which results in a decrease of the spreading velocity or, eventually, to a complete stop of the spreading process.

5) The surface area of the bubbles. A small surface area permits a small spreading distance and diminishes the chance of film rupture. Furthermore, the lateral size of the films in foams with small bubble-size distributions is small. This also decreases the chance that a droplet arrives in a film surface.
6) In relation with point 5) the time scale of spreading affects the outcome of the spreading process. When the spreading is too fast the restricted surface area allows not a sufficient spreading distance to induce film rupture. On the other hand, when the spreading velocity is too low the film has time to restore the thinning part of the film which underlies the spreading droplet.
7) When the liquid films are thicker they are more stable against spreading particles. However, it has to be mentioned that spreading particles can rupture much thicker films than hydrophobic particles of the same size.
8) The viscosity of the film liquid has a positive effect on the chance of film rupture due to the spreading process. This is due to an increased effect of the shear stress exerted by the moving surface on the underlying film liquid. The higher the bulk viscosity of the film liquid, the better film liquid is dragged along with the moving surface.
9) The droplet size has an effect. This study made clear that smaller droplets are more effective than larger ones. This is due to a combination of spreading distance and the restricted surface area of spreading. In theory larger droplets are capable to rupture thicker films but due to their own dimensions in relation to the available surface area, i.e. spreading distance, they may not be able to spread far and long enough to rupture the film.

10) The surface rheological behaviour of the aqueous phase in compression. This was found to be important when the surface areas of the films are small. The decrease in surface tension upon compression may stop the spreading process before the film ruptures. Therefore, measurement of the surface dilational viscosity in compression at time scales of spreading, provides valuable information. It is known that the minor components have a large effect on the surface rheological behaviour in compression. The overflowing cylinder technique where, due to the expansion of the surface the minor components play a minor role, delivers important surface rheological information on the interfaces of spreading droplet. Regarding the compression of the 'clean' aqueous surface the minor components are far more important because due to compression of the surface the minor components are accumulated in the surface and have a much bigger influence on the surface rheological behaviour. The extent of this influence can be found back in the surface dilational viscosity and the surface dilational modulus. A higher surface dilational viscosity and a higher surface dilational modulus would result in a bigger deceleration of the spreading droplet due to a steeper decrease of the surface tension of the 'clean' surface upon compression. This would stop the spreading process in an earlier stage which is in favour of film stability instead of film rupture. This effect will appear more pronounced when the bubbles, i.e. area of bubble surface, is smaller.

Before the present investigation had been carried out a few researchers had already speculated about the spreading particle mechanism. Others had made an attempt to describe the film rupture with theories based on the longitudinal wave theory and the penetration theory. Although a lot of questions are still not answered we may conclude that our approach based on the hydrodynamic coupling between surface and bulk liquid movement as is used in the overflowing cylinder has been proved to be fruitful. Therefore, the overflowing cylinder is a good technique to study what is happening when a droplet spreads over an aqueous surface of a film. The spreading behaviour did not follow the longitudinal wave theory but it has to be

mentioned that the latter was originally meant for spreading of monolayers. Further investigations should focus on the rheological behaviour of surfaces and interfaces at large deformation rates during both expansion and compression. Regarding the spreading velocities the possibility of film instability due to a shock wave should not be forgotten.

Now an idea has been formed of the parameters affecting the spreading behaviour, more tools have become available to control the influence of spreading particles on the stability of thin liquid films.

REFERENCES CHAPTER 5.

Bergink-Martens, D.J.M., "Interface dilation, the overflowing cylinder technique", PhD Thesis, Agricultural University Wageningen (1993).

Joos, P., Pintens, J., J. Coll. Int. Sci., **60(3)**:507 (1977).

Prins A., "Foam Stability as affected by the presence of small spreading particles." In: Surfactants in Solution, Vol. 10, Ed. K.L. Mittal, pp. 91 (1989).

Ronteltap, A.D., PhD Thesis, Agricultural University Wageningen (1989).

LIST OF SYMBOLS

A	surface area	m^2
A_C	work of isothermal formation of a nucleus	Nm
A_c	maximum surface area of new formed surface	m^2
A_P	surface area where particle is pressing against film surface	m^2
a	radius	m
a	relative surface expansion rate as function of time	s^{-1}
b	radius	m
c	radius	m
D	diffusion coefficient	m^2s^{-1}
d	distance	m
E	surface dilational modulus	Nm^{-1}
E_c	entering coefficient	Nm^{-1}
E_d	storage modulus	Nm^{-1}
$\|E\|$	amplitude of the ratio between surface stress and strain	Nm^{-1}
F_S	Stokes' force	N
F_c	counteracting force	N
f_c	force	N
$f_{c,max}$	maximum resistance force of liquid surface	N
f_D	frequency of the intensity fluctuations in the reflected light	s^{-1}
G	force	N
g	acceleration due to gravity	ms^{-2}
H	hydrostatic height	m
h	height	m
$h_{capillary}$	height of wetting film	m
K'	constant (eq. 2.44)	ms^{-1}
k	Boltzman's constant	NmK^{-1}
L	film length	m
l	slit length	m

P	penetration depth of liquid flow	m
P_c	capillary suction	Nm^{-2}
P^*	penetration depth of diffusion	m
ΔP	pressure difference	Nm^{-2}
ΔP_{OL}	Laplace pressure jump across the oil-liquid interface	Nm^{-2}
ΔP_{OA}	Laplace pressure jump across the oil-air interface	Nm^{-2}
Q	flow rate	m^3s^{-1}
R	radius	m
R_F	film radius	m
R_l	maximum spreading distance of oil layer	m
R_P	particle radius	m
R_{OA}	radius of curvature of oil-air surface	m
R_m	maximum radius	m
R'_{OL}	radius of curvature of oil-liquid interface	m
R''_{OL}	radius of curvature of oil-liquid interface	m
r	radius	m
r_c	critical wetting perimeter	m
S	displacement of the film surface	m
S_c	spreading coefficient	Nm^{-1}
T	temperature	K
t	time	s
t_c	drainage time to reach critical film thickness	s
t_e	falling time of the film to induce film rupture	s
$t_{rupture}$	spreading time to induce film rupture	s
t_s	spreading time	s
t_x	time for film element to fall to distance x from the slit	s
U	energy of resistance	Nm
v_A	angular velocity	ms^{-1}

v_B	bursting velocity of the falling film	ms^{-1}
v_L	spreading velocity according to the longitudinal wave theory	ms^{-1}
v_P	particle velocity perpendicular to the light fringe pattern	ms^{-1}
v_f	velocity of front or longitudinal wave	ms^{-1}
v_r	radial velocity	ms^{-1}
v_t	spreading velocity of monolayer as function of time	ms^{-1}
v_x	falling velocity of the film at distance x from the slit	ms^{-1}
v_z	velocity component perpendicular to the film surface	ms^{-1}
v_ξ	spreading velocity of monolayer as function of distance	ms^{-1}
v_0	initial velocity	ms^{-1}
W_A	work of adhesion	Nm
W_C	work of cohesion	Nm
x	distance	m
x_r	distance from the slit where the falling film will rupture	m
z	distance	m

Π	disjoining pressure	Nm^{-2}
Φ	amount of liquid draining from a vertical film	m^2s^{-1}
ψ	theoretical slope	m^{-1}
α	Mach angle	deg
α	angle from the centre of a spherical particle to its wetting perimeter	deg
α_c	angle defining the position of a spherical particle with respect to the undisturbed liquid surface	deg
α_P	dimensionless factor	-
β_P	dimensionless factor	-
γ	surface tension	Nm^{-1}

γ_F	surface tension of a film	Nm^{-1}
γ_{LA}	surface tension of the liquid-air surface	Nm^{-1}
γ_{OA}	surface tension of the oil-air surface	Nm^{-1}
γ_{OL}	interfacial tension of the oil-liquid interface	Nm^{-1}
γ_P	surface tension of Plateau border	Nm^{-1}
$\gamma_{O'L'}$	interfacial tension of oil-liquid interface: mutual saturated	Nm^{-1}
$\gamma_{L'A}$	surface tension of the liquid-air surface: liquid saturated with oil	Nm^{-1}
$\gamma_{O'A}$	surface tension of the oil-air surface: oil saturated with liquid	Nm^{-1}
γ_{dyn}	dynamic surface tension (in compression or expansion)	Nm^{-1}
$\gamma_{eq.}$	equilibrium surface tension	Nm^{-1}
γ_x	surface tension at distance x from the slit of the falling film	Nm^{-1}
$\Delta\gamma$	surface tension difference	Nm^{-1}
δ	film thickness	m
ζ	excluded time for spreading droplet	s
η	dynamic bulk viscosity	Nsm^{-2}
η_s^d	surface dilational viscosity	Nsm^{-1}
θ_B	angle between laser light beams	deg
θ_{OA}	Neumann angle of oil-air surface	deg
θ_{OL}	Neumann angle of oil-liquid surface	deg
θ_c	critical film thickness for rupture	m
θ_f	film thickness	m
$\theta_{f,0}$	initial thickness of a vertical film	m
θ_r	wetting perimeter	m
θ_x	film thickness at distance x from the slit of the falling film	m
θ_0	width of the slit of the free falling liquid film apparatus	m
κ	line force	N
λ	wave length of laser light	m

ν	kinematic viscosity	m^2s^{-1}
ξ	spreading distance	m
$\xi_{rupture}$	spreading distance to induce film rupture	m
ρ	density	kgm^{-3}
σ	shear stress	Nm^{-2}
τ	time	s
ω	frequency	s^{-1}

SUMMARY

Foam is a dispersion of gas in liquid that can be generated by for instance agitation at the gas liquid interface, leading gas through a glass sinter or a grit with very small holes in it or by the nucleation of gas bubbles when the liquid is supersaturated with gas. Foaming is mainly a physical phenomenon in which the chemical composition of the system plays an important role. The lifetime of the foam is for different reasons of great importance. Unwanted foam can create many problems. It can lead to major disruption of operations when it, for instance, interferes with process instruments, sensors, pumps and filters or when it initiates unwanted separation and segregation of process ingredients. On the other hand controlling the instability of foam is a functional part in products as beer and champagne. In order to understand the control of foams, one must first be aware of the factors that contribute to foam stability.

The three main physical processes that contribute to foam stability are drainage, disproportionation and coalescence. These processes are interrelated and occur simultaneously in a foam. They are determined by the surface and bulk properties of the foaming system. Amongst others, temperature, pH and surfactant concentration all influence the properties of the liquid surfaces of the films in a foam and therefore affect foam stability.

The most fragile structures (for rupture) in a foam are the thin liquid films between the bubbles. Therefore, the physical structure in a foam on which this study was focusing is the thin liquid film. The spreading behaviour of oil droplets and the mechanism of film thinning and eventually film rupture due to the spreading of droplets over the surface of the films between the bubbles in a foam, was subject of investigation in this study. It was the aim to describe the local thinning of a liquid film when, due to spreading of surface active material out of a particle over the film surface, film liquid is dragged away from the center of spreading to such an extent that the film ruptures. The hydrodynamic

processes, that take place in the film during spreading, were quantified theoretically.

The following steps in the whole process were distinguished: 1) transport of the particle to the film surface, 2) dewetting of the particle ensuring physical contact between the particle surface and the film surface, 3) spreading of the particle over the film surface and 4) movement of the film bulk liquid induced by the surface movement due to spreading material.

Experiments were performed to characterize the spreading process in terms of dewetting, spreading, spreading velocity and film rupture. However, due to the difficulties to determine the spreading behaviour of very small droplets (i.e. a radius of 1-100 μm) over thin liquid films experiments were done to investigate the spreading behaviour of relatively large oil droplets (i.e. a radius of 0.5-1 mm) over the surfaces of liquid bulk systems instead of thin liquid films. It was assumed that this kind of spreading behaviour provides information to be used to describe the spreading behaviour of very small droplets over the surface of thin liquid films. This was confirmed by the developed theory and performed experiments

From the results of this study several main parameters could be distinguished to be important in the spreading mechanism. A droplet has to be dewetted at the film surface, i.e. the entering coefficient must bigger than zero. This appeared to be important in both the cases when the droplets are present in the film or when droplets come into the film surface out of the gas phase. A particle starts to spread when the spreading coefficient is bigger than zero. In this context the interfacial tension of the oil phase is important because it determines up to a large extent the value of the spreading coefficient. Lower values of the interfacial tension increase the capability of droplets to spread over surfaces of foaming liquids. On the other hand, a lower interfacial tension results in a larger spreading coefficient which decreases the maximum film thickness that can be ruptured.

Without experimental evidence it could be concluded that the chance of film rupture increases when the droplets arrive in the film surface out of the gas phase. In that case the droplets are not in equilibrium with the aqueous phase and, therefore, they can develop still the lowest possible interfacial tension which is in favour of the spreading process.

The dynamic surface rheological properties of the involved interfaces were found to play an important role. In the case of the dewetting process out of the film liquid the oil-air surface is expanded and the oil-aqueous interface is compressed. Are the droplets coming out of the gas phase, the situation is vice versa. Regarding the spreading process both the oil-air and the oil-aqueous interfaces are expanded. Therefore, it became clear that study of the dynamic surface tensions of these interfaces in compression and expansion would give information about the dewetting and spreading behaviour and not the equilibrium interfacial tensions. At the time scales of spreading these interfacial tensions may increase which results in a decrease of the spreading velocity or, eventually, to a complete stop of the spreading process. The surface area of the bubbles plays also an important role in the result of a spreading process. A small surface area permits a small spreading distance and diminishes the chance of film rupture. Furthermore, the lateral size of the films in foams with small bubble-size distributions is small. This also decreases the chance that a droplet arrives in a film surface.

The time scale of spreading affects the outcome of the spreading process. When the spreading is too fast the restricted surface area of a bubble surface does not allow a sufficient spreading distance to induce film rupture. On the other hand, when the spreading velocity is too low the film has time to restore the thinning part of the film which underlies the spreading droplet.

When the liquid films are thicker they are more stable against spreading particles. However, it has to be mentioned that spreading particles can rupture much thicker films than hydrophobic particles of the same size.

The viscosity of the film liquid has a positive effect on the chance of film rupture due to the spreading process. This is due to an increased effect of the shear stress exerted by the moving surface on the underlying film liquid. The higher the bulk viscosity of the film liquid, the better film liquid is dragged along with the moving surface.

This study made clear that smaller droplets are more effective than larger ones. This is due to a combination of spreading distance and the restricted surface area of spreading. In theory larger droplets are capable to rupture thicker films but due to their own dimensions in relation to the available surface area, i.e. spreading distance, they may not be able to spread far and long enough to rupture the film.

The surface rheological behaviour of the aqueous phase in compression was found to be important when the surface areas of the films are small. The decrease in surface tension upon compression may stop the spreading process before the film ruptures. Therefore, the surface dilational viscosity in compression and the surface dilational modulus at time scales of spreading, provided valuable information. A higher surface dilational viscosity and a higher surface dilational modulus resulted in a bigger deceleration of the spreading droplet due to a steeper decrease of the surface tension of the 'clean' surface upon compression. This would stop the spreading process in an earlier stage which is in favour of film stability instead of film rupture.

SAMENVATTING

Schuim is een dispersie van een gas in een vloeistof en kan gemaakt worden door bijvoorbeeld opkloppen, gas door een glas sinter te leiden dat kleine gaatjes bevat of door nucleatie van gasbellen wanneer de oplossing met het gas oververzadigd is. Schuimvorming is voornamelijk een fysisch fenomeen waarbij de chemische samenstelling van de vloeistof een grote rol speelt. Ongewenst schuim kan veel problemen veroorzaken. Het kan tot obstructie van produktieprocessen leiden als het, bijvoorbeeld, storing veroorzaakt bij machines, sensoren, pompen en filters of als het separatie en segregatie van ingredienten teweegbrengt. Aan de andere kant is een gecontroleerde schuimstabiliteit van belang in produkten als bier en champagne. Om een schuimstabiliteit in de hand te kunnen hebben is het zaak de factoren die bijdragen aan de schuimstabiliteit te onderkennen.

De drie belangrijkste fysische processen die de schuimstabiliteit bepalen zijn drainage, disproportionering en coalescentie. Deze processen zijn onderling verbonden en vinden tergelijkertijd plaats in het schuim. Zij worden bepaald door de oppervlakte- en bulk-reologische eigenschappen van het schuimende systeem. Naast andere factoren beinvloeden temperatuur, pH en surfactant concentratie de eigenschappen van de vloeistofoppervlakken in een schuim en daarmee de schuimstabiliteit.

De meest gevoelige structuren voor breuk in een schuim zijn de dunne vloeistoffilms tussen de gasbellen. In deze studie is daarom de aandacht gericht op deze dunne vloeistoffilm. Het spreidingsgedrag van oliedruppels en het mechanisme van het dunner worden van de film en het eventueel breken ervan veroorzaakt door spreidende druppels was onderwerp van dit onderzoek. Het was het doel om te beschrijven hoe een vloeistoffilm breekt als gevolg van het spreiden van een druppel over het filmoppervlak waardoor onderliggende vloeistof wordt meegesleurd en de film plaatselijk te dun wordt.

De hydrodynamische processen die tijdens het spreiden plaatsvinden werden theoretisch gekwantificeerd.

Er werd onderscheid gemaakt tussen de volgende stappen in het gehele proces: 1) het transport van het deeltje naar het filmoppervlak, 2) het droogvallen van het deeltje waardoor fysisch kontakt tussen het deeltje en het oppervlak onstaat, 3) het spreiden van het deeltje over het filmoppervlak en 4) het bewegen van de filmvloeistof veroorzaakt door de oppervlaktebeweging dat het spreiden met zich meebrengt.

Er werden experimenten uitgevoerd om het spreidingsproces te karakteriseren uit oogpunt van droogvallen, spreiden, spreidsnelheid en filmbreuk. Echter door experimentele moeilijkheden om het spreidingsgedrag van zeer kleine druppeltjes (radius 1-100 μm) over dunne vloeistoffilms te bestuderen werden experimenten uitgevoerd waarin het spreidingsgedrag van relatief grote driuppels (radius 0.5-1 mm) over de oppervlakken van bulk vloeistof systemen in plaats van dunne vloeistoffilms werd onderzocht. Er werd aangenomen dat dit soort spreiding bruikbare informatie zou leveren om het spreidingsgedrag van zeer kleine druppeltjes te kunnen beschrijven. Dit werd door de ontwikkelde theorie en de experimentele resultaten bevestigd.

Uit de resultaten van dit onderzoek kon onderscheid worden gemaakt tussen verscheidende voor het spreidingsproces belangrijke parameters. Een druppel moet droogvallen aan het filmoppervlak. Dit betekend dat de zogenaamde "entering coefficient" positief moet zijn. Dit bleek belangrijk te zijn in het geval de druppel in de film aanwezig is maar ook als de druppel vanuit de gasfase in het filmoppervlak komt. Een druppel begint te spreiden als de zogenaamde "spreading coefficient" groter is dan nul. Hierbij speelt de grensvlakspanning van de olie een belangrijke rol omdat het in hoge mate de waarde van de "spreading coefficient" bepaald. Lagere grensvlakspanningen verhogen de spreidingsmogelijkheden van druppels over oppervlakken van schuimende vloeistoffen. Aan de andere kant resulteerd een lagere grensvlakspanning in

een grotere "spreading coefficient" waardoor de maximale dikte van een film die nog gebroken kan worden afneemt.

Zonder experimenteel bewijs kon geconcludeerd worden dat de kans op filmbreuk groter wordt indien de druppels vanuit de gasfase in het filmoppervlak arriveren. In dit geval zijn de druppels niet in evenwicht met de filmvloeistof en kunnen ze nog steeds de laagst mogelijke grensvlakspanning ontwikkelen wat een voordeel is voor het spreidingsproces.

De dynamische reologische eigenschappen van de betrokken grensvlakken spelen een belangrijke rol. In het geval van droogvallen vanuit de filmvloeistof wordt het olie-lucht oppervlak geëxpandeerd en wordt het olie-water grensvlak gecomprimeerd. Wanneer de druppels uit de gasfase in het filmoppervlak komen is de situatie andersom. Tijdens het spreiden worden beide grensvlakken geëxpandeerd. Het werd daarom duidelijk dat het bestuderen van de dynamische opervlakte- en grensvlak-spanningen bruikbare informatie zou leveren over het droogvallen en het spreidingsgedrag. Bij tijdschalen van toepassing voor spreiding kunnen deze grensvlakspanning hoger worden wat een lagere spreidingssnelheid of, eventueel, een complete stop van het spreiden tot gevolg kan hebben. De oppervlakte van de gasbellen speelt eveneens een belangrijke rol in het uiteindelijke resultaat van het spreidingsproces. Een kleine oppervlakte staat een kleine spreidingsafstand toe een verkleint daarmee de kans op filmbreuk. Bovendien is de laterale grootte van de films in een schuim met een kleine bellengrootteverdeling klein. Hierdoor wordt de kans dat een deeltje in het oppervlak komt eveneens verkleint.

De tijd van spreiding beïnvloedt het resultaat van het spreidingsproces. Als het spreiden te snel gaat wordt door het beperkte oppervlak van een gasbel de mogelijke spreidingsafstand gelimiteerd waardoor de kans op filmbreuk wederom wordt beperkt. Aan de andere kant is het zo dat wanneer de

spreidingssnelheid te laag is de film tijd heeft om het dunner wordende deel te herstellen doordat filmvloeistof kan terugvloeien.

Als de vloeistoffilms dikker zijn is hun stabiliteit tegen spreidende deeltjes groter. Niettemin moet gezegd worden dat spreidende deeltjes veel dikkere films kunnen breken dan hydrofobe deeltje met dezelfde grootte.

De viscositeit van de filmvloeistof heeft een positief effect op de kans op filmbreuk door het spreidingsproces. Dit komt door de grotere afschuifkrachten die door het bewegende oppervlak op de onderliggende vloeistof wordt uitgeoefend. Hoe hoger de bulkviscositeit van de filmvloeistof, hoe beter de filmvloeistof met het bewegende filmoppervlak wordt meegesleurd.

Dit onderzoek maakte duidelijk dat kleinere oliedruppeltjes effectiever zijn dan grotere. Dit komt door een combinatie van spreidingsafstand en het beperkte oppervlak van een gasbel waarover spreiding kan plaatsvinden. Theoretisch zouden grotere druppels dikkere films kunnen breken maar door hun eigen dimensies in relatie met het beschikbare oppervlak (spreidingsafstand) is het niet mogelijk dat ze ver en lang genoeg te spreiden om tot filmbreuk te leiden.

De oppervlaktereologische eigenschappen van het wateroppervlak in compressie bleek belangrijk te zijn als de oppervlakken van de films klein zijn. De verlaging van de oppervlaktespanning in compressie kan het spreiden stoppen nog voor de film breekt. Daarom geven de oppervlakte dilatatie viscositeit en de oppervlakte dilatatie modulus bij tijdschalen die bij spreiding voorkomen bruikbare informatie. Een hoge oppervlakte dilatatie viscositeit en een hoge oppervlakte dilatatie modulus resulteren in een grotere afremming van de spreidende druppel doordat de oppervlaktespanning van het nog "schone" beloppervlak sneller daalt. Dit zou het spreidingsproces in een vroeger stadium kunnen stoppen waardoor de kans op filmbreuk kleiner wordt.

CURRICULUM VITAE

Curriculum Vitae C.G.J. Bisperink

Christiaan Gerrit Jan Bisperink was born on the 8th of March 1962 in Borculo, The Netherlands. In 1982 he passed his examination Athenaeum_β successful at the Rijksscholengemeenschap Lochem in Lochem, The Netherlands. The same year he started his study Food Technology at the Agricultural University Wageningen, The Netherlands. During the period of practical training he worked at the dairy factory "Zuid-Oost-Hoek" in Oosterwolde, The Netherlands. The main topics during his study were dairy science and technology and food physics. In 1989 he graduated in Dairy Technology and Food Physics on the final project titled 'About the Mechanism of Rebodying Milk Fat Globules and the role of the Fat Crystals in it'.
From March 1989 to May 1994 he was employed as a research worker at the Food Physics group of the Agricultural University Wageningen, The Netherlands within the Eureka project BUFOM (EU267): 'Sparkling wines and foaming beverages'. His research topics were bubble formation and growth in carbonized liquids, the effect of malt lipids on beer foam behaviour, the development of the Foam Analyzer which is now successfully used in practice to measure amongst other parameters the bubble-size distribution in aqueous foams, and the mechanism of coalescence initiated by the rupture of the thin liquid films between bubbles in a foam due to spreading of particles over the surface of those films. The last topic was studied for a period of one and a half year and the results will be used in this Ph.D.-thesis. Within the framework of this project he presented two lectures and three posters on conferences and symposia within the Netherlands and abroad.
Since August 1994 he works at the Nestlé Research Center in Lausanne Switzerland in the Food Technology Department within the Texture and Structure group. Since May 1995 he is there product area coordinator for the ice cream research.